Measurement of the Mass of the τ Lepton

J. Z. Bai,[1] O. Bardon,[6] R. A. Becker-Szendy,[7] T. H. Burnett,[10] J. S. Campbell,[9] S. J. Chen,[1] S. M. Chen,[1] Y. Q. Chen,[1] Z. D. Cheng,[1] J. A. Coller,[2] R. F. Cowan,[6] H. C. Cui,[1] X. Z. Cui,[1] H. L. Ding,[1] Z. Z. Du,[1] W. Dunwoodie,[7] C. Fang,[1] M. J. Fero,[6] M. L. Gao,[1] S. Q. Gao,[1] W. X. Gao,[1] Y. N. Gao,[1] J. H. Gu,[1] S. D. Gu,[1] W. X. Gu,[1] Y. N. Guo,[1] Y. Y. Guo,[1] Y. Han,[1] M. Hatanaka,[3] J. He,[1] D. G. Hitlin,[3] G. Y. Hu,[1] T. Hu,[1] D. Q. Huang,[1] Y. Z. Huang,[1] J. M. Izen,[9] Q. P. Jia,[1] C. H. Jiang,[1] Z. J. Jiang,[1] A. S. Johnson,[2] L. A. Jones,[3] M. H. Kelsey,[3] Y. F. Lai,[1] P. F. Lang,[1] A. Lankford,[4] F. Li,[1] J. Li,[1] P. Q. Li,[1] Q. M. Li,[1] R. B. Li,[1] W. Li,[1] W. D. Li,[1] W. G. Li,[1] Y. S. Li,[1] S. Z. Lin,[1] H. M. Liu,[1] Q. Liu,[1] R. G. Liu,[1] Y. Liu,[1] B. Lowery,[9] J. G. Lu,[1] D. H. Ma,[1] E. C. Ma,[1] J. M. Ma,[1] M. Mandelkern,[4] H. Marsiske,[7] H. S. Mao,[1] Z. P. Mao,[1] X. C. Meng,[1] H. L. Ni,[1] L. J. Pan,[1] J. H. Panetta,[3] F. C. Porter,[3] E. N. Prabhakar,[3] N. D. Qi,[1] Y. K. Que,[1] J. Quigley,[6] G. Rong,[1] B. Schmid,[4] J. Schultz,[4] J. T. Shank,[2] Y. Y. Shao,[1] D. L. Shen,[1] H. Y. Sheng,[1] H. Z. Shi,[1] A. Smith,[4] E. Soderstrom,[7] X. F. Song,[1] D. P. Stoker,[4] H. S. Sun,[1] J. Synodinos,[7] W. H. Toki,[5] G. L. Tong,[1] E. Torrence,[6] L. Z. Wang,[1] M. Wang,[1] P. Wang,[1] P. L. Wang,[1] T. J. Wang,[1] Y. Y. Wang,[1] J. S. Whitaker,[2] R. J. Wilson,[2] W. J. Wisniewski,[8] X. D. Wu,[1] D. M. Xi,[1] X. M. Xia,[1] P. P. Xie,[1] X. X. Xie,[1] R. S. Xu,[1] Z. Q. Xu,[1] S. T. Xue,[1] R. K. Yamamoto,[6] J. Yan,[1] W. G. Yan,[1] C. M. Yang,[1] C. Y. Yang,[1] H. B. Yao,[1] M. H. Ye,[1] S. Z. Ye,[1] Z. Q. Yu,[1] B. Y. Zhang,[1] C. C. Zhang,[1] D. H. Zhang,[1] H. L. Zhang,[1] H. Y. Zhang,[1] J. W. Zhang,[1] L. S. Zhang,[1] S. Q. Zhang,[1] Y. Zhang,[1] D. X. Zhao,[1] M. Zhao,[1] P. D. Zhao,[1] W. R. Zhao,[1] J. P. Zheng,[1] L. S. Zheng,[1] Z. P. Zheng,[1] G. P. Zhou,[1] H. S. Zhou,[1] L. Zhou,[1] L. Zhou,[1] X. F. Zhou,[1] Y. H. Zhou,[1] Q. M. Zhu,[1] Y. C. Zhu,[1] Y. S. Zhu,[1] and G. Zioulas[4]

(BES Collaboration)

[1] *Institute of High Energy Physics, Beijing 100039, People's Republic of China*
[2] *Boston University, Boston, Massachusetts 02215*
[3] *California Institute of Technology, Pasadena, California 91125*
[4] *University of California, Irvine, California 92717*
[5] *Colorado State University, Fort Collins, Colorado 80523*
[6] *Massachusetts Institute of Technology, Cambridge, Massachusetts 02139*
[7] *Stanford Linear Accelerator Center, Stanford University, Stanford, California 94309*
[8] *Superconducting Super Collider Laboratory, Dallas, Texas 75237-3946*
[9] *University of Texas at Dallas, Richardson, Texas 75083-0688*
[10] *University of Washington, Seattle, Washington 98195*
(Received 7 August 1992)

The mass of the τ lepton has been measured at the Beijing Electron-Positron Collider using the Beijing Spectrometer. A search near threshold for $e^+e^- \rightarrow \tau^+\tau^-$ was performed. Candidate events were identified by requiring that one τ decay via $\tau \rightarrow e\nu\bar{\nu}$, and the other via $\tau \rightarrow \mu\nu\bar{\nu}$. The mass value, obtained from a fit to the energy dependence of the $\tau^+\tau^-$ cross section, is $m_\tau = 1776.9^{+0.4}_{-0.5} \pm 0.2$ MeV.

PACS numbers: 14.60.Jj, 13.10.+q

For a conventional charged lepton l, the electronic branching ratio B_l^e, lifetime τ_l, mass m_l, and weak coupling constant $G_{l \rightarrow e\nu\bar{\nu}}$ are related by

$$\frac{B_l^e}{\tau_l} = \frac{G^2_{l \rightarrow e\nu\bar{\nu}}}{192\pi^3} m_l^5 , \qquad (1)$$

up to small radiative and electroweak corrections. Equation (1) then implies the following relationship among the above parameters for the τ and μ leptons:

$$\left(\frac{G_{\tau \rightarrow e\nu\bar{\nu}}}{G_{\mu \rightarrow e\nu\bar{\nu}}} \right)^2 = \left(\frac{m_\mu}{m_\tau} \right)^5 \frac{B_\tau^e}{B_\mu^e} \frac{\tau_\mu}{\tau_\tau} . \qquad (2)$$

Particle Data Group (PDG) [1] averages for the above quantities yield $(G_{\tau \rightarrow e\nu\bar{\nu}}/G_{\mu \rightarrow e\nu\bar{\nu}})^2 = 0.941 \pm 0.025$, implying a 2.4 standard deviation disagreement with lepton universality [2]. Note that the τ mass enters to the fifth power in this test of lepton universality.

A measurement of the $\tau^+\tau^-$ production cross section in the region most sensitive to the τ mass—a few MeV around threshold—provides the opportunity to measure the τ mass with greatly improved precision. This paper presents such a measurement made using the Beijing Spectrometer (BES) at the Beijing Electron-Positron Collider (BEPC). The $\tau^+\tau^-$ events are identified by means of the $e\mu$ topology, which provides the best combination of high detection efficiency and low background; the mass value is obtained from a fit to the energy dependence of the cross section. The measurement is independent of the ν_τ mass.

The BEPC [3] operates in the 3 to 5 GeV center-of-mass energy range. Near $\tau^+\tau^-$ threshold, the peak luminosity is 5×10^{30} cm^{-2}s^{-1}, the luminosity-weighted uncertainty in the mean center-of-mass energy is 0.10 MeV, and the spread in the center-of-mass energy of the collider is ≈ 1.4 MeV. The absolute energy scale and energy spread are determined by interpolation between the results of repeated scans of the J/ψ and $\psi(2S)$ resonances.

The BES is a solenoidal detector [3] with a 0.4-T magnetic field. Charged track reconstruction is performed by means of a cylindrical drift chamber which provides solid angle coverage of 85% of 4π. The momentum resolution is $\sigma_p/p=0.021(1+p^2)^{1/2}$ (p in GeV/c). Measurements of dE/dx with resolution 8.5% allow particle identification. An inner drift chamber is used for trigger purposes. Scintillation counters measure the time of flight of charged particles over 76% of 4π with a Bhabha resolution of 330 ps. A cylindrical 12-radiation-length Pb/gas electromagnetic calorimeter operating in limited streamer mode covering 80% of 4π achieves energy resolution $\sigma_E/E=0.25/\sqrt{E\text{ (GeV)}}$, and spatial resolution $\sigma_\phi=4.5$ mrad, $\sigma_z=2$ cm. End-cap time-of-flight counters and shower counters are not used in this analysis. Finally, a three-layer iron flux return instrumented for muon identification yields spatial resolutions $\sigma_z=5$ cm, $\sigma_{r\phi}=3$ cm over 68% of 4π for muons with momentum greater than 550 MeV/c.

In the data analysis, the event selection for $e\mu$ candidates requires the following: (1) exactly two oppositely charged tracks having momentum between 350 MeV/c and the maximum for an electron from τ decay; (2) each track's point of closest approach to the intersection point to satisfy $|x|<1.5$ cm, $|y|<1.5$ cm, and $|z|<15$ cm; (3) $2.5°<\theta_{\text{acol}}<177.5°$, $\theta_{\text{acop}}>10°$ (see Ref. [4]), and $\theta_{\text{acol}}+\theta_{\text{acop}}>50°$; (4) no isolated photons [5]; (5) one track well identified as a muon in the muon counter, with calorimeter energy <500 MeV, and the other track well identified as an electron using a combination of calorimeter, dE/dx, and time-of-flight information.

Monte Carlo simulations yield a detection efficiency of $\approx 14\%$ for these selection criteria, independent of energy in the threshold region. The background is estimated by applying the same requirements to 5×10^6 events from a data sample taken at the J/ψ energy; seven events meet these criteria, corresponding to a background of 0.12 event in the entire $\tau^+\tau^-$ sample.

The likelihood function used to estimate the τ mass incorporates the $\tau^+\tau^-$ cross section near threshold. Including the center-of-mass energy spread Δ, initial state radiation [6] $F(x,W)$, and vacuum polarization corrections [7] $\Pi(W)$, the cross section is

$$\sigma(W,m_\tau)=\frac{1}{\sqrt{2\pi}\Delta}\int_0^\infty dW'e^{-(W-W')^2/2\Delta^2}\int_0^{1-4m_\tau^2/W'^2}dx\,F(x,W')\sigma_1(W'\sqrt{1-x},m_\tau)\,, \tag{3}$$

where σ_1 is

$$\sigma_1(W,m_\tau)=\frac{4\pi\alpha^2}{3W^2}\frac{\beta(3-\beta^2)}{2}\frac{F_c(\beta)F_r(\beta)}{[1-\Pi(W)]^2}\,, \tag{4}$$

W is the center-of-mass energy, and $\beta=[1-(2m_\tau/W)^2]^{1/2}$. The Coulomb interaction and final-state radiation corrections are described [8] by the functions $F_c(\beta)$ and $F_r(\beta)$.

The likelihood function is a product of Poisson distributions, one for each center-of-mass energy. At each point, the number of expected $e\mu$ events $\langle N\rangle$ is given by

$$\langle N\rangle=[\epsilon B\sigma(W,m_\tau)+\sigma_B]\mathcal{L}\,. \tag{5}$$

Here, ϵ is the detection efficiency, B is the product branching fraction for $\tau^+\tau^-$ to $e\mu$, $\mathcal{L}$ is the integrated luminosity, and σ_B is the effective background cross section estimated from the J/ψ data sample ($\sigma_B=0.024$ pb).

Since the range of center-of-mass energies where the $\tau^+\tau^-$ cross section is most sensitive to the τ mass is of the order of the beam energy spread around $\tau^+\tau^-$ threshold, it is important to devise a running strategy to maximize the integrated luminosity in this region. The beam energy is set initially assuming the world average for the τ mass; in this case, the PDG value is 1784.1 MeV [1]. Then, after each 250–400 nb^{-1} of integrated luminosity, a new estimate of the mass is made using all the data accumulated to that point; in this way, a new prediction of the most sensitive energy at which to run is obtained. The energy is changed to this new value if the difference is more than the BEPC step size (≈ 0.4 MeV). Following this strategy, an integrated luminosity of ≈ 4.3 pb^{-1} has been accumulated at ten energies within a range of 24 MeV. It has been verified by Monte Carlo simulation that this data-driven search strategy provides an unbiased measurement.

The sequence of energies is shown in Fig. 1; the corresponding data are summarized in Table I [9]. The ten-step search yielded seven $e\mu$ events. The eleventh and twelfth points in Table I, taken well above threshold where the cross section varies slowly with energy, provide an improved estimate of the absolute $\tau^+\tau^-$ cross section.

In order to account for uncertainties in the efficiency ϵ, the branching fraction product, and the luminosity, ϵ is treated as a free parameter in a two-dimensional maximum-likelihood fit for m_τ and ϵ to the data of Table I.

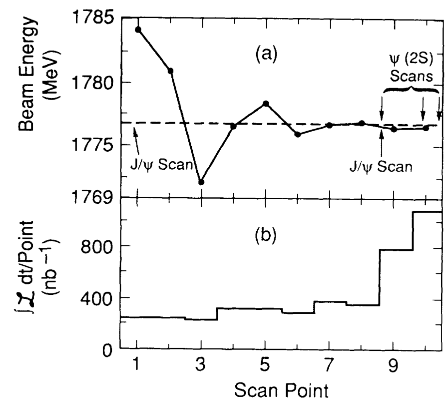

FIG. 1. (a) The convergence of the predicted mass with each consecutive scan point. (b) The integrated luminosity accumulated at each point.

The estimates obtained are $m_\tau = 1776.9$ MeV and $\epsilon = 14.1\%$. The uncertainty in ϵ is equivalent to the uncertainty in the absolute normalization, and is treated as a source of systematic error. The statistical error [10] in m_τ, $^{+0.4}_{-0.5}$ MeV, is determined from the one-parameter likelihood function with ϵ fixed to 14.1% (Fig. 2). The efficiency-corrected cross-section data as a function of corrected beam energy and the curve which results from the likelihood fit are shown in Fig. 2. The quality of the fit is checked by forming the likelihood ratio λ, with the result [11] $-2\ln\lambda = 3.6$.

Four independent sources of systematic error are considered: uncertainties in the product $\epsilon B\mathcal{L}$, in the absolute beam energy scale, in the beam energy spread, and in the background.

The systematic uncertainty in $\epsilon B\mathcal{L}$ is determined by fixing m_τ at its best-estimate value and finding the values of ϵ corresponding to $\pm 1\sigma$ variations in the likelihood function; these efficiencies are 18.3% and 10.6%. Fixing the efficiency to each of these values in turn and fitting for m_τ yields changes in the predicted mass of $\Delta m_\tau = ^{+0.16}_{-0.20}$ MeV.

TABLE I. A chronological summary of the $\tau^+\tau^-$ data.

Scan point	$W/2$ (MeV)	Δ (MeV)	$\mathcal{L}$ (nb^{-1})	N ($e\mu$ events)
1	1784.19	1.34	245.8	2
2	1780.99	1.33	248.9	1
3	1772.09	1.36	232.8	0
4	1776.57	1.37	323.0	0
5	1778.49	1.44	322.5	2
6	1775.95	1.43	296.9	0
7	1776.75	1.47	384.0	0
8	1776.98	1.47	360.8	1
9	1776.45	1.44	794.1	0
10	1776.62	1.40	1109.1	1
11	1799.51	1.44	499.7	5
12	1789.55	1.43	250.0	2

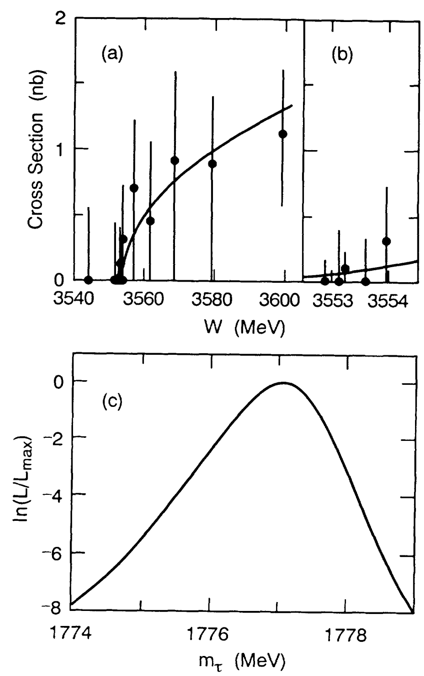

FIG. 2. (a) The center-of-mass energy dependence of the $\tau^+\tau^-$ cross section resulting from the likelihood fit (curve), compared to the efficiency-corrected data. The error bar on each data point is computed by integrating the Poisson likelihood function to obtain the interval containing 68% of the area. It should be emphasized that the curve does not result from a direct fit to these data points. (b) An expanded version of (a), in the immediate vicinity of $\tau^+\tau^-$ threshold. (c) The dependence of the logarithm of the likelihood function on m_τ, with efficiency fixed at 14.1%.

The energy scale is determined from several scans of the J/ψ and $\psi(2S)$ performed during the search (see Fig. 1). The reproducibility of the fits to these scans, together with the other uncertainties listed in Table II, yields a systematic uncertainty [12] of $\Delta m_\tau = \pm 0.09$ MeV.

Fits to the two resonances were also used to measure the beam energy spread and its variation with center-of-mass energy and beam current. The uncertainty in center-of-mass energy spread is ± 0.08 MeV, yielding a systematic error $\Delta m_\tau = \pm 0.02$ MeV.

TABLE II. Contributions to the uncertainty in the energy scale.

Quantity	Error (MeV)
W_M: BEPC measured center-of-mass energy	$\delta W_M = 0.10$
M_ψ: BEPC value for J/ψ mass	$\delta M_\psi = 0.18$
$M_{\psi'}$: BEPC value of $\psi(2S)$ mass	$\delta M_{\psi'} = 0.15$
T_ψ: PDG value for J/ψ mass[a]	$\delta T_\psi = 0.09$
$T_{\psi'}$: PDG value for $\psi(2S)$ mass[a]	$\delta T_{\psi'} = 0.10$

[a]Reference [1].

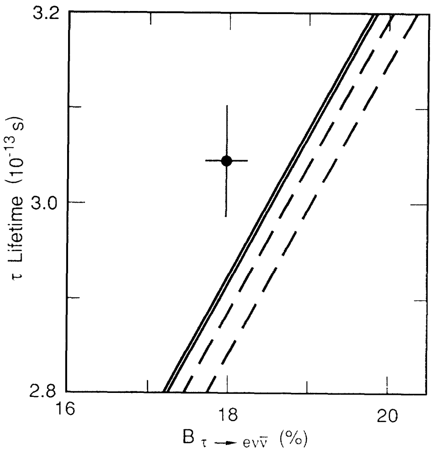

FIG. 3. The variation of τ_τ with B_τ^e, given by Eq. (1) under the assumption of lepton universality; the $\pm 1\sigma$ bands obtained using m_τ from this experiment (solid lines) and using the PDG value (dashed lines) are shown in comparison to the point corresponding to the PDG values (1σ error bars).

Finally, the systematic error due to uncertainty in the background is estimated from the 1σ Poisson errors on the seven J/ψ background events and the uncertainty in the hadronic cross section at $\tau^+\tau^-$ threshold. The resulting uncertainty is $\Delta m_\tau = \pm 0.01$ MeV.

These independent systematic errors are added in quadrature to yield a total systematic error of $\Delta m_\tau = ^{+0.18}_{-0.22}$ MeV.

In conclusion, using a maximum-likelihood fit to $\tau^+\tau^-$ cross-section data near threshold, the mass of the τ lepton has been measured as $m_\tau = 1776.9^{+0.4}_{-0.5} \pm 0.2$ MeV, where the first error is statistical and the second systematic. This result is 7.2 MeV below the PDG average [1] ($1784.1^{+2.7}_{-3.6}$ MeV) and has significantly smaller errors [13]. Inserting this new value in Eq. (2), the coupling strength ratio becomes

$$(G_{\tau \to e\nu\bar{\nu}}/G_{\mu \to e\nu\bar{\nu}})^2 = 0.960 \pm 0.024\,, \tag{6}$$

so that the deviation from lepton universality is reduced from 2.4 to 1.7 standard deviations (see Fig. 3). It should be noted also that this new result for m_τ yields a reduction in the upper limit on m_{ν_τ} (see Ref. [13]).

We would like to thank the BEPC staff and the Computer Center at IHEP for their outstanding efforts, and also Y. S. Tsai and J. M. Wu for helpful discussions about the $\tau^+\tau^-$ cross section near threshold. This work was supported in part by the National Natural Science Foundation of China under Contract No. 19290400 (IHEP); by the Department of Energy under Contracts No. DE-AC03-76SF00515 (SLAC), No. DE-FG03-92ER40701 (Caltech), No. DE-FG03-91ER40679 (UC Irvine), No. DE-FG02-91ER40676 (Boston University), No. DE-AC02-76ER03069 (MIT), No. DE-AC35-89ER40486 (SSC), and No. DE-FG05-92ER40736 (UT Dallas); by the Texas National Research Laboratory Commission (Rocky Mountain Consortium for High Energy Physics) under Contracts No. RGFY91B5 and No. RGFY92B5 (Colorado State); and by the National Science Foundation (University of Washington).

[1] Particle Data Group, K. Hikasa *et al.*, Phys. Rev. D **45**, S1 (1992).

[2] W. J. Marciano, Phys. Rev. D **45**, 721 (1992). The measurements quoted in this reference have been superseded by Ref. [1].

[3] M. H. Ye and Z. P. Zheng, in *Proceedings of the 1989 International Symposium on Lepton and Photon Interactions at High Energies* (Stanford University, Stanford, 1989), p. 122.

[4] Acoplanarity, $\theta_{\rm acop}$, is defined as the angle between the planes spanned by the beam direction and the momentum vector of e and μ, respectively. Acollinearity, $\theta_{\rm acol}$, is defined as the angle between the momentum vectors of e and μ.

[5] An isolated photon has an energy > 60 MeV and is separated from the nearest charged track by $> 12°$.

[6] É. A. Kuraev and V. S. Fadin, Yad. Fiz. **41**, 733 (1985) [Sov. J. Nucl. Phys. **41**, 466 (1985)].

[7] F. A. Berends and G. J. Komen, Phys. Lett. **63B**, 432 (1976).

[8] M. B. Voloshin, Report No. TPI-MINN-89-33-T, 1989 (unpublished).

[9] Δ was determined according to the equation $\Delta = (A\bar{I} + B)(CW^2 + D)$, where $\bar{I}$ is the average beam current. A, B, C, and D are fitted to beam current measurements and to measurements of the energy spreads at the J/ψ and $\psi(2S)$ resonances.

[10] It has been verified by simulation that this uncertainty corresponds to a 68% confidence interval.

[11] In the large statistics limit, $-2\ln\lambda$ would obey a χ^2 distribution for 10 degrees of freedom.

[12] Assuming a linear relation between measured energy W_M, and the corrected value W, the latter is given by $W = T_\psi + (W_M - M_\psi)[(T_{\psi'} - T_\psi)/(M_{\psi'} - M_\psi)]$ in the notation of Table II. At $\tau^+\tau^-$ threshold the resulting mass scale correction is $W - W_M = -0.74$ MeV, with corresponding uncertainty $\delta W = 0.18$ MeV.

[13] The ARGUS Collaboration has also reported [H. Albrecht *et al.*, Report No. DESY 92-086, 1992 (to be published)] a new measurement of the τ mass, $m_\tau = 1776.3 \pm 2.4 \pm 1.4$ MeV.

Direct Measurement of the Pseudoscalar Decay Constant, f_{D_s}

J. Z. Bai,[1] O. Bardon,[6] I. Blum,[11] A. Breakstone,[9] T. Burnett,[12] G. P. Chen,[1] H. F. Chen,[4] J. Chen,[5] S. J. Chen,[1] S. M. Chen,[1] Y. Chen,[1] Y. B. Chen,[1] Y. Q. Chen,[1] B. S. Cheng,[1] R. F. Cowan,[6] H. C. Cui,[1] X. Z. Cui,[1] H. L. Ding,[1] Z. Z. Du,[1] W. Dunwoodie,[8] X. L. Fan,[1] J. Fang,[1] M. Fero,[6] C. S. Gao,[1] M. L. Gao,[1] S. Q. Gao,[1] W. X. Gao,[1] P. Gratton,[11] J. H. Gu,[1] S. D. Gu,[1] W. X. Gu,[1] Y. F. Gu,[1] Y. N. Guo,[1] S. W. Han,[1] Y. Han,[1] F. A. Harris,[9] M. Hatanaka,[3] J. He,[1] K. R. He,[1] M. He,[7] D. G. Hitlin,[3] G. Y. Hu,[1] H. B. Hu,[1] T. Hu,[1] X. Q. Hu,[1] D. Q. Huang,[1] Y. Z. Huang,[1] J. M. Izen,[11] Q. P. Jia,[5] C. H. Jiang,[1] Y. Jin,[1] L. Jones,[3] S. H. Kang,[1] M. H. Kelsey,[3] B. K. Kim,[11] Y. F. Lai,[1] H. B. Lan,[1] P. F. Lang,[1] A. Lankford,[10] F. Li,[1] J. Li,[1] P. Q. Li,[1] Q. Li,[7] R. B. Li,[1] W. Li,[1] W. D. Li,[1] W. G. Li,[1] X. Li,[1] X. N. Li,[1] S. Z. Lin,[1] H. M. Liu,[1] J. H. Liu,[1] Q. Liu,[1] R. G. Liu,[1] Y. Liu,[1] Z. A. Liu,[1] X. C. Lou,[11] B. Lowery,[11] J. G. Lu,[1] A. M. Ma,[1] E. C. Ma,[1] J. M. Ma,[1] H. S. Mao,[1] Z. P. Mao,[1] R. Malchow,[5] M. Mandelkern,[10] X. C. Meng,[1] H. L. Ni,[1] J. Nie,[1] S. L. Olsen,[9] J. Oyang,[3] D. Paluselli,[9] L. J. Pan,[9] J. Panetta,[3] F. Porter,[3] E. Prabhakar,[3] N. D. Qi,[1] Y. K. Que,[1] J. Quigley,[6] G. Rong,[1] M. Schernau,[10] B. Schmid,[10] J. Schultz,[10] Y. Y. Shao,[1] D. L. Shen,[1] H. Shen,[1] X. Y. Shen,[1] H. Y. Sheng,[1] H. Z. Shi,[1] X. R. Shi,[3] A. Smith,[10] E. Soderstrom,[8] X. F. Song,[1] J. Standifird,[11] D. Stoker,[10] F. Sun,[1] H. S. Sun,[1] S. J. Sun,[1] J. Synodinos,[8] Y. P. Tan,[1] S. Q. Tang,[1] W. Toki,[5] G. L. Tong,[1] E. Torrence,[6] F. Wang,[1] L. S. Wang,[1] L. Z. Wang,[1] M. Wang,[1] P. Wang,[1] P. L. Wang,[1] S. M. Wang,[1] T. J. Wang,[1] W. Wang,[1] Y. Y. Wang,[1] S. Whittaker,[2] R. Wilson,[5] W. J. Wisniewski,[13,*] D. M. Xi,[1] X. M. Xia,[1] P. P. Xie,[1] D. Z. Xu,[1] R. S. Xu,[1] Z. Q. Xu,[1] S. T. Xue,[1] R. Yamamoto,[6] J. Yan,[1] W. G. Yan,[1] C. M. Yang,[1] C. Y. Yang,[1] W. Yang,[1] H. B. Yao,[1] M. H. Ye,[1] S. Z. Ye,[1] C. S. Yu,[1] C. X. Yu,[1] Z. Q. Yu,[1] C. Z. Yuan,[1] B. Y. Zhang,[1] C. C. Zhang,[1] D. H. Zhang,[1] H. L. Zhang,[1] J. Zhang,[1] J. W. Zhang,[1] L. S. Zhang,[1] S. Q. Zhang,[1] Y. Zhang,[1] Y. Y. Zhang,[1] D. X. Zhao,[1] J. W. Zhao,[1] M. Zhao,[1] P. D. Zhao,[1] W. R. Zhao,[1] W. X. Zhao,[1] J. P. Zheng,[1] L. S. Zheng,[1] Z. P. Zheng,[1] G. P. Zhou,[1] H. S. Zhou,[1] Li Zhou,[1] X. F. Zhou,[1] Y. H. Zhou,[1] Q. M. Zhu,[1] Y. C. Zhu,[1] Y. S. Zhu,[1] B. A. Zhuang,[1] and G. Zioulas[10]

(BES Collaboration)

[1]*Institute of High Energy Physics, Beijing 100039, People's Republic of China*
[2]*Boston University, Boston, Massachusetts 02215*
[3]*California Institute of Technology, Pasadena, California 91125*
[4]*China's University of Science and Technology, Hefei 230026, People's Republic of China*
[5]*Colorado State University, Fort Collins, Colorado 80523*
[6]*Massachusetts Institute of Technology, Cambridge, Massachusetts 02139*
[7]*Shandong University, Jinan 250100, People's Republic of China*
[8]*Stanford Linear Accelerator Center, Stanford, California 94309*
[9]*University of Hawaii, Honolulu, Hawaii 96822*
[10]*University of California at Irvine, Irvine, California 92717*
[11]*University of Texas at Dallas, Richardson, Texas 75083-0688*
[12]*University of Washington, Seattle, Washington 98195*
[13]*Superconducting Supercollider Laboratory, Dallas, Texas 75237-3946*

(Received 22 December 1994)

The Beijing Spectrometer (BES) experiment has observed purely leptonic decays of the D_s meson in the reaction $e^+e^- \to D_s^+ D_s^-$ at a c.m. energy of 4.03 GeV. Three events are observed in which one D_s decays hadronically to $\phi\pi$, $\overline{K}^{*0}K$, or $\overline{K}^0 K$, and the other decays leptonically to $\mu\nu_\mu$ or $\tau\nu_\tau$. With the assumption of μ-τ universality, values of the branching fraction, $B(D_s \to \mu\nu_\mu) = (1.5^{+1.3+0.3}_{-0.6-0.2})\%$, and the D_s pseudoscalar decay constant, $f_{D_s} = (4.3^{+1.5+0.4}_{-1.3-0.4}) \times 10^2$ MeV, are obtained.

PACS numbers: 13.20.Fc, 14.40.Lb

Purely leptonic decays of the D_s meson proceed via the annihilation of the charm and antistrange quarks to a virtual W boson. The rate of this process is determined by the quark wave function at the origin, and is characterized by the pseudoscalar decay constant, f_{D_s}. The leptonic decay width of the D_s can be written as [1]

$$\Gamma(D_s \longrightarrow \ell\nu_\ell) = \frac{G_F^2 |V_{cs}|^2}{8\pi} f_{D_s}^2 m_{D_s} m_\ell^2 \left(1 - \frac{m_\ell^2}{m_{D_s}^2}\right)^2, \quad (1)$$

where m_{D_s} is the D_s mass, m_ℓ is the lepton mass, $V_{cs} = 0.974$ is the $c \to s$ Cabibbo-Kobayashi-Maskawa (CKM) matrix element [2], and G_F is the Fermi constant.

Predictions for f_{D_s} and the Cabbibo-suppressed decay constant of the charged D meson, f_D, varying from 90 to 350 MeV, have been made using various theoretical models [3–7]. Many models can more reliably predict the ratios $f_{D_s} : f_D : f_B$, where f_B is the decay constant for the charged B meson [8]. Since f_B relates measured quantities, such as B^0-$\overline{B}^0$ mixing, to CKM matrix elements, its determination is of considerable importance. Measurements of the charm decay constants will help discriminate among the different models and improve the reliability of estimates of f_B. The first experimental measurement, $f_{D_s} = (2.32 \pm 0.45 \pm 0.20 \pm 0.48) \times 10^2$ MeV, was reported by the WA75 group [9], using muons from D_s leptonic decays seen in emulsions; the third error is due to uncertainty in the D_s production rate. The CLEO group [10] measured $f_{D_s} = (3.44 \pm 0.37 \pm 0.52 \pm 0.42) \times 10^2$ MeV using the decays $D_s^* \to \gamma D_s$, $D_s \to \mu\nu$; here the third error is due to uncertainty in the normalizing D_s branching fraction.

In this paper, direct, model-independent measurements of f_{D_s} and the D_s leptonic branching fraction are reported. The data were obtained using the BES detector at the Beijing e^+e^- Collider (BEPC), and correspond to an integrated luminosity of 22.3 pb^{-1} (obtained from large angle Bhabha scattering events) at c.m. energy 4.03 GeV. This is just above the $e^+e^- \to D_s^+ D_s^-$ threshold, but below that for $D_s^{*+} D_s^-$ [11]. Thus, if a D_s meson decay is fully reconstructed in a given event, the recoil system corresponds to the decay of the charge conjugate D_s meson. Events for which one D_s is fully reconstructed are termed singly tagged. For such a data sample, the detection of the decays $D_s \to \mu\nu_\mu$ or $\tau\nu_\tau$ among the recoil systems permits an absolute measurement of f_{D_s} and the leptonic branching fractions.

The BES is a conventional cylindrical detector, which is described in detail in Ref. [12]. A four-layer central drift chamber surrounding the beampipe provides trigger information. Charged tracks are reconstructed in a forty-layer main drift chamber (MDC) with a momentum resolution of $1.7\%\sqrt{1 + p^2}$ (p in GeV/c), and energy loss (dE/dx) resolutions of 8.5% for Bhabha electrons and 11% for hadrons. Scintillation counters provide time-of-flight (TOF) measurements, with resolutions of ~330 ps for Bhabha events and ~450 ps for hadrons. A 12-radiation-length, lead-gas barrel shower counter (BSC), operating in limited streamer mode, measures the energies of electrons and photons over ~80% of the total solid angle. A solenoidal magnet provides a 0.4 T magnetic field in the central tracking region of the detector. Three double-layer muon counters (MUC) instrument the magnet flux return, and serve to identify muons of momentum greater than 500 MeV/c. They cover ~68% of the total solid angle with longitudinal (transverse) spatial resolution of 5 cm (3 cm).

In this experiment, singly tagged D_s mesons are detected via hadronic decay to $\phi\pi$, $\overline{K}^{*0}K$, or $\overline{K}^0 K$, with $\phi \to K^+K^-$, $\overline{K}^{*0} \to K^-\pi^+$, and $\overline{K}^0 \to K_S^0 \to \pi^+\pi^-$. For a candidate three-charged-track combination, each track must be well reconstructed and consistent with an origin in the interaction region (candidate pions from K_S^0 decay need not satisfy the latter requirement). In addition, the dE/dx and TOF information associated with each track must be consistent with the assigned mass interpretation with a confidence level >0.1%. Finally, if the confidence level as a kaon is greater than that as a pion, the track is considered to be a kaon, and vice versa.

With the resulting mass assignments, the energy sum over the candidate tracks may be calculated; for particle-antiparticle production, this energy should be close to that of the beam. Requiring that the energy difference be <50 MeV selects such events without bias in mass, and effectively suppresses background from D^+ decay. In order to improve the invariant mass resolution, surviving candidates are subjected to a one-constraint (1-C) fit requiring overall event four-momentum balance and that the candidate and recoil systems have the same (but unspecified) invariant mass. Candidates yielding fit confidence levels >20% are retained, and the decay mode to $\phi\pi$, $\overline{K}^{*0}K$, or $\overline{K}^0 K$ defined by requiring that the invariant mass of the ϕ (K^+K^-), $\overline{K}^{*0}$ ($K^-\pi^+$), or $\overline{K}^0$ ($\pi^+\pi^-$) be within 25, 50, or 20 MeV, respectively, of nominal [2]. For the $\overline{K}^{*0}$ sample, significant background reduction is achieved by further requiring $|\cos\theta_K| > 0.4$, where θ_K is the helicity angle of the K^- in the $\overline{K}^{*0}$ rest frame. Similarly, background in the $\overline{K}^0$ sample is reduced by requiring that the $\overline{K}^0$ have a significant flight path whose direction is consistent (within 26°) with the $\overline{K}^0$ momentum vector.

The resulting distributions in invariant mass, calculated using the momentum vectors from the 1-C fit, are shown in Fig. 1; each exhibits a clear signal at the D_s mass position. An unbinned maximum likelihood fit [13] to the combined distribution of Fig. 1(d) yields a singly tagged D_s meson signal of 94.3 ± 12.5 events, and a D_s mass value 1968.7 ± 0.6(stat) ± 0.5(syst) MeV.

The search for D_s leptonic decay candidates among the systems recoiling against singly tagged D_s candidates includes all of the events of Fig. 1(d), not only those in the D_s signal region. For this sample, the recoil system is required to contain a single, vertex-associated charged track of charge opposite that of the tagging system. Events containing at least one isolated photon [14] are removed, and for the remaining events the recoil charged track is subjected to the following lepton identification criteria.

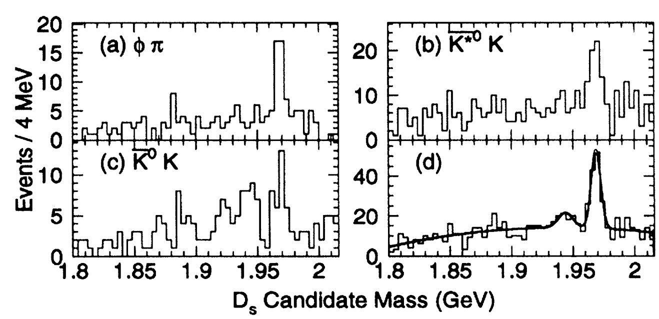

FIG. 1. The invariant mass distributions, calculated using 1-C fit momentum vectors, for (a) $\phi\pi$, (b) $\overline{K}^{*0}K$, and (c) $\overline{K}^0 K$ D_s decay candidates; the combined distribution is shown in (d), where the curve corresponds to the fit described in the text.

An electron candidate is required to have momentum ≥ 400 MeV/c and direction $|\cos\theta| \leq 0.75$, with TOF and dE/dx measurements consistent with the electron hypothesis. The TOF-measured velocity of the track must be $> 0.7c$, and the measured dE/dx should be within 4σ of the expected value for an electron. The energy deposition in the BSC must be consistent with that expected for an electron in both magnitude and distribution in depth. Applying these criteria to radiative Bhabha scattering events leads to an identification efficiency of more than 80% over the full momentum range, and $\sim 90\%$ for electrons with momenta above 1 GeV/c. Known pions are misidentified as electrons at a rate of $\sim 5\%$, with a modest momentum dependence.

A muon candidate is required to have momentum between 550 and 1250 MeV/c and direction $|\cos\theta| < 0.65$, with TOF and dE/dx information consistent with the muon interpretation. There must be hits in the MUC detector which are well associated with the track in transverse projection; the required number of hits is momentum dependent. For a sample of cosmic rays, the identification efficiency is $\sim 85\%$, while for a sample of well-identified pions the average misidentification rate is $\sim 4\%$.

Events satisfying the above selection criteria are subjected to a visual scan. This serves to remove events containing cosmic rays as well as those having unreconstructed low-angle track(s), which are typically recognized by a pattern of hits in the CDC and the innermost two layers of the MDC.

The distributions of tagging D_s mass for the events of Fig. 1(d) which have an identified single electron or muon candidate are shown in Figs. 2(a) and 2(b), respectively. The characteristics of these events are summarized in Table I; in each case the D_s and subsystem masses agree well with the expected values.

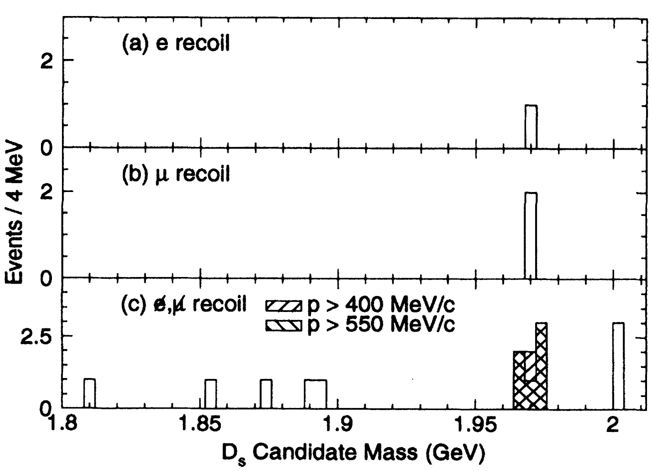

FIG. 2. The distribution of Fig. 1(d) requiring that the recoil system consist of a single charged track identified as (a) an electron; (b) a muon; (c) neither an electron nor a muon. Shading in (c) indicates signal region events which satisfy the lepton kinematic requirements described in the text.

TABLE I. Three candidates for D_s leptonic decay.

Event	1	2	3
Tagging D_s decay	$\phi\pi^+$	$\overline{K}^{*0}K^+$	$\overline{K}^0K^+$
Subsystem mass (MeV)	1019.3	873.4	491.5
D_s mass (MeV)	1970.2	1970.9	1969.0
Recoil lepton	μ^-	μ^-	e^-
$p_{\rm lepton}$ (MeV/c)	751	1216	489
$M^2_{\rm miss}$ (GeV^2)	0.778	-0.115	1.627
D_s leptonic decay	$\tau\nu(\mu 3\nu)$	$\mu\nu$	$\tau\nu(e3\nu)$

From Monte Carlo simulations, it is found that the detection efficiencies for the tagging and leptonic D_s decays are independent, to a good approximation. The expected number of $D_s^+D_s^-$ events for which one D_s is from the signal region of Fig. 1(d) and the other corresponds to a particular leptonic decay mode is then obtained as the product of the singly tagged signal, the D_s branching fraction to the mode in question, and the detection efficiency for that mode. The latter efficiency is found to be 51% for the decay $D_s \to \mu\nu_\mu$, 6.3% for $D_s \to \tau\nu_\tau$, $\tau \to \mu\nu\nu$, and 8.2% for $D_s \to \tau\nu_\tau$, $\tau \to e\nu\nu$, including the τ branching fractions [2]. Since the D_s decay rate to $e\nu_e$ is negligible, leptonic events with an electron recoil result only from the τ decay sequence.

A Monte Carlo study shows that background contributions to the leptonic decay samples result mainly from hadron misidentification in the processes $D_s \to K_L^0 K$ and $D_s \to \tau\nu_\tau$ with $\tau \to \pi\nu_\tau$. In the present analysis, this contribution is estimated from the singly tagged events in the D_s signal region of Fig. 1(d) which have a single recoil track satisfying neither the electron nor the muon identification criteria. The tagging mass distribution for these events is shown in Fig. 2(c); seven events in the D_s signal region satisfy the momentum and polar angle criteria for electrons, while only six satisfy those for muons. The misidentification rates discussed previously yield background estimates of 0.35 events for the electron sample and 0.24 for the muon sample (of which 0.04 contribute to $D_s \to \mu\nu_\mu$).

The values of the D_s leptonic branching fractions are estimated by maximizing a likelihood function containing a Poisson distribution factor for the expected number of events (including background), and a factor for the expected missing-mass-squared distribution for each channel (the distributions for $D_s \to \mu\nu_\mu$ vs $D_s \to \tau\nu_\tau$, $\tau \to \mu\nu\nu$ are well separated). Maximizing the likelihood function for the branching fractions to $\mu\nu_\mu$ and $\tau\nu_\tau$ independently, the values $B(D_s \to \mu\nu_\mu) = (2.0^{+4.4}_{-1.7})\%$ and $B(D_s \to \tau\nu_\tau) = (12^{+20}_{-10})\%$ are obtained. Assuming μ-τ universality and the theoretical prediction of the ratio $B(\tau\nu_\tau)/B(\mu\nu_\mu) = 9.74$, the result is $B(D_s \to \mu\nu_\mu) = [1.5^{+1.3}_{-0.6}(\text{stat})^{+0.3}_{-0.2}(\text{syst})]\%$ and $B(D_s \to \tau\nu_\tau) = [15^{+13}_{-6}(\text{stat})^{+3}_{-2}(\text{syst})]\%$.

If in addition, the relation

$$B(D_s \longrightarrow \ell\nu_\ell) = \frac{\tau_{D_s}}{\hbar}\,\Gamma(D_s \longrightarrow \ell\nu_\ell)$$

is used with Eq. (1), the likelihood function may be maximized with respect to f_{D_s} directly, as shown in Fig. 3. The result is

$$f_{D_s} = (4.3^{+1.5+0.4}_{-1.3-0.4}) \times 10^2 \text{ MeV}.$$

The first errors are statistical, and correspond to the 68.3% confidence interval shown in Fig. 3; the second errors are systematic, and result from uncertainties in lepton mode detection efficiencies, background estimates, and the D_s lifetime [2].

Although the branching fraction and f_{D_s} values obtained in the present analysis have sizable uncertainties, it should be emphasized that the results are independent of luminosity and $D_s^+ D_s^-$ cross section, and do not require model-dependent assumptions. The central value of f_{D_s} is larger than, but consistent with, current theoretical predictions, which range from 90 to 350 MeV.

We would like to thank the staffs of the BEPC accelerator, the Computing Center at the Institute of High Energy Physics (Beijing), and the Texas High Performance Computing Center. We thank Professor Chaohsi Chang for useful discussions of D_s physics.

Work supported in part by the National Natural Science Foundation of China under Contract No. 19290400 and the Chinese Academy of Sciences under Contract No. KJ85 (IHEP); by the Department of Energy under Contract No. DE-FG02-91ER40676 (Boston University), No. DE-FG03-92ER40701 (Caltech), No. DE-FG03-93ER40788 (Colorado State University), No. DE-AC02-76ER03069 (MIT), No. DE-AC03-76SF00515 (SLAC), No. DE-FG03-91ER40679 (UC Irvine), No. DE-FG03-94ER40833 (U Hawaii), No. DE-FG05-92ER40736 (UT Dallas), and No. DE-AC35-89ER40486 (SSC Lab); by the U.S. National Science Foundation, Grant No. PHY9203212 (University of Washington); and by the Texas National Research Laboratory Commission under Contract No. RGFY91B5, No. RGFY92B5 (Colorado State), and No. RCFY93-316H (UT Dallas).

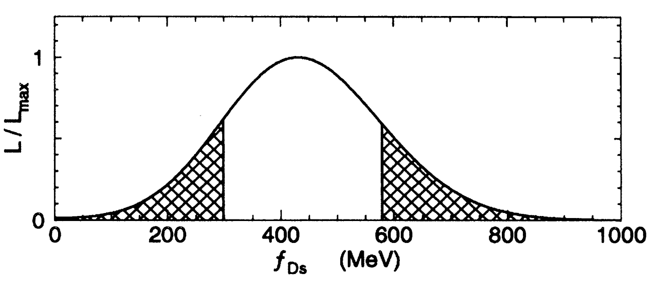

FIG. 3. The variation of the normalized likelihood function with respect to f_{D_s}, under the assumption of μ-τ universality; the unshaded area under the curve denotes the 68.3% confidence interval.

*Present address: Stanford Linear Accelerator Center, Stanford, California 94309.

[1] See, for example, J.L. Rosner, Phys. Rev. D **42**, 3732 (1990); C.H. Chang and Y.Q. Chen, *ibid.* **46**, 3845 (1992); **49**, 3399 (1994).
[2] Particle Data Group, L. Montanet *et al.*, Phys. Rev. D **50**, 1173 (1994).
[3] T.A. DeGrand and R.D. Loft, Phys. Rev. D **38**, 954 (1988); D.S. Du, *ibid.* **34**, 3428 (1986).C. Bernard *et al.*, Phys. Rev. D **38**, 3540 (1988); M.B. Gavela *et al.*, Phys. Lett. B **206**, 113 (1988);
[4] J.G. Bian and T. Huang, Modern Phys. Lett. **8**, 635 (1993); C. Dominguez and N. Paver, Phys. Lett. B **197**, 423 (1987); S. Narison, Phys. Lett. B **198**, 104 (1987); M.A. Shifman, Ups. Fix. Nauk **151**, 193 (1987).
[5] H. Krasemann, Phys. Lett. **96B**, 397 (1980); M. Suzuki, *ibid.* **162B**, 391 (1985); S.N. Sinha, Phys. Lett. B **178**, 110 (1986); P. Cea *et al.*, *ibid.* **206**, 691 (1988); P. Colangelo, G. Nardulli, and M. Pietroni, Phys. Rev. D **43**, 3002 (1991).
[6] D. Bortoletto and S. Stone, Phys. Rev. Lett. **65**, 2951 (1990); J.L. Rosner, Phys. Rev. D **42**, 3732 (1990).
[7] S. Capstick and S. Godfrey, Phys. Rev. D **41**, 2856 (1988).E.V. Shuryak, Nucl. Phys. **B198**, 83 (1982); R.R. Mendel and H.D. Trottier, Phys. Lett. B **231**, 312 (1989);
[8] I. Claudio *et al.*, Phys. Rev. D **41**, 1522 (1990);M. Witherell, "Charm Weak Decay," in Proceedings of the XVI International Symposium on Photon-Lepton Physics, Cornell University, Ithaca, New York, August 1993; F.J. Gilman and M.B. Wise, *ibid.* **27**, 1128 (1983).
[9] S. Aoki *et al.*, Prog. Theor. Phys. **89**, 131 (1993).
[10] D. Acosta *et al.*, Phys. Rev. D **49**, 5690 (1993).
[11] Throughout the paper, reference to a particular charge configuration implies reference to the charge conjugate configuration as well.
[12] J.Z. Bai *et al.*, Nucl. Instrum. Methods Phys. Res., Sect. A **344**, 319 (1994); J.Z. Bai *et al.*, Phys. Rev. Lett. **69**, 3021 (1992).
[13] The D_s signal is represented by a Gaussian distribution, and the background by a polynomial. Additional background in the $\overline{K}^0 K$ mode resulting from $D^* D$ events is represented by a second Gaussian at ~1940 MeV.
[14] An isolated photon is defined as an e.m. shower of energy >60 MeV and separated by at least 18° from the direction of the nearest charged track.

$\psi(2S)$ Hadronic Decays to Vector-Tensor Final States

J. Z. Bai,[1] J. G. Bian,[1] I. Blum,[11] Z. W. Chai,[1] G. P. Chen,[1] H. F. Chen,[10] J. Chen,[3] J. C. Chen,[1] Y. Chen,[1] Y. B. Chen,[1] Y. Q. Chen,[1] B. S. Cheng,[1] X. Z. Cui,[1] H. L. Ding,[1] L. Y. Ding,[1] L. Y. Dong,[1] Z. Z. Du,[1] W. Dunwoodie,[7] S. Feng,[1] C. S. Gao,[1] M. L. Gao,[1] S. Q. Gao,[1] P. Gratton,[11] J. H. Gu,[1] S. D. Gu,[1] W. X. Gu,[1] Y. F. Gu,[1] Y. N. Guo,[1] S. W. Han,[1] Y. Han,[1] F. A. Harris,[8] J. He,[1] J. T. He,[1] M. He,[5] D. G. Hitlin,[2] G. Y. Hu,[1] H. M. Hu,[1] J. L. Hu,[1] Q. H. Hu,[1] T. Hu,[1] X. Q. Hu,[1] J. D. Huang,[1] Y. Z. Huang,[1] J. M. Izen,[11] C. H. Jiang,[1] Y. Jin,[1] Z. J. Ke,[1] M. H. Kelsey,[2] B. K. Kim,[11] D. Kong,[8] Y. F. Lai,[1] P. F. Lang,[1] A. Lankford,[9] C. G. Li,[1] D. Li,[1] H. B. Li,[1] J. Li,[1] P. Q. Li,[1] R. B. Li,[1] W. Li,[1] W. D. Li,[1] W. G. Li,[1] X. H. Li,[1] X. N. Li,[1] H. M. Liu,[1] J. Liu,[1] J. H. Liu,[1] R. G. Liu,[1] Y. Liu,[1] X. C. Lou,[11] B. Lowery,[11] F. Lu,[1] J. G. Lu,[1] J. Y. Lu,[1] L. C. Lu,[1] C. H. Luo,[1] A. M. Ma,[1] E. C. Ma,[1] J. M. Ma,[1] R. Malchow,[3] H. S. Mao,[1] Z. P. Mao,[1] X. C. Meng,[1] J. Nie,[1] S. L. Olsen,[8] J. Oyang,[2] D. Paluselli,[8] L. J. Pan,[8] J. Panetta,[2] F. Porter,[2] N. D. Qi,[1] X. R. Qi,[1] C. D. Qian,[6] J. F. Qiu,[1] Y. H. Qu,[1] Y. K. Que,[1] G. Rong,[1] M. Schernau,[9] Y. Y. Shao,[1] B. W. Shen,[1] D. L. Shen,[1] H. Shen,[1] X. Y. Shen,[1] H. Y. Sheng,[1] H. Z. Shi,[1] X. F. Song,[1] J. Standifird,[11] F. Sun,[1] H. S. Sun,[1] S. Q. Tang,[1] W. Toki,[3] G. L. Tong,[1] F. Wang,[1] L. S. Wang,[1] L. Z. Wang,[1] M. Wang,[1] Meng Wang,[1] P. Wang,[1] P. L. Wang,[1] S. M. Wang,[1] T. J. Wang,[1,*] Y. Y. Wang,[1] M. Weaver,[2] C. L. Wei,[1] Y. G. Wu,[1] D. M. Xi,[1] X. M. Xia,[1] P. P. Xie,[1] Y. Xie,[1] Y. H. Xie,[1] W. J. Xiong,[1] C. C. Xu,[1] G. F. Xu,[1] S. T. Xue,[1] J. Yan,[1] W. G. Yan,[1] C. M. Yang,[1] C. Y. Yang,[1] J. Yang,[1] W. Yang,[3] X. F. Yang,[1] M. H. Ye,[1] S. W. Ye,[10] Y. X. Ye,[10] K. Yi,[1] C. S. Yu,[1] C. X. Yu,[1] Y. H. Yu,[4] Z. Q. Yu,[1] Z. T. Yu,[1] C. Z. Yuan,[1] Y. Yuan,[1] B. Y. Zhang,[1] C. C. Zhang,[1] D. H. Zhang,[1] Dehong Zhang,[1] H. L. Zhang,[1] J. Zhang,[1] J. L. Zhang,[1] J. W. Zhang,[1] L. S. Zhang,[1] Q. J. Zhang,[1] S. Q. Zhang,[1] X. Y. Zhang,[5] Y. Zhang,[1] Y. Y. Zhang,[1] D. X. Zhao,[1] H. W. Zhao,[1] J. W. Zhao,[1] M. Zhao,[1] W. R. Zhao,[1] Z. G. Zhao,[1] J. P. Zheng,[1] L. S. Zheng,[1] Z. P. Zheng,[1] G. P. Zhou,[1] H. S. Zhou,[1] L. Zhou,[1] Q. M. Zhu,[1] Y. C. Zhu,[1] Y. S. Zhu,[1] and B. A. Zhuang[1]

(BES Collaboration)

[1]*Institute of High Energy Physics, Beijing 100039, People's Republic of China*
[2]*California Institute of Technology, Pasadena, California 91125*
[3]*Colorado State University, Fort Collins, Colorado 80523*
[4]*Hangzhou University, Hangzhou 310028, People's Republic of China*
[5]*Shandong University, Jinan 250100, People's Republic of China*
[6]*Shanghai Jiaotong University, Shanghai 200030, People's Republic of China*
[7]*Stanford Linear Accelerator Center, Stanford, California 94309*
[8]*University of Hawaii, Honolulu, Hawaii 96822*
[9]*University of California at Irvine, Irvine, California 92717*
[10]*University of Science and Technology of China, Hefei 230026, People's Republic of China*
[11]*University of Texas at Dallas, Richardson, Texas 75083-0688*
(Received 19 August 1998)

The decays of the $\psi(2S)$ into vector plus tensor meson final states have been studied for the first time using the BES detector. We determine upper limits on branching fractions for $\psi(2S)$ decays into ωf_2, ρa_2, $K^{*0}\overline{K}_2^{*0}$ + c.c., and $\phi f_2'(1525)$ that are, in each case, significantly smaller than the corresponding branching fractions for the J/ψ meson, scaled according to the expectations of perturbative QCD. [S0031-9007(98)07836-3]

PACS numbers: 13.25.Gv, 12.38.Qk

One of the most dramatic problems confronting the understanding of hadronic charmonium decays is the strong suppression of $\psi(2S) \to \rho\pi$ and $K^*\overline{K}$ + c.c. decays. In perturbative QCD, the most important lowest-order diagram for J/ψ and $\psi(2S)$ decays to hadrons corresponds to the annihilation of the constituent c and $\bar{c}$ quarks into three gluons. In this case, the partial width for the decay is proportional to $|\Psi(0)|^2$, where $\Psi(0)$ is the wave function at the origin in the nonrelativistic quark model for $c\bar{c}$. Thus, it is reasonable to expect that, for any final hadronic state h, the J/ψ and $\psi(2S)$ decay branching ratios will scale as [1]

$$Q_h \equiv \frac{B(\psi(2S) \to h)}{B(J/\psi \to h)} \cong \frac{B(\psi(2S) \to e^+e^-)}{B(J/\psi \to e^+e^-)}, \\ = (14.6 \pm 2.2)\%, \tag{1}$$

where the leptonic branching fractions are taken from the Particle Data Group (PDG) tables [2]. It was first observed by the Mark II experiment [3] that, while this is true for a number of exclusive hadronic decay channels, it is badly violated for the vector plus pseudoscalar-meson (VP) final states, $\rho\pi$ and $K^*\overline{K}$. The preliminary BES results confirm the Mark II measurements at higher sensitivity. The present experimental limits on $Q_{\rho\pi}$ and

 0031-9007/98/81(23)/5080(5)$15.00

$Q_{K^*\overline{K}}$ indicate order-of-magnitude discrepancies with the expected ratio of branching fractions [2,4]. This anomaly, called the $\rho\pi$ puzzle, has generated considerable interest, and a number of theoretical explanations have been proposed [1]. However, meager experimental progress has hindered the resolution of the puzzle. Until recently, no other examples of substantial differences between J/ψ and $\psi(2S)$ hadronic decays have been documented.

In this Letter, we report the results of a study of $\psi(2S)$ decays into vector plus tensor meson (VT) final states and present branching fraction limits for $\psi(2S) \to \omega f_2$, ρa_2, $K^{*0}\overline{K}_2^{*0}$ + c.c., and $\phi f_2'(1525)$. The data were taken with the BES detector at the BEPC e^+e^- storage ring and correspond to a total sample of $(3.79 \pm 0.31) \times 10^6$ produced $\psi(2S)$ events. The BES detector is described in detail elsewhere [5]. A 40-layer main drift chamber in a 0.4 T magnetic field provides tracking and energy-loss (dE/dx) information. The momentum resolution is $\sigma_p/p = 1.7\%\sqrt{1 + p^2(\mathrm{GeV}/c)}$, and the dE/dx resolution for hadron tracks for this data sample is about 9%. The tracking chamber is surrounded by an array of 48 time-of-flight (TOF) counters with a resolution of about 450 ps for hadrons. Radially outside of the TOF are an electromagnetic calorimeter with a resolution of $\sigma_E/E = 0.22/\sqrt{E(\mathrm{GeV})}$, $\sigma_\phi = 4.5$ mrad, and $\sigma_\theta = 12$ mrad, and an array of μ counters that are interspersed inside the steel plates that return the solenoid's magnetic flux.

For the $\psi(2S) \to \omega f_2$ and ρa_2 decay channels, we use the reaction $\psi(2S) \to \pi^+\pi^-\pi^+\pi^-\pi^0$; for the $\psi(2S) \to K^{*0}\overline{K}_2^{*0}$ + c.c. and $\phi f_2'$ decays, we use $\pi^+\pi^-K^+K^-$ and $K^+K^-K^+K^-$ final states, respectively. Each analysis requires events to have four charged tracks with total charge zero and, in the case of the $\pi^+\pi^-\pi^+\pi^-\pi^0$ final state, at least two photons. Tracks consistent with being electrons in the electromagnetic calorimeter or being muons in the muon detector are discarded. The dE/dx and TOF measurements are used to select π or K tracks with a confidence level larger than 0.003 for each track and 0.01 for four tracks combined. Events are kinematically fit to four energy-momentum constraints, and those with a fit probability greater than 0.01 are accepted. Photon pairs that have a $\gamma\gamma$ invariant mass within 2.5σ ($\sigma = 14$ MeV) of the π^0 mass are assigned as candidate π^0s. The detection efficiency is determined using 1×10^4 or 2×10^4 Monte Carlo (MC)-simulated events that are generated with a uniform phase space distribution. The π or K decays in the detector according to the PDG [2] lifetimes and branching fractions. The relative uncertainty of efficiency obtained in this way is estimated to be 20%. Efficiencies given in this paper refer to the specific VT final states.

In the $\pi^+\pi^-\pi^+\pi^-\pi^0$ sample, the major background contributions are from $\psi(2S) \to \pi^+\pi^-J/\psi$ followed by $J/\psi \to \pi^+\pi^-\pi^0$ and from $\psi(2S) \to \eta J/\psi$, where $\eta \to \pi^+\pi^-\pi^0$ and the J/ψ decays to leptons. The former is rejected by removing events where any $\pi^+\pi^-\pi^0$ combination has an invariant mass within 50 MeV of the J/ψ mass. The latter is removed by eliminating events where any $\pi^+\pi^-$ pair has an invariant mass greater than 2.9 GeV/c^2. There are 939 events selected as $\psi(2S) \to \pi^+\pi^-\pi^+\pi^-\pi^0$ candidate events. The $\pi^+\pi^-\pi^0$ mass spectrum of the selected events, shown in Fig. 1, has a clear ω signal with a mass resolution $\sigma = 13.4$ MeV. Candidate ω mesons are required to have a $\pi^+\pi^-\pi^0$ combination with an invariant mass in the range $740 < m_{\pi^+\pi^-\pi^0} < 820$ MeV. Figure 2 shows the invariant mass spectrum for $\pi^+\pi^-$ pairs recoiling against candidate ω mesons. There is no obvious signal in the region of the $f_2(1270)$. A fit to the spectrum using a Breit-Wigner function with mass and width fixed at the PDG values ($m = 1275$ MeV, $\Gamma = 185$ MeV) and convoluted with a Gaussian resolution function with $\sigma = 12.3$ MeV, together with a quadratic background shape, yields 8.8 ± 9.2 ωf_2 events, which imply a 90% confidence level upper limit of 23.8 events. Using the isospin ratio 2:1 for f_2 decays into $\pi^+\pi^-$ to $\pi^0\pi^0$ and the experimental efficiency of 0.074, we determine an upper limit on the branching fraction of

$$B(\psi(2S) \to \omega f_2) < 1.7 \times 10^{-4} \qquad (\mathrm{C.L.} = 90\%).$$

We use the $\psi(2S) \to \pi^+\pi^-\pi^+\pi^-\pi^0$ sample with the events that are consistent with $\omega\pi^+\pi^-$ removed to search for $\psi(2S) \to \rho a_2 \to \rho\rho\pi$. Here we select the $\pi^+\pi^-$ and $\pi^0\pi^\pm$ combination that has the minimum value of the quantity [6]

$$\sqrt{(m_{\pi^+\pi^-} - m_{\rho^0})^2 + (m_{\pi^0\pi^\pm} - m_{\rho^\pm})^2}$$

and require this minimum value to be less than 200 MeV. The combined $\rho^0\pi^\pm$ and $\rho^\pm\pi^\mp$ invariant mass plot, shown in Fig. 3, has no indication of an $a_2(1320)$ meson signal. A fit to this spectrum with the a_2 represented by a resolution-broadened Breit-Wigner line shape with mass and width fixed at PDG values ($m = 1318.1$ MeV, $\Gamma = 107$ MeV) and a quadratic background function gives 3.9 ± 15.7 a_2 events, which correspond to less than 29.6 events at the 90% confidence level. Using isospin

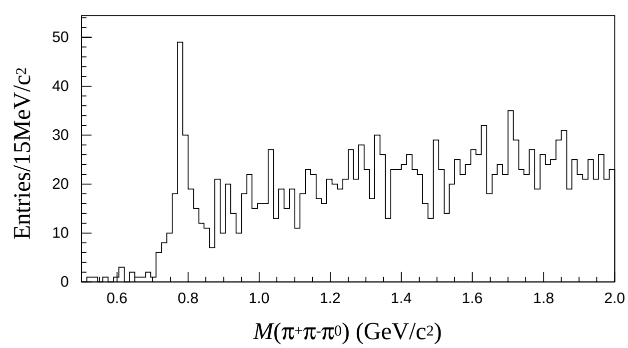

FIG. 1. The $\pi^+\pi^-\pi^0$ invariant mass distribution for $\psi(2S) \to \pi^+\pi^-\pi^+\pi^-\pi^0$ events (four entries/event).

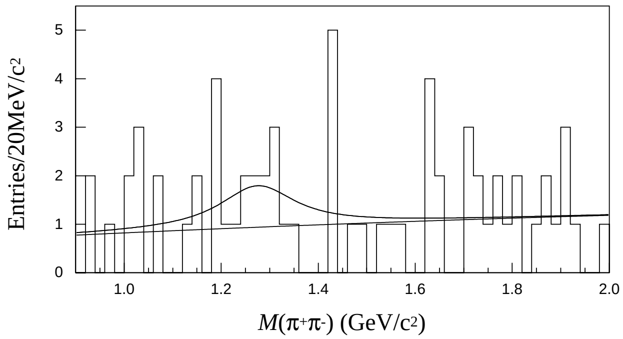

FIG. 2. The invariant mass distribution of $\pi^+\pi^-$ pairs recoiling against candidate ω mesons for events of the type $\psi(2S) \to \omega\pi^+\pi^-$. The curve shows a fit to quadratic background plus a f_2 resonance (see text).

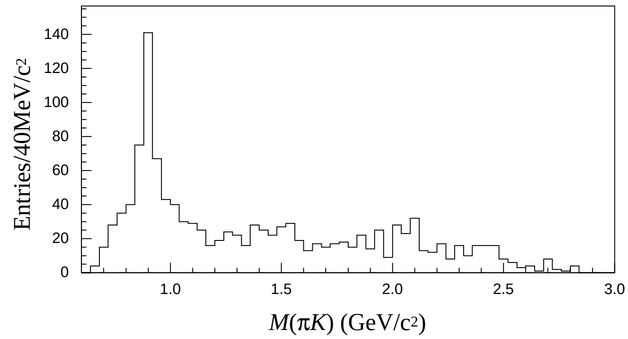

FIG. 4. The $\pi^\pm K^\mp$ invariant mass distribution for $\psi(2S) \to \pi^+\pi^-K^+K^-$ events (four entries/event).

invariance to correct for the unseen $a_2 \to \rho\pi$ decay channels and the MC-determined experimental efficiency of 0.074, we determine

$$B(\psi(2S) \to \rho a_2) < 2.3 \times 10^{-4} \qquad (\text{C.L.} = 90\%).$$

In the selection of $\pi^+\pi^-K^+K^-$ final states, each event has four possible π^+, π^-, K^+, and K^- track assignments. For each assignment that satisfies the four-constraint kinematic fit with a probability greater than 0.01, the TOF and dE/dx measurements and the kinematic fit quality are combined to determine a global χ^2. The track assignment with the smallest global χ^2 is selected as a candidate $\pi^+\pi^-K^+K^-$ event. The main background which remains from $\psi(2S) \to \pi^+\pi^-J/\psi$ is eliminated by requiring the mass recoiling against the $\pi^+\pi^-$ to differ from $m_{J/\psi}$ by more than 50 MeV. There are 614 events after the above selections. Those $K^\pm\pi^\mp$ pairs with an invariant mass in the range $800 < m_{K^\pm\pi^\mp} < 1000$ MeV are considered to be K^{*0} candidates. The contamination from $\psi(2S) \to \phi\pi^+\pi^-$ with $\phi \to K^+K^-$ is found to be negligible. The $K^\pm\pi^\mp$ mass spectrum, shown in Fig. 4, has a pronounced peak at the mass of the K^{*0}. The invariant mass distribution of $K^\pm\pi^\mp$ tracks recoiling against the K^{*0} candidates, shown in Fig. 5, is fit with two Breit-Wigner functions with masses and widths fixed at the PDG values for the K^{*0} ($m = 896.1$ MeV, $\Gamma = 50.5$ MeV) and K_2^{*0} ($m = 1432.4$ MeV, $\Gamma = 109$ MeV), together with a quadratic background. The MC-determined experimental mass resolutions are 4.9 MeV for the K^{*0} and 6.7 MeV for the K_2^{*0}. The fit yields 1.4 ± 8.6 $K^{*0}K_2^{*0}$ events, which imply a 90% confidence level upper limit of 17.2 events. Using the isospin ratio $K^\pm\pi^\mp{:}K^0\pi^0 = 2{:}1$ for both the K^{*0} and K_2^{*0} decays and the MC-determined efficiency of 0.171, we determine the limit

$$B(\psi(2S) \to K^{*0}\overline{K}_2^{*0} + \text{c.c.}) < 1.2 \times 10^{-4} \quad (\text{C.L.} = 90\%).$$

In the selection of $K^+K^-K^+K^-$ final states, the TOF and dE/dx measurements are used to select kaon tracks. Events are kinematically fit to four energy-momentum constraints, and those with a fit probability greater than 0.01 are accepted. Backgrounds from other $\psi(2S)$ decays are negligible. Figure 6 shows the K^+K^- mass spectrum for the 41 selected $K^+K^-K^+K^-$ candidate events; there is a strong $\phi(1020)$ signal. Here the experimental mass resolution is $\sigma = 4.1$ MeV. We identify all K^+K^-

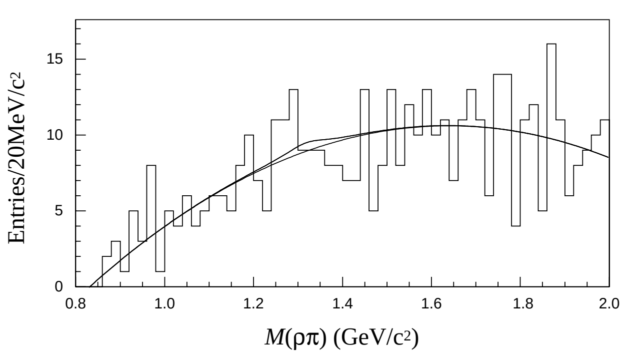

FIG. 3. The $\rho\pi$ invariant mass distribution for events of the type $\psi(2S) \to \rho^0\rho^\mp\pi^\pm$. The curve shows a fit to quadratic background plus an a_2 resonance (see text).

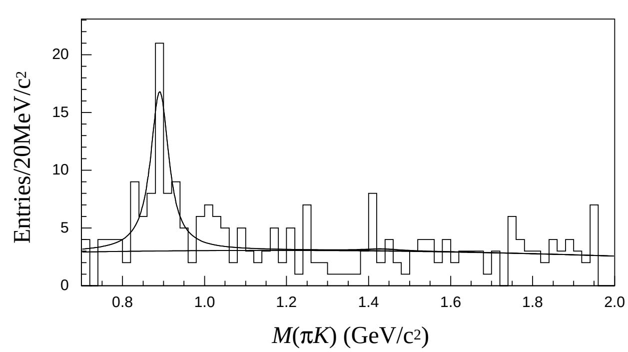

FIG. 5. The invariant mass distribution for $\pi^\pm K^\mp$ tracks recoiling against a K^{*0} for $\psi(2S) \to \pi^+\pi^-K^+K^-$ events. The curve shows a fit to quadratic background plus K^{*0} and K_2^{*0} resonances (see text).

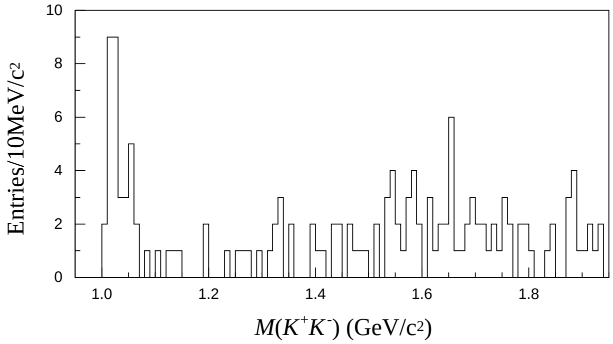

FIG. 6. The K^+K^- invariant mass distribution for $\psi(2S) \to K^+K^-K^+K^-$ events (four entries/event).

pairs with $m_{K^+K^-} < 1040$ MeV as candidate ϕ mesons. Figure 7 shows the invariant mass distribution for the K^+K^- pairs that are recoiling against candidate ϕ mesons. No evidence for an enhancement at the mass of the f_2' resonance is apparent. There are three events in the Fig. 7 distribution within ± 80 MeV of the f_2' mass ($m = 1525$ MeV, $\Gamma = 76$ MeV). The 90% confidence level upper limit on this number of events is 6.68. Using the MC-determined efficiency of 0.181, we determine an upper limit for the branching fraction of

$$B(\psi(2S) \to \phi f_2'(1525)) < 4.5 \times 10^{-5} \quad (\text{C.L.} = 90\%).$$

Table I summarizes the results of branching fraction measurements for the $\psi(2S) \to VT$ decay modes reported here. For comparison, the table includes the data for the corresponding J/ψ decays [7] as well as the ratios of the $\psi(2S)$ to J/ψ branching fractions. All four $\psi(2S) \to VT$ decay modes are suppressed by a factor of at least 3 compared to the expectations of Eq. (1). An even higher statistics study would be required to determine whether or not the suppression of the VT decays is as severe as that of the $\rho\pi$ and $K^*\overline{K}$ decay channels. It is noted that, in a perturbative QCD quark scheme, VP decays are forbidden by hadron helicity conservation (HHC) [8], whereas VT decays are HHC allowed [9].

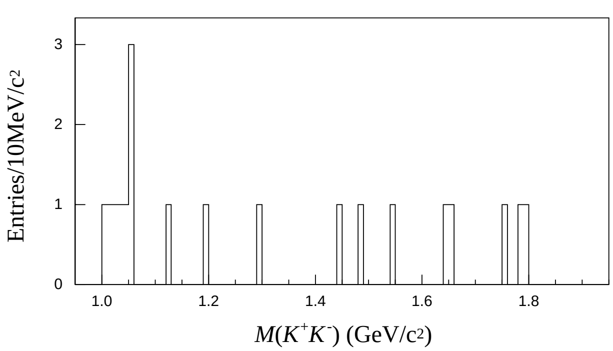

FIG. 7. The invariant mass distribution of K^+K^- pairs recoiling against candidate ϕ mesons for $\psi(2S) \to K^+K^-K^+K^-$ events. Three events fall into 80 MeV$/c^2$ region around the f_2' mass.

TABLE I. Branching fractions measured for $\psi(2S) \to$ vector plus tensor meson final states. Results for the corresponding J/ψ branching fractions [7] are also given as well as the ratios $Q_h \equiv B(\psi(2S))/B(J/\psi)$. All limits are at the 90% confidence level.

Final state	$B(\psi(2S))$ $(\times 10^{-4})$	$B(J/\psi)$ $(\times 10^{-3})$	Q_h
ωf_2	<1.7	4.3 ± 0.6	<0.040
ρa_2	<2.3	10.9 ± 2.2	<0.021
$K^{*0}\overline{K}_2^{*0}$	<1.2	6.7 ± 2.6	<0.018
$\phi f_2'$	<0.45	$1.23 \pm 0.06 \pm 0.20$	<0.037

In conclusion, we have presented first measurements of $\psi(2S)$ decays to ωf_2, ρa_2, $K^{*0}\overline{K}_2^{*0}$, and $\phi f_2'(1525)$. The upper limits established for the branching fractions for each of these decay modes are well below the level obtained by scaling the corresponding J/ψ branching fraction according to expectations based on perturbative QCD. The puzzle of the hadronic decays of the J/ψ and $\psi(2S)$ extends from the VP decay to the VT decays.

We gratefully acknowledge the efforts of the staffs of the BEPC accelerator and the computing center at the Institute of High Energy Physics (Beijing). The authors also thank G. D. Zhao, S. J. Brodsky, and S. F. Tuan for enlightening discussions. This work was supported in part by the National Natural Science Foundation of China under Contract No. 19290400; the Chinese Academy of Sciences under Contract No. KJ85 (IHEP); and by the Department of Energy under Contracts No. DE-FG03-92ER40701 (Caltech), No. DE-FG03-93ER40788 (Colorado State University), No. DE-AC03-76SF00515 (SLAC), No. DE-FG03-91ER40679 (UC Irvine), No. DE-FG03-94ER40833 (U Hawaii), and No. DE-FG03-95ER40925 (UT Dallas).

*Deceased.

[1] W. S. Hou and A. Soni, Phys. Rev. Lett. **50**, 569 (1983); G. Karl and W. Roberts, Phys. Lett. **144B**, 243 (1984); S. J. Brodsky *et al.*, Phys. Rev. Lett. **59**, 621 (1987); M. Chaichian *et al.*, Nucl. Phys. **B323**, 75 (1989); S. S. Pinsky, Phys. Lett. B **236**, 479 (1990); X. Q. Li *et al.*, Phys. Rev. D **55**, 1421 (1997); S. J. Brodsky and M. Karliner, Phys. Rev. Lett. **78**, 4682 (1997); Yu-Qi Chen and Eric Braaten, Phys. Rev. Lett. **80**, 5060 (1998).
[2] Particle Data Group, R. M. Barnett *et al.*, Phys. Rev. D **54**, 1 (1996).
[3] M. E. B. Franklin *et al.*, Phys. Rev. Lett. **51**, 963 (1983).
[4] BES Collaboration, J. Z. Bai *et al.*, Phys. Rev. D **54**, 1221 (1996); **57**, 3187(E) (1998).
[5] BES Collaboration, J. Z. Bai *et al.*, Nucl. Instrum. Methods Phys. Res., Sect. A **344**, 319 (1994).
[6] DM2 Collaboration, J. E. Augustin *et al.*, Nucl. Phys. **B320**, 1 (1989).

[7] For the first three decays, we use the PDG [2] recommended values of the J/ψ branching fractions. For J/ψ decay to $\phi f_2'$, there is poor consistency between the two existing measurements, Mark II and DM2 [2]. Instead of the PDG average with 50% error, we use the more recent data of DM2, which was a high statistics measurement, giving smaller errors and including the interference with $f_J(1710)$.

[8] S.J. Brodsky and G.P. Lepage, Phys. Rev. D **24**, 2848 (1981).

[9] Y.F. Gu and S.F. Tuan, Mod. Phys. Lett. A **10**, 615 (1995).

Measurements of the Cross Section for $e^+e^- \rightarrow$ Hadrons at Center-of-Mass Energies from 2 to 5 GeV

J. Z. Bai,[1] Y. Ban,[10] J. G. Bian,[1] A. D. Chen,[1] H. F. Chen,[16] H. S. Chen,[1] J. C. Chen,[1] X. D. Chen,[1] Y. B. Chen,[1] B. S. Cheng,[1] S. P. Chi,[1] Y. P. Chu,[1] J. B. Choi,[3] X. Z. Cui,[1] Y. S. Dai,[19] L. Y. Dong,[1] Z. Z. Du,[1] W. Dunwoodie,[14] H. Y. Fu,[1] L. P. Fu,[7] C. S. Gao,[1] S. D. Gu,[1] Y. N. Guo,[1] Z. J. Guo,[2] S. W. Han,[1] Y. Han,[1] F. A. Harris,[15] J. He,[1] J. T. He,[1] K. L. He,[1] M. He,[11] X. He,[1] T. Hong,[1] Y. K. Heng,[1] G. Y. Hu,[1] H. M. Hu,[1] Q. H. Hu,[1] T. Hu,[1] G. S. Huang,[2] X. P. Huang,[1] Y. Z. Huang,[1] J. M. Izen,[17] X. B. Ji,[11] C. H. Jiang,[1] Y. Jin,[1] B. D. Jones,[17] J. S. Kang,[8] Z. J. Ke,[1] H. J. Kim,[13] S. K. Kim,[13] T. Y. Kim,[13] D. Kong,[15] Y. F. Lai,[1] D. Li,[1] H. B. Li,[1] H. H. Li,[6] J. Li,[1] J. C. Li,[1] P. Q. Li,[1] Q. J. Li,[1] R. Y. Li,[1] W. Li,[1] W. G. Li,[1] X. N. Li,[1] X. Q. Li,[9] B. Liu,[1] F. Liu,[6] Feng Liu,[1] H. M. Liu,[1] J. Liu,[1] J. P. Liu,[18] T. R. Liu,[1] R. G. Liu,[1] Y. Liu,[1] Z. X. Liu,[1] X. C. Lou,[17] G. R. Lu,[5] F. Lu,[1] J. G. Lu,[1] Z. J. Lu,[1] X. L. Luo,[1] E. C. Ma,[1] J. M. Ma,[1] R. Malchow,[4] H. S. Mao,[1] Z. P. Mao,[1] X. C. Meng,[1] X. H. Mo,[1] J. Nie,[1] Z. D. Nie,[1] S. L. Olsen,[15] D. Paluselli,[15] H. Park,[8] N. D. Qi,[1] X. R. Qi,[1] C. D. Qian,[12] J. F. Qiu,[1] Y. K. Que,[1] G. Rong,[1] Y. Y. Shao,[1] B. W. Shen,[1] D. L. Shen,[1] H. Shen,[1] X. Y. Shen,[1] H. Y. Sheng,[1] F. Shi,[1] H. Z. Shi,[1] X. F. Song,[1] J. Y. Suh,[8] H. S. Sun,[1] L. F. Sun,[1] Y. Z. Sun,[1] S. Q. Tang,[1] W. Toki,[4] G. L. Tong,[1] G. S. Varner,[15] J. Wang,[1] J. Z. Wang,[1] L. Wang,[1] L. S. Wang,[1] P. Wang,[1] P. L. Wang,[1] S. M. Wang,[1] Y. Y. Wang,[1] Z. Y. Wang,[1] C. L. Wei,[1] N. Wu,[1] D. M. Xi,[1] X. M. Xia,[1] X. X. Xie,[1] G. F. Xu,[1] Y. Xu,[1] S. T. Xue,[1] W. B. Yan,[1] W. G. Yan,[1] C. M. Yang,[1] C. Y. Yang,[1] G. A. Yang,[1] H. X. Yang,[1] W. Yang,[4] X. F. Yang,[1] M. H. Ye,[2] S. W. Ye,[16] Y. X. Ye,[16] C. S. Yu,[1] C. X. Yu,[1] G. W. Yu,[1] Y. Yuan,[1] B. Y. Zhang,[1] C. Zhang,[1] C. C. Zhang,[1] D. H. Zhang,[1] H. L. Zhang,[1] H. Y. Zhang,[1] J. Zhang,[1] J. W. Zhang,[1] L. Zhang,[1] L. S. Zhang,[1] P. Zhang,[1] Q. J. Zhang,[1] S. Q. Zhang,[1] X. Y. Zhang,[11] Y. Y. Zhang,[1] Z. P. Zhang,[16] D. X. Zhao,[1] H. W. Zhao,[1] Jiawei Zhao,[16] J. W. Zhao,[1] M. Zhao,[1] P. P. Zhao,[1] W. R. Zhao,[1] Y. B. Zhao,[1] Z. G. Zhao,[1] J. P. Zheng,[1] L. S. Zheng,[1] Z. P. Zheng,[1] B. Q. Zhou,[1] G. M. Zhou,[1] L. Zhou,[1] K. J. Zhu,[1] Q. M. Zhu,[1] Y. C. Zhu,[1] Y. S. Zhu,[1] Z. A. Zhu,[1] B. A. Zhuang,[1] and B. S. Zou[1]

(BES Collaboration)

[1]*Institute of High Energy Physics, Beijing 100039, People's Republic of China*
[2]*China Center of Advanced Science and Technology, Beijing 100080, People's Republic of China*
[3]*Chonbuk National University, Chonju 561-756, Korea*
[4]*Colorado State University, Fort Collins, Colorado 80523*
[5]*Henan Normal University, Xinxiang 453002, People's Republic of China*
[6]*Huazhong Normal University, Wuhan 430079, People's Republic of China*
[7]*Hunan University, Changsha 410082, People's Republic of China*
[8]*Korea University, Seoul 136-701, Korea*
[9]*Nankai University, Tianjin 300071, People's Republic of China*
[10]*Peking University, Beijing 100871, People's Republic of China*
[11]*Shandong University, Jinan 250100, People's Republic of China*
[12]*Shanghai Jiaotong University, Shanghai 200030, People's Republic of China*
[13]*Seoul National University, Seoul 151-742, Korea*
[14]*Stanford Linear Accelerator Center, Stanford, California 94309*
[15]*University of Hawaii, Honolulu, Hawaii 96822*
[16]*University of Science and Technology of China, Hefei 230026, People's Republic of China*
[17]*University of Texas at Dallas, Richardson, Texas 75083-0688*
[18]*Wuhan University, Wuhan 430072, People's Republic of China*
[19]*Zhejiang University, Hangzhou 310028, People's Republic of China*

(Received 3 February 2001; published 25 February 2002)

We report values of $R = \sigma(e^+e^- \rightarrow \text{hadrons})/\sigma(e^+e^- \rightarrow \mu^+\mu^-)$ for 85 center-of-mass energies between 2 and 5 GeV measured with the upgraded Beijing Spectrometer at the Beijing Electron-Positron Collider.

DOI: 10.1103/PhysRevLett.88.101802 PACS numbers: 13.85.Lg, 12.15.–y

In precision tests of the Standard Model (SM) [1], the quantities $\alpha(M_Z^2)$, the QED running coupling constant evaluated at the Z pole, and $a_\mu = (g - 2)/2$, the anomalous magnetic moment of the muon, are of fundamental importance. The dominant uncertainties in both $\alpha(M_Z^2)$ and a_μ^{SM} are due to the effects of hadronic vacuum polarization, which cannot be reliably calculated in the low energy region. Instead, with the application of dispersion relations, experimentally measured R values are used to determine the vacuum polarization, where R is the lowest order cross section for $e^+e^- \to \gamma^* \to$ hadrons in units of the lowest-order QED cross section for $e^+e^- \to \mu^+\mu^-$, namely, $R = \sigma(e^+e^- \to \text{hadrons})/\sigma(e^+e^- \to \mu^+\mu^-)$, where $\sigma(e^+e^- \to \mu^+\mu^-) = \sigma^0_{\mu\mu} = 4\pi\alpha^2(0)/3s$.

Values of R in the center-of-mass (c.m.) energy ($E_{\text{c.m.}}$) range below 5 GeV were measured about 20 years ago with a precision of 15%–20% [2–4]. In this Letter, we report measurements of R at 85 c.m. energies between 2 and 4.8 GeV, with an average precision of 6.6% [5]. The measurements were carried out with the upgraded Beijing Spectrometer (BESII) [6] at the Beijing Electron-Positron Collider (BEPC).

Experimentally, the value of R is determined from the number of observed hadronic events, $N^{\text{obs}}_{\text{had}}$, by the relation

$$R = \frac{N^{\text{obs}}_{\text{had}} - N_{\text{bg}} - \sum_l N_{ll} - N_{\gamma\gamma}}{\sigma^0_{\mu\mu} L \epsilon_{\text{trg}} \bar{\epsilon}_{\text{had}}(1 + \delta)}, \tag{1}$$

where N_{bg} is the number of beam-associated background events, $\sum_l N_{ll}$ ($l = e, \mu, \tau$) are the numbers of lepton-pair events from one-photon processes, $N_{\gamma\gamma}$ is the number of two-photon process events that are misidentified as hadronic events, L is the integrated luminosity, δ is the effective initial state radiative (ISR) correction, $\bar{\epsilon}_{\text{had}}$ is the average detection efficiency for hadronic events, and ϵ_{trg} is the trigger efficiency. The triggers and the integrated luminosity measurement were the same as those used in a preliminary scan that measured R at six energy points between 2.6 and 5 GeV [7].

The hadronic event selection is similar with that used in the first R scan [7] but with improvements that include the following: for good track selection, the distance of closest approach requirement (<18 cm) of a track to the interaction point along the beam axis is not imposed; for event-level selection, the selected tracks must not all point into the forward ($\cos\theta > 0$) or the backward ($\cos\theta < 0$) hemisphere. Some distributions comparing data and Monte Carlo data are shown in Figs. 1(a)–1(c). The cuts used for selecting hadronic events were varied over a wide range, e.g., $|\cos\theta|$ from 0.75 to 0.90, E_{sum} from $0.24E_{\text{beam}}$ to $0.32E_{\text{beam}}$ (E_{sum} is the total deposited energy, E_{beam} the beam energy), to estimate the systematic error arising from the event selection; this is the dominant component of the systematic error as indicated in Table II.

The numbers of hadronic events and beam-associated background events are determined by fitting the distribution of event vertices along the beam direction with a Gaussian to describe the hadronic events and a polynomial of degree one to three for the beam-associated background. This background varies from 3% to 10% of the selected hadronic event candidates, depending on the energy. The fit using a second degree polynomial, shown in Fig. 1(d), turned out to be the best. The difference between using a polynomial of degree one or three to that of degree two is about 1%, which is included in the systematic error in the event selection.

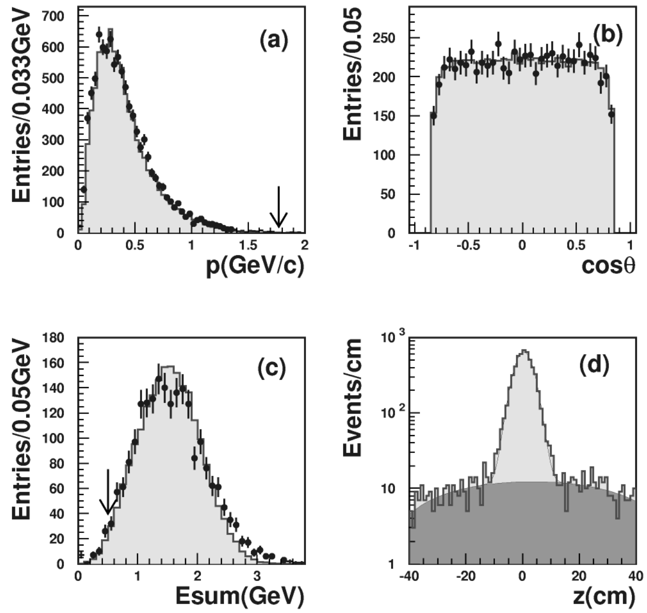

FIG. 1. Distributions for $E_{\text{c.m.}} = 3.0$ GeV of (a) track momentum, (b) track $\cos\theta$, (c) total energy deposited in the Barrel Shower Counter (BSC), and (d) event vertex position along the beam (z) axis. Histograms and dots in (a)–(c) represent Monte Carlo and real data, respectively; the beam associated background in (c) has been removed by sideband subtraction.

A special joint effort was made by the Lund group and the BES Collaboration to develop the LUARLW generator, which uses a formalism based on the Lund Model Area Law, but without the extreme-high-energy approximations used in JETSET's string fragmentation algorithm [8]. The final states simulated in LUARLW are exclusive, in contrast to JETSET, where they are inclusive. Above

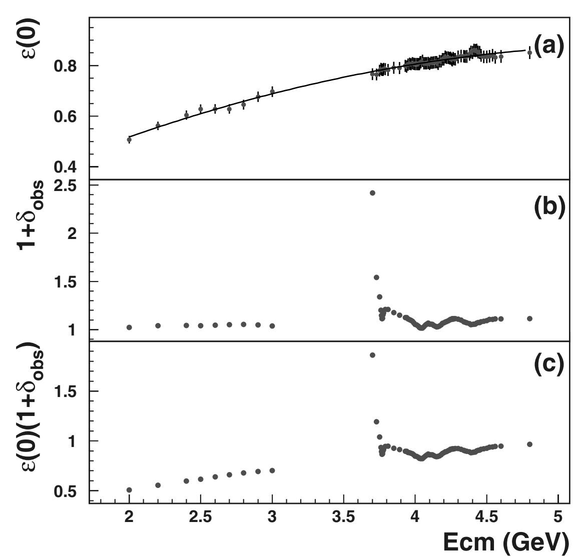

FIG. 2. (a) The c.m. energy dependence of the detection efficiency for hadronic events estimated using the LUARLW generator. The error bars are the total systematic errors. (b) The calculated radiative correction and (c) the product of (a) and (b).

TABLE I. Some values used in the determination of R at a few typical energy points.

$E_{\mathrm{c.m.}}$ (GeV)	$N_{\mathrm{had}}^{\mathrm{obs}}$	$N_{ll}+N_{\gamma\gamma}$	L (nb^{-1})	$\epsilon(0)$ (%)	$1+\delta_{\mathrm{obs}}$	R	Stat. error	Syst. error
2.000	1155.4	19.5	47.3	49.50	1.024	2.18	0.07	0.18
3.000	2055.4	24.3	135.9	67.55	1.038	2.21	0.05	0.11
4.000	768.7	58.0	48.9	80.34	1.055	3.16	0.14	0.15
4.800	1215.3	92.6	84.4	86.79	1.113	3.66	0.14	0.19

3.77 GeV, the production of D, D^*, D_s, and D_s^* is included in the generator according to the Eichten Model [9]. A Monte Carlo event generator has been developed to handle decays of the resonances in the radiative return processes $e^+e^- \rightarrow \gamma J/\psi$ or $\gamma\psi(2S)$ [10].

The parameters in LUARLW are tuned to reproduce 14 distributions of kinematic variables over the entire energy region covered by the scan [11]. We find that one set of parameter values is required for the c.m. energy region below open charm threshold and that a second set is required for higher energies. In an alternative approach, the parameter values were tuned point by point throughout the entire energy range. The detection efficiencies determined using individually tuned parameters are consistent with those determined with globally tuned parameters to within 2%. This difference is included in the systematic errors. The detection efficiencies were also determined using JETSET74 for the energies above 3 GeV. The difference between the JETSET74 and LUARLW results is about 1% and is also taken into account in estimating the systematic uncertainty. Figure 2(a) shows the variation of the detection efficiency as a function of c.m. energy.

We changed the fractions of D, D^*, D_s, and D_s^* production by 50% and find that the detection efficiency varies less than 1%. We also varied the fraction of the continuum under the broad resonances by 20% and find the change of the detection efficiency is about 1%. These variations are included in the systematic errors.

Different schemes for the initial state radiative corrections were compared [12–15], as reported in Ref. [7]. Below charm threshold, the four different schemes agree with each other to within 1%, while above charm threshold, where resonances are important, the agreement is within 1% to 3%. The radiative correction used in this analysis is based on Ref. [15], and the differences with the other schemes are included in the systematic error [16]. In practice, the radiative effects in the detection efficiency were moved into the radiative correction factor by making the replacement $\bar{\epsilon}_{\mathrm{had}}(1+\delta) \rightarrow \epsilon(0)(1+\delta_{\mathrm{obs}})$, where $\epsilon(k)$ is the efficiency for events with a radiative photon of energy k, and δ_{obs} contains a modification of the bremsstrahlung term to reflect the k dependence of the hadronic acceptance.

To calculate δ_{obs}, a cutoff in s', the effective c.m. energy after ISR to produce hadrons, has to be made. In our calculation, the minimum value of s' should be the threshold for producing two pions, corresponding to $k_{\max} = 1 - s'/s = (0.9805 - 0.9969)$ in the 2–5 GeV range. Our criteria to select hadronic events is such that ϵ approaches zero when k is close to 0.90, which makes us insensitive to events with high ISR photon energy.

In calculating the radiative correction for the narrow resonances J/ψ and $\psi(2S)$, the theoretical cross section is convoluted with the energy distribution of the colliding beams, which is treated as a Gaussian with a relative beam energy spread of $1.32 \times 10^{-4} E_{\mathrm{c.m.}}$ ($E_{\mathrm{c.m.}}$ in GeV). For the broad resonances at 3770, 4040, 4160, and 4416 MeV, the interferences and the energy dependence of total widths were taken into consideration. Initially the resonance parameters from PDG2000 [17] were used; then the parameters were allowed to vary and were determined from our fit. The calculation converged after a few iterations.

We varied the input parameters (masses and widths) of the J/ψ, $\psi(2S)$, and the broad resonances used in the radiative correction determination by 1 standard deviation from the values quoted in Ref. [17] and find that the changes in the R value are less than 1% for most points. Points close to the resonance at 4.0 GeV have errors from 1% to 1.7%. Figure 2(b) shows the radiative correction as a function of c.m. energy, where the structure at higher energy is related to the radiative tail of the $\psi(2S)$ and the broad resonances in this energy region. Tables I and II

TABLE II. Contributions to systematic errors: experimental selection of hadronic events, luminosity determination, theoretical modeling of hadronic events, trigger efficiency, radiative corrections, and total systematic error. All errors are in percentages (%).

$E_{\mathrm{c.m.}}$ (GeV)	Hadron selection	L	MC modeling	Trigger	Radiative correction	Total
2.000	7.07	2.81	2.62	0.5	1.06	8.13
3.000	3.30	2.30	2.66	0.5	1.32	5.02
4.000	2.64	2.43	2.25	0.5	1.82	4.64
4.800	3.58	1.74	3.05	0.5	1.02	5.14

TABLE III. Values of R from this experiment; the first error is statistical, the second systematic ($E_{\mathrm{c.m.}}$ in GeV).

$E_{\mathrm{c.m.}}$	R	$E_{\mathrm{c.m.}}$	R	$E_{\mathrm{c.m.}}$	R	$E_{\mathrm{c.m.}}$	R
2.000	$2.18 \pm 0.07 \pm 0.18$	3.890	$2.64 \pm 0.11 \pm 0.15$	4.120	$4.11 \pm 0.24 \pm 0.23$	4.340	$3.27 \pm 0.15 \pm 0.18$
2.200	$2.38 \pm 0.07 \pm 0.17$	3.930	$3.18 \pm 0.14 \pm 0.17$	4.130	$3.99 \pm 0.15 \pm 0.17$	4.350	$3.49 \pm 0.14 \pm 0.14$
2.400	$2.38 \pm 0.07 \pm 0.14$	3.940	$2.94 \pm 0.13 \pm 0.19$	4.140	$3.83 \pm 0.15 \pm 0.18$	4.360	$3.47 \pm 0.13 \pm 0.18$
2.500	$2.39 \pm 0.08 \pm 0.15$	3.950	$2.97 \pm 0.13 \pm 0.17$	4.150	$4.21 \pm 0.18 \pm 0.19$	4.380	$3.50 \pm 0.15 \pm 0.17$
2.600	$2.38 \pm 0.06 \pm 0.15$	3.960	$2.79 \pm 0.12 \pm 0.17$	4.160	$4.12 \pm 0.15 \pm 0.16$	4.390	$3.48 \pm 0.16 \pm 0.16$
2.700	$2.30 \pm 0.07 \pm 0.13$	3.970	$3.29 \pm 0.13 \pm 0.13$	4.170	$4.12 \pm 0.15 \pm 0.19$	4.400	$3.91 \pm 0.16 \pm 0.19$
2.800	$2.17 \pm 0.06 \pm 0.14$	3.980	$3.13 \pm 0.14 \pm 0.16$	4.180	$4.18 \pm 0.17 \pm 0.18$	4.410	$3.79 \pm 0.15 \pm 0.20$
2.900	$2.22 \pm 0.07 \pm 0.13$	3.990	$3.06 \pm 0.15 \pm 0.18$	4.190	$4.01 \pm 0.14 \pm 0.14$	4.420	$3.68 \pm 0.14 \pm 0.17$
3.000	$2.21 \pm 0.05 \pm 0.11$	4.000	$3.16 \pm 0.14 \pm 0.15$	4.200	$3.87 \pm 0.16 \pm 0.16$	4.430	$4.02 \pm 0.16 \pm 0.20$
3.700	$2.23 \pm 0.08 \pm 0.08$	4.010	$3.53 \pm 0.16 \pm 0.20$	4.210	$3.20 \pm 0.16 \pm 0.17$	4.440	$3.85 \pm 0.17 \pm 0.17$
3.730	$2.10 \pm 0.08 \pm 0.14$	4.020	$4.43 \pm 0.16 \pm 0.21$	4.220	$3.62 \pm 0.15 \pm 0.20$	4.450	$3.75 \pm 0.15 \pm 0.17$
3.750	$2.47 \pm 0.09 \pm 0.12$	4.027	$4.58 \pm 0.18 \pm 0.21$	4.230	$3.21 \pm 0.13 \pm 0.15$	4.460	$3.66 \pm 0.17 \pm 0.16$
3.760	$2.77 \pm 0.11 \pm 0.13$	4.030	$4.58 \pm 0.20 \pm 0.23$	4.240	$3.24 \pm 0.12 \pm 0.15$	4.480	$3.54 \pm 0.17 \pm 0.18$
3.764	$3.29 \pm 0.27 \pm 0.29$	4.033	$4.32 \pm 0.17 \pm 0.22$	4.245	$2.97 \pm 0.11 \pm 0.14$	4.500	$3.49 \pm 0.14 \pm 0.15$
3.768	$3.80 \pm 0.33 \pm 0.25$	4.040	$4.40 \pm 0.17 \pm 0.19$	4.250	$2.71 \pm 0.12 \pm 0.13$	4.520	$3.25 \pm 0.13 \pm 0.15$
3.770	$3.55 \pm 0.14 \pm 0.19$	4.050	$4.23 \pm 0.17 \pm 0.22$	4.255	$2.88 \pm 0.11 \pm 0.14$	4.540	$3.23 \pm 0.14 \pm 0.18$
3.772	$3.12 \pm 0.24 \pm 0.23$	4.060	$4.65 \pm 0.19 \pm 0.19$	4.260	$2.97 \pm 0.11 \pm 0.14$	4.560	$3.62 \pm 0.13 \pm 0.16$
3.776	$3.26 \pm 0.26 \pm 0.19$	4.070	$4.14 \pm 0.20 \pm 0.19$	4.265	$3.04 \pm 0.13 \pm 0.14$	4.600	$3.31 \pm 0.11 \pm 0.16$
3.780	$3.28 \pm 0.12 \pm 0.12$	4.080	$4.24 \pm 0.21 \pm 0.18$	4.270	$3.26 \pm 0.12 \pm 0.16$	4.800	$3.66 \pm 0.14 \pm 0.19$
3.790	$2.62 \pm 0.11 \pm 0.10$	4.090	$4.06 \pm 0.17 \pm 0.18$	4.280	$3.08 \pm 0.12 \pm 0.15$		
3.810	$2.38 \pm 0.10 \pm 0.12$	4.100	$3.97 \pm 0.16 \pm 0.18$	4.300	$3.11 \pm 0.12 \pm 0.12$		
3.850	$2.47 \pm 0.11 \pm 0.13$	4.110	$3.92 \pm 0.16 \pm 0.19$	4.320	$2.96 \pm 0.12 \pm 0.14$		

list some of the values used in the determination of R and the contributions to the uncertainty in the value of R at a few typical energy points in the scanned energy range, respectively.

Table III lists the values of R from this experiment. They are displayed in Fig. 3, together with BESII values from Ref. [7] and those measured by Mark I Collaboration, $\gamma\gamma 2$ Collaboration, and Pluto Collaboration [2–4]. The R values from BESII have an average uncertainty of about 6.6%, which represents a factor of 2 to 3 improvement in precision in the 2 to 5 GeV energy region. Of this error, 3.3% is common to all points. These improved measurements have a significant impact on the global fit to the electroweak data and the determination of the SM prediction for the mass of the Higgs particle [18]. In addition, they are expected to provide an improvement in the precision of the calculated value of a_μ^{SM} [19,20] and test the QCD sum rules down to 2 GeV [21,22].

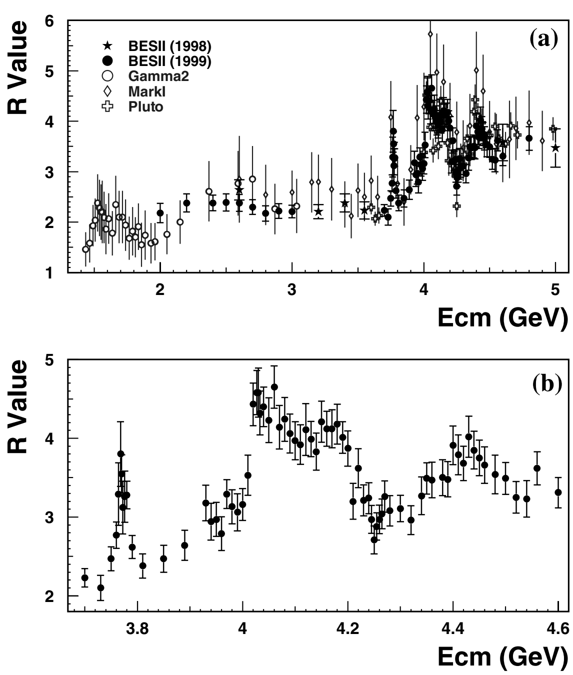

FIG. 3. (a) A compilation of measurements of R in the c.m. energy range from 1.4 to 5 GeV. (b) R values from this experiment in the resonance region between 3.7 and 4.6 GeV.

We thank the staff of the BEPC Accelerator Center and IHEP Computing Center for their efforts. We thank B. Andersson for helping in the development of the LUARLW generator. We also acknowledge useful discussions with M. Davier, B. Pietrzyk, T. Sjöstrand, A. D. Martin, and M. L. Swartz. We especially thank M. Tigner for major contributions not only to BES but also to the operation of the BEPC during the R scan. This work is supported in part by the National Natural Science Foundation of China under Contracts No. 19991480, No. 19805009, and No. 19825116; the Chinese Academy of Sciences under Contracts No. KJ95T-03, and No. E-01 (IHEP); and by the Department of Energy under Contracts No. DE-FG03-93ER40788 (Colorado State University), No. DE-AC03-76SF00515 (SLAC), No. DE-FG03-94ER40833 (University of Hawaii), No. DE-FG03-95ER40925 (University of Texas at Dallas), and by the Ministry of Science and Technology of Korea under Contract No. KISTEP I-03-037 (Korea).

[1] Z. G. Zhao, Int. J. Mod. Phys. A **15**, 3739 (2000).
[2] Mark I Collaboration, J. L. Siegrist *et al.,* Phys. Rev. D **26**, 969 (1982).
[3] $\gamma\gamma 2$ Collaboration, C. Bacci *et al.,* Phys. Lett. **86B**, 234 (1979).
[4] Pluto Collaboration, L. Criegee *et al.,* Phys. Rep. **83**, 151 (1982); Ch. Berger *et al.,* Phys. Lett. **81B**, 410 (1979).
[5] Z. G. Zhao, Nucl. Phys. **A675**, 13c (2000).
[6] BES Collaboration, J. Z. Bai *et al.,* Nucl. Instrum. Methods Phys. Res., Sect. A **458**, 627 (2001).
[7] BES Collaboration, J. Z. Bai *et al.,* Phys. Rev. Lett. **84**, 594 (2000).
[8] B. Andersson and Haiming Hu, hep-ph/9910285.
[9] E. Eichten *et al.,* Phys. Rev. D **21**, 203 (1980).
[10] J. C. Chen *et al.,* Phys. Rev. D **62**, 034003 (2000).
[11] Haiming Hu *et al.,* High Energy Phys. Nucl. Phys. (in Chinese) **25**, 1035 (2001).
[12] F. A. Berends and R. Kleiss, Nucl. Phys. **B178**, 141 (1981).
[13] G. Bonneau and F. Martin, Nucl. Phys. **B27**, 387 (1971).
[14] E. A. Kuraev and V. S. Fadin, Sov. J. Nucl. Phys. **41**, 3 (1985).
[15] A. Osterheld *et al.,* SLAC Report No. SLAC-PUB-4160, 1986.
[16] Haiming Hu *et al.,* High Energy Phys. Nucl. Phys. (in Chinese) **25**, 701 (2001).
[17] Particle Data Group, D. E. Groom *et al.,* Eur. Phys. J. C **15**, 1 (2000).
[18] H. Burkhardt and B. Pietrzyk, Phys. Lett. B **513**, 46 (2001).
[19] B. Pietrzyk, in *Proceedings of the 30th International Conference on High Energy Physics, Osaka, Japan, 2000,* edited by C. S. Lim and Taku Yamanaka (World Scientific, Singapore, River Edge, NJ, 2001); Robert Carey, *ibid.*; Atul Gurtu, *ibid.*
[20] A. Martin *et al.,* Phys. Lett. B **492**, 69 (2000).
[21] M. Davier and A. Hoecker, Phys. Lett. B **419**, 419 (1998).
[22] J. H. Kuehn and M. Steinhauser, Phys. Lett. B **437**, 425 (1998).

Observation of a Near-Threshold Enhancement in the $p\bar{p}$ Mass Spectrum from Radiative $J/\psi \to \gamma p\bar{p}$ Decays

J. Z. Bai,[1] Y. Ban,[9] J. G. Bian,[1] X. Cai,[1] J. F. Chang,[1] H. F. Chen,[16] H. S. Chen,[1] J. Chen,[3] Jie Chen,[8] J. C. Chen,[1] Y. B. Chen,[1] S. P. Chi,[1] Y. P. Chu,[1] X. Z. Cui,[1] Y. M. Dai,[7] Y. S. Dai,[19] L. Y. Dong,[1] S. X. Du,[18] Z. Z. Du,[1] W. Dunwoodie,[13] J. Fang,[1] S. S. Fang,[1] C. D. Fu,[1] H. Y. Fu,[1] L. P. Fu,[6] C. S. Gao,[1] M. L. Gao,[1] Y. N. Gao,[14] M. Y. Gong,[1] W. X. Gong,[1] S. D. Gu,[1] Y. N. Guo,[1] Y. Q. Guo,[1] Z. J. Guo,[2] S. W. Han,[1] F. A. Harris,[15] J. He,[1] K. L. He,[1] M. He,[10] X. He,[1] Y. K. Heng,[1] T. Hong,[1] H. M. Hu,[1] T. Hu,[1] G. S. Huang,[1] L. Huang,[6] X. P. Huang,[1] J. M. Izen,[17] X. B. Ji,[1] C. H. Jiang,[1] X. S. Jiang,[1] D. P. Jin,[1] S. Jin,[1] Y. Jin,[1] B. D. Jones,[17] Z. J. Ke,[1] D. Kong,[15] Y. F. Lai,[1] F. Li,[1] G. Li,[1] H. H. Li,[5] J. Li,[1] J. C. Li,[1] K. Li,[6] Q. J. Li,[1] R. B. Li,[1] R. Y. Li,[1] W. Li,[1] W. G. Li,[1] X. Q. Li,[8] X. S. Li,[14] C. F. Liu,[18] C. X. Liu,[1] Fang Liu,[16] F. Liu,[5] H. M. Liu,[1] J. B. Liu,[1] J. P. Liu,[18] R. G. Liu,[1] Y. Liu,[1] Z. A. Liu,[1] Z. X. Liu,[1] X. C. Lou,[17] G. R. Lu,[4] F. Lu,[1] H. J. Lu,[16] J. G. Lu,[1] Z. J. Lu,[1] X. L. Luo,[1] E. C. Ma,[1] F. C. Ma,[7] J. M. Ma,[1] R. Malchow,[3] Z. P. Mao,[1] X. C. Meng,[1] X. H. Mo,[2] J. Nie,[1] Z. D. Nie,[1] S. L. Olsen,[15] D. Paluselli,[15] H. P. Peng,[16] N. D. Qi,[1] C. D. Qian,[11] J. F. Qiu,[1] G. Rong,[1] D. L. Shen,[1] H. Shen,[1] X. Y. Shen,[1] H. Y. Sheng,[1] F. Shi,[1] L. W. Song,[1] H. S. Sun,[1] S. S. Sun,[16] Y. Z. Sun,[1] Z. J. Sun,[1] S. Q. Tang,[1] X. Tang,[1] D. Tian,[1] Y. R. Tian,[14] W. Toki,[3] G. L. Tong,[1] G. S. Varner,[15] J. Wang,[1] J. Z. Wang,[1] L. Wang,[1] L. S. Wang,[1] M. Wang,[1] Meng Wang,[1] P. Wang,[1] P. L. Wang,[1] W. F. Wang,[1] Y. F. Wang,[1] Zhe Wang,[1] Z. Wang,[1] Zheng Wang,[1] Z. Y. Wang,[2] C. L. Wei,[1] N. Wu,[1] X. M. Xia,[1] X. X. Xie,[1] G. F. Xu,[1] Y. Xu,[1] S. T. Xue,[1] M. L. Yan,[16] W. B. Yan,[1] G. A. Yang,[1] H. X. Yang,[14] J. Yang,[16] S. D. Yang,[1] M. H. Ye,[2] Y. X. Ye,[16] J. Ying,[9] C. S. Yu,[1] G. W. Yu,[1] C. Z. Yuan,[1] J. M. Yuan,[1] Y. Yuan,[1] Q. Yue,[1] S. L. Zang,[1] Y. Zeng,[6] B. X. Zhang,[1] B. Y. Zhang,[1] C. C. Zhang,[1] D. H. Zhang,[1] H. Y. Zhang,[1] J. Zhang,[1] J. M. Zhang,[4] J. W. Zhang,[1] L. S. Zhang,[1] Q. J. Zhang,[1] S. Q. Zhang,[1] X. Y. Zhang,[10] Y. J. Zhang,[9] Yiyun Zhang,[12] Y. Y. Zhang,[1] Z. P. Zhang,[16] D. X. Zhao,[1] Jiawei Zhao,[16] J. W. Zhao,[1] P. P. Zhao,[1] W. R. Zhao,[1] Y. B. Zhao,[1] Z. G. Zhao,[1,*] J. P. Zheng,[1] L. S. Zheng,[1] Z. P. Zheng,[1] X. C. Zhong,[1] B. Q. Zhou,[1] G. M. Zhou,[1] L. Zhou,[1] N. F. Zhou,[1] K. J. Zhu,[1] Q. M. Zhu,[1] Yingchun Zhu,[1] Y. C. Zhu,[1] Y. S. Zhu,[1] Z. A. Zhu,[1] B. A. Zhuang,[1] and B. S. Zou.[1]

(BES Collaboration)

[1]*Institute of High Energy Physics, Beijing 100039, People's Republic of China*
[2]*China Center of Advanced Science and Technology, Beijing 100080, People's Republic of China*
[3]*Colorado State University, Fort Collins, Colorado 80523, USA*
[4]*Henan Normal University, Xinxiang 453002, People's Republic of China*
[5]*Huazhong Normal University, Wuhan 430079, People's Republic of China*
[6]*Hunan University, Changsha 410082, People's Republic of China*
[7]*Liaoning University, Shenyang 110036, People's Republic of China*
[8]*Nankai University, Tianjin 300071, People's Republic of China*
[9]*Peking University, Beijing 100871, People's Republic of China*
[10]*Shandong University, Jinan 250100, People's Republic of China*
[11]*Shanghai Jiaotong University, Shanghai 200030, People's Republic of China*
[12]*Sichuan University, Chengdu 610064, People's Republic of China*
[13]*Stanford Linear Accelerator Center, Stanford, California 94309, USA*
[14]*Tsinghua University, Beijing 100084, People's Republic of China*
[15]*University of Hawaii, Honolulu, Hawaii 96822, USA*
[16]*University of Science and Technology of China, Hefei 230026, People's Republic of China*
[17]*University of Texas at Dallas, Richardson, Texas 75083-0688, USA*
[18]*Wuhan University, Wuhan 430072, People's Republic of China*
[19]*Zhejiang University, Hangzhou 310028, People's Republic of China*
(Received 7 March 2003; published 10 July 2003)

We observe a narrow enhancement near $2m_p$ in the invariant mass spectrum of $p\bar{p}$ pairs from radiative $J/\psi \to \gamma p\bar{p}$ decays. No similar structure is seen in $J/\psi \to \pi^0 p\bar{p}$ decays. The results are based on an analysis of a 58×10^6 event sample of J/ψ decays accumulated with the BESII detector at the Beijing electron-positron collider. The enhancement can be fit with either an S- or P-wave Breit-Wigner resonance function. In the case of the S-wave fit, the peak mass is below $2m_p$ at $M = 1859^{+3}_{-10}\,(\mathrm{stat})^{+5}_{-25}(\mathrm{syst})\ \mathrm{MeV}/c^2$ and the total width is $\Gamma < 30\ \mathrm{MeV}/c^2$ at the 90% confidence level. These mass and width values are not consistent with the properties of any known particle.

DOI: 10.1103/PhysRevLett.91.022001 PACS numbers: 13.75.Cs, 12.39.Mk, 12.40.Yx, 13.20.Gd

There is an accumulation of evidence for anomalous behavior in the proton-antiproton ($p\overline{p}$) system very near the $M_{p\overline{p}} = 2m_p$ mass threshold. The observed cross section for $e^+e^- \to$ hadrons has a narrow diplike structure at a center of mass energy of $\sqrt{s} \simeq 2m_p c^2$ [1]. The proton's timelike magnetic form factor, determined from high statistics measurements of the $p\overline{p} \to e^+e^-$ annihilation process, exhibits a very steep falloff just above the $p\overline{p}$ mass threshold [2]. The authors of Ref. [1] attribute these features to a narrow, subthreshold $J^{PC} = 1^{--}$ resonance with mass 1870 ± 10 MeV$/c^2$ and width $\Gamma = 10 \pm 5$ MeV$/c^2$. In studies of $\overline{p}$ annihilations at rest in deuterium, anomalies in the charged pion momentum spectrum from $\overline{p}d \to \pi^-\pi^0 p$ and $\pi^+\pi^- n$ reactions [3] and the proton spectrum from $\overline{p}d \to p2\pi^+3\pi^-$ [4] have been interpreted as effects of narrow, below-threshold resonances. There are no well established mesons that could be associated with such a state. The proximity in mass to $2m_p$ is suggestive of nucleon-antinucleon ($N\overline{N}$) bound states, an idea that has a long history. In 1949, Fermi and Yang [5] proposed that the pion was a tightly bound $N\overline{N}$ state. Nambu and Jona-Lasinio [6] expanded on this in 1961 with a model based on chiral symmetry that has, in addition to a low-mass pion, a scalar $p\overline{p}$ composite state with mass equal to $2m_p$. Although these ideas have been superseded by the quark model [7], the possibility of bound $N\overline{N}$ states with mass near $2m_p$, generally referred to as *baryonium,* continues to be considered [8]. Recently Belle has reported observations of the decays $B^+ \to K^+ p\overline{p}$ [9] and $\overline{B}^0 \to D^0 p\overline{p}$ [10]. In both processes there are enhancements in the $p\overline{p}$ invariant mass distributions near $M_{p\overline{p}} \simeq 2m_p$. An investigation of low-mass $p\overline{p}$ systems with different quantum numbers may help clarify the situation.

In this Letter we report a study of the low-mass $p\overline{p}$ pairs produced via radiative decays in a sample of 58×10^6 J/ψ events accumulated in the upgraded Beijing Spectrometer (BESII) located at the Beijing Electron-Positron Collider (BEPC) at the Beijing Institute of High Energy Physics. This reaction produces $p\overline{p}$ systems with even C parity and, thus, probes states with different quantum numbers than those studied in Refs. [1,2].

BESII is a large solid-angle magnetic spectrometer that is described in detail in Ref. [11]. Charged particle momenta are determined with a resolution of $\sigma_p/p = 1.78\%\sqrt{1 + p^2(\mathrm{GeV}^2)}$ in a 40-layer cylindrical drift chamber. Particle identification is accomplished by specific ionization (dE/dx) measurements in the drift chamber and time-of-flight (TOF) measurements in a barrel-like array of 48 scintillation counters. The dE/dx resolution is $\sigma_{dE/dx} = 8.0\%$; the TOF resolution is $\sigma_{\mathrm{TOF}} = 180$ ps; both systems independently provide more than 3σ separation of protons from any other charged particle species for the entire momentum range considered in this experiment. Radially outside of the time-of-flight counters is a 12-radiation-length barrel shower counter (BSC) comprised of gas proportional tubes interleaved with lead sheets. The BSC measures the energies and directions of photons with resolutions of $\sigma_E/E \simeq 21\%/\sqrt{E(\mathrm{GeV})}$, $\sigma_\phi = 7.9$ mrad, and $\sigma_z = 2.3$ mrad. The iron flux return of the magnet is instrumented with three double layers of counters that are used to identify muons.

For this analysis we use events with a high energy gamma ray and two oppositely charged tracks each of which is well fitted to a helix originating near the interaction point. Candidate γ's are associated with energy clusters in the BSC that have less than 80% of their total energy in any one readout layer and do not match the extrapolated position of any charged track. Since antiprotons that stop in the material of the TOF or BSC can produce annihilation products that are reconstructed elsewhere in the detector as γ rays, no restrictions are placed on the total number of neutral clusters in the event. We use charged tracks and γ's that are within the polar angle region $|\cos\theta| < 0.8$ and reject events where both tracks are identified as muons, or produce high energy showers in the BSC that are characteristic of electrons. The dE/dx information is used to form particle identification confidence levels $\mathcal{P}^i_{\mathrm{pid}}$, where i denotes π, K, and p. We require that both charged tracks have $\mathcal{P}^p_{\mathrm{pid}} > \mathcal{P}^K_{\mathrm{pid}}$ and $\mathcal{P}^p_{\mathrm{pid}} > \mathcal{P}^\pi_{\mathrm{pid}}$. A study based on a kinematically selected sample of $J/\psi \to K^{*\pm}K^\mp \to K^+K^-\pi^0$ events indicates that the probability for a charged kaon to satisfy this requirement is less than 1% per track.

We subject the surviving events to four-constraint kinematic fits to the hypotheses $J/\psi \to \gamma p\overline{p}$ and $J/\psi \to \gamma K^+K^-$. For events with more than one γ, we select the γ that has the highest fit confidence level (C.L.). We select events that have fit confidence level $\mathrm{C.L.}_{\gamma p\overline{p}} > 0.05$ and reject events that have $\mathrm{C.L.}_{\gamma K^+K^-} > \mathrm{C.L.}_{\gamma p\overline{p}}$.

Figure 1 shows the $p\overline{p}$ invariant mass distribution for surviving events. The distribution has a peak near $M_{p\overline{p}} = 2.98$ GeV$/c^2$ that is consistent in mass, width, and yield with expectations for $J/\psi \to \gamma\eta_c$, $\eta_c \to p\overline{p}$ [12], a broad enhancement around $M_{p\overline{p}} \sim 2.2$ GeV$/c^2$, and a narrow,

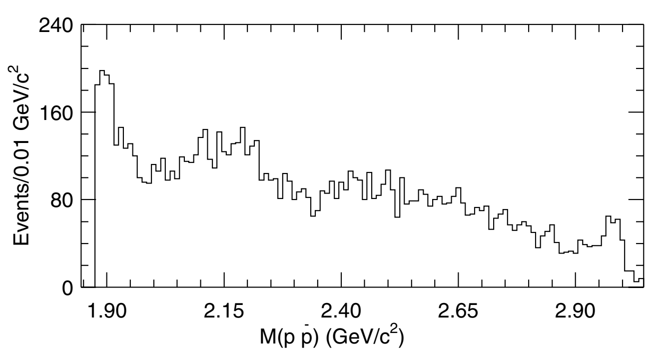

FIG. 1. The $p\overline{p}$ invariant mass distribution for the $J/\psi \to \gamma p\overline{p}$-enriched event sample.

low-mass peak at the $p\overline{p}$ mass threshold that is the subject of this Letter.

Backgrounds from processes involving charged particles that are not protons and antiprotons are negligibly small. In addition to being well separated from other charged particles by the dE/dx measurements and the kinematic fit, the protons and antiprotons from the low $M_{p\overline{p}}$ region stop in the TOF counters and, thus, have very characteristic BSC responses: protons do not produce any matching signals in the BSC while secondary particles from antiproton annihilation usually produce large signals. This asymmetric behavior is quite distinct from that for K^+K^-, $\pi^+\pi^-$, or e^+e^- pairs, where the positive and negative tracks produce similar, nonzero BSC responses. The observed BSC energy distributions for the selected $J/\psi \to \gamma p\overline{p}$ events with $M_{p\overline{p}} \leq 1.9\ \mathrm{GeV}/c^2$ closely match expectations for protons and antiprotons and show no evidence for contamination from other particle species.

There is, however, a large background from $J/\psi \to \pi^0 p\overline{p}$ events with an asymmetric $\pi^0 \to \gamma\gamma$ decay where one of the photons has most of the π^0's energy. This is studied using a sample of $J/\psi \to \pi^0 p\overline{p}$ decays reconstructed from the same data sample. For these, we select events with oppositely charged tracks that are identified as protons and with two or more photons, apply a four-constraint kinematic fit to the hypothesis $J/\psi \to \gamma\gamma p\overline{p}$, and require $\mathrm{C.L.}_{\gamma\gamma p\overline{p}} > 0.005$. For events with more than two γ's, we select the γ pair that produces the best fit. In the $M_{\gamma\gamma}$ distribution of the selected events there is a distinct π^0 signal; we require $|M_{\gamma\gamma} - M_{\pi^0}| < 0.03\ \mathrm{GeV}/c^2$ $(\pm 2\sigma)$. The distribution of events vs $M_{p\overline{p}} - 2m_p$ near the $M_{p\overline{p}} = 2m_p$ threshold, shown in Fig. 2(a), is reasonably well described by a function of the form $f_{\mathrm{bkg}}(\delta) = N(\delta^{1/2} + a_1\delta^{3/2} + a_2\delta^{5/2})$, where $\delta \equiv M_{p\overline{p}} - 2m_p$ and the shape parameters a_1 and a_2 are determined from a fit to simulated Monte Carlo (MC) events that were generated uniformly in phase space. This is shown in the figure as a smooth curve. There is no indication of a narrow peak at low $p\overline{p}$ invariant masses. Monte Carlo simulations of other J/ψ decay processes with final-state $p\overline{p}$ pairs indicate that backgrounds from processes other than $J/\psi \to \pi^0 p\overline{p}$ are negligibly small.

The $M_{p\overline{p}} - 2m_p$ distribution for the $\pi^0 p\overline{p}$ phase-space MC events that pass the $\gamma p\overline{p}$ selection is shown in Fig. 2(b). There is no clustering at threshold; the smooth curve is the result of a fit to $f_{\mathrm{bkg}}(\delta)$ with the same shape parameter values.

In BESII, the detection efficiency for protons and antiprotons falls sharply for three momenta below $0.4\ \mathrm{GeV}/c$. This produces a mass dependence in the experimental acceptance near $M_{p\overline{p}} \simeq 2m_p$ for $J/\psi \to \gamma p\overline{p}$ and $\pi^0 p\overline{p}$. For both processes, when $M_{p\overline{p}}$ is very near $2m_p$, the p and $\overline{p}$ both have three momenta very near $0.5\ \mathrm{GeV}/c$ and are well detected. For increasing $p\overline{p}$ masses, more asymmetric energy sharing is possible and the acceptance decreases until $M_{p\overline{p}} \simeq 2.0\ \mathrm{GeV}/c^2$, where it is $\simeq 0.65$ of its value at $M_{p\overline{p}} = 2m_p$.

Figure 3(a) shows the threshold region for the selected $J/\psi \to \gamma p\overline{p}$ events. The dotted curve in the figure indicates how the acceptance varies with invariant mass. The solid curve shows the result of a fit using an acceptance-weighted S-wave Breit-Wigner (BW) function [13] to represent the low-mass enhancement plus $f_{\mathrm{bkg}}(\delta)$ to

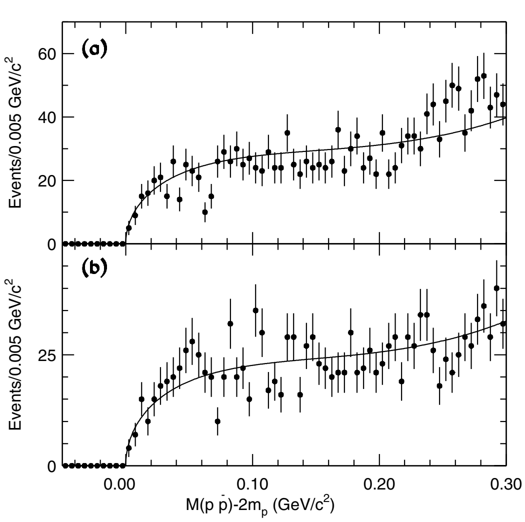

FIG. 2. The $M_{p\overline{p}} - 2m_p$ distribution for (a) selected $J/\psi \to \pi^0 p\overline{p}$ decays and (b) MC $J/\psi \to \pi^0 p\overline{p}$ events that satisfy the $\gamma p\overline{p}$ selection criteria. The smooth curves are the result of fits described in the text.

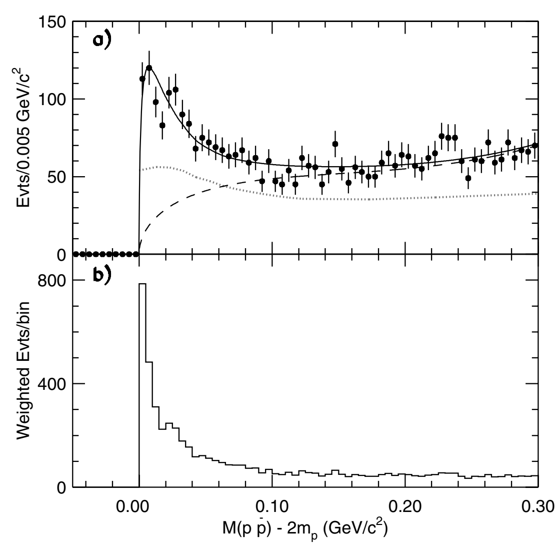

FIG. 3. (a) The near threshold $M_{p\overline{p}} - 2m_p$ distribution for the $\gamma p\overline{p}$ event sample. The solid curve is the result of the fit described in the text; the dashed curve shows the fitted background function. The dotted curve indicates how the acceptance varies with $p\overline{p}$ invariant mass. (b) The $M_{p\overline{p}} - 2m_p$ distribution with events weighted by q_0/q.

represent the background. The mass and width of the BW signal function are allowed to vary and the shape parameters of $f_{\text{bkg}}(\delta)$ are fixed at the values derived from the fit to the $\pi^0 p\overline{p}$ phase-space MC sample [14]. This fit yields 928 ± 57 events [15] in the BW function with a peak mass of $M = 1859^{+3}_{-10}$ MeV$/c^2$ and a full width of $\Gamma = 0 \pm 21$ MeV$/c^2$. Here the errors are statistical only: those for the event yield and the width are derived from the fit; the determination of the statistical errors for the mass is discussed below. The fit confidence level is 46.2% (χ^2/d.o.f. $= 56.3/56$).

Monte Carlo studies indicate that in the presence of background, the determination of the peak mass for a below-threshold resonance is more unreliable the further the peak position is below threshold. This produces an asymmetric distribution of mass input values that can produce our measured result. Moreover, the rms spread of these values increases for lower input masses, indicating that the statistical error returned by our mass fit underestimates the negative error. Because of this, we quote statistical errors for the mass that are derived from the rms spreads of fit results for an ensemble of MC experiments with different input mass values.

Further evidence that the peak mass is below the $2m_p$ threshold is provided in Fig. 3(b), which shows the $M_{p\overline{p}} - 2m_p$ distribution when the kinematic threshold behavior is removed by weighting each event by q_0/q, where q is the proton momentum in the $p\overline{p}$ rest frame and q_0 is the value for $M_{p\overline{p}} = 2$ GeV$/c^2$. The sharp and monotonic increase at threshold that is observed in this weighted histogram can occur only for an S-wave BW function when the peak mass is below $2m_p$.

An S-wave $p\overline{p}$ system with even C parity would correspond to a 0^{-+} pseudoscalar state. We also tried to fit the signal with a P-wave BW function, which would correspond to a 0^{++} (^3_0P) scalar state that occurs in some models [6,8]. This fit yields a peak mass $M = 1876.4 \pm 0.9$ MeV$/c^2$, which is very nearly equal to $2m_p$, and a very narrow total width: $\Gamma = 4.6 \pm 1.8$ MeV$/c^2$ (statistical errors only). The fit quality, χ^2/d.o.f. $= 59.0/56$, is worse than that for the S-wave BW but still acceptable. A fit with a D-wave BW fails badly with χ^2/d.o.f. $= 1405/56$.

In addition we tried fits that use known particle resonances to represent the low-mass peak. There are two spin-zero resonances listed in the Particle Data Group (PDG) tables in this mass region [16]: the $\eta(1760)$ with $M_{\eta(1760)} = 1760 \pm 11$ MeV$/c^2$ and $\Gamma_{\eta(1760)} = 60 \pm 16$ MeV$/c^2$, and the $\pi(1800)$ with $M_{\pi(1800)} = 1801 \pm 13$ MeV$/c^2$ and $\Gamma_{\pi(1800)} = 210 \pm 15$ MeV. A fit with f_{bkg} and an acceptance-weighted S-wave BW function with mass and width fixed at the PDG values for the $\eta(1760)$ produces χ^2/d.o.f. $= 323.4/58$. A fit using a BW with the $\pi(1800)$ parameters is worse.

For both the scalar and pseudoscalar case, the polar angle of the photon, θ_γ, would be distributed according to $1 + \cos^2\theta_\gamma$. Figure 4 shows the background-subtracted, acceptance-corrected $|\cos\theta_\gamma|$ distribution for events with $M_{p\overline{p}} \leq 1.9$ GeV and $|\cos\theta_\gamma| \leq 0.8$. Here we have subtracted the $|\cos\theta_{\pi^0}|$ distribution from the $\pi^0 p\overline{p}$ data sample, normalized to the area of $f_{\text{bkg}}(\delta)$ for $M_{p\overline{p}} < 1.9$ GeV$/c^2$ to account for background. The solid curve shows the result of a fit for $1 + \cos^2\theta_\gamma$ to the $|\cos\theta_\gamma| < 0.8$ region; the dashed line shows the result of a similar fit to $\sin^2\theta_\gamma$. Although the data are not precise enough to establish a $1 + \cos^2\theta_\gamma$ behavior, the distribution is consistent with expectations for a radiative transition to a pseudoscalar or scalar meson [17].

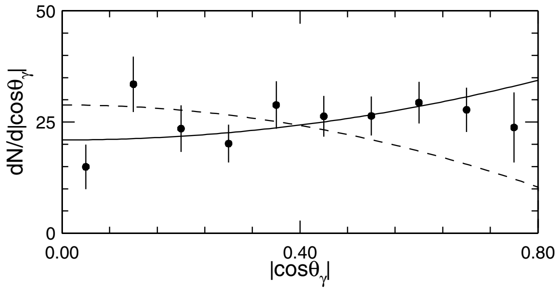

FIG. 4. The background-subtracted, acceptance-corrected $|\cos\theta_\gamma|$ distribution for $J/\psi \to \gamma p\overline{p}$-enriched events with $M_{p\overline{p}} \leq 1.9$ GeV$/c^2$. The solid curve is a fit to a $1 + \cos^2\theta_\gamma$ shape for the region $|\cos\theta_\gamma| \leq 0.8$; the dashed curve is the result of a fit to $\sin^2\theta_\gamma$.

We evaluate systematic errors on the mass and width from changes observed in the fitted values for fits with different bin sizes, with background shape parameters left as free parameters, different shapes for the acceptance variation, and different resolutions. The ensemble Monte Carlo studies mentioned above indicate that in the presence of background, the determination of the parameters of a subthreshold BW resonance can be biased. We include the range of differences between input and output values seen in the MC study in the systematic errors.

For the mass, we determine a systematic error of $^{+5}_{-25}$ MeV$/c^2$. For the total width, we determine a 90% confidence level upper limit of $\Gamma < 30$ MeV$/c^2$, where the limit includes the systematic error.

Using a Monte Carlo determined acceptance of 23%, we determine a product of branching fractions $\mathcal{B}(J/\psi \to \gamma X)\mathcal{B}(X \to p\bar{p}) = 7.0 \pm 0.4(\text{stat})^{+1.9}_{-0.8}(\text{syst}) \times 10^{-5}$, where the systematic error includes uncertainties in the acceptance (10%), the total number of J/ψ decays in the data sample (5%), and the effects of changing the various inputs to the fit ($^{+24\%}_{-2\%}$).

In summary, we observe a strong, near-threshold enhancement in the $p\overline{p}$ invariant mass distribution in the radiative decay process $J/\psi \to \gamma p\overline{p}$. No similar structure is seen in $J/\psi \to \pi^0 p\overline{p}$ decays. The structure has properties consistent with either a $J^{PC} = 0^{-+}$ or 0^{++} quantum number assignment and cannot be attributed to the effects of any known meson resonance. If interpreted as a single

0^{-+} resonance, its peak mass is below the $M_{p\bar{p}} = 2m_p$ threshold at $1859^{+3}_{-10}(\text{stat})^{+5}_{-25}(\text{syst})$ MeV/c^2 and its width is $\Gamma < 30$ MeV/c^2 at the 90% C.L. These mass and width values are close to those of the 1^{--} state discussed in Ref. [1], which suggests that these states may be related. A search for a state with these properties in radiative J/ψ decays to mesonic final states is in progress.

We thank the staffs of BEPC and the computing center for their strong efforts. This work is supported in part by the National Natural Science Foundation of China under Contracts No. 19991480, No. 10225524, and No. 10225525 and the Chinese Academy of Sciences under Contract No. KJ 95T-03, the 100 Talents Program of CAS under Contracts No. U-24 and No. U-25, and the Knowledge Innovation Project of CAS under Contracts No. U-602 and No. U-34 (IHEP); by the National Natural Science Foundation of China under Contract No. 10175060 (USTC); and by the Department of Energy under Contracts No. DE-FG03-93ER40788 (Colorado State University), No. DE-AC03-76SF00515 (SLAC), No. DE-FG03-94ER40833 (U. Hawaii), and No. DE-FG03-95ER40925 (UT Dallas).

*Visiting scientist at the University of Michigan, Ann Arbor, MI 48109, USA.

[1] FENICE Collaboration, A. Antonelli *et al.*, Nucl. Phys. **B517**, 3 (1998).

[2] G. Bardin *et al.*, Nucl. Phys. **B411**, 3 (1994).

[3] D. Bridges *et al.*, Phys. Lett. B **180**, 313 (1986).

[4] O. D. Dalkarov *et al.*, Phys. Lett. B **392**, 229 (1997).

[5] E. Fermi and C. N. Yang, Phys. Rev. **76**, 1739 (1949).

[6] Y. Nambu and G. Jona-Lasinio, Phys. Rev. **122**, 345 (1961); **124**, 246 (1961).

[7] R. Delbourgo and M. D. Scadron, Phys. Rev. Lett. **48**, 379 (1982); T. Hatsuda and T. Kunihiro, Prog. Theor. Phys. **74**, 765 (1985); Phys. Rep. **247**, 221 (1994).

[8] For recent reviews of this subject, see E. Klempt *et al.*, Phys. Rep. **368**, 119 (2002); J.-M. Richard, Nucl. Phys. B (Proc. Suppl.) **86**, 361 (2000).

[9] Belle Collaboration, K. Abe *et al.*, Phys. Rev. Lett. **88**, 181803 (2002).

[10] Belle Collaboration, K. Abe *et al.*, Phys. Rev. Lett. **89**, 151802 (2002).

[11] BES Collaboration, J. Z. Bai *et al.*, Nucl. Instrum. Methods Phys. Res., Sect. A **458**, 627 (2001).

[12] BES Collaboration, J. Z. Bai *et al.*, Phys. Lett. B **555**, 174 (2003).

[13] For the BW, we use the form $\mathrm{BW}(M) \propto \frac{q^{(2\ell+1)}k^3}{(M^2-M_0^2)^2+M_0^2\Gamma^2}$, where Γ is a constant (determined from the fit), q is the proton momentum in the $p\bar{p}$ rest frame, ℓ is the $p\bar{p}$ orbital angular momentum, and k is the photon momentum. Note that for $M_0 < 2m_p$, the BW tail above $M_{p\bar{p}} = 2m_p$ is substantial, even for $\Gamma = 0$.

[14] The $p\bar{p}$ mass resolution varies from $\sigma \simeq 1.2$ MeV/c^2 at $M_{p\bar{p}} \simeq 2m_p$ to ~ 3 MeV/c^2 at higher masses. Convolving the fitting function with a Gaussian with a width in this range has no significant effect on the results.

[15] The background level in the fit is about twice the level of $J/\psi \to \pi^0 p\bar{p}$ feedthrough predicted by the MC. This indicates that there is some contribution from nonresonant three-body $J/\psi \to \gamma p\bar{p}$ decays.

[16] Particle Data Group, D. Groom *et al.*, Eur. Phys. J. C **15**, 1 (2000).

[17] The $1 + \cos^2\theta_\gamma$ fit has $\chi^2/\text{d.o.f.} = 3.7/7$; the $\sin^2\theta_\gamma$ fit has $\chi^2/\text{d.o.f.} = 10.3/7$.

Observation of the Decay $\psi(2S) \to K_S^0 K_L^0$

J. Z. Bai,[1] Y. Ban,[10] J. G. Bian,[1] X. Cai,[1] J. F. Chang,[1] H. F. Chen,[16] H. S. Chen,[1] H. X. Chen,[1] J. Chen,[1] J. C. Chen,[1] Jun Chen,[6] M. L. Chen,[1] Y. B. Chen,[1] S. P. Chi,[1] Y. P. Chu,[1] X. Z. Cui,[1] H. L. Dai,[1] Y. S. Dai,[18] Z. Y. Deng,[1] L. Y. Dong,[1] S. X. Du,[1] Z. Z. Du,[1] J. Fang,[1] S. S. Fang,[1] C. D. Fu,[1] H. Y. Fu,[1] L. P. Fu,[6] C. S. Gao,[1] M. L. Gao,[1] Y. N. Gao,[14] M. Y. Gong,[1] W. X. Gong,[1] S. D. Gu,[1] Y. N. Guo,[1] Y. Q. Guo,[1] Z. J. Guo,[15] S. W. Han,[1] F. A. Harris,[15] J. He,[1] K. L. He,[1] M. He,[11] X. He,[1] Y. K. Heng,[1] H. M. Hu,[1] T. Hu,[1] G. S. Huang,[1] L. Huang,[6] X. P. Huang,[1] X. B. Ji,[1] Q. Y. Jia,[10] C. H. Jiang,[1] X. S. Jiang,[1] D. P. Jin,[1] S. Jin,[1] Y. Jin,[1] Y. F. Lai,[1] F. Li,[1] G. Li,[1] H. H. Li,[1] J. Li,[1] J. C. Li,[1] Q. J. Li,[1] R. B. Li,[1] R. Y. Li,[1] S. M. Li,[1] W. Li,[1] W. G. Li,[1] X. L. Li,[7] X. Q. Li,[7] X. S. Li,[14] Y. F. Liang,[13] H. B. Liao,[5] C. X. Liu,[1] Fang Liu,[16] F. Liu,[5] H. M. Liu,[1] J. B. Liu,[1] J. P. Liu,[17] R. G. Liu,[1] Y. Liu,[1] Z. A. Liu,[1] Z. X. Liu,[1] G. R. Lu,[4] F. Lu,[1] J. G. Lu,[1] C. L. Luo,[8] X. L. Luo,[1] F. C. Ma,[7] J. M. Ma,[1] L. L. Ma,[11] X. Y. Ma,[1] Z. P. Mao,[1] X. C. Meng,[1] X. H. Mo,[1] J. Nie,[1] Z. D. Nie,[1] S. L. Olsen,[15] H. P. Peng,[16] N. D. Qi,[1] C. D. Qian,[12] H. Qin,[8] J. F. Qiu,[1] Z. Y. Ren,[1] G. Rong,[1] L. Y. Shan,[1] L. Shang,[1] D. L. Shen,[1] X. Y. Shen,[1] H. Y. Sheng,[1] F. Shi,[1] X. Shi,[10] L. W. Song,[1] H. S. Sun,[1] S. S. Sun,[16] Y. Z. Sun,[1] Z. J. Sun,[1] X. Tang,[1] N. Tao,[16] Y. R. Tian,[14] G. L. Tong,[1] G. S. Varner,[15] D. Y. Wang,[1] J. Z. Wang,[1] L. Wang,[1] L. S. Wang,[1] M. Wang,[1] Meng Wang,[1] P. Wang,[1] P. L. Wang,[1] S. Z. Wang,[1] W. F. Wang,[1] Y. F. Wang,[1] Zhe Wang,[1] Z. Wang,[1] Zheng Wang,[1] Z. Y. Wang,[1] C. L. Wei,[1] N. Wu,[1] Y. M. Wu,[1] X. M. Xia,[1] X. X. Xie,[1] B. Xin,[7] G. F. Xu,[1] H. Xu,[1] Y. Xu,[1] S. T. Xue,[1] M. L. Yan,[16] W. B. Yan,[1] F. Yang,[9] H. X. Yang,[14] J. Yang,[16] S. D. Yang,[1] Y. X. Yang,[3] L. H. Yi,[6] Z. Y. Yi,[1] M. Ye,[1] M. H. Ye,[2] Y. X. Ye,[16] C. S. Yu,[1] G. W. Yu,[1] C. Z. Yuan,[1] J. M. Yuan,[1] Y. Yuan,[1] Q. Yue,[1] S. L. Zang,[1] Y. Zeng,[6] B. X. Zhang,[1] B. Y. Zhang,[1] C. C. Zhang,[1] D. H. Zhang,[1] H. Y. Zhang,[1] J. Zhang,[1] J. M. Zhang,[4] J. Y. Zhang,[1] J. W. Zhang,[1] L. S. Zhang,[1] Q. J. Zhang,[1] S. Q. Zhang,[1] X. M. Zhang,[1] X. Y. Zhang,[11] Yiyun Zhang,[13] Y. J. Zhang,[10] Y. Y. Zhang,[1] Z. P. Zhang,[16] Z. Q. Zhang,[4] D. X. Zhao,[1] J. B. Zhao,[1] J. W. Zhao,[1] P. P. Zhao,[1] W. R. Zhao,[1] X. J. Zhao,[1] Y. B. Zhao,[1] Z. G. Zhao,[1] H. Q. Zheng,[10] J. P. Zheng,[1] L. S. Zheng,[1] Z. P. Zheng,[1] X. C. Zhong,[1] B. Q. Zhou,[1] G. M. Zhou,[1] L. Zhou,[1] N. F. Zhou,[1] K. J. Zhu,[1] Q. M. Zhu,[1] Yingchun Zhu,[1] Y. C. Zhu,[1] Y. S. Zhu,[1] Z. A. Zhu,[1] B. A. Zhuang,[1] and B. S. Zou[1]

(BES Collaboration)

[1]*Institute of High Energy Physics, Beijing 100039, People's Republic of China*
[2]*China Center of Advanced Science and Technology, Beijing 100080, People's Republic of China*
[3]*Guangxi Normal University, Guilin 541004, People's Republic of China*
[4]*Henan Normal University, Xinxiang 453002, People's Republic of China*
[5]*Huazhong Normal University, Wuhan 430079, People's Republic of China*
[6]*Hunan University, Changsha 410082, People's Republic of China*
[7]*Liaoning University, Shenyang 110036, People's Republic of China*
[8]*Nanjing Normal University, Nanjing 210097, People's Republic of China*
[9]*Nankai University, Tianjin 300071, People's Republic of China*
[10]*Peking University, Beijing 100871, People's Republic of China*
[11]*Shandong University, Jinan 250100, People's Republic of China*
[12]*Shanghai Jiaotong University, Shanghai 200030, People's Republic of China*
[13]*Sichuan University, Chengdu 610064, People's Republic of China*
[14]*Tsinghua University, Beijing 100084, People's Republic of China*
[15]*University of Hawaii, Honolulu, Hawaii 96822, USA*
[16]*University of of Science and Technology of China, Hefei 230026, People's Republic of China*
[17]*Wuhan University, Wuhan 430072, People's Republic of China*
[18]*Zhejiang University, Hangzhou 310028, People's Republic of China*
(Received 13 October 2003; published 5 February 2004)

The decay $\psi(2S) \to K_S^0 K_L^0$ is observed using $\psi(2S)$ data collected with the Beijing Spectrometer at the Beijing Electron-Positron Collider; the branching fraction is determined to be $\mathcal{B}(\psi(2S) \to K_S^0 K_L^0) = (5.24 \pm 0.47 \pm 0.48) \times 10^{-5}$. Compared with $J/\psi \to K_S^0 K_L^0$, the $\psi(2S)$ branching fraction is enhanced relative to the prediction of the perturbative QCD "12%" rule. The result, together with the branching fractions of $\psi(2S)$ decays to other pseudoscalar meson pairs ($\pi^+\pi^-$ and K^+K^-), is used to investigate the relative phase between the three-gluon and the one-photon annihilation amplitudes of $\psi(2S)$ decays.

DOI: 10.1103/PhysRevLett.92.052001 PACS numbers: 13.25.Gv, 12.38.Qk, 14.40.Gx

It has been determined that for many two-body exclusive J/ψ decays, such as vector pseudoscalar (VP), vector-vector, pseudoscalar-pseudoscalar (PP) meson decays, and nucleon-antinucleon decays, the relative phases between the three-gluon and the one-photon annihilation amplitudes are near 90° [1–6]. For $\psi(2S)$ decays, the available information about the phase is much more limited because there are fewer experimental measurements. It has been argued that the relative phases in $\psi(2S)$ decays should be similar to those in J/ψ decays [1,7], but the analysis of $\psi(2S)$ to VP decays in Ref. [1] indicates this phase is likely to be around 180°. Another analysis of this mode though shows the relative phase observed in J/ψ decays could also fit these decays [8], but it could not rule out the 180° possibility due to the big uncertainties in the experimental data. Therefore it is important to measure phases in other $\psi(2S)$ decay modes.

In $\psi(2S) \to$ PP, the currently available measurements on $\pi^+\pi^-$ and K^+K^- are from DASP (DESY double-arm spectrometer) [9], with huge errors. These do not provide enough information to extract the phase since there are three free parameters in the parametrization of the PP amplitudes [4,5,10]. The result for $\psi(2S) \to K_S^0 K_L^0$ is also needed to get the phase [11].

Furthermore, there is a long-standing "$\rho\pi$ puzzle" between J/ψ and $\psi(2S)$ decays in some decay modes; many $\psi(2S)$ decay channels compared with the corresponding J/ψ decays are suppressed relative to the perturbative QCD (pQCD) predicted "12% rule" [12]. It is of great interest to check this in more channels.

In this Letter, the decay $\psi(2S) \to K_S^0 K_L^0$ is reported, and its branching fraction is used to determine the phase between the three-gluon and one-photon annihilation amplitudes and to test the 12% rule between J/ψ and $\psi(2S)$ decays. The data used for the analysis are taken with the Beijing Spectrometer (BESII) detector at the Beijing Electron-Positron Collider (BEPC) storage ring at a center-of-mass energy corresponding to $M_{\psi(2S)}$. The data sample contains a total of $(14.0 \pm 0.7) \times 10^6$ $\psi(2S)$ decays, as determined from inclusive $\psi(2S)$ hadronic decays [13].

BESII is a conventional solenoidal magnet detector that is described in detail in Refs. [14,15]. The subdetectors relevant to this analysis are the main drift chamber (MDC) and the barrel shower counter (BSC). MDC is a 40-layer drift chamber, which provides trajectory and energy loss (dE/dx) information for charged tracks over 85% of the total solid angle. The momentum resolution is $\sigma_p/p = 0.017\sqrt{1+p^2}$ (p in GeV$/c$). The BSC is a 12 r.l., lead-gas electromagnetic calorimeter. It measures the energies of electrons and photons over ~80% of the total solid angle with an energy resolution of $\sigma_E/E = 22\%/\sqrt{E}$ (E in GeV).

A Monte Carlo simulation is used for the determination of the detection efficiency. For the signal channel, $\psi(2S) \to K_S^0 K_L^0$, the angular distribution of the K_S^0 or K_L^0 is generated as $\sin^2\theta$, where θ is the polar angle in the laboratory system. The K_L^0 is allowed to decay and interact with the material in the detector, and for the K_S^0, only $K_S^0 \to \pi^+\pi^-$ is generated. The detector response is simulated using a GEANT3 based Monte Carlo program. Reasonable agreement between data and Monte Carlo simulation has been observed in various channels tested, including $e^+e^- \to (\gamma)e^+e^-$, $e^+e^- \to (\gamma)\mu^+\mu^-$, $J/\psi \to p\bar{p}$, and $\psi(2S) \to \pi^+\pi^- J/\psi$, $J/\psi \to \ell^+\ell^-$ ($\ell = e, \mu$).

Candidate events are required to satisfy the following selection criteria: (i) The number of charged tracks is required to be two with net charge zero. (ii) Each track should satisfy $|\cos\theta| < 0.8$, where θ is the polar angle in the MDC, and should have a good helix fit so that the error matrix from track fitting is available for secondary vertex finding. (iii) $E_\gamma^{\rm tot} < 1.0$ GeV, where $E_\gamma^{\rm tot}$ is the total energy of the neutral clusters in the BSC which are not associated with the charged tracks.

The two tracks are assumed to be π^+ and π^-. To find the intersection of the two tracks, an iterative, nonlinear least squares technique is used. The intersection is taken as the K_S^0 vertex, and the momentum of the K_S^0 is calculated at this point. Figure 1 shows a scatter plot of the $\pi^+\pi^-$ invariant mass versus the decay length in the transverse plane (L_{xy}) for events that satisfy the above selection criteria and have $\pi^+\pi^-$ momentum greater than 1.7 GeV$/c$. The cluster of events with mass consistent with the nominal K_S^0 mass and with a long decay length indicates a clear K_S^0 signal. The lack of events at $L_{xy} > 0.1$ m is due to the trigger, which is discussed later.

Fits of the $\pi^+\pi^-$ invariant mass distributions (not shown) indicate good agreement between data and Monte Carlo simulation in both mass and the mass resolution. After requiring $L_{xy} > 1$ cm and $\pi^+\pi^-$ mass within twice the mass resolution around the K_S^0 nominal mass, the K_S^0 momentum distribution, shown in Fig. 2(a), is obtained. In the plot, there is a clear peak at around 1.77 GeV$/c$ with low background, as indicated by the K_S^0 mass sideband (3σ away from the K_S^0 nominal mass on both sides) events. The excess at lower momentum, which

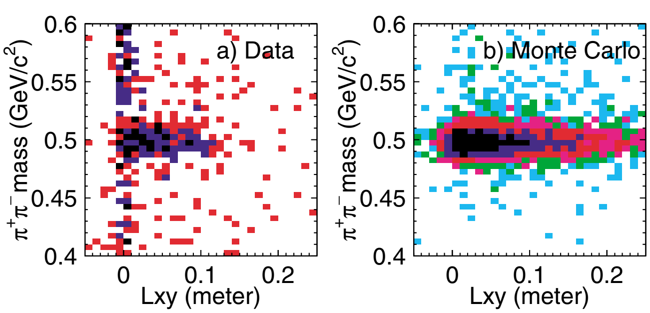

FIG. 1 (color online). Scatter plot of $\pi^+\pi^-$ invariant mass versus the decay length in the transverse plane for events with $\pi^+\pi^-$ momentum greater than 1.7 GeV$/c$ for (a) data and (b) Monte Carlo simulation.

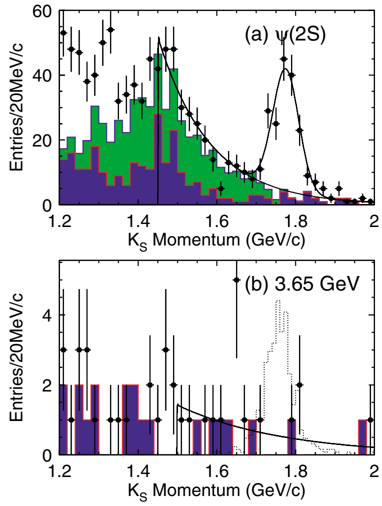

FIG. 2 (color online). The K_S^0 momentum distributions for data at the $\psi(2S)$ peak (a) and at $\sqrt{s} = 3.65$ GeV (b). The dots with error bars are data and the curves shown in the plots are the best fit of the data. For (a), the dark shaded histogram is from K_S^0 mass sideband events, and the light shaded histogram is from the Monte Carlo simulated backgrounds. For (b), the shaded histogram is for K_S^0 mass sideband events, while the dotted histogram is the expected shape of a $K_S^0K_L^0$ signal as determined by Monte Carlo simulation (not normalized).

is not explained by the sideband background, is due to the contribution of the background channels with K_S^0 production.

The main K_S^0 production backgrounds near the signal region are from $\psi(2S) \to K^{*0}(892)\overline{K}^0$ + c.c. and $\psi(2S) \to \gamma\chi_{c1}$, $\chi_{c1} \to K^{*0}(892)\overline{K}^0$ + c.c., where the K^{*0} decays into K^0 and π^0 and one of the K^0s becomes a K_S^0 and the other one becomes a K_L^0. The background from $\psi(2S) \to \gamma\chi_{cJ}(J = 0, 2)$, $\chi_{cJ} \to K_S^0K_S^0$, where one of the K_S^0 decays into $\pi^+\pi^-$ and the other decays into $\pi^0\pi^0$, is removed almost entirely (more than 95%) by the $E_\gamma^{\rm tot}$ requirement, according to the Monte Carlo simulation. The decay $\psi(2S) \to J/\psi + X$ with J/ψ decaying into K_S^0X has a big branching fraction, but the K_S^0 momentum is much lower. The decays χ_{c0} and $\chi_{c2} \to K_S^0K_L^0$ violate CP conservation, and $\chi_{c1} \to K_S^0K_L^0$ violates parity conservation, so they do not contribute to the background. The light shaded histogram in Fig. 2(a) shows the contribution of the background channels normalized to the known branching fractions [16,17]. It can be seen that the agreement between the background estimation and data is good near the $K_S^0K_L^0$ peak, indicating that the estimation of the background under the $K_S^0K_L^0$ peak is reliable.

Under SU(3) symmetry, $K_S^0K_L^0$ production via virtual photon annihilation is forbidden. This is checked by applying the same selection criteria to the data sample taken below the $\psi(2S)$ peak, at $\sqrt{s} = 3.650$ GeV, with an integrated luminosity of about one-third of that at the $\psi(2S)$ peak. Figure 2(b) shows the K_S^0 momentum spectrum of the selected events; the events in the signal region agree well with expectation from the K_S^0 mass sideband events. Taking all four candidates with momentum between 1.7 and 1.9 GeV/c as signal, the upper limit of the production cross section at the 90% C.L. is measured to be $\sigma < 5.9$ pb. The background from the continuum contribution is thus neglected in the following analysis since no evidence for $K_S^0K_L^0$ production via the virtual photon process is observed.

The K_S^0 momentum spectrum of the selected events is fitted from 1.45 to 2.0 GeV/c with a Gaussian distribution for the signal and an exponential for the background using the unbinned maximum likelihood method. The result is shown in Fig. 2(a). The backgrounds from the K_S^0 mass sidebands and the simulated background channels are also shown, and they agree with the fitted background reasonably well near the signal region, considering the uncertainties in the global normalization of the background channels. The peak K_S^0 momentum is (1775.0 ± 3.3) MeV/c, which is in good agreement with the Monte Carlo expectation for $\psi(2S) \to K_S^0K_L^0$. The momentum resolution also agrees well with the Monte Carlo (MC) simulation. The fit yields $n^{\rm obs} = 156 \pm 14$ events, and the efficiency for detecting $\psi(2S) \to K_S^0K_L^0$, with $K_S^0 \to \pi^+\pi^-$ is $\varepsilon_{\rm MC} = (41.59 \pm 0.48)\%$ from the Monte Carlo simulation, where the error is due to the limited statistics of the Monte Carlo sample. The statistical significance of the signal is 13.7σ obtained by comparing fits with signal and with no signal.

Because of the long decay length of the high momentum K_S^0 particles and the trigger requirement for hits in the vertex chamber (VC), the trigger efficiency of $K_S^0K_L^0$ events is very different than for normal hadronic events. Since the trigger system is not included in the Monte Carlo simulation, the trigger efficiency is measured using $K_S^0K_L^0$ events by comparing the number of events beyond and within the outer radius of the VC with what would be expected for an exponential decay, which yields a trigger efficiency of $\varepsilon_{\rm trig} = (76.0 \pm 1.8)\%$. The systematic errors in the branching fraction measurement from this source and all other sources are listed in Table I.

TABLE I. Summary of systematic errors.

Source	Systematic errors (%)
MC statistics	1.2
Trigger efficiency	2.4
Secondary vertex finding	4.1
$E_\gamma^{\rm tot} < 1.0$ GeV	2
MDC tracking	4
Fit range	2.4
Background shape	3.0
$N_{\psi(2S)}$	5
$\mathcal{B}(K_S^0 \to \pi^+\pi^-)$	0.4
Total systematic error	9.2

The efficiency of the secondary vertex finding, ε_{2nd}, is studied using $J/\psi \to K^*(892)\overline{K}$ + c.c. events. It is found that the Monte Carlo simulates data fairly well. Extrapolating the difference between data and Monte Carlo simulation to the K_S^0 momentum range under study and correcting by the polar angle dependence of the efficiency, a correction factor of $(98.1 \pm 4.0)\%$ is obtained to the Monte Carlo efficiency.

The effect of the requirement on the total energy of the photon candidates is checked with $J/\psi \to K_S^0 K_L^0$ events. The efficiency is very high (>90%), and the efficiency difference between data and Monte Carlo simulation is measured to be 0.99 ± 0.01; data are slightly lower than Monte Carlo simulation. No correction to the final efficiency is made, and 2% is taken as the systematic error on the efficiency associated with this requirement.

The simulation of the tracking efficiency agrees with data to within 1%–2% for each charged track as measured using channels like $J/\psi \to \Lambda\overline{\Lambda}$ and $\psi(2S) \to \pi^+\pi^- J/\psi$, $J/\psi \to \mu^+\mu^-$. The systematic error for the channel of interest is taken conservatively as 4%.

The Monte Carlo simulated mass resolution and momentum resolution of the K_S^0 agree with those determined from data within the statistical uncertainties. The requirement that the K_S^0 mass be within 2 standard deviations introduces a very small systematic bias and is neglected.

Varying the lower and upper bounds of the fitting range results in a 2.4% change in the number of the events; using a second order polynomial for the background parametrization causes a 3% change in the number of events. These are taken as systematic errors. The systematic error in the total number of $\psi(2S)$ events, $N_{\psi(2S)}$, which is measured using inclusive hadrons in the same way as in Ref. [13], is taken as 5%. The systematic error on the branching fraction $\mathcal{B}(K_S^0 \to \pi^+\pi^-)$ is obtained from Ref. [17] directly.

Figure 3 shows the cosine of the K_S^0 polar angle for $K_S^0 K_L^0$ events from $\psi(2S)$ decays; agreement between data and Monte Carlo simulation is observed. This distribution is also checked with a larger sample from $J/\psi \to K_S^0 K_L^0$, where the Monte Carlo simulation agrees with data very well. This indicates that the angular distribution used in the Monte Carlo generator is correct.

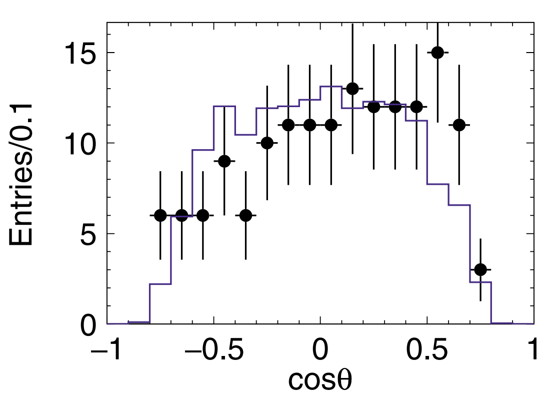

FIG. 3 (color online). Distribution of the cosine of the K_S^0 polar angle of $K_S^0 K_L^0$ events from $\psi(2S)$ decays. Dots with error bars are data, and the histogram is the Monte Carlo simulation.

The branching fraction of $\psi(2S) \to K_S^0 K_L^0$ is calculated with

$$\mathcal{B}(\psi(2S) \to K_S^0 K_L^0) = \frac{n^{\mathrm{obs}}/(\varepsilon_{\mathrm{MC}} \cdot \varepsilon_{\mathrm{trig}} \cdot \varepsilon_{2\mathrm{nd}})}{N_{\psi(2S)} \mathcal{B}(K_S^0 \to \pi^+\pi^-)}.$$

Using numbers from above (listed in Table II), one obtains

$$\mathcal{B}(\psi(2S) \to K_S^0 K_L^0) = (5.24 \pm 0.47 \pm 0.48) \times 10^{-5},$$

where the first error is statistical and the second systematic.

Comparing with the corresponding branching fraction for $J/\psi \to K_S^0 K_L^0$ from BESII $[(1.82 \pm 0.14) \times 10^{-4}]$ [18], one gets

$$Q_h = \frac{\mathcal{B}(\psi(2S) \to K_S^0 K_L^0)}{\mathcal{B}(J/\psi \to K_S^0 K_L^0)} = (28.8 \pm 3.7)\%,$$

where the common errors in the J/ψ and $\psi(2S)$ analyses are removed in the calculation. The result indicates that $\psi(2S)$ decays are enhanced by more than 4σ relative to the 12% rule expected from pQCD, while for almost all other channels where the deviations from the 12% rule are observed, $\psi(2S)$ decays are suppressed.

The branching fraction of $K_S^0 K_L^0$, together with branching fractions of $\psi(2S) \to \pi^+\pi^-$ and $\psi(2S) \to K^+K^-$, can be used to extract the relative phase between the three-gluon and the one-photon annihilation amplitudes of the $\psi(2S)$ decays to pseudoscalar meson pairs. It is found that a relative phase of $(-82 \pm 29)^\circ$ or $(+121 \pm 27)^\circ$ can explain the experimental results [11], where the errors are from the uncertainties of $\mathcal{B}(\psi(2S) \to K_S^0 K_L^0)$ in this analysis and $\pi^+\pi^-$ form factor and $\mathcal{B}(\psi(2S) \to K^+K^-)$ used in Ref. [11].

In summary, the flavor-SU(3)-breaking decay to $K_S^0 K_L^0$ is observed in $\psi(2S)$ decays with the BESII $\psi(2S)$ data sample, and the branching fraction is determined to be $\mathcal{B}(\psi(2S) \to K_S^0 K_L^0) = (5.24 \pm 0.47 \pm 0.48) \times 10^{-5}$.

TABLE II. Numbers used in the branching fraction calculation and the branching fraction result.

Quantity	Value
n^{obs}	156 ± 14
$\varepsilon_{\mathrm{MC}}$ (%)	41.59 ± 0.48
$\varepsilon_{\mathrm{trig}}$ (%)	76.0 ± 1.8
$\varepsilon_{2\mathrm{nd}}$ (%)	98.1 ± 4.0
$N_{\psi(2S)}(10^6)$	14.0 ± 0.7
$\mathcal{B}(K_S^0 \to \pi^+\pi^-)$	0.6860 ± 0.0027 [17]
$\mathcal{B}(\psi(2S) \to K_S^0 K_L^0)(10^{-5})$	$5.24 \pm 0.47 \pm 0.48$

Compared with the branching fraction of $J/\psi \rightarrow K_S^0 K_L^0$, $\psi(2S)$ decays are enhanced relative to the "12%" pQCD prediction. The phases of the three-gluon and the one-photon annihilation amplitudes of $\psi(2S)$ decays to pseudoscalar meson pairs are found to be nearly orthogonal.

The BES Collaboration thanks the staff of BEPC for their hard efforts. This work is supported in part by the National Natural Science Foundation of China under Contracts No. 19991480, No. 10225524, and No. 10225525, by the Chinese Academy of Sciences under Contract No. KJ 95T-03, by the 100 Talents Program of CAS under Contracts No. U-11, No. U-24, and No. U-25, by the Knowledge Innovation Project of CAS under Contracts No. U-602, U-34 (IHEP), by the National Natural Science Foundation of China under Contract No. 10175060 (USTC), and by the Department of Energy under Contract No. DE-FG03-94ER40833 (University of Hawaii).

[1] M. Suzuki, Phys. Rev. D **63**, 054021 (2001); J. L. Rosner, Phys. Rev. D **60**, 074029 (1999).
[2] J. Jousset *et al.*, Phys. Rev. D **41**, 1389 (1990).
[3] D. Coffman *et al.*, Phys. Rev. D **38**, 2695 (1988).
[4] M. Suzuki, Phys. Rev. D **60**, 051501 (1999).
[5] L. Köpke and N. Wermes, Phys. Rep. **174**, 67 (1989).
[6] R. Baldini *et al.*, Phys. Lett. B **444**, 111 (1998).
[7] J. M. Gérard and J. Weyers, Phys. Lett. B **462**, 324 (1999).
[8] P. Wang, C. Z. Yuan, and X. H. Mo, hep-ph/0303144 [Phys. Rev. D (to be published)].
[9] R. Brandelik *et al.*, Z. Phys. C **1**, 233 (1979).
[10] H. E. Haber and J. Perrier, Phys. Rev. D **32**, 2961 (1985).
[11] C. Z. Yuan, P. Wang, and X. H. Mo, Phys. Lett. B **567**, 73 (2003).
[12] BES Collaboration, J. Z. Bai *et al.*, Phys. Rev. D **67**, 052002 (2003).
[13] BES Collaboration, J. Z. Bai *et al.*, Phys. Lett. B **550**, 24 (2002).
[14] BES Collaboration, J. Z. Bai *et al.*, Nucl. Instrum. Methods Phys. Res., Sect. A **344**, 319 (1994).
[15] BES Collaboration, J. Z. Bai *et al.*, Nucl. Instrum. Methods Phys. Res., Sect. A **458**, 627 (2001).
[16] BES Collaboration, J. Z. Bai *et al.*, Phys. Rev. D **60**, 072001 (1999).
[17] Particle Data Group, K. Hagiwara *et al.*, Phys. Rev. D **66**, 010001 (2002).
[18] BES Collaboration, J. Z. Bai *et al.*, Phys. Rev. D **69**, 012003 (2004).

Available online at www.sciencedirect.com
SCIENCE DIRECT®
Physics Letters B 605 (2005) 63–71
PHYSICS LETTERS B
www.elsevier.com/locate/physletb

Evidence of $\psi(3770)$ non-$D\bar{D}$ decay to $J/\psi\pi^+\pi^-$

BES Collaboration

J.Z. Bai [a], Y. Ban [h], J.G. Bian [a], X. Cai [a], J.F. Chang [a], H.F. Chen [n], H.S. Chen [a], J. Chen [g], J.C. Chen [a], Y.B. Chen [a], S.P. Chi [a], Y.P. Chu [a], X.Z. Cui [a], Y.M. Dai [f], Y.S. Dai [p], L.Y. Dong [a], S.X. Du [o], Z.Z. Du [a], J. Fang [a], S.S. Fang [a], C.D. Fu [a], H.Y. Fu [a], L.P. Fu [e], C.S. Gao [a], M.L. Gao [a], Y.N. Gao [l], M.Y. Gong [a], W.X. Gong [a], S.D. Gu [a], Y.N. Guo [a], Y.Q. Guo [a], Z.J. Guo [m], S.W. Han [a], F.A. Harris [m], J. He [a], K.L. He [a], M. He [i], X. He [a], Y.K. Heng [a], T. Hong [a], H.M. Hu [a], T. Hu [a], G.S. Huang [a], L. Huang [e], X.P. Huang [a], X.B. Ji [a], C.H. Jiang [a], X.S. Jiang [a], D.P. Jin [a], S. Jin [a], Y. Jin [a], Z.J. Ke [a], Y.F. Lai [a], F. Li [a], G. Li [a], H.H. Li [d], J. Li [a], J.C. Li [a], K. Li [e], Q.J. Li [a], R.B. Li [a], R.Y. Li [a], W. Li [a], W.G. Li [a], X.Q. Li [g], X.S. Li [l], C.F. Liu [o], C.X. Liu [a], Fang Liu [n], F. Liu [d], H.M. Liu [a], J.B. Liu [a], J.P. Liu [o], R.G. Liu [a], Y. Liu [a], Z.A. Liu [a], Z.X. Liu [a], G.R. Lu [c], F. Lu [a], H.J. Lu [n], J.G. Lu [a], Z.J. Lu [a], X.L. Luo [a], E.C. Ma [a], F.C. Ma [f], J.M. Ma [a], L.L. Ma [i], Z.P. Mao [a], X.C. Meng [a], X.H. Mo [b], J. Nie [a], Z.D. Nie [a], S.L. Olsen [m], H.P. Peng [n], N.D. Qi [a], C.D. Qian [j], J.F. Qiu [a], G. Rong [a], D.L. Shen [a], H. Shen [a], X.Y. Shen [a], H.Y. Sheng [a], F. Shi [a], L.W. Song [a], H.S. Sun [a], S.S. Sun [n], Y.Z. Sun [a], Z.J. Sun [a], S.Q. Tang [a], X. Tang [a], D. Tian [a], Y.R. Tian [l], G.L. Tong [a], G.S. Varner [m], J. Wang [a], J.Z. Wang [a], L. Wang [a], L.S. Wang [a], M. Wang [a], Meng Wang [a], P. Wang [a], P.L. Wang [a], W.F. Wang [a], Y.F. Wang [a], Zhe Wang [a], Z. Wang [a], Zheng Wang [a], Z.Y. Wang [b], C.L. Wei [a], N. Wu [a], X.M. Xia [a], X.X. Xie [a], G.F. Xu [a], Y. Xu [a], S.T. Xue [a], M.L. Yan [n], W.B. Yan [a], G.A. Yang [a], H.X. Yang [l], J. Yang [n], S.D. Yang [a], M.H. Ye [b], Y.X. Ye [n], J. Ying [h], C.S. Yu [a], G.W. Yu [a], J.M. Yuan [a], Y. Yuan [a], Q. Yue [a], S.L. Zang [a], Y. Zeng [e], B.X. Zhang [a], B.Y. Zhang [a], C.C. Zhang [a], D.H. Zhang [a], H.Y. Zhang [a], J. Zhang [a], J.M. Zhang [c], J.W. Zhang [a], L.S. Zhang [a], Q.J. Zhang [a], S.Q. Zhang [a], X.Y. Zhang [i], Y.J. Zhang [h], Yiyun Zhang [k], Y.Y. Zhang [a], Z.P. Zhang [n], D.X. Zhao [a], Jiawei Zhao [n], J.W. Zhao [a], P.P. Zhao [a], W.R. Zhao [a], Y.B. Zhao [a], Z.G. Zhao [a,1], J.P. Zheng [a], L.S. Zheng [a], Z.P. Zheng [a], X.C. Zhong [a], B.Q. Zhou [a], G.M. Zhou [a], L. Zhou [a], N.F. Zhou [a], K.J. Zhu [a], Q.M. Zhu [a], Yingchun Zhu [a], Y.C. Zhu [a], Y.S. Zhu [a], Z.A. Zhu [a], B.A. Zhuang [a], B.S. Zou [a]

doi:10.1016/j.physletb.2004.11.029

[a] *Institute of High Energy Physics, Beijing 100039, People's Republic of China*
[b] *China Center of Advanced Science and Technology, Beijing 100080, People's Republic of China*
[c] *Henan Normal University, Xinxiang 453002, People's Republic of China*
[d] *Huazhong Normal University, Wuhan 430079, People's Republic of China*
[e] *Hunan University, Changsha 410082, People's Republic of China*
[f] *Liaoning University, Shenyang 110036, People's Republic of China*
[g] *Nankai University, Tianjin 300071, People's Republic of China*
[h] *Peking University, Beijing 100871, People's Republic of China*
[i] *Shandong University, Jinan 250100, People's Republic of China*
[j] *Shanghai Jiaotong University, Shanghai 200030, People's Republic of China*
[k] *Sichuan University, Chengdu 610064, People's Republic of China*
[l] *Tsinghua University, Beijing 100084, People's Republic of China*
[m] *University of Hawaii, Honolulu, HI 96822, USA*
[n] *University of Science and Technology of China, Hefei 230026, People's Republic of China*
[o] *Wuhan University, Wuhan 430072, People's Republic of China*
[p] *Zhejiang University, Hangzhou 310028, People's Republic of China*

Received 7 July 2004; accepted 10 November 2004

Available online 19 November 2004

Editor: M. Doser

Abstract

Evidence of $\psi(3770)$ decays to a non-$D\bar{D}$ final state is observed. A total of $11.8 \pm 4.8 \pm 1.3$ $\psi(3770) \to J/\psi\pi^+\pi^-$ events are obtained from a data sample of 27.7 pb^{-1} taken at center-of-mass energies around 3.773 GeV using the BES-II detector at the BEPC. The branching fraction is determined to be $\text{BF}(\psi(3770) \to J/\psi\pi^+\pi^-) = (0.34 \pm 0.14 \pm 0.09)\%$, corresponding to the partial width of $\Gamma(\psi(3770) \to J/\psi\pi^+\pi^-) = (80 \pm 33 \pm 23)$ keV.

1. Introduction

The $\psi(3770)$ resonance is believed to be a mixture of the 1^3D_1 and 2^3S_1 states of the $c\bar{c}$ system [1]. Since its mass is above the open charm-pair threshold and its width is two orders of magnitude larger than that of the $\psi(2S)$, it is thought to decay almost entirely to pure $D\bar{D}$ [2]. However, Lipkin pointed out that the $\psi(3770)$ could decay to non-$D\bar{D}$ final states with a large branching fraction [3]. There are theoretical calculations [4–7] that estimate the partial width for $\Gamma(\psi(3770) \to J/\psi\pi^+\pi^-)$ based on the multipole expansion in QCD. Recently Kuang [7] used the Chen–Kuang potential model to obtain a partial width for $\psi(3770) \to J/\psi\pi\pi$ in the range from 37 to 170 keV, corresponding to 25 to 113 keV for $\psi(3770) \to J/\psi\pi^+\pi^-$ from isospin symmetry. In this Letter, we report evidence for $\psi(3770) \to J/\psi\pi^+\pi^-$ based on a data sample of 27.7 pb^{-1} taken in the center-of-mass (c.m.) energy region from 3.738 to 3.885 GeV using the upgraded Beijing spectrometer (BES-II) at the Beijing electron–positron collider (BEPC).

2. The BES-II detector

The BES-II is a conventional cylindrical magnetic detector that is described in detail in Ref. [8]. A 12-layer vertex chamber (VC) surrounding the beryllium beam pipe provides input to the event trigger, as well as coordinate information. A forty-layer main drift chamber (MDC) located just outside the VC yields precise measurements of charged particle trajectories

E-mail address: rongg@mail.ihep.ac.cn (G. Rong).

[1] Visiting professor to University of Michigan, Ann Arbor, MI 48109, USA.

with a solid angle coverage of 85% of 4π; it also provides ionization energy loss (dE/dx) measurements which are used for particle identification. Momentum resolution of $1.7\%\sqrt{1+p^2}$ (p in GeV/c) and dE/dx resolution of 8.5% for Bhabha scattering electrons are obtained for the data taken at $\sqrt{s} = 3.773$ GeV. An array of 48 scintillation counters surrounding the MDC measures the time of flight (TOF) of charged particles with a resolution of about 180 ps for electrons. Outside the TOF, a 12 radiation length, lead-gas barrel shower counter (BSC), operating in limited streamer mode, measures the energies of electrons and photons over 80% of the total solid angle with an energy resolution of $\sigma_E/E = 0.22/\sqrt{E}$ (E in GeV) and spatial resolutions of $\sigma_\phi = 7.9$ mrad and $\sigma_Z = 2.3$ cm for electrons. A solenoidal magnet outside the BSC provides a 0.4 T magnetic field in the central tracking region of the detector. Three double-layer muon counters instrument the magnet flux return and serve to identify muons with momentum greater than 500 MeV/c. They cover 68% of the total solid angle.

3. Data analysis

3.1. Monte Carlo simulation

To understand the main source of background in the study of the decay $\psi(3770) \to J/\psi\pi^+\pi^-$, we developed a Monte Carlo generator. The Monte Carlo simulation includes the initial state radiation (ISR) at one-loop order, in which the actual center-of-mass energies after ISR are generated according to Ref. [9]. The $\psi(2S)$ and $\psi(3770)$ are generated using energy dependent Breit–Wigner functions according to Eq. (38.53) of Ref. [10] in which the ratio of $\Gamma_{\mathrm{el}}(s)/\Gamma_{\mathrm{tot}}(s) = \Gamma_{\psi(2S)\to e^+e^-}/\Gamma_{\mathrm{tot}}$ and the branching fraction of $\psi(2S) \to J/\psi\pi^+\pi^-$ in the formula are assumed to be constant. The beam energy spread ($\sigma_{E_{\mathrm{beam}}} = 1.37$ MeV) is taken into account in the simulation. Since there is no unique description and solution for the low energy $\pi\pi$ production amplitude [11], the correction of the decay rate due to the $\pi\pi$ production amplitude is neglected in the making of the event generator. However, the effect of the variations in the correction to the decay rate on the estimated number of $\psi(2S) \to J/\psi\pi^+\pi^-$ is considered in the final background subtraction in Section 3.5. Fig. 1 shows the distribution of $J/\psi\pi^+\pi^-$ events with $J/\psi \to l^+l^-$ ($l = e$ or μ) as a function of the actual energy remaining after initial state photon radiation, which is determined by our Monte Carlo generator, where the branching fraction for $\psi(3770) \to J/\psi\pi^+\pi^-$ is set to be 0.35%, while the branching fractions for $\psi(2S) \to J/\psi\pi^+\pi^-$ and $J/\psi \to l^+l^-$ are taken from the Particle Data Group (PDG) [10].

There are two peaks which are around 3.686 and 3.773 GeV in Fig. 1, where the $J/\psi\pi^+\pi^-$ events from the $\psi(2S)$ decay are given by the dotted histogram, while the events from the $\psi(3770)$ decay are given by the solid histogram. There are two components in the higher mass peak. One is from $\psi(3770)$ production, and the another is from $\psi(2S)$ production which is due to the tail of $\psi(2S)$ Breit–Wigner function. This type of $\psi(2S)$ production (called type B of $\psi(2S)$ in this Letter) is indicated by the dotted histogram around 3.773 GeV. The $J/\psi\pi^+\pi^-$ events in the lower mass peak are produced around the peak of the $\psi(2S)$ Breit–Wigner function (called type A of $\psi(2S)$ in this Letter), and are due to ISR energy re-

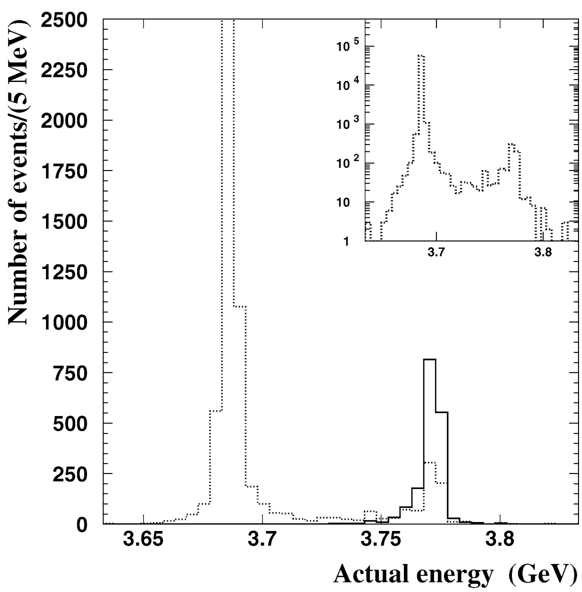

Fig. 1. The numbers of $\psi(3770) \to J/\psi\pi^+\pi^-$ (solid line) and $\psi(2S) \to J/\psi\pi^+\pi^-$ (dotted line) as a function of the actual energy remaining after ISR, where J/ψ is set to decay to l^+l^-; the events are generated with the Monte Carlo generator at the c.m. energies at which the data were collected from 3.738 to 3.885 GeV. The insert on the right-top shows the distribution of the energy at which $\psi(2S) \to J/\psi\pi^+\pi^-$ events are produced.

turn to the $\psi(2S)$ peak. The "type B" of $\psi(2S)$ is the main source of background events in the experimental study of the decay $\psi(3770) \to J/\psi\pi^+\pi^-$. This background event has the same topology as that as the decay of $\psi(3770) \to J/\psi\pi^+\pi^-$. To get the number of $\psi(3770) \to J/\psi\pi^+\pi^-$ signal events, the number of the background events of $\psi(2S) \to J/\psi\pi^+\pi^-$ has to be subtracted from the observed candidate events of $J/\psi\pi^+\pi^-$ based on analyzing the Monte Carlo events.

In the energy region from 3.738 to 3.885 GeV in Fig. 1, there are 1724 $\psi(3770) \to J/\psi\pi^+\pi^-$ events and 747 $\psi(2S) \to J/\psi\pi^+\pi^-$ events. The generated events as shown in Fig. 1 are put through the full detector simulation based on the GEANT simulation package. The fully simulated events are used for study of the main background.

3.2. Events selection

To search for the decay of $\psi(3770) \to J/\psi\pi^+\pi^-$, $J/\psi \to e^+e^-$ or $\mu^+\mu^-$, $\mu^+\mu^-\pi^+\pi^-$ and $e^+e^-\pi^+\pi^-$ candidate events are selected. These are required to have four charged tracks with zero total charge. Each track is required to have a good helix fit, to be consistent with originating from the primary event vertex, and to satisfy $|\cos\theta| < 0.85$, where θ is the polar angle.

Pions and leptons must satisfy particle identification requirements. For pions, the combined confidence level (CL), calculated for the π hypothesis using the dE/dx and TOF measurements, is required to be greater than 0.1%. In order to reduce γ conversion background, in which the e^+ and e^- from a converted γ are misidentified as π^+ and π^-, an opening angle cut, $\theta_{\pi^+\pi^-} > 20°$, is imposed. For electron identification, the combined confidence level, calculated for the e hypothesis using the dE/dx, TOF and BSC measurements, is required to be greater than 1%, and the ratio $CL_e/(CL_e + CL_\mu + CL_\pi + CL_K)$ is required to be greater than 0.7. If a charged track hits the muon counter, and the z and $r\phi$ positions of the hit match with the extrapolated positions of the reconstructed MDC track, the charged track is identified as a muon.

The candidate events of $e^+e^-\pi^+\pi^-$ or $\mu^+\mu^-\pi^+\pi^-$ satisfying the above selection criteria are further analyzed by using two different analysis methods to be discussed in Sections 3.3 and 3.4.

3.3. Analysis of the $\pi^+\pi^-$ recoil mass

The mass recoiling against the $\pi^+\pi^-$ system is calculated using

$$M_{\mathrm{REC}}(\pi^+\pi^-) = \sqrt{(E_{\mathrm{cm}} - E_{\pi^+\pi^-})^2 - |\vec{P}_{\pi^+\pi^-}|^2},$$

where E_{cm} is the c.m. energy, $E_{\pi^+\pi^-}$ and $\vec{P}_{\pi^+\pi^-}$ are the total energy and momentum of the $\pi^+\pi^-$ system, respectively.

Fig. 2 shows the distribution of the masses recoiling against the $\pi^+\pi^-$ system for candidate events with total energy within $\pm 2.5\sigma_{E_{\pi^+\pi^-l^+l^-}}$ of the nominal c.m. energy at which the events were obtained and with a dilepton invariant mass within ± 150 MeV of the J/ψ mass, where $\sigma_{E_{\pi^+\pi^-l^+l^-}}$ is the standard deviation of the distribution of the energy of the $\pi^+\pi^-l^+l^-$. Two peaks are observed. The higher one is from the "type A" of $\psi(2S)$ events produced by radiative return to the peak of the $\psi(2S)$, while the small enhancement around 3.1 GeV is mostly from $\psi(3770)$ decays, but also contains the contamination of the "type B" of $\psi(2S)$ decays. This is confirmed by analyzing the Monte Carlo sample generated with the Monte Carlo generator as mentioned before. Fig. 3 shows the

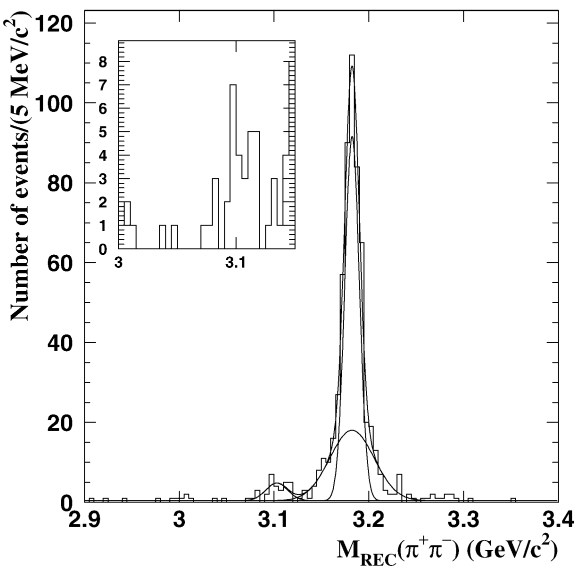

Fig. 2. The distribution of the masses recoiling from the $\pi^+\pi^-$ system for $l^+l^-\pi^+\pi^-$ events; the insert on the left-top shows the mass distribution in a local region around 3.1 GeV; the curves give the best fit to the recoil mass spectrum, see text.

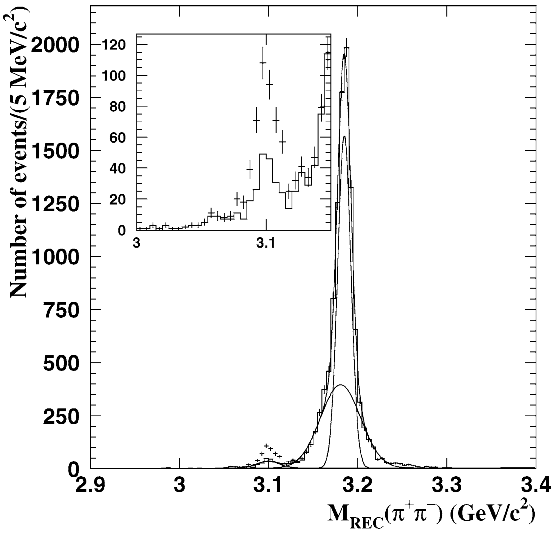

Fig. 3. The distribution of the masses recoiling from $\pi^+\pi^-$ for the Monte Carlo events of $\psi(2S) \to J/\psi\pi^+\pi^-$ and $\psi(3770) \to J/\psi\pi^+\pi^-$ with $J/\psi \to l^+l^-$; these events are generated with the Monte Carlo generator; where the error bars represent the sum total of the two components, while the histogram is for the $\psi(2S) \to J/\psi\pi^+\pi^-$ from both the "type A" and "type B" of $\psi(2S)$; the curves give the best fits to the recoil mass spectrum from the Monte Carlo $\psi(2S) \to J/\psi\pi^+\pi^-$ events only; the insert on the left-top shows the mass distribution in a local region around 3.1 GeV; here two components from the $\psi(3770) \to J/\psi\pi^+\pi^-$ and the "type B" of $\psi(2S) \to J/\psi\pi^+\pi^-$ are clearly seen.

same distribution from analysis of the Monte Carlo events for $\psi(2S)$ and $\psi(3770)$ production and decays to $J/\psi\pi^+\pi^-$ with $J/\psi \to l^+l^-$ final states. The Monte Carlo events are generated at the c.m. energies at which the data were collected. The size of the Monte Carlo sample is twenty times larger than the data. There are also two peaks; the higher one is from the "type A" of $\psi(2S)$ events; the small enhancement around 3.1 GeV consist of two components. One is from the "type B" of $\psi(2S)$ event production and decays as shown by the solid line histogram; the other one is from $\psi(3770)$ production and decays which come from the events as shown by the solid histogram in Fig. 1. The error bars in Fig. 3 are based on the total number of observed events of $\psi(3770) \to J/\psi\pi^+\pi^-$ and $\psi(2S) \to J/\psi\pi^+\pi^-$. The differences between the error bars and the histogram as shown around 3.1 GeV correspond to $\psi(3770)$ production and decay to $J/\psi\pi^+\pi^-$.

Monte Carlo studies show that the distributions of the masses recoiling from the $\pi^+\pi^-$ system for the

Table 1
Summary of the fitted results of the data and the Monte Carlo sample in Figs. 2 and 3

Figures	Peak	Mass [MeV]	σ_M [MeV]
Fig. 2	Peak1	3097.8 ± 3.0	9.9 ± 2.4
	Peak2	3182.4 ± 1.8	23.3 ± 2.8
	Peak3	3182.5 ± 0.6	7.6 ± 0.7
Fig. 3	Peak1	3099.4 ± 1.3	13.1 ± 2.9
	Peak2	3180.8 ± 0.4	22.4 ± 0.7
	Peak3	3185.0 ± 0.2	7.4 ± 0.2

"type A" of $\psi(2S)$ events can be described by two Gaussian functions. One Gaussian function is for the "type A" of $\psi(2S)$ production from the events for which the nominal c.m. energy is set at 3.773 GeV, and the other one is from the events for which the nominal c.m. energies are set off 3.773 GeV. Using triple Gaussian functions, one of which describes the peak near the J/ψ mass and two of which represent the second and the third peaks of the events from the "type A" of $\psi(2S)$, and a first order polynomial to represent the background to fit the mass distributions as shown by the solid histograms for both the data (Fig. 2) and the Monte Carlo (Fig. 3) sample, we obtain a total of 25.5 ± 5.9 $J/\psi \to l^+l^-$ signal events from both the $\psi(3770) \to J/\psi\pi^+\pi^-$ and the "type B" of $\psi(2S) \to J/\psi\pi^+\pi^-$ events and 220.5 ± 26.0 "type B" of $\psi(2S) \to J/\psi\pi^+\pi^-$ events, respectively. The curves give the best fits to the data and the Monte Carlo sample. The fitted peak positions and standard deviations of the Gaussian functions used for the fits in Figs. 2 and 3 are listed in Table 1.

3.4. Kinematic fit

In order to reduce background and improve momentum resolution, candidate events are subjected to four-constraint kinematic fits to either the $e^+e^- \to \mu^+\mu^-\pi^+\pi^-$ or the $e^+e^- \to e^+e^-\pi^+\pi^-$ hypothesis. Events with a confidence level greater than 1% are accepted. Fig. 4 shows the dilepton masses determined from the fitted lepton momenta of the accepted events. There are clearly two peaks. The lower mass peak is mostly due to $\psi(3770) \to J/\psi\pi^+\pi^-$, while the higher one is due to the "type A" of $\psi(2S) \to J/\psi\pi^+\pi^-$. Since the higher mass peak is produced by the radiative return to the $\psi(2S)$ peak, its energy will be approximately 3.686 GeV, while the c.m. energy is set to the nominal energy in the kine-

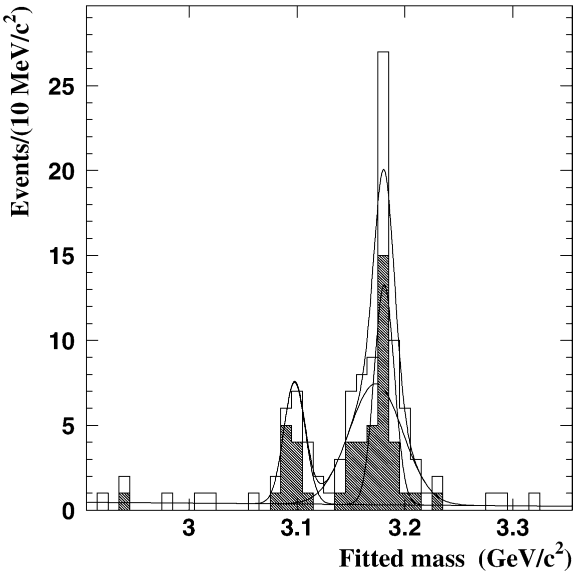

Fig. 4. The distribution of the fitted dilepton masses for the events of $l^+l^-\pi^+\pi^-$ from the data; the hatched histogram is for $\mu^+\mu^-\pi^+\pi^-$, while the open one is for $e^+e^-\pi^+\pi^-$; the curves give the best fit to the data.

matic fitting. Therefore, the dilepton masses calculated based on the fitted lepton momenta from $\psi(2S) \to J/\psi\pi^+\pi^-$, $J/\psi \to l^+l^-$ are shifted upward to about 3.18 GeV.

A maximum likelihood fit to the mass distribution in Fig. 4, using three Gaussian functions to describe the mass distribution of the $l^+l^-\pi^+\pi^+$ combinations and a first order polynomial to represent the broad background as used to fit the $\pi^+\pi^-$ recoil mass distributions in Figs. 2 and 3, yields a J/ψ mass value of 3097.8 ± 3.0 MeV and a signal of 17.8 ± 4.8 $J/\psi \to l^+l^-$ events. The curves give the best fit to the data.

As discussed in Section 3.3, there is a contribution from the "type B" of $\psi(2S) \to J/\psi\pi^+\pi^-$ that can pass the event selection criteria and can lead to an accumulation of the recoil masses of the $\pi^+\pi^-$ and/or the fitted dilepton masses around 3.097 GeV. This is the main source of background to $\psi(3770) \to J/\psi\pi^+\pi^-$. Fig. 5 shows the distribution of the fitted dilepton masses of the Monte Carlo events of $\psi(3770) \to J/\psi\pi^+\pi^-$ and $\psi(2S) \to J/\psi\pi^+\pi^-$ with $J/\psi \to l^+l^-$ as shown in Fig. 1. Here the histogram shows the dilepton mass distribution for $\psi(2S) \to J/\psi\pi^+\pi^-$ only. The higher mass peak is due to the "type A" of $\psi(2S) \to J/\psi\pi^+\pi^-$ events,

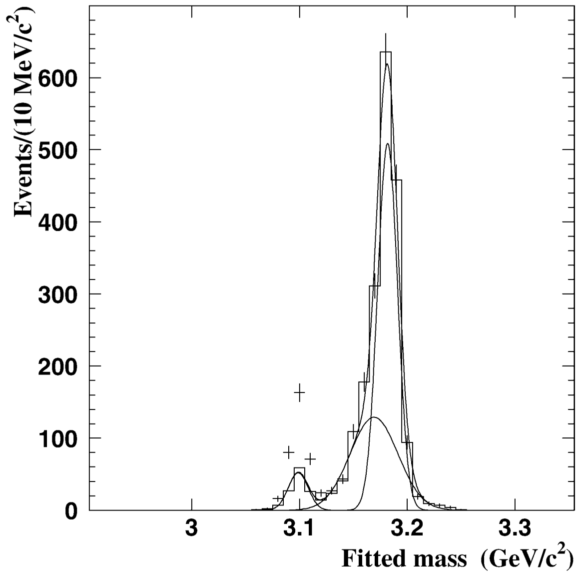

Fig. 5. The distribution of the fitted dilepton masses for the events of $l^+l^-\pi^+\pi^-$ from the Monte Carlo sample of $\psi(3770) \to J/\psi\pi^+\pi^-$ and $\psi(2S) \to J/\psi\pi^+\pi^-$ which are generated with the Monte Carlo generator (see Section 3.1); the histogram is for $\psi(2S) \to J/\psi\pi^+\pi^-$, while the error bars are the sum of $\psi(3770) \to J/\psi\pi^+\pi^-$ and $\psi(2S) \to J/\psi\pi^+\pi^-$, where the J/ψ is set to decay to l^+l^-.

and the lower one is from the "type B" of $\psi(2S) \to J/\psi\pi^+\pi^-$ events. The error bars show the sum total of the observed events of $\psi(2S) \to J/\psi\pi^+\pi^-$ and $\psi(3770) \to J/\psi\pi^+\pi^-$. The differences between the error bars and the histogram correspond to the observed events of $\psi(3770) \to J/\psi\pi^+\pi^-$. Fitting the mass distribution for the $\psi(2S)$ events only (histogram) with the same triple Gaussian functions as mentioned before yields 119 ± 12.1 J/ψ events from the "type B" of $\psi(2S) \to J/\psi\pi^+\pi^-$ decays.

3.5. Other background and background subtraction

3.5.1. Other background

Some physics processes, such as two-photon events, $e^+e^- \to e^+e^-\mu^+\mu^-$ (where the slow muons are misidentified as pions) and $e^+e^- \to e^+e^-\pi^+\pi^-$, $e^+e^- \to \tau^+\tau^-$ and $e^+e^- \to D\bar{D}$ could be sources of background.

To check if there are some background contaminations in the observed $J/\psi\pi^+\pi^-$ events due to the possible sources of background, we generated 1×10^5

two-photon Monte Carlo events (which is about 4 times larger than the data), 6×10^5 $e^+e^- \to$ *hadrons* Monte Carlo events (which is about 1.6 times larger than the data), and 2.3×10^6 $e^+e^- \to D\bar{D}$ Monte Carlo events (which is about 13 times larger than the data), where the D and $\bar{D}$ mesons are set to decay to all possible final states according to the decay modes and branching fractions quoted from PDG [10]. These Monte Carlo events are fully simulated with the GEANT-based simulation package. None of the simulated possible background events were misidentified as $J/\psi\pi^+\pi^-$ events.

The candidate $J/\psi\pi^+\pi^-$ events could also be produced in the continuum process, such as $e^+e^- \to l^+l^-\pi^+\pi^-$ and $e^+e^- \to \tau^+\tau^-$, and satisfy the selection criteria. From analyzing a sample of 6.6 pb^{-1} taken at 3.65 GeV with the BES-II detector, a sample of 5.1 pb^{-1} taken in the energy region from 3.544 to 3.600 GeV and a sample of 22.3 pb^{-1} taken at 4.03 GeV with the BES-I detector, no significant $J/\psi\pi^+\pi^-$, $J/\psi \to l^+l^-$ events are observed. Fig. 6 shows the distribution of the fitted dilepton masses of the events of $l^+l^-\pi^+\pi^-$ which satisfy the selection criteria; these events are from the data taken with the BES-I detector at 4.03 GeV. The distribution of the fitted dilepton masses is flat, which is consistent with the background distribution. Hence the continuum background is negligible.

3.5.2. Number of background

After normalizing to the total luminosity of the data set, we estimate that there are $11.0 \pm 1.3 \pm 2.4$ background events from the "type B" of $\psi(2S) \to J/\psi\pi^+\pi^-$ in the 25.5 ± 5.9 $J/\psi \to l^+l^-$ signal events obtained by fitting to the $\pi^+\pi^-$ recoil mass distribution of Fig. 2 and $6.0 \pm 0.5 \pm 1.3$ background events from the "type B" of $\psi(2S) \to J/\psi\pi^+\pi^-$ in the 17.8 ± 4.8 $J/\psi \to l^+l^-$ signal events obtained by fitting to the fitted dilepton mass distribution of Fig. 4, where the first errors are statistical and the second are systematic. The later arise from the uncertainties (± 1.1) and (± 0.6) in the $\psi(2S)$ resonance parameters and the uncertainties (± 2.2) and (± 1.2) coming from the ambiguities of the knowledge of the low energy $\pi\pi$ production amplitude in $\psi(2S) \to J/\psi\pi^+\pi^-$. The two terms correspond to the uncertainty on the production amplitude predicted by different theoretical models [11] for analyzing the $\pi^+\pi^-$ recoil mass spectrum and the fitted dilepton mass spectrum, respectively. The theoretical models are based on the PCAC and current algebra or chiral perturbative theory predictions in which the various $\pi^+\pi^-$ rescattering corrections are taken into account to get better unitarity behavior at higher energy.

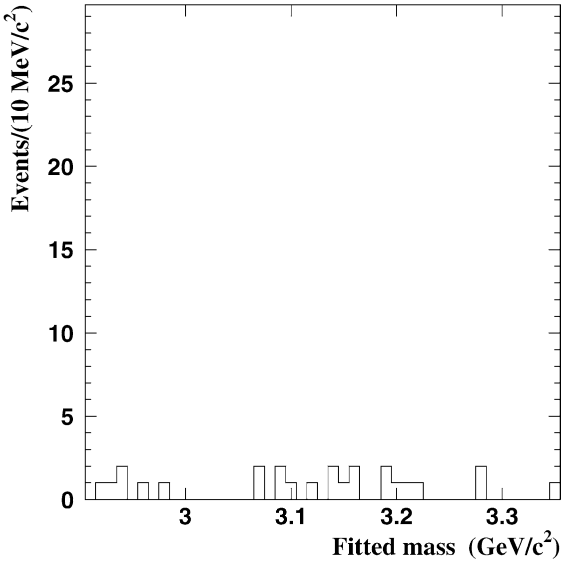

Fig. 6. The distribution of the dilepton masses of the events of $l^+l^-\pi^+\pi^-$ from the data taken at 4.03 GeV with the BES-I at the BEPC.

3.6. Number of signal events $\psi(3770) \to J/\psi\pi^+\pi^-$

The probability that the 17.8 events observed are due to a fluctuation of the $6.0 \pm 0.5 \pm 1.3$ events is 1.1×10^{-3}. After subtracting the numbers of the background events, $14.5 \pm 6.4 \pm 2.4$ and $11.8 \pm 4.8 \pm 1.3$ signal events of $\psi(3770) \to J/\psi\pi^+\pi^-$ are retained from analyzing the recoil masses of $\pi^+\pi^-$ (see Fig. 2) and the fitted dilepton masses (see Fig. 4) of the events $l^+l^-\pi^+\pi^-$, respectively.

In this analysis, the possible interference between the $\psi(2S)$ background and the $\psi(3770)$ signal is neglected since the decay wave functions of $\psi(3770)$ and $\psi(2S)$ are orthogonal [6]. The BES detector is symmetric enough in the spatial direction and there is no bias for the event selections about the momentum direction of the particles. Therefore the interference terms cancel after integrating over the pion momenta.

To test whether there is any bias in the kinematic fit, we examine the $\pi^+\pi^-$ recoil mass distribution

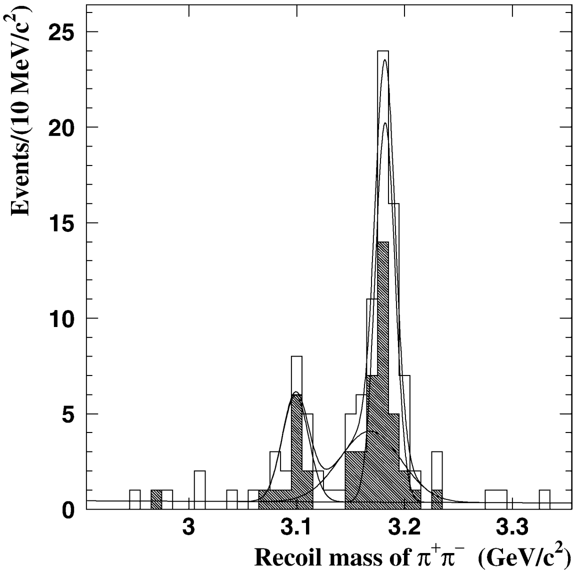

Fig. 7. The distribution of the masses recoiling against the $\pi^+\pi^-$ system calculated using the measured momenta for events that pass the kinematic fit requirement, where the hatched histogram is for events of $\mu^+\mu^-\pi^+\pi^-$ and the open one is for $e^+e^-\pi^+\pi^-$.

for the events passing the kinematic fit requirements. Fig. 7 shows the recoil mass distribution, where the recoil masses are calculated as mentioned in Section 3.3, but the events are not required to satisfy the total energy cut and dilepton invariant mass cut. There are also two peaks, similar to those in Fig. 4, observed clearly. Fitting to the mass spectrum with the same functions as described above yields a J/ψ mass value of 3100.1 ± 3.8 MeV and a signal of 17.2 ± 5.0 events, consistent with the 17.8 ± 4.8 signal events obtained by fitting to the dilepton mass distribution in Fig. 4.

Table 2 summarizes the fitted peak positions and standard deviations of the Gaussian functions used for the fits in Figs. 4, 5 and 7.

3.7. The number of $\psi(3770)$ produced

The total number of $\psi(3770)$ events is obtained from our measured luminosities at each c.m. energy and from calculated cross sections for $\psi(3770)$ production at these energies. The Born level cross section at energy E is given by

$$\sigma^B_{\psi(3770)}(E) = \frac{12\pi\Gamma_{ee}\Gamma_{\text{tot}}(E)}{(E^2 - M^2)^2 + M^2\Gamma^2_{\text{tot}}(E)},$$

Table 2
Summary of the fitted results of the data and Monte Carlo sample in Figs. 4, 5 and 7

Figures	Peak	Mass [MeV]	σ_M [MeV]
Fig. 4	Peak1	3097.8 ± 3.0	9.9 ± 2.4
	Peak2	3173.1 ± 5.5	24.8 ± 5.7
	Peak3	3180.9 ± 2.4	9.3 (fixed)
Fig. 5	Peak1	3098.8 ± 0.7	9.1 ± 0.5
	Peak2	3169.2 ± 0.7	22.2 ± 0.5
	Peak3	3181.8 ± 0.2	9.3 (fixed)
Fig. 7	Peak1	3100.1 ± 3.8	13.2 ± 3.5
	Peak2	3177.1 ± 3.9	19.6 (fixed)
	Peak3	3185.4 (fixed)	7.0 (fixed)

where the $\psi(3770)$ resonance parameters, Γ_{ee} and M, are taken from the PDG [10] and $\Gamma_{\text{tot}}(E)$ is chosen to be energy dependent and normalized to the total width Γ_{tot} at the peak of the resonance [10,12,13]. In order to obtain the observed cross section, it is necessary to correct for ISR. The observed $\psi(3770)$ cross section, $\sigma^{\text{obs}}_{\psi(3770)}(s_{\text{nom}})$, is reduced by a factor $g(s_{\text{nom}}) = \sigma^{\text{obs}}_{\psi(3770)}(s_{\text{nom}})/\sigma^B_{\psi(3770)}(s_{\text{nom}})$, where s_{nom} is the c.m. energy squared and $\sigma^B_{\psi(3770)}(s_{\text{nom}})$ is the Born cross section. The ISR correction for $\psi(3770)$ production is calculated using a Breit–Wigner function and the radiative photon energy spectrum [9,13]. With the calculated cross sections for $\psi(3770)$ production at each energy point around 3.773 GeV and the corresponding luminosities, the total number of $\psi(3770)$ events in the data sample is determined to be $N^{\text{prod}}_{\psi(3770)} = (1.85 \pm 0.37) \times 10^5$, where the error is mainly due to the uncertainty in the observed cross section for $\psi(3770)$ production.

4. Result

4.1. Monte Carlo efficiency

The efficiencies for reconstruction of the events of $\psi(3770) \to J/\psi\pi^+\pi^-$ with $J/\psi \to e^+e^-$ and $J/\psi \to \mu^+\mu^-$ are estimated by Monte Carlo simulation. Monte Carlo study shows that the efficiencies are $\epsilon_{\psi(3770)\to J/\psi\pi^+\pi^-, J/\psi\to e^+e^-} = 0.146 \pm 0.003$ and $\epsilon_{\psi(3770)\to J/\psi\pi^+\pi^-, J/\psi\to\mu^+\mu^-} = 0.174 \pm 0.003$, where the errors are statistical. These give the averaged efficiency for detection of $J/\psi \to e^+e^-$ and

$J/\psi \to \mu^+\mu^-$ events to be

$$\epsilon_{\psi(3770)\to J/\psi\pi^+\pi^-, J/\psi\to l^+l^-} = 0.160 \pm 0.002.$$

4.2. Branching fraction and partial width

Using these numbers and the known branching fractions for $J/\psi \to e^+e^-$ and $\mu^+\mu^-$ [10], the branching fraction for the non-$D\bar{D}$ decay $\psi(3770) \to J/\psi\pi^+\pi^-$ is measured to be

$$\mathrm{BF}\big(\psi(3770) \to J/\psi\pi^+\pi^-\big) = (0.338 \pm 0.143 \pm 0.086)\%,$$

where the first error is statistical and the second systematic arising from the uncertainties in the total number of $\psi(3770)$ produced (20%), tracking efficiency (2.0% per track), particle identification (2.2%), background shape (6%), $\psi(2S) \to J/\psi\pi^+\pi^-$ background subtraction (12%) and the averaged branching fraction for $J/\psi \to l^+l^-$ (1.2%). Adding these uncertainties in quadrature yields the total systematic error of 25.5%.

Using Γ_{tot} from the PDG [10], this branching fraction corresponds to a partial width of

$$\Gamma\big(\psi(3770) \to J/\psi\pi^+\pi^-\big) = (80 \pm 33 \pm 23)\ \mathrm{keV},$$

where the first error is statistical and the second systematic. The systematic uncertainty in the measured partial width arises from the systematic uncertainty in the measured branching fraction (25.5%) and the uncertainty in the total width of $\psi(3770)$ (11.5%) [10].

As a consistency check, we can use the number of signal events $\psi(3770) \to J/\psi\pi^+\pi^-$ obtained from analyzing the recoil masses of the $\pi^+\pi^-$ from the events $l^+l^-\pi^+\pi^-$ to calculate the branching fraction. The detection efficiency is

$$\epsilon_{\psi(3770)\to J/\psi\pi^+\pi^-, J/\psi\to l^+l^-} = 0.194.$$

These numbers yield a branching fraction $\mathrm{BF}(\psi(3770) \to J/\psi\pi^+\pi^-) = (0.342 \pm 0.142 \pm 0.097)\%$, which is in good agreement with the value obtained above, indicating that the kinematic fit result is reliable.

5. Summary

In summary, the branching fraction for $\psi(3770) \to J/\psi\pi^+\pi^-$ has been measured. From a total of $(1.85 \pm 0.37) \times 10^5$ $\psi(3770)$ events, $11.8 \pm 4.8 \pm 1.3$ non-$D\bar{D}$ decays of $\psi(3770) \to J/\psi\pi^+\pi^-$ events are observed, leading to a branching fraction of $\mathrm{BF}(\psi(3770) \to J/\psi\pi^+\pi^-) = (0.34 \pm 0.14 \pm 0.09)\%$, and a partial width $\Gamma(\psi(3770) \to J/\psi\pi^+\pi^-) = (80 \pm 33 \pm 23)$ keV.

Acknowledgements

We would like to thank the BEPC staff for their strong efforts and the members of the IHEP computing center for their helpful assistance. We acknowledge Professor Yu-Ping Kuang and Professor Kuang-Ta Chao for many helpful discussions on the non-$D\bar{D}$ decay of $\psi(3770)$. This work is supported in part by the National Natural Science Foundation of China under contracts Nos. 19991480, 10225524, 10225525, the Chinese Academy of Sciences under contract No. KJ 95T-03, the 100 Talents Program of CAS under Contract Nos. U-24, U-25, and the Knowledge Innovation Project of CAS under Contract Nos. U-602, U-34(IHEP); by the National Natural Science Foundation of China under Contract No. 10175060(USTC); and by the Department of Energy under Contract No. DE-FG03-94ER40833 (U Hawaii).

References

[1] P.A. Rapidis, et al., MARK-I Collaboration, Phys. Rev. Lett. 39 (1978) 526.
[2] W. Bacino, et al., DELCO Collaboration, Phys. Rev. Lett. 40 (1978) 671.
[3] H.J. Lipkin, Phys. Lett. B 179 (1986) 278.
[4] K. Lane, Harvard Report No. HUTP-86/A045, 1986.
[5] Y.P. Kuang, T.M. Yan, Phys. Rev. D 24 (1981) 2874.
[6] Y.P. Kuang, T.M. Yan, Phys. Rev. D 41 (1990) 155.
[7] Y.P. Kuang, Phys. Rev. D 65 (2002) 094024.
[8] J.Z. Bai, et al., BES Collaboration, Nucl. Instrum. Methods A 458 (2001) 627.
[9] E.A. Kuraev, V.S. Fadin, Sov. J. Nucl. Phys. 41 (1985) 466.
[10] S. Eidelman, et al., Particle Data Group, Phys. Lett. B 592 (2004) 1.
[11] R.L. Goble, J.L. Rosner, Phys. Rev. D 5 (1972) 2345;
H.Q. Zheng, et al., Nucl. Phys. A 733 (2004) 235;
L.S. Brown, Phys. Rev. Lett. 35 (1975) 1.
[12] R.H. Schindler, et al., Phys. Rev. D 21 (1980) 2716.
[13] M. Ablikim, et al., BES Collaboration, Phys. Lett. B 603 (2004) 130, hep-ex/0411013.

Available online at www.sciencedirect.com
SCIENCE DIRECT®
Physics Letters B 619 (2005) 247–254
PHYSICS LETTERS B
www.elsevier.com/locate/physletb

Partial wave analysis of $\psi' \to \pi^+\pi^-\pi^0$ at BESII

BES Collaboration

M. Ablikim [a], J.Z. Bai [a], Y. Ban [j], J.G. Bian [a], X. Cai [a], J.F. Chang [a], H.F. Chen [p], H.S. Chen [a], H.X. Chen [a], J.C. Chen [a], Jin Chen [a], Jun Chen [f], M.L. Chen [a], Y.B. Chen [a], S.P. Chi [b], Y.P. Chu [a], X.Z. Cui [a], H.L. Dai [a], Y.S. Dai [r], Z.Y. Deng [a], L.Y. Dong [a], S.X. Du [a], Z.Z. Du [a], J. Fang [a], S.S. Fang [b], C.D. Fu [a], H.Y. Fu [a], C.S. Gao [a], Y.N. Gao [n], M.Y. Gong [a], W.X. Gong [a], S.D. Gu [a], Y.N. Guo [a], Y.Q. Guo [a], Z.J. Guo [o], F.A. Harris [o], K.L. He [a], M. He [k], X. He [a], Y.K. Heng [a], H.M. Hu [a], T. Hu [a], G.S. Huang [a,1], L. Huang [f], X.P. Huang [a], X.B. Ji [a], Q.Y. Jia [j], C.H. Jiang [a], X.S. Jiang [a], D.P. Jin [a], S. Jin [a], Y. Jin [a], Y.F. Lai [a], F. Li [a], G. Li [a], H.H. Li [a], J. Li [a], J.C. Li [a], Q.J. Li [a], R.B. Li [a], R.Y. Li [a], S.M. Li [a], W.G. Li [a], X.L. Li [g], X.Q. Li [i], X.S. Li [n], Y.F. Liang [m], H.B. Liao [e], C.X. Liu [a], F. Liu [e], Fang Liu [p], H.M. Liu [a], J.B. Liu [a], J.P. Liu [q], R.G. Liu [a], Z.A. Liu [a], Z.X. Liu [a], F. Lu [a], G.R. Lu [d], J.G. Lu [a], C.L. Luo [h], X.L. Luo [a], F.C. Ma [g], J.M. Ma [a], L.L. Ma [k], Q.M. Ma [a], X.Y. Ma [a], Z.P. Mao [a], X.H. Mo [a], J. Nie [a], Z.D. Nie [a], S.L. Olsen [o], H.P. Peng [p], N.D. Qi [a], C.D. Qian [l], H. Qin [h], J.F. Qiu [a], Z.Y. Ren [a], G. Rong [a], L.Y. Shan [a], L. Shang [a], D.L. Shen [a], X.Y. Shen [a], H.Y. Sheng [a], F. Shi [a], X. Shi [j], H.S. Sun [a], S.S. Sun [p], Y.Z. Sun [a], Z.J. Sun [a], X. Tang [a], N. Tao [p], Y.R. Tian [n], G.L. Tong [a], G.S. Varner [o], D.Y. Wang [a], J.Z. Wang [a], K. Wang [p], L. Wang [a], L.S. Wang [a], M. Wang [a], P. Wang [a], P.L. Wang [a], S.Z. Wang [a], W.F. Wang [a], Y.F. Wang [a], Zhe Wang [a], Z. Wang [a], Zheng Wang [b], Z.Y. Wang [a], C.L. Wei [a], D.H. Wei [c], N. Wu [a], Y.M. Wu [a], X.M. Xia [a], X.X. Xie [a], B. Xin [g], G.F. Xu [a], H. Xu [a], Y. Xu [a], S.T. Xue [a], M.L. Yan [p], F. Yang [i], H.X. Yang [a], J. Yang [p], S.D. Yang [a], Y.X. Yang [c], M. Ye [a], M.H. Ye [b], Y.X. Ye [p], L.H. Yi [f], Z.Y. Yi [a], C.S. Yu [a], G.W. Yu [a], C.Z. Yuan [a], J.M. Yuan [a], Y. Yuan [a], Q. Yue [a], S.L. Zang [a], Yu Zeng [a], Y. Zeng [f], B.X. Zhang [a], B.Y. Zhang [a], C.C. Zhang [a], D.H. Zhang [a], H.Y. Zhang [a], J. Zhang [a], J.Y. Zhang [a], J.W. Zhang [a], L.S. Zhang [a], Q.J. Zhang [a], S.Q. Zhang [a], X.M. Zhang [a], X.Y. Zhang [k], Y.J. Zhang [j], Y.Y. Zhang [a], Yiyun Zhang [m], Z.P. Zhang [p], Z.Q. Zhang [d], D.X. Zhao [a], J.B. Zhao [a], J.W. Zhao [a], M.G. Zhao [i], P.P. Zhao [a], W.R. Zhao [a], X.J. Zhao [a], Y.B. Zhao [a], Z.G. Zhao [a,2], H.Q. Zheng [j], J.P. Zheng [a], L.S. Zheng [a], Z.P. Zheng [a], X.C. Zhong [a], B.Q. Zhou [a],

0370-2693
doi:10.1016/j.physletb.2005.05.038

G.M. Zhou [a], L. Zhou [a], N.F. Zhou [a], K.J. Zhu [a], Q.M. Zhu [a], Y.C. Zhu [a], Y.S. Zhu [a], Yingchun Zhu [a], Z.A. Zhu [a], B.A. Zhuang [a], B.S. Zou [a]

[a] *Institute of High Energy Physics, Beijing 100039, People's Republic of China*
[b] *China Center for Advanced Science and Technology (CCAST), Beijing 100080, People's Republic of China*
[c] *Guangxi Normal University, Guilin 541004, People's Republic of China*
[d] *Henan Normal University, Xinxiang 453002, People's Republic of China*
[e] *Huazhong Normal University, Wuhan 430079, People's Republic of China*
[f] *Hunan University, Changsha 410082, People's Republic of China*
[g] *Liaoning University, Shenyang 110036, People's Republic of China*
[h] *Nanjing Normal University, Nanjing 210097, People's Republic of China*
[i] *Nankai University, Tianjin 300071, People's Republic of China*
[j] *Peking University, Beijing 100871, People's Republic of China*
[k] *Shandong University, Jinan 250100, People's Republic of China*
[l] *Shanghai Jiaotong University, Shanghai 200030, People's Republic of China*
[m] *Sichuan University, Chengdu 610064, People's Republic of China*
[n] *Tsinghua University, Beijing 100084, People's Republic of China*
[o] *University of Hawaii, Honolulu, HA 96822, USA*
[p] *University of Science and Technology of China, Hefei 230026, People's Republic of China*
[q] *Wuhan University, Wuhan 430072, People's Republic of China*
[r] *Zhejiang University, Hangzhou 310028, People's Republic of China*

Received 22 February 2005; received in revised form 15 May 2005; accepted 16 May 2005

Available online 24 May 2005

Editor: L. Rolandi

Abstract

The decay $\psi' \to \pi^+\pi^-\pi^0$ is analyzed using a sample of 14 million ψ' events taken with the BESII detector at the BEPC, and the branching fraction is measured to be $\mathcal{B}(\psi' \to \pi^+\pi^-\pi^0) = (18.1 \pm 1.8 \pm 1.9) \times 10^{-5}$. A partial wave analysis is carried out using the helicity amplitude method. $\psi' \to \rho(770)\pi$ is observed, and the branching fraction is measured to be $\mathcal{B}(\psi' \to \rho(770)\pi) = (5.1 \pm 0.7 \pm 1.1) \times 10^{-5}$, where the first error is statistical and the second one is systematic. A high mass enhancement with mass around 2.15 GeV/c^2 is also observed. Attributing this enhancement to the $\rho(2150)$ resonance, the branching fraction is measured to be $\mathcal{B}(\psi' \to \rho(2150)\pi \to \pi^+\pi^-\pi^0) = (19.4 \pm 2.5^{+11.5}_{-3.4}) \times 10^{-5}$. The results will help in the understanding of the longstanding "$\rho\pi$ puzzle" between J/ψ and ψ' hadronic decays.

From perturbative QCD (pQCD), it is expected that both J/ψ and ψ' decaying into light hadrons are dominated by the annihilation of $c\bar{c}$ into three gluons or one virtual photon, with a width proportional to the square of the wave function at the origin [1]. This yields the pQCD "12% rule"

$$Q_h = \frac{\mathcal{B}_{\psi' \to h}}{\mathcal{B}_{J/\psi \to h}} = \frac{\mathcal{B}_{\psi' \to e^+e^-}}{\mathcal{B}_{J/\psi \to e^+e^-}} \approx 12\%. \tag{1}$$

A large violation of this rule was first observed in decays to $\rho\pi$ and $K^{*+}K^- +$ c.c. by Mark II [2], known as *the $\rho\pi$ puzzle*, where only upper limits on the branching fractions were reported in ψ' decays. Since then, many two-body decay modes of the ψ' have been measured by the BES Collaboration and recently by the CLEO Collaboration; some decays obey the rule while others violate it [3,4].

E-mail address: wangz@mail.ihep.ac.cn (Zheng Wang).
[1] Current address: Purdue University, West Lafayette, IN 47907, USA.
[2] Current address: University of Michigan, Ann Arbor, MI 48109, USA.

In the study of the $\rho\pi$ puzzle, $\psi' \to \rho\pi$ is a key decay mode and is of great interest to both theorists and experimentalists. Many theoretical attempts, using, for instance, intermediate vector glueballs, hadronic form factors, final state interactions, etc., have been made to solve the puzzle [5]. A recent calculation of the $\psi' \to \rho\pi$ branching fraction, done in the framework of SU(3) symmetry and taking into consideration interference between ψ' resonance decay and the continuum amplitude, predicts a branching fraction of $\psi' \to \rho\pi$ around 1×10^{-4} in Ref. [6] where the relative phase between ψ' strong and electromagnetic decay amplitudes is taken as $-90°$. The measurement of the $\psi' \to \rho\pi$ mode is a direct test of the many models proposed to solve the $\rho\pi$ puzzle [5,6].

The data used for this analysis are taken with the Beijing Spectrometer (BESII) detector at the Beijing Electron Positron Collider (BEPC) storage ring operating at the ψ' energy. The number of ψ' events is 14 ± 0.6 million [7], determined from the number of inclusive hadrons, and the luminosity is $(19.72 \pm 0.86)\ \mathrm{pb}^{-1}$ [8] as measured using large angle Bhabha events.

BESII is a conventional solenoidal magnet detector that is described in detail in Refs. [9,10]. A 12-layer vertex chamber (VC) surrounding the beam pipe provides coordinate and trigger information. A forty-layer main drift chamber (MDC), located radially outside the VC, provides trajectory and energy loss (dE/dx) information for tracks over 85% of the total solid angle. The momentum resolution is $\sigma_p/p = 0.017\sqrt{1+p^2}$ (p in GeV/c), and the dE/dx resolution for hadron tracks is $\sim 8\%$. An array of 48 scintillation counters surrounding the MDC measures the time-of-flight (TOF) of tracks with a resolution of ~ 200 ps for hadrons. Radially outside the TOF system is a 12 radiation length, lead-gas barrel shower counter (BSC). This measures the energies of electrons and photons over $\sim 80\%$ of the total solid angle with an energy resolution of $\sigma_E/E = 22\%/\sqrt{E}$ (E in GeV). Outside of the solenoidal coil, which provides a 0.4 Tesla magnetic field over the tracking volume, is an iron flux return that is instrumented with three double layers of counters that identify muons of momentum greater than 0.5 GeV/c.

A phase space Monte Carlo sample of 2 million $\psi' \to \pi^+\pi^-\pi^0$ events is generated for the efficiency determination in the partial wave analysis (PWA). Monte Carlo samples of Bhabha, dimuon, and inclusive hadronic events generated with Lundcharm [11] are used for background studies. The simulation of the detector uses a Geant3 [12] based program, which simulates the detector response, including the interactions of secondary particles with the detector material. Reasonable agreement between data and Monte Carlo simulation has been observed in various channels tested [13], including $e^+e^- \to (\gamma)e^+e^-$, $e^+e^- \to (\gamma)\mu^+\mu^-$, $J/\psi \to p\bar{p}$, and $\psi' \to J/\psi\pi^+\pi^-$, $J/\psi \to \ell^+\ell^-$ ($\ell = e, \mu$).

The final state of interest includes two charged pions and one neutral pion which is reconstructed from two photons. The candidate events must satisfy the following selection criteria:

(1) A neutral cluster is considered to be a photon candidate when the deposited energy in the BSC is greater than 80 MeV, the angle between the nearest track and the cluster is greater than 16°, the first hit of the cluster is in the beginning six radiation lengths of the BSC, and the angle between the cluster development direction in the BSC and the photon emission direction is less than 37°, and the angle between two nearest photons is required to be larger than 7°. The number of photon candidates after selection is required to be two.

(2) There are two tracks in the MDC with net charge zero. A track must have a good helix fit and satisfy $|\cos\theta| < 0.80$, where θ is the polar angle of the track in the MDC.

(3) For each track, the TOF and dE/dx measurements are used to calculate χ^2 values and the corresponding confidence levels for the hypotheses that the particle is a pion, kaon, or proton ($Prob_\pi$, $Prob_K$, $Prob_p$). At least one track is required to satisfy $Prob_\pi > Prob_K$ and $Prob_\pi > Prob_p$. Radiative Bhabha background is removed by requiring the tracks have small dE/dx or small energy deposited in the BSC. Dimuon background is removed using the hit information in the muon counter.

(4) A four-constraint kinematic fit is performed under the hypothesis $\psi' \to \gamma\gamma\pi^+\pi^-$, and the confidence level of the fit is required to be greater than 1%. A four-constraint kinematic fit is also performed under the hypothesis of $\psi' \to \gamma\gamma K^+K^-$,

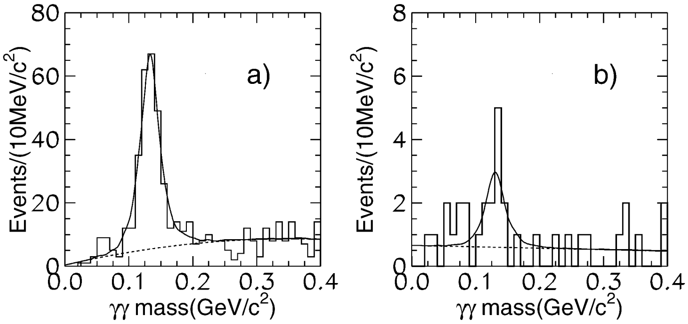

Fig. 1. Two photon invariant mass distribution after final selection for (a) ψ' data and (b) continuum data. The histograms are data, and the curves show the best fits.

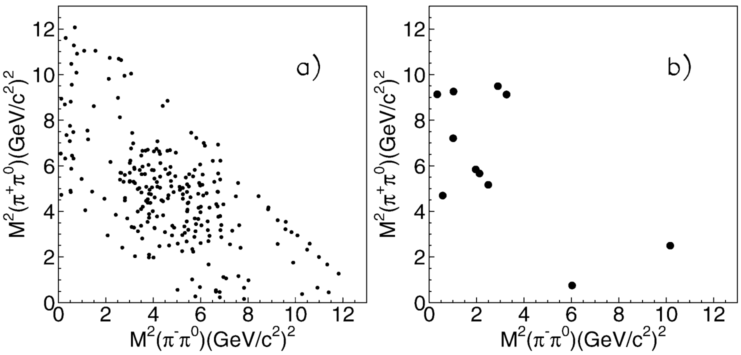

Fig. 2. Dalitz plots of $\pi^+\pi^-\pi^0$ for (a) ψ' data and (b) continuum data after the final selection.

and $\chi^2_{\gamma\gamma\pi\pi} < \chi^2_{\gamma\gamma KK}$ is required to remove $K^+K^-\pi^0$ events.

(5) To remove background produced by ψ' decays to $\gamma\gamma J/\psi$ and $\pi^0\pi^0 J/\psi$ with $J/\psi \to \pi^+\pi^-$ or $J/\psi \to \mu^+\mu^-$, where the muons are misidentified as pions, the invariant mass of $\pi^+\pi^-$ is required to be less than 2.95 GeV/c^2.

After applying the above selection criteria, the invariant mass distribution of the two photons is shown in Fig. 1(a). A clear π^0 signal can be seen. A fit to the mass spectrum (shown in Fig. 1(a)) using a π^0 signal shape determined from Monte Carlo simulation and a polynomial background yields 260 ± 19 π^0 events.

The contribution from the continuum is measured using (6.42 ± 0.24) pb^{-1} [8] of data taken at $\sqrt{s} =$ 3.65 GeV ("continuum data"). Fig. 1(b) shows the $\gamma\gamma$ invariant mass distribution and the fit. The number of π^0 events from the fit (10.0 ± 4.2) is subtracted incoherently from the number of π^0 events in the ψ' data, after normalizing by the ratio of the two luminosities times a factor to account for the $1/s^2$ dependence of the cross section. This yields 229 ± 23 observed $\psi' \to \pi^+\pi^-\pi^0$ events.

Dalitz plots of the $\pi^+\pi^-\pi^0$ system for the ψ' and continuum data are shown in Fig. 2 after requiring that the invariant mass of the two photons lie within ± 30 MeV/c^2 of the nominal π^0 mass. (The mass resolution from Monte Carlo simulation is 17.5 MeV/c^2.) For the ψ' sample, 250 events are obtained with 13% non-π^0 background, while for the continuum sample, 11 events are obtained with 42% non-π^0 background. Here the fractions of non-π^0 background are obtained from the π^0 mass sidebands as shown in Fig. 1. In ψ' decays, besides clear ρ bands at the edges of the Dalitz plot, there is a prominent cluster of events in the center. This is very different than the Dalitz plot for $J/\psi \to \pi^+\pi^-\pi^0$ decays [14], indicating different decay dynamics between J/ψ and $\psi' \to \pi^+\pi^-\pi^0$.

The comparison of the $\pi\pi$ mass distribution between the ψ' data and the scaled continuum data is shown in Fig. 3(a). With the limited statistics, no

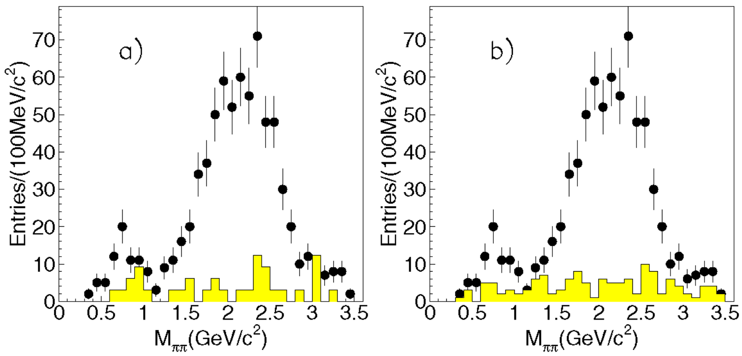

Fig. 3. (a) The comparison of the $\pi\pi$ mass distribution between the ψ' data and the scaled continuum data (shaded histogram, including about 42% non-π^0 background). (b) The comparison of the $\pi\pi$ mass distribution between the ψ' data and the non-π^0 background estimated by the M_{π^0} sideband events (shaded histogram). Dots with error bars are ψ' data. In these plots, the distributions for the three different dipion charge configurations are combined.

clear structure can be seen for the continuum data in Figs. 3(a) or 2(b). The $\pi\pi$ mass distribution of the non-π^0 background, estimated using the M_{π^0} sideband events, is shown in Fig. 3(b). The non-π^0 background contribution for the $\pi\pi$ mass spectrum is approximately uniform.

We now proceed to study the resonant substructure. Here, no continuum subtraction is made, and the selected events are fitted in the helicity amplitude formalism with an unbinned maximum likelihood method using MINUIT [15]. For the process

$$e^+e^- \to \gamma^* \to \rho(1^-) + \pi(0^-) \hookrightarrow \pi(0^-) + \pi(0^-),$$

the intensity distribution dI for the final state is written as

$$dI = \sum_{i=\pm1} \left(|A_i|^2 + |C_i|^2\right) d(\mathrm{LIPS}),$$

where C_i is an incoherent non-π^0 background term, that is assumed to be either a constant or to have the same angular distribution as A_i. The differences between these two fits, 7.3% and 1.4% for $\rho(770)$ and $\rho(2150)$ respectively, are taken as the systematic error on the background description. LIPS denotes the Lorentz-invariant phase space, and the amplitude

$$A_i = A_i^0(\pi^-, \pi^+) + A_i^+(\pi^+, \pi^0) + A_i^-(\pi^0, \pi^-),$$

where $i = +1$ or -1 is the helicity of the γ^*, the first pion in each set of parentheses is the one designated to define the direction, and

$$A_{\pm1}^c = B(m^2) \sin\theta_\pi (\cos\phi_\pi \pm i \cos\theta \sin\phi_\pi) e^{\pm i\phi}.$$

Here $c = 0, +1$, or -1 is the net charge of the dipion system, θ and ϕ are the polar and azimuthal angles of the ρ in the e^+e^- system, θ_π and ϕ_π are the polar and azimuthal angles of the designated pion in the ρ rest frame, and $B(m^2)$ describes the dependence of the amplitude on the dipion mass m:

$$B(m^2) = \frac{BW_{\rho(770)}(m^2) + \sum_j c_j e^{i\beta_j} BW_j(m^2)}{1 + \sum_j c_j},$$

where, $BW(m^2)$ is the Breit–Wigner form of the $\rho(770)$ or its excited states. Here, the Gounaris–Sakurai parameterization [16] is used; β_j and c_j are the relative phase and the relative strength, respectively, between the excited ρ state j and the $\rho(770)$.

Since the number of events is limited, the masses and the widths of all states in the fit are fixed to their PDG values [17], and the number of background events is fixed to the number determined from the $\gamma\gamma$ invariant mass fit. A fit with $\rho(770)$, $\rho(1450)$, $\rho(1700)$ and $\rho(2150)$ results in insignificant $\rho(1450)$ and $\rho(1700)$ contributions. The fit after removing these two components yields a likelihood decrease of 10.7 with four less free parameters. The fit results are shown in Fig. 4; the fit describes the data reasonably well. It is noted that the data do not determine the mass and width of the high mass ρ; the $\rho(2150)$ serves as an effective description of the high mass enhancement near 2.15 GeV/c^2 in $\pi\pi$ mass.

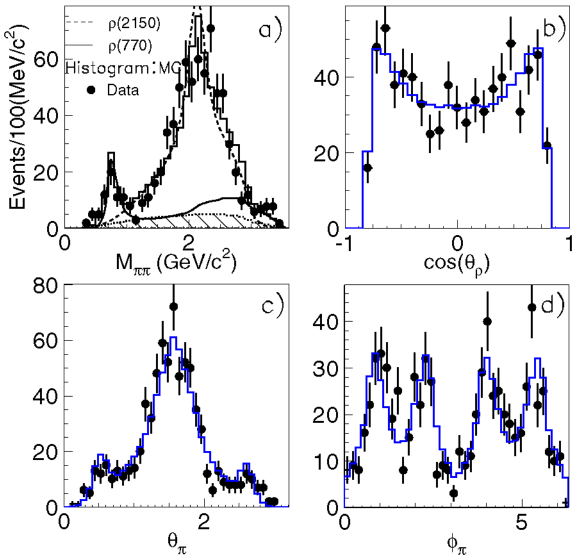

Fig. 4. Comparison between data (dots with error bars) and the final fit (solid histograms) for (a) two pion invariant mass, with a solid line for the $\rho(770)\pi$, a dashed line for the $\rho(2150)\pi$, and a hatched histogram for background; (b) the ρ polar angle in the ψ' rest frame; and (c) and (d) for the polar and azimuthal angles of the designated π in ρ helicity frame.

Table 1
$\psi' \to \pi^+\pi^-\pi^0$ fitting parameters and the assumed values or fitting results. For the assumed values (the numbers with no errors), the values are taken from PDG [17] and fixed in the fit

Quantity	Fit parameters
$M_{\rho(770)}$ (GeV/c^2)	0.7758
$\Gamma_{\rho(770)}$ (GeV/c^2)	0.1503
$\beta_{\rho(2150)}$ (°)	-102 ± 10
$M_{\rho(2150)}$ (GeV/c^2)	2.149
$\Gamma_{\rho(2150)}$ (GeV/c^2)	0.363
$\mathcal{B}(3\pi):\mathcal{B}(\rho(770)\pi)$	$1.0:(0.28\pm0.03)$
$:\mathcal{B}(\rho(2150)\pi)$	$:(1.07\pm0.09)$

The fit parameters and results are given in Table 1, where for results without errors, the parameter is fixed. The fit yields $(28 \pm 3)\%$ $\rho(770)\pi$ in all $\pi^+\pi^-\pi^0$ events (corrected for detection efficiency). By comparing the likelihood difference with and without the $\rho(770)\pi$ in the fit, the significance of $e^+e^- \to \rho(770)\pi$ at $\sqrt{s} = 3.686\,\text{GeV}$ is 7.4σ and varies between 6.1σ to 7.7σ for the fit variations described below in the determination of systematic errors. The significance of $\rho(2150)\pi$ is larger than 10σ. Adding free parameters in front of the $\rho^+\pi^-$ and $\rho^-\pi^+$ amplitudes allows a test of isospin symmetry in the three $\rho(770)\pi$ modes; the fit yields the relative numbers of $\rho(770)^0\pi^0$, $\rho(770)^+\pi^-$ and $\rho(770)^-\pi^+$ events are $1:2.28\pm0.63:0.96\pm0.27$, in fair agreement with the expectation of $1:1:1$. A fit with the $\rho(770)$, $\rho(2150)$ and an additional P wave phase space shows that the contribution of the direct 3π process is small.

The fit quality is checked using Pearson's χ^2 test by dividing the Dalitz plots into small areas with at least 20 events and comparing the number of events between data and normalized Monte Carlo simulation. A $\chi^2/\text{ndf} = 14.6/7 = 2.1$ is obtained, which corresponds to a confidence level of 4%. A fit with the $\rho(2150)$ width or mass free; or a fit with $\rho(770)$, $\rho(1450)$, $\rho(1700)$, and $\rho(2150)$; or even with an extra excited ρ state does not improve the fit quality significantly. Considering these cases, the number of $\rho(770)\pi$ events changes by less than 9.1%, which is included in the systematic error. The number of $\rho(2150)\pi$ events increases by 57% when other excited ρ states are added in the fit due to the large destructive interference between them; this is also included in the systematic error.

Using the parameters of the fit in the Monte Carlo generator, the efficiency of $\psi' \to \pi^+\pi^-\pi^0$ is estimated to be 9.02%, and the corresponding efficiencies for $\rho(770)\pi$ and $\rho(2150)\pi$ are 10.54% and 8.70%, respectively. The efficiency is considered in the PWA.

Systematic errors in the $\psi' \to \pi^+\pi^-\pi^0$ branching fraction measurement come from the kinematic fit, the MDC tracking, particle identification, photon identification, background estimation, continuum subtraction, etc. Most of the errors are measured using clean exclusive J/ψ and ψ' decay samples [14,18], while some were described above. The uncertainty in the continuum subtraction listed in Table 2 is the error of the luminosity normalization factor between the continuum and ψ' data. The fluctuation of the continuum counts relative to the ψ' yield is taken into consideration in the $\pi^+\pi^-\pi^0$ event subtraction, so this error is included in the first error of the following branching fraction calculation.

To determine $\mathcal{B}(\psi' \to \rho(770)\pi \to \pi^+\pi^-\pi^0)$ and $\mathcal{B}(\psi' \to \rho(2150)\pi \to \pi^+\pi^-\pi^0)$, we assume that the ratios of branching fractions in Table 1 are the same for the ψ' data as for the continuum cross sections and use these ratios and the continuum subtracted $\mathcal{B}(\psi' \to \pi^+\pi^-\pi^0)$ to obtain the desired branching fractions.

Table 2
Summary of relative systematic errors (%). (The sources marked with a * were treated in common for all three modes)

Source	$\mathcal{B}(\psi' \to \pi^+\pi^-\pi^0)$	$\mathcal{B}(\psi' \to \rho(770)\pi)$	$\mathcal{B}(\psi' \to \rho(2150)\pi)$
Trigger*	0.5	0.5	0.5
MDC tracking*	4.0	4.0	4.0
Kinematic fit*	6.0	6.0	6.0
Photon efficiency*	4.0	4.0	4.0
Number of photons*	2.0	2.0	2.0
Background estimation*	3.6	3.6	3.6
Particle ID*	negligible	negligible	negligible
Total number of ψ'*	4.0	4.0	4.0
Continuum subtraction*	3.0	3.0	3.0
Background shape in PWA	no	7.3	1.4
Different PWA fits	no	9.1	$^{+57}_{-0.0}$
Continuum resonant structure	no	16.0	13.7
Total	±10.5	±22.4	$^{+59.3}_{-17.5}$

This subtracts the continuum with the stated assumption.

For $\rho(770)\pi$ and $\rho(2150)\pi$, the uncertainties associated with the possibility of different resonant structure between the continuum and the ψ' data, 16.0% and 13.7% respectively, and the uncertainties of fitting with different high mass ρ states and with the $\rho(2150)$ width or mass free, etc., are also included. Here, 16.0% is obtained from the difference of the $\psi' \to \rho(770)\pi$ events between the $\rho(770)\pi$ subtraction using the component ratio in the PWA and the $\rho(770)\pi$ subtraction estimated by CLEO-c's continuum measurement [4], and the 13.7% is the difference of $\psi' \to \rho(2150)\pi$ events between the $\rho(2150)\pi$ subtraction using the component ratio in the PWA and CLEO-c's zero subtraction of $\rho(2150)\pi$ events. Table 2 summarizes the systematic errors for all channels. The total systematic error for $\psi' \to \pi^+\pi^-\pi^0$ is 10.5%, and those for $\psi' \to \rho(770)\pi$ and $\rho(2150)\pi$ are 22.4% and $^{+59.3}_{-17.5}$%, respectively.

Using the numbers obtained above, the branching fractions of $\psi' \to \pi^+\pi^-\pi^0$, $\rho(770)\pi$ and $\rho(2150)\pi$ are

$$\mathcal{B}\big(\pi^+\pi^-\pi^0\big) = (18.1 \pm 1.8 \pm 1.9) \times 10^{-5},$$

$$\mathcal{B}\big(\rho(770)\pi \to \pi^+\pi^-\pi^0\big) = (5.1 \pm 0.7 \pm 1.1) \times 10^{-5},$$

$$\mathcal{B}\big(\rho(2150)\pi \to \pi^+\pi^-\pi^0\big) = \big(19.4 \pm 2.5^{+11.5}_{-3.4}\big) \times 10^{-5},$$

where the second errors are systematic, while the first error of $\mathcal{B}(\pi^+\pi^-\pi^0)$ is the statistical error which contains the error from the continuum 3π yield subtraction; and the first errors of $\mathcal{B}(\rho(770)\pi \to \pi^+\pi^-\pi^0)$ and $\mathcal{B}(\rho(2150)\pi \to \pi^+\pi^-\pi^0)$ are the combinations of the PWA fit errors (shown in Table 1) and the first error of $\mathcal{B}(\pi^+\pi^-\pi^0)$.

Our $\mathcal{B}(\psi' \to \pi^+\pi^-\pi^0)$ agrees with the Mark II [2] result within 1.8σ and agrees well with the CLEO-c measurement [4]. Our $\mathcal{B}(\psi' \to \rho(770)\pi)$ is below the Mark II [2] upper limit and in agreement with the model prediction of $\mathcal{B}(\psi' \to \rho(770)\pi) = (1.11 \pm 0.87) \times 10^{-4}$ [6]. This measurement is about 2σ higher than the result of CLEO-c [4]; this is due to the different analysis procedure, namely the interference between $\rho(770)$ and $\rho(2150)$ considered in this analysis but not in the CLEO-c analysis and the difference in the continuum subtractions in the two analyses. The continuum amplitude, which is considered incoherently in both analyses, could change the $\rho(770)\pi$ branching fraction due to interference with the resonance [6]. This should be considered in a higher statistics experiment [19].

Comparing with the corresponding J/ψ decay branching fractions, it is found that both $\pi^+\pi^-\pi^0$ and $\rho(770)\pi$ are highly suppressed compared with the "12% rule", while for $\rho(2150)\pi$, there is no measurement in J/ψ decays. It could be enhanced in ψ' decays since the phase space in J/ψ decays is limited due to the large mass of the excited ρ state. Using the J/ψ and $\psi' \to \rho\pi$ branching fractions, the $\psi'' \to \rho\pi$ branching fraction is expected to be on the order of 10^{-4} and the $e^+e^- \to \rho\pi$ cross section at $\sqrt{s} = 3.773$ GeV extremely small in the S- and D-wave mixing model [20], which is proposed as a solution of the $\rho\pi$ puzzle in ψ' decays.

In summary, $\psi' \to \pi^+\pi^-\pi^0$ is analyzed and the branching fraction is measured to be $\mathcal{B}(\psi' \to \pi^+\pi^-\pi^0) = (18.1 \pm 1.8 \pm 1.9) \times 10^{-5}$. $\psi' \to \rho(770)\pi$ is observed in ψ' decays, and the branching fraction is measured to be $\mathcal{B}(\psi' \to \rho(770)\pi) = (5.1 \pm 0.7 \pm 1.1) \times 10^{-5}$. A high mass enhancement at mass around 2.15 GeV/c^2 is also observed. Using the $\rho(2150)$ to describe this resonance, the branching fraction is measured to be $\mathcal{B}(\psi' \to \rho(2150)\pi \to \pi^+\pi^-\pi^0) = (19.4 \pm 2.5^{+11.5}_{-3.4}) \times 10^{-5}$. The results will help in the understanding of the longstanding "$\rho\pi$ puzzle" between J/ψ and ψ' hadronic decays.

Acknowledgements

The BES Collaboration thanks the staff of BEPC for their hard efforts and the members of IHEP computing center for their helpful assistance. This work is supported in part by the National Natural Science Foundation of China under contracts Nos. 10491303, 10225524, 10225525, the Chinese Academy of Sciences under contract No. KJ 95T-03, the 100 Talents Program of CAS under Contract Nos. U-11, U-24, U-25, and the Knowledge Innovation Project of CAS under Contract Nos. U-602, U-34 (IHEP); by the National Natural Science Foundation of China under Contract No. 10175060 (USTC), and No. 10225522 (Tsinghua University); and by the US Department of Energy under Contract No. DE-FG03-94ER40833 (U Hawaii).

References

[1] T. Appelquist, H.D. Politzer, Phys. Rev. Lett. 34 (1975) 43; A. De Rújula, S.L. Glashow, Phys. Rev. Lett. 34 (1975) 46.
[2] Mark II Collaboration, M.E.B. Franklin, et al., Phys. Rev. Lett. 51 (1983) 963.
[3] Many results may be found in Ref. [17]; More recent results may be found in BES Collaboration, J.Z. Bai, et al., Phys. Rev. D 69 (2004) 072001; BES Collaboration, J.Z. Bai, et al., Phys. Rev. Lett. 92 (2004) 052001; BES Collaboration, M. Ablikim, et al., Phys. Rev. D 70 (2004) 112007; BES Collaboration, M. Ablikim, et al., Phys. Rev. D 70 (2004) 112003; BES Collaboration, M. Ablikim, et al., Phys. Lett. B 614 (2005) 37.
[4] CLEO Collaboration, N.E. Adam, et al., Phys. Rev. Lett. 94 (2005) 012005.
[5] W.S. Hou, A. Soni, Phys. Rev. Lett. 50 (1983) 569; S.J. Brodsky, M. Karliner, Phys. Rev. Lett. 78 (1997) 4682; M. Chaichian, N.A. Törnqvist, Nucl. Phys. B 323 (1989) 75; S.S. Pinsky, Phys. Lett. B 236 (1990) 479; G. Karl, W. Roberts, Phys. Lett. B 144 (1984) 263; X.Q. Li, D.V. Bugg, B.S. Zou, Phys. Rev. D 55 (1997) 1421; Y.Q. Chen, E. Braaten, Phys. Rev. Lett. 80 (1998) 5060; J.M. Gérard, J. Weyers, Phys. Lett. B 462 (1999) 324; T. Feldmann, P. Kroll, Phys. Rev. D 62 (2000) 074006.
[6] P. Wang, C.Z. Yuan, X.H. Mo, Phys. Rev. D 69 (2003) 057502, the branching fraction 1×10^{-4} is obtained from $\mathcal{B}(\psi' \to \rho^0\pi^0)$.
[7] X.H. Mo, et al., High Energy Phys. Nucl. Phys. 27 (2004) 455, hep-ex/0407055.
[8] S.P. Chi, X.H. Mo, Y.S. Zhu, High Energy Phys. Nucl. Phys. 28 (2004) 1135.
[9] BES Collaboration, J.Z. Bai, et al., Nucl. Instrum. Methods A 344 (1994) 319.
[10] BES Collaboration, J.Z. Bai, et al., Nucl. Instrum. Methods A 458 (2001) 627.
[11] J.C. Chen, et al., Phys. Rev. D 62 (2000) 034003.
[12] GEANT: detector description and simulation tool, V3.21, CERN Program Library Long Writeup W5013, October 1994.
[13] BES Collaboration, M. Ablikim, et al., physics/0503001, Nucl. Instrum. Methods, in press.
[14] BES Collaboration, J.Z. Bai, et al., Phys. Rev. D 70 (2004) 012005.
[15] CERN Program Library Long Writeup D506.
[16] G.J. Gounaris, J.J. Sakurai, Phys. Rev. Lett. 21 (1968) 244.
[17] Particle Data Group, S. Eidelman, et al., Phys. Lett. B 592 (2004) 1.
[18] BES Collaboration, J.Z. Bai, et al., Phys. Rev. D 69 (2004) 072001.
[19] P. Wang, C.Z. Yuan, X.H. Mo, D.H. Zhang, Phys. Lett. B 593 (2004) 89.
[20] P. Wang, X.H. Mo, C.Z. Yuan, Phys. Lett. B 574 (2003) 41.

Observation of a Resonance $X(1835)$ in $J/\psi \to \gamma\pi^+\pi^-\eta'$

M. Ablikim,[1] J. Z. Bai,[1] Y. Ban,[11] J. G. Bian,[1] X. Cai,[1] H. F. Chen,[16] H. S. Chen,[1] H. X. Chen,[1] J. C. Chen,[1] Jin Chen,[1] Y. B. Chen,[1] S. P. Chi,[2] Y. P. Chu,[1] X. Z. Cui,[1] Y. S. Dai,[18] Z. Y. Deng,[1] L. Y. Dong,[1,*] Q. F. Dong,[14] S. X. Du,[1] Z. Z. Du,[1] J. Fang,[1] S. S. Fang,[2] C. D. Fu,[1] C. S. Gao,[1] Y. N. Gao,[14] S. D. Gu,[1] Y. T. Gu,[4] Y. N. Guo,[1] Y. Q. Guo,[1] Z. J. Guo,[15] F. A. Harris,[15] K. L. He,[1] M. He,[12] Y. K. Heng,[1] H. M. Hu,[1] T. Hu,[1] G. S. Huang,[1,†] X. P. Huang,[1] X. T. Huang,[12] X. B. Ji,[1] X. S. Jiang,[1] J. B. Jiao,[12] D. P. Jin,[1] S. Jin,[1] Yi Jin,[1] Y. F. Lai,[1] G. Li,[2] H. B. Li,[1] H. H. Li,[1] J. Li,[1] R. Y. Li,[1] S. M. Li,[1] W. D. Li,[1] W. G. Li,[1] X. L. Li,[8] X. Q. Li,[10] Y. L. Li,[4] Y. F. Liang,[13] H. B. Liao,[6] C. X. Liu,[1] F. Liu,[6] Fang Liu,[16] H. H. Liu,[1] H. M. Liu,[1] J. Liu,[11] J. B. Liu,[1] J. P. Liu,[17] R. G. Liu,[1] Z. A. Liu,[1] F. Lu,[1] G. R. Lu,[5] H. J. Lu,[16] J. G. Lu,[1] C. L. Luo,[9] F. C. Ma,[8] H. L. Ma,[1] L. L. Ma,[1] Q. M. Ma,[1] X. B. Ma,[5] Z. P. Mao,[1] X. H. Mo,[1] J. Nie,[1] S. L. Olsen,[15] H. P. Peng,[16] N. D. Qi,[1] H. Qin,[9] J. F. Qiu,[1] Z. Y. Ren,[1] G. Rong,[1] L. Y. Shan,[1] L. Shang,[1] D. L. Shen,[1] X. Y. Shen,[1] H. Y. Sheng,[1] F. Shi,[1] X. Shi,[11,‡] H. S. Sun,[1] J. F. Sun,[1] S. S. Sun,[1] Y. Z. Sun,[1] Z. J. Sun,[1] Z. Q. Tan,[4] X. Tang,[1] Y. R. Tian,[14] G. L. Tong,[1] G. S. Varner,[15] D. Y. Wang,[1] L. Wang,[1] L. S. Wang,[1] M. Wang,[1] P. Wang,[1] P. L. Wang,[1] W. F. Wang,[1,§] Y. F. Wang,[1] Z. Wang,[1] Z. Y. Wang,[1] Zhe Wang,[1] Zheng Wang,[2] C. L. Wei,[1] D. H. Wei,[1] N. Wu,[1] X. M. Xia,[1] X. X. Xie,[1] B. Xin,[8,†] G. F. Xu,[1] Y. Xu,[10] M. L. Yan,[16] F. Yang,[10] H. X. Yang,[1] J. Yang,[16] Y. X. Yang,[3] M. H. Ye,[2] Y. X. Ye,[16] Z. Y. Yi,[1] G. W. Yu,[1] C. Z. Yuan,[1] J. M. Yuan,[1] Y. Yuan,[1] S. L. Zang,[1] Y. Zeng,[7] Yu Zeng,[1] B. X. Zhang,[1] B. Y. Zhang,[1] C. C. Zhang,[1] D. H. Zhang,[1] H. Y. Zhang,[1] J. W. Zhang,[1] J. Y. Zhang,[1] Q. J. Zhang,[1] X. M. Zhang,[1] X. Y. Zhang,[12] Y. Y. Zhang,[13] Z. P. Zhang,[16] Z. Q. Zhang,[5] D. X. Zhao,[1] J. W. Zhao,[1] M. G. Zhao,[10] P. P. Zhao,[1] W. R. Zhao,[1] Z. G. Zhao,[1,∥] H. Q. Zheng,[11] J. P. Zheng,[1] Z. P. Zheng,[1] L. Zhou,[1] N. F. Zhou,[1] K. J. Zhu,[1] Q. M. Zhu,[1] Y. C. Zhu,[1] Yingchun Zhu,[1,¶] Y. S. Zhu,[1] Z. A. Zhu,[1] B. A. Zhuang,[1] X. A. Zhuang,[1] and B. S. Zou[1]

(BES Collaboration)

[1]*Institute of High Energy Physics, Beijing 100049, People's Republic of China*
[2]*China Center for Advanced Science and Technology (CCAST), Beijing 100080, People's Republic of China*
[3]*Guangxi Normal University, Guilin 541004, People's Republic of China*
[4]*Guangxi University, Nanning 530004, People's Republic of China*
[5]*Henan Normal University, Xinxiang 453002, People's Republic of China*
[6]*Huazhong Normal University, Wuhan 430079, People's Republic of China*
[7]*Hunan University, Changsha 410082, People's Republic of China*
[8]*Liaoning University, Shenyang 110036, People's Republic of China*
[9]*Nanjing Normal University, Nanjing 210097, People's Republic of China*
[10]*Nankai University, Tianjin 300071, People's Republic of China*
[11]*Peking University, Beijing 100871, People's Republic of China*
[12]*Shandong University, Jinan 250100, People's Republic of China*
[13]*Sichuan University, Chengdu 610064, People's Republic of China*
[14]*Tsinghua University, Beijing 100084, People's Republic of China*
[15]*University of Hawaii, Honolulu, Hawaii 96822, USA*
[16]*University of Science and Technology of China, Hefei 230026, People's Republic of China*
[17]*Wuhan University, Wuhan 430072, People's Republic of China*
[18]*Zhejiang University, Hangzhou 310028, People's Republic of China*
(Received 11 August 2005; published 28 December 2005)

The decay channel $J/\psi \to \gamma\pi^+\pi^-\eta'$ is analyzed using a sample of 5.8×10^7 J/ψ events collected with the BESII detector. A resonance, the $X(1835)$, is observed in the $\pi^+\pi^-\eta'$ invariant-mass spectrum with a statistical significance of 7.7σ. A fit with a Breit-Wigner function yields a mass $M = 1833.7 \pm 6.1(\mathrm{stat}) \pm 2.7(\mathrm{syst})$ MeV/c^2, a width $\Gamma = 67.7 \pm 20.3(\mathrm{stat}) \pm 7.7(\mathrm{syst})$ MeV/c^2, and a product branching fraction $B(J/\psi \to \gamma X) \cdot B(X \to \pi^+\pi^-\eta') = [2.2 \pm 0.4(\mathrm{stat}) \pm 0.4(\mathrm{syst})] \times 10^{-4}$. The mass and width of the $X(1835)$ are not compatible with any known meson resonance. Its properties are consistent with expectations for the state that produces the strong $p\bar{p}$ mass threshold enhancement observed in the $J/\psi \to \gamma p\bar{p}$ process at BESII.

DOI: 10.1103/PhysRevLett.95.262001 PACS numbers: 12.39.Mk, 12.40.Yx, 13.20.Gd, 13.75.Cs

An anomalous enhancement near the mass threshold in the $p\bar{p}$ invariant-mass spectrum from $J/\psi \to \gamma p\bar{p}$ decays was reported by the BES II experiment [1]. This enhancement was fitted with a subthreshold S-wave Breit-

Wigner resonance function with a mass $M = 1859^{+3+5}_{-10-25}$ MeV/c^2, a width $\Gamma < 30$ MeV/c^2 (at the 90% C.L.), and a product branching fraction (BF) $B(J/\psi \to \gamma X) \cdot B(X \to p\bar{p}) = [7.0 \pm 0.4(\mathrm{stat})^{+1.9}_{-0.8}(\mathrm{syst})] \times 10^{-5}$. This surprising experimental observation has stimulated a number of theoretical speculations [2–7] and motivated further investigations on baryon-antibaryon mass threshold structures, which led to the subsequent experimental observation of a strong $p\bar{\Lambda}$ mass threshold enhancement in $J/\psi \to pK^-\bar{\Lambda}$ decay [8]. Among various theoretical interpretations of the $p\bar{p}$ mass threshold enhancement, the most intriguing one is that of a $p\bar{p}$ bound state, sometimes called *baryonium* [2,5,9], which has been the subject of many experimental searches [10]. However, it should be noted that many theoretical predictions on the mass and width of a baryonium state depend on the details of models.

The baryonium interpretation of the $p\bar{p}$ mass enhancement requires a new resonance with a mass around 1.85 GeV/c^2, and it would be supported by the observation of the resonance in other decay channels. Possible decay modes for a $p\bar{p}$ bound state, suggested in Refs. [4,5], include $\pi^+\pi^-\eta'$. In this Letter, we report an analysis on the $J/\psi \to \gamma\pi^+\pi^-\eta'$ decay channel and the observation of a resonance in the $\pi^+\pi^-\eta'$ mass spectrum with a mass around 1835 MeV/c^2, where the η' meson is detected in two decay modes, $\eta' \to \pi^+\pi^-\eta(\eta \to \gamma\gamma)$ and $\eta' \to \gamma\rho$. In the following, this resonance is designated as the $X(1835)$. The results reported here are based on a sample of 5.8×10^7 J/ψ decays detected with the upgraded Beijing Spectrometer (BESII) at the Beijing Electron-Positron Collider (BEPC).

BESII is a large solid-angle magnetic spectrometer that is described in detail in Ref. [11]. Charged particle momenta are determined with a resolution of $\sigma_p/p = 1.78\%\sqrt{1 + p^2\ (\mathrm{GeV}/c^2)}$ in a 40-layer cylindrical main drift chamber (MDC). Particle identification is accomplished by specific ionization (dE/dx) measurements in the MDC and time-of-flight (TOF) measurements in a barrel-like array of 48 scintillation counters. The dE/dx resolution is $\sigma_{dE/dx} = 8.0\%$; the TOF resolution is measured to be $\sigma_{\mathrm{TOF}} = 180$ ps for Bhabha events. Outside of the time-of-flight counters is a 12-radiation-length barrel shower counter (BSC) comprised of gas tubes interleaved with lead sheets. The BSC measures the energies and directions of photons with resolutions of $\sigma_E/E \simeq 21\%/\sqrt{E\ (\mathrm{GeV})}$, $\sigma_\phi = 7.9$ mrad, and $\sigma_z = 2.3$ cm. The iron flux return of the magnet is instrumented with three double layers of counters that are used to identify muons. In this analysis, a GEANT3-based Monte Carlo (MC) package with detailed consideration of the detector performance is used. The consistency between data and MC has been carefully checked in many high-purity physics channels, and the agreement is reasonable [12].

For the $J/\psi \to \gamma\pi^+\pi^-\eta'(\eta' \to \pi^+\pi^-\eta, \eta \to \gamma\gamma)$ channel, candidate events are required to have four charged tracks, each of which is well fitted to a helix that is within the polar angle region $|\cos\theta| < 0.8$ and with a transverse momentum larger than 70 MeV/c. The total charge of the four tracks is required to be zero. For each track, the TOF and dE/dx information are combined to form particle identification confidence levels for the π, K, and p hypotheses; the particle type with the highest confidence level is assigned to each track. At least three of the charged tracks are required to be identified as pions. Candidate photons are required to have an energy deposit in the BSC greater than 60 MeV and to be isolated from charged tracks by more than 5°; the number of photons is required to be three. A four-constraint (4C) energy-momentum conservation kinematic fit is performed to the $\pi^+\pi^-\pi^+\pi^-\gamma\gamma\gamma$ hypothesis, and the χ^2_{4C} is required to be less than 8 and also less than the χ^2 for the kinematically similar $K^+K^-\pi^+\pi^-\gamma\gamma\gamma$ hypothesis. An η signal is evident in the $\gamma\gamma$ invariant-mass distribution of all $\gamma\gamma$ pairings [Fig. 1(a)]. In order to reduce combinatorial backgrounds from $\pi^0 \to \gamma\gamma$ decays, we require that the invariant masses of all $\gamma\gamma$ pairings are greater than 0.22 GeV/c^2. Candidate η mesons are selected by requiring $|M_{\gamma\gamma} - m_\eta| < 0.05$ GeV/c^2. The events are then subjected to a five-constraint (5C) fit where the invariant mass of the $\gamma\gamma$ pair associated with the η is constrained to m_η, and $\chi^2_{5C} < 15$ is required. The 5C fit improves the $M_{\pi^+\pi^-\eta}$ mass resolution from 20 MeV/c^2 (for the 4C fit) to 7 MeV/c^2. Figure 1(b) shows the $\pi^+\pi^-\eta$ invariant-mass distribution after the 5C fit, where a clear η' signal is visible. For η' candidates, we select $\pi^+\pi^-\eta$ combinations with $|M_{\pi^+\pi^-\eta} - m_{\eta'}| < 0.015$ GeV/c^2. In a small fraction of events, more than one combination passes the above selection. In these cases, the combination with $M_{\pi^+\pi^-\eta}$ closest to η' mass is used [13]. The $\pi^+\pi^-\eta'$ invariant-mass spectrum for the selected events is shown in Fig. 1(c), where a peak at a mass around 1835 MeV/c^2 is observed.

For the $J/\psi \to \gamma\pi^+\pi^-\eta'(\eta' \to \gamma\rho)$ channel, events with four charged tracks (with zero net charge) and two photons are selected. At least three of the charged tracks are required to be identified as pions. These events are subjected to a 4C kinematic fit to the $\pi^+\pi^-\pi^+\pi^-\gamma\gamma$ hypothesis, and the χ^2_{4C} is required to be less than 8 and less than the χ^2 for the $K^+K^-\pi^+\pi^-\gamma\gamma$ hypothesis. At this stage of the analysis, the primary remaining background contributions are due to $J/\psi \to \pi^+\pi^-\pi^+\pi^-\pi^0$, $J/\psi \to \pi^+\pi^-\pi^+\pi^-\eta$, and $J/\psi \to \omega(\omega \to \gamma\pi^0)\pi^+\pi^-\pi^+\pi^-$; these produce peaks at m_{π^0}, m_η, and m_ω in the $\gamma\gamma$ invariant-mass distribution shown in Fig. 2(a). We suppress these backgrounds by rejecting events with $M_{\gamma\gamma} < 0.22$ GeV/c^2, $|M_{\gamma\gamma} - m_\eta| < 0.05$ GeV/c^2, or 0.72 GeV/$c^2 < M_{\gamma\gamma} < 0.82$ GeV/c^2. To select ρ and η' signals, all $\pi^+\pi^-$ and $\gamma\pi^+\pi^-$ combinations are consid-

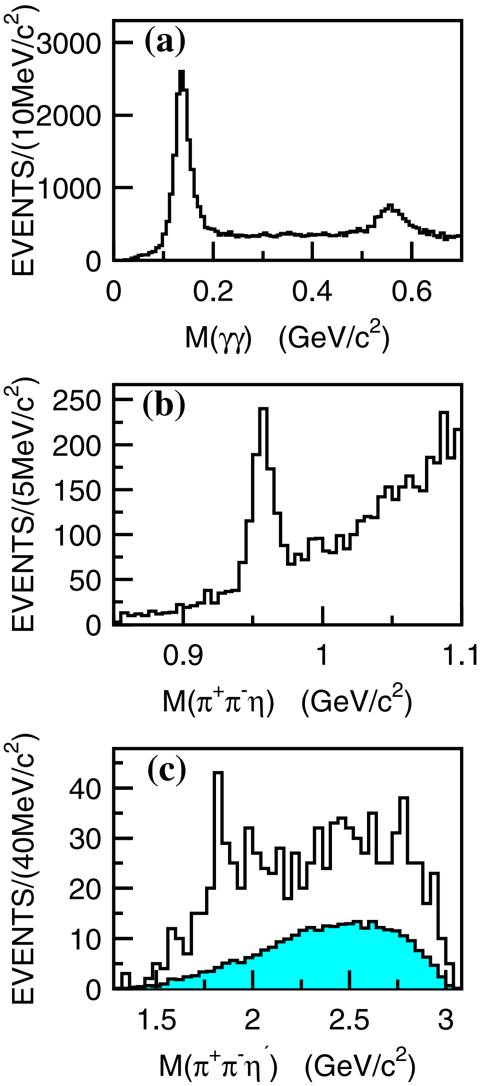

FIG. 1 (color online). Invariant-mass distributions for selected $J/\psi \to \gamma\pi^+\pi^-\eta'(\eta' \to \pi^+\pi^-\eta, \eta \to \gamma\gamma)$ candidate events. (a) The invariant-mass distribution of $\gamma\gamma$ pairs. (b) The $\pi^+\pi^-\eta$ invariant-mass distribution. (c) The $\pi^+\pi^-\eta'$ invariant-mass distributions; the open histogram is data and the shaded histogram is $J/\psi \to \gamma\pi^+\pi^-\eta'$ phase-space MC events (with arbitrary normalization).

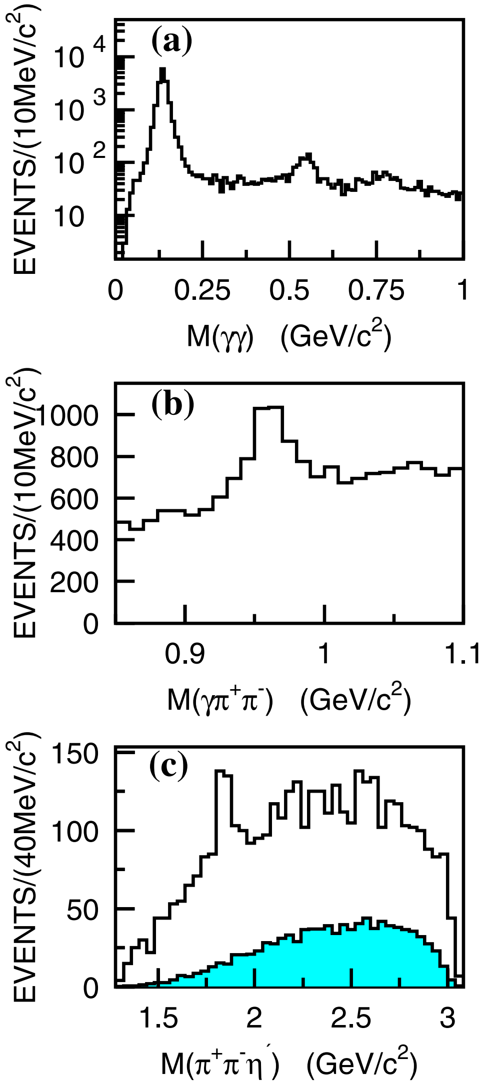

FIG. 2 (color online). Invariant-mass distributions for the selected $J/\psi \to \gamma\pi^+\pi^-\eta'(\eta' \to \gamma\rho)$ candidate events. (a) The invariant-mass distribution for $\gamma\gamma$ pairs. (b) The $\gamma\pi^+\pi^-$ invariant-mass distribution. (c) The $\pi^+\pi^-\eta'$ invariant-mass distributions; the open histogram is data and the shaded histogram is from $J/\psi \to \gamma\pi^+\pi^-\eta'$ phase-space MC events (with arbitrary normalization).

ered. The $\gamma\pi^+\pi^-$ invariant-mass distribution shows an η' signal [Fig. 2(b)]. We require that $|M_{\pi^+\pi^-} - m_\rho| < 0.2\ \mathrm{GeV}/c^2$ and $|M_{\gamma\pi^+\pi^-} - m_{\eta'}| < 0.025\ \mathrm{GeV}/c^2$. If more than one combination passes these criteria, the combination with $M_{\gamma\pi^+\pi^-}$ closest to $m_{\eta'}$ is selected [13]. For this channel, there is also a distinct peak near $1835\ \mathrm{MeV}/c^2$ in the $\pi^+\pi^-\eta'$ invariant-mass spectrum [Fig. 2(c)].

To ensure that the peak near $1835\ \mathrm{MeV}/c^2$ is not due to background, we have made extensive studies of potential background processes using both data and MC. Non-η' processes are studied with η' mass-sideband events. The main background channel $J/\psi \to \pi^0\pi^+\pi^-\eta'$ and other background processes with multiphotons and/or with kaons are reconstructed with the data. In addition, we also checked for possible backgrounds with a MC sample of 60×10^6 J/ψ decays generated by the LUND model [14]. None of these background sources produce a peak around $1835\ \mathrm{MeV}/c^2$ in the $\pi^+\pi^-\eta'$ invariant-mass spectrum.

Figure 3 shows the $\pi^+\pi^-\eta'$ invariant-mass spectrum for the combined $J/\psi \to \gamma\pi^+\pi^-\eta'(\eta' \to \pi^+\pi^-\eta)$ and $J/\psi \to \gamma\pi^+\pi^-\eta'(\eta' \to \gamma\rho)$ samples [i.e., the sum of the histograms in Figs. 1(c) and 2(c)]. This spectrum is fitted

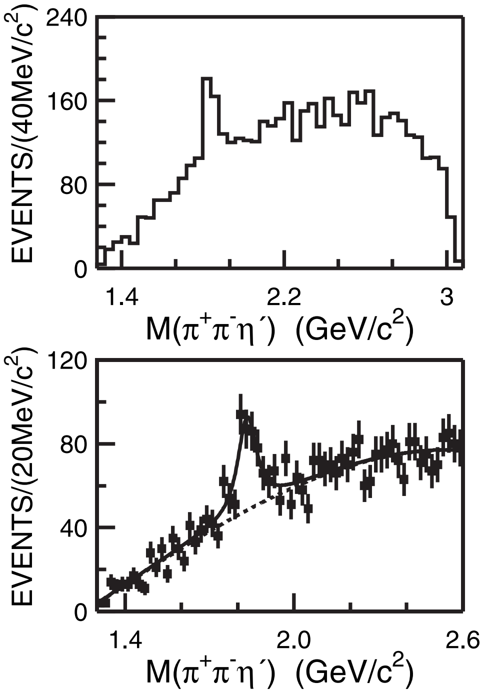

FIG. 3. The $\pi^+\pi^-\eta'$ invariant-mass distribution for selected events from both the $J/\psi \to \gamma\pi^+\pi^-\eta'(\eta' \to \pi^+\pi^-\eta, \eta \to \gamma\gamma)$ and $J/\psi \to \gamma\pi^+\pi^-\eta'(\eta' \to \gamma\rho)$ analyses. The bottom panel shows the fit (solid curve) to the data (points with error bars); the dashed curve indicates the background function.

with a Breit-Wigner (BW) function convolved with a Gaussian mass resolution function (with $\sigma = 13$ MeV/c^2) to represent the $X(1835)$ signal plus a smooth polynomial background function. The mass and width obtained from the fit (shown in the bottom panel in Fig. 3) are $M = 1833.7 \pm 6.1$ MeV/c^2 and $\Gamma = 67.7 \pm 20.3$ MeV/c^2. The signal yield from the fit is 264 ± 54 events with a confidence level 45.5% (χ^2/d.o.f. $= 57.6/57$) and $-2\ln L = 58.4$. A fit to the mass spectrum without a BW signal function returns $-2\ln L = 126.5$. The change in $-2\ln L$ with Δ(d.o.f.) $= 3$ corresponds to a statistical significance of 7.7σ for the signal.

Using MC-determined selection efficiencies of 3.72% and 4.85% for the $\eta' \to \pi^+\pi^-\eta$ and $\eta' \to \gamma\rho$ modes, respectively, we determine a product BF of

$$B(J/\psi \to \gamma X(1835)) \cdot B(X(1835) \to \pi^+\pi^-\eta') = (2.2 \pm 0.4) \times 10^{-4}.$$

The consistency between the two η' decay modes is checked by fitting the distributions in Figs. 1(c) and 2(c) separately with the method described above. The fit to Fig. 1(c) gives $M = 1827.4 \pm 8.1$ MeV/c^2 and $\Gamma = 54.2 \pm 34.5$ MeV/c^2 with a statistical significance of 5.1σ. From the 68 ± 26 signal events obtained from the fit, the product BF is $B(J/\psi \to \gamma X(1835)) \cdot B(X(1835) \to \pi^+\pi^-\eta') = (1.8 \pm 0.7) \times 10^{-4}$. Similar results are obtained if we apply only a 4C kinematic fit in this analysis. For the fit to Fig. 2(c), the mass and width are determined to be $M = 1836.3 \pm 7.9$ MeV/c^2 and $\Gamma = 70.3 \pm 23.1$ MeV/c^2 with a statistical significance of 6.0 σ. For this mode alone, the signal yield of 193 ± 43 signal events corresponds to $B(J/\psi \to \gamma X(1835)) \cdot B(X(1835) \to \pi^+\pi^-\eta') = (2.3 \pm 0.5) \times 10^{-4}$. The $X(1835)$ mass, width, and product BF values determined from the two η' decay modes separately are in good agreement with each other.

The systematic uncertainties on the mass and width are determined by varying the functional form used to represent the background, the fitting range of the mass spectrum, the mass calibration, and possible biases due to the fitting procedure. The latter are estimated from differences between the input and output mass and width values from MC studies. The total systematic errors on the mass and width are 2.7 and 7.7 MeV/c^2, respectively. The systematic error on the branching fraction measurement comes mainly from the uncertainties of MDC simulation (including systematic uncertainties of the tracking efficiency and the kinematic fits), the photon detection efficiency, the particle identification efficiency, the η' decay branching fractions to $\pi^+\pi^-\eta$ and $\gamma\rho$, the background function parametrization, the fitting range of the mass spectrum, the requirements on numbers of photons, the invariant-mass distributions of $\gamma\gamma$ pairs in the two analyses, the $\pi^+\pi^-$ invariant-mass distribution in $\eta' \to \gamma\pi^+\pi^-$ decays, MC statistics, the total number of J/ψ events [15], and the unknown spin-parity of the $X(1835)$. For the latter, we use the difference between phase space and a $J^{PC} = 0^{-+}$ hypothesis for the $X(1835)$. The total relative systematic error on the product branching fraction is 20.2%.

In summary, the decay channel $J/\psi \to \gamma\pi^+\pi^-\eta'$ is analyzed using two η' decay modes, $\eta' \to \pi^+\pi^-\eta$ and $\eta' \to \gamma\rho$. A resonance, the $X(1835)$, is observed with a high statistical significance of 7.7σ in the $\pi^+\pi^-\eta'$ invariant-mass spectrum. From a fit with a Breit-Wigner function, the mass is determined to be $M = 1833.7 \pm 6.1(\text{stat}) \pm 2.7(\text{syst})$ MeV/c^2, the width is $\Gamma = 67.7 \pm 20.3(\text{stat}) \pm 7.7(\text{syst})$ MeV/c^2, and the product branching fraction is $B(J/\psi \to \gamma X) \cdot B(X \to \pi^+\pi^-\eta') = [2.2 \pm 0.4(\text{stat}) \pm 0.4(\text{syst})] \times 10^{-4}$. The mass and width of the $X(1835)$ are not compatible with any known meson resonance [16]. In Ref. [16], the candidate closest in mass to the $X(1835)$ is the (unconfirmed) 2^{-+} $\eta_2(1870)$ with $M = 1842 \pm 8$ MeV/c^2. The width of this state, $\Gamma = 225 \pm 14$ MeV/c^2, is considerably larger than that of the $X(1835)$ (see also [17], where the 2^{-+} component in the $\eta\pi\pi$ mode of J/ψ radiative decay has a mass 1840 ± 15 MeV/c^2 and a width 170 ± 40 MeV/c^2).

We examined the possibility that the $X(1835)$ is responsible for the $p\bar{p}$ mass threshold enhancement observed in radiative $J/\psi \to \gamma p\bar{p}$ decays [1]. It has been pointed out that the S-wave BW function used for the fit in Ref. [1]

should be modified to include the effect of final-state interactions (FSI) on the shape of the $p\bar{p}$ mass spectrum [6,7]. Redoing the S-wave BW fit to the $p\bar{p}$ invariant-mass spectrum of Ref. [1], including the zero isospin, S-wave FSI factor of Ref. [7], yields a mass $M = 1831 \pm 7\ \mathrm{MeV}/c^2$ and a width $\Gamma < 153\ \mathrm{MeV}/c^2$ (at the 90% C.L.) [systematic uncertainties are not included in the error of the mass and the upper limit of the width. In contrast to Ref. [7], the isospin $= 1$ FSI factor is not used to redo the fit since the isospin $= 1$ states are strongly suppressed in J/ψ radiative decays]; these values are in good agreement with the mass and width of $X(1835)$ reported here. Moreover, according to Ref. [5], the $\pi\pi\eta'$ decay mode is expected to be strong for a $p\bar{p}$ bound state. Thus, the $X(1835)$ resonance is a prime candidate for the source of the $p\bar{p}$ mass threshold enhancement in the $J/\psi \to \gamma p\bar{p}$ process. In this case, the J^{PC} and I^G of the $X(1835)$ could only be 0^{-+} and 0^+, which can be tested in future experiments. Also in this context, the relative $p\bar{p}$ decay strength is quite strong: $B(X \to p\bar{p})/B(X \to \pi^+\pi^-\eta') \sim 1/3$ [the product BF determined from the fit that includes FSI effects on the $p\bar{p}$ mass spectrum is within the systematic errors of the result reported in Ref. [1]]. Since decays to $p\bar{p}$ are kinematically allowed only for a small portion of the high-mass tail of the resonance and have very limited phase space, the large $p\bar{p}$ branching fraction implies an unusually strong coupling to $p\bar{p}$, as expected for a $p\bar{p}$ bound state [9,18]. However, other possible interpretations of the $X(1835)$ that have no relation to the $p\bar{p}$ mass threshold enhancement are not excluded.

We thank many Chinese theorists for their helpful discussions and suggestions and Dr. A. Sibirtsev *et al.* for providing the FSI functions. The BES Collaboration acknowledges the staff of BEPC for the excellent performance of the machine. This work is supported in part by the National Natural Science Foundation of China under Contracts No. 10491300, No. 10225524, No. 10225525, No. 10425523, the Chinese Academy of Sciences under Contract No. KJ 95T-03, the 100 Talents Program of CAS under Contracts No. U-11, No. U-24, No. U-25, and the Knowledge Innovation Project of CAS under Contracts No. KJCX2-SW-N10, No. U-602, No. U-34 (IHEP); by the National Natural Science Foundation of China under Contract No. 10175060 (USTC); and by the Department of Energy under Contract No. DE-FG04ER41291 (University of Hawaii).

*Present address: Iowa State University, Ames, IA 50011-3160, USA.
†Present address: Purdue University, West Lafayette, IN 47907, USA.
‡Present address: Cornell University, Ithaca, NY 14853, USA.
§Present address: Laboratoire de l'Accélératear Linéaire, Orsay, F-91898, France.
‖Present address: University of Michigan, Ann Arbor, MI 48109, USA.
¶Present address: DESY, D-22607, Hamburg, Germany.

[1] J.Z. Bai *et al.* (BES Collaboration), Phys. Rev. Lett. **91**, 022001 (2003).
[2] A. Datta and P.J. O'Donnell, Phys. Lett. B **567**, 273 (2003); M.L. Yan *et al.*, Phys. Rev. D **72**, 034027 (2005); B. Loiseau and S. Wycech, Phys. Rev. C **72**, 011001 (2005).
[3] J. Ellis, Y. Frishman, and M. Karliner, Phys. Lett. B **566**, 201 (2003); J.L. Rosner, Phys. Rev. D **68**, 014004 (2003).
[4] C.S. Gao and S.L. Zhu, Commun. Theor. Phys. **42**, 844 (2004).
[5] G.J. Ding and M.L. Yan, Phys. Rev. C **72**, 015208 (2005).
[6] B.S. Zou and H.C. Chiang, Phys. Rev. D **69**, 034004 (2004).
[7] A. Sibirtsev *et al.*, Phys. Rev. D **71**, 054010 (2005).
[8] M. Ablikim *et al.* (BES Collaboration), Phys. Rev. Lett. **93**, 112002 (2004).
[9] I.S. Shapiro, Phys. Rep. **35**, 129 (1978); C.B. Dover and M. Goldhaber, Phys. Rev. D **15**, 1997 (1977).
[10] For recent reviews of this subject, see E. Klempt *et al.*, Phys. Rep. **368**, 119 (2002); J-M. Richard, Nucl. Phys. B, Proc. Suppl. **86**, 361 (2000).
[11] J.Z. Bai *et al.* (BES Collaboration), Nucl. Instrum. Methods Phys. Res., Sect. A **458**, 627 (2001).
[12] M. Ablikim *et al.* (BES Collaboration), Nucl. Instrum. Methods Phys. Res., Sect. A **552**, 344 (2005).
[13] The selection criteria are optimized by maximizing $N_s/\sqrt{N_{\mathrm{tot}}}$, where N_s is the expected number of $J/\psi \to \gamma\pi^+\pi^-\eta'$ signal events and N_{tot} is the total expected number of signal and background events. In order not to bias the $\pi^+\pi^-\eta'$ invariant-mass spectrum, we do not include any resonance in the optimization.
[14] J.C. Chen *et al.*, Phys. Rev. D **62**, 034003 (2000).
[15] S.S. Fang *et al.*, High Energy Phys. Nucl. Phys. **27**, 277 (2003).
[16] S. Eidelman *et al.* (Particle Data Group), Phys. Lett. B **592**, 1 (2004).
[17] J.Z. Bai *et al.* (BES Collaboration), Phys. Lett. B **446**, 356 (1999).
[18] S.L. Zhu and C.S. Gao, hep-ph/0507050.

Observation of a Charged Charmoniumlike Structure in $e^+e^- \to \pi^+\pi^- J/\psi$ at $\sqrt{s} = 4.26$ GeV

M. Ablikim,[1] M. N. Achasov,[6] X. C. Ai,[1] O. Albayrak,[3] D. J. Ambrose,[39] F. F. An,[1] Q. An,[40] J. Z. Bai,[1] R. Baldini Ferroli,[17a] Y. Ban,[26] J. Becker,[2] J. V. Bennett,[16] M. Bertani,[17a] J. M. Bian,[38] E. Boger,[19,*] O. Bondarenko,[20] I. Boyko,[19] R. A. Briere,[3] V. Bytev,[19] H. Cai,[44] X. Cai,[1] O. Cakir,[34a] A. Calcaterra,[17a] G. F. Cao,[1] S. A. Cetin,[34b] J. F. Chang,[1] G. Chelkov,[19,*] G. Chen,[1] H. S. Chen,[1] J. C. Chen,[1] M. L. Chen,[1] S. J. Chen,[24] X. Chen,[26] Y. B. Chen,[1] H. P. Cheng,[14] Y. P. Chu,[1] D. Cronin-Hennessy,[38] H. L. Dai,[1] J. P. Dai,[1] D. Dedovich,[19] Z. Y. Deng,[1] A. Denig,[18] I. Denysenko,[19,†] M. Destefanis,[43a,43c] W. M. Ding,[28] Y. Ding,[22] L. Y. Dong,[1] M. Y. Dong,[1] S. X. Du,[46] J. Fang,[1] S. S. Fang,[1] L. Fava,[43b,43c] C. Q. Feng,[40] P. Friedel,[2] C. D. Fu,[1] J. L. Fu,[24] O. Fuks,[19,*] Q. Gao,[1] Y. Gao,[33] C. Geng,[40] K. Goetzen,[7] W. X. Gong,[1] W. Gradl,[18] M. Greco,[43a,43c] M. H. Gu,[1] Y. T. Gu,[9] Y. H. Guan,[36] A. Q. Guo,[25] L. B. Guo,[23] T. Guo,[23] Y. P. Guo,[25] Y. L. Han,[1] F. A. Harris,[37] K. L. He,[1] M. He,[1] Z. Y. He,[25] T. Held,[2] Y. K. Heng,[1] Z. L. Hou,[1] C. Hu,[23] H. M. Hu,[1] J. F. Hu,[35] T. Hu,[1] G. M. Huang,[4] G. S. Huang,[40] J. S. Huang,[12] L. Huang,[1] X. T. Huang,[28] Y. Huang,[24] Y. P. Huang,[1] T. Hussain,[42] C. S. Ji,[40] Q. Ji,[1] Q. P. Ji,[25] X. B. Ji,[1] X. L. Ji,[1] L. L. Jiang,[1] X. S. Jiang,[1] J. B. Jiao,[28] Z. Jiao,[14] D. P. Jin,[1] S. Jin,[1] F. F. Jing,[33] N. Kalantar-Nayestanaki,[20] M. Kavatsyuk,[20] B. Kopf,[2] M. Kornicer,[37] W. Kühn,[35] W. Lai,[1] J. S. Lange,[35] M. Lara,[16] P. Larin,[11] M. Leyhe,[2] C. H. Li,[1] Cheng Li,[40] Cui Li,[40] D. M. Li,[46] F. Li,[1] G. Li,[1] H. B. Li,[1] J. C. Li,[1] K. Li,[10] Lei Li,[1] Q. J. Li,[1] S. L. Li,[1] W. D. Li,[1] W. G. Li,[1] X. L. Li,[28] X. N. Li,[1] X. Q. Li,[25] X. R. Li,[27] Z. B. Li,[32] H. Liang,[40] Y. F. Liang,[30] Y. T. Liang,[35] G. R. Liao,[33] X. T. Liao,[1] D. Lin,[11] B. J. Liu,[1] C. L. Liu,[3] C. X. Liu,[1] F. H. Liu,[29] Fang Liu,[1] Feng Liu,[4] H. Liu,[1] H. B. Liu,[9] H. H. Liu,[13] H. M. Liu,[1] H. W. Liu,[1] J. P. Liu,[44] K. Liu,[33] K. Y. Liu,[22] Kai Liu,[36] P. L. Liu,[28] Q. Liu,[36] S. B. Liu,[40] X. Liu,[21] Y. B. Liu,[25] Z. A. Liu,[1] Zhiqiang Liu,[1] Zhiqing Liu,[1] H. Loehner,[20] X. C. Lou,[1,‡] G. R. Lu,[12] H. J. Lu,[14] J. G. Lu,[1] Q. W. Lu,[29] X. R. Lu,[36] Y. P. Lu,[1] C. L. Luo,[23] M. X. Luo,[45] T. Luo,[37] X. L. Luo,[1] M. Lv,[1] C. L. Ma,[36] F. C. Ma,[22] H. L. Ma,[1] Q. M. Ma,[1] S. Ma,[1] T. Ma,[1] X. Y. Ma,[1] F. E. Maas,[11] M. Maggiora,[43a,43c] Q. A. Malik,[42] Y. J. Mao,[26] Z. P. Mao,[1] J. G. Messchendorp,[20] J. Min,[1] T. J. Min,[1] R. E. Mitchell,[16] X. H. Mo,[1] Y. J. Mo,[10] H. Moeini,[20] C. Morales Morales,[11] K. Moriya,[16] N. Yu. Muchnoi,[6] H. Muramatsu,[39] Y. Nefedov,[19] C. Nicholson,[36] I. B. Nikolaev,[6] Z. Ning,[1] S. L. Olsen,[27] Q. Ouyang,[1] S. Pacetti,[17b] J. W. Park,[27] M. Pelizaeus,[2] H. P. Peng,[40] K. Peters,[7] J. L. Ping,[23] R. G. Ping,[1] R. Poling,[38] E. Prencipe,[18] M. Qi,[24] S. Qian,[1] C. F. Qiao,[36] L. Q. Qin,[28] X. S. Qin,[1] Y. Qin,[26] Z. H. Qin,[1] J. F. Qiu,[1] K. H. Rashid,[42] G. Rong,[1] X. D. Ruan,[9] A. Sarantsev,[19,§] B. D. Schaefer,[16] M. Shao,[40] C. P. Shen,[37,‖] X. Y. Shen,[1] H. Y. Sheng,[1] M. R. Shepherd,[16] W. M. Song,[1] X. Y. Song,[1] S. Spataro,[43a,43c] B. Spruck,[35] D. H. Sun,[1] G. X. Sun,[1] J. F. Sun,[12] S. S. Sun,[1] Y. J. Sun,[40] Y. Z. Sun,[1] Z. J. Sun,[1] Z. T. Sun,[40] C. J. Tang,[30] X. Tang,[1] I. Tapan,[34c] E. H. Thorndike,[39] D. Toth,[38] M. Ullrich,[35] I. Uman,[34b] G. S. Varner,[37] B. Q. Wang,[26] D. Wang,[26] D. Y. Wang,[26] K. Wang,[1] L. L. Wang,[1] L. S. Wang,[1] M. Wang,[28] P. Wang,[1] P. L. Wang,[1] Q. J. Wang,[1] S. G. Wang,[26] X. F. Wang,[33] X. L. Wang,[40] Y. D. Wang,[17a] Y. F. Wang,[1] Y. Q. Wang,[18] Z. Wang,[1] Z. G. Wang,[1] Z. Y. Wang,[1] D. H. Wei,[8] J. B. Wei,[26] P. Weidenkaff,[18] Q. G. Wen,[40] S. P. Wen,[1] M. Werner,[35] U. Wiedner,[2] L. H. Wu,[1] N. Wu,[1] S. X. Wu,[40] W. Wu,[25] Z. Wu,[1] L. G. Xia,[33] Y. X. Xia,[15] Z. J. Xiao,[23] Y. G. Xie,[1] Q. L. Xiu,[1] G. F. Xu,[1] G. M. Xu,[26] Q. J. Xu,[10] Q. N. Xu,[36] X. P. Xu,[31] Z. R. Xu,[40] F. Xue,[4] Z. Xue,[1] L. Yan,[40] W. B. Yan,[40] Y. H. Yan,[15] H. X. Yang,[1] Y. Yang,[4] Y. X. Yang,[8] H. Ye,[1] M. Ye,[1] M. H. Ye,[5] B. X. Yu,[1] C. X. Yu,[25] H. W. Yu,[26] J. S. Yu,[21] S. P. Yu,[28] C. Z. Yuan,[1] Y. Yuan,[1] A. A. Zafar,[42] A. Zallo,[17a] S. L. Zang,[24] Y. Zeng,[15] B. X. Zhang,[1] B. Y. Zhang,[1] C. Zhang,[24] C. C. Zhang,[1] D. H. Zhang,[1] H. H. Zhang,[32] H. Y. Zhang,[1] J. Q. Zhang,[1] J. W. Zhang,[1] J. Y. Zhang,[1] J. Z. Zhang,[1] LiLi Zhang,[15] R. Zhang,[36] S. H. Zhang,[1] X. J. Zhang,[1] X. Y. Zhang,[28] Y. Zhang,[1] Y. H. Zhang,[1] Z. P. Zhang,[40] Z. Y. Zhang,[44] Zhenghao Zhang,[4] G. Zhao,[1] H. S. Zhao,[1] J. W. Zhao,[1] K. X. Zhao,[23] Lei Zhao,[40] Ling Zhao,[1] M. G. Zhao,[25] Q. Zhao,[1] S. J. Zhao,[46] T. C. Zhao,[1] X. H. Zhao,[24] Y. B. Zhao,[1] Z. G. Zhao,[40] A. Zhemchugov,[19,*] B. Zheng,[41] J. P. Zheng,[1] Y. H. Zheng,[36] B. Zhong,[23] L. Zhou,[1] X. Zhou,[44] X. K. Zhou,[36] X. R. Zhou,[40] C. Zhu,[1] K. Zhu,[1] K. J. Zhu,[1] S. H. Zhu,[1] X. L. Zhu,[33] Y. C. Zhu,[40] Y. M. Zhu,[25] Y. S. Zhu,[1] Z. A. Zhu,[1] J. Zhuang,[1] B. S. Zou,[1] and J. H. Zou[1]

(BESIII Collaboration)

[1]*Institute of High Energy Physics, Beijing 100049, People's Republic of China*
[2]*Bochum Ruhr-University, D-44780 Bochum, Germany*
[3]*Carnegie Mellon University, Pittsburgh, Pennsylvania 15213, USA*
[4]*Central China Normal University, Wuhan 430079, People's Republic of China*
[5]*China Center of Advanced Science and Technology, Beijing 100190, People's Republic of China*
[6]*G. I. Budker Institute of Nuclear Physics SB RAS (BINP), Novosibirsk 630090, Russia*
[7]*GSI Helmholtzcentre for Heavy Ion Research GmbH, D-64291 Darmstadt, Germany*
[8]*Guangxi Normal University, Guilin 541004, People's Republic of China*

[9]GuangXi University, Nanning 530004, People's Republic of China
[10]Hangzhou Normal University, Hangzhou 310036, People's Republic of China
[11]Helmholtz Institute Mainz, Johann-Joachim-Becher-Weg 45, D-55099 Mainz, Germany
[12]Henan Normal University, Xinxiang 453007, People's Republic of China
[13]Henan University of Science and Technology, Luoyang 471003, People's Republic of China
[14]Huangshan College, Huangshan 245000, People's Republic of China
[15]Hunan University, Changsha 410082, People's Republic of China
[16]Indiana University, Bloomington, Indiana 47405, USA
[17a]INFN Laboratori Nazionali di Frascati, I-00044 Frascati, Italy
[17b]INFN and University of Perugia, I-06100 Perugia, Italy
[18]Johannes Gutenberg University of Mainz, Johann-Joachim-Becher-Weg 45, D-55099 Mainz, Germany
[19]Joint Institute for Nuclear Research, 141980 Dubna, Moscow region, Russia
[20]KVI, University of Groningen, NL-9747 AA Groningen, The Netherlands
[21]Lanzhou University, Lanzhou 730000, People's Republic of China
[22]Liaoning University, Shenyang 110036, People's Republic of China
[23]Nanjing Normal University, Nanjing 210023, People's Republic of China
[24]Nanjing University, Nanjing 210093, People's Republic of China
[25]Nankai University, Tianjin 300071, People's Republic of China
[26]Peking University, Beijing 100871, People's Republic of China
[27]Seoul National University, Seoul 151-747 Korea
[28]Shandong University, Jinan 250100, People's Republic of China
[29]Shanxi University, Taiyuan 030006, People's Republic of China
[30]Sichuan University, Chengdu 610064, People's Republic of China
[31]Soochow University, Suzhou 215006, People's Republic of China
[32]Sun Yat-Sen University, Guangzhou 510275, People's Republic of China
[33]Tsinghua University, Beijing 100084, People's Republic of China
[34a]Ankara University, Dogol Caddesi, 06100 Tandogan, Ankara, Turkey
[34b]Dogus University, 34722 Istanbul, Turkey
[34c]Uludag University, 16059 Bursa, Turkey
[35]Universität Giessen, D-35392 Giessen, Germany
[36]University of Chinese Academy of Sciences, Beijing 100049, People's Republic of China
[37]University of Hawaii, Honolulu, Hawaii 96822, USA
[38]University of Minnesota, Minneapolis, Minnesota 55455, USA
[39]University of Rochester, Rochester, New York 14627, USA
[40]University of Science and Technology of China, Hefei 230026, People's Republic of China
[41]University of South China, Hengyang 421001, People's Republic of China
[42]University of the Punjab, Lahore 54590, Pakistan
[43a]University of Turin, I-10125 Turin, Italy
[43b]University of Eastern Piedmont, I-15121 Alessandria, Italy
[43c]INFN, I-10125 Turin, Italy
[44]Wuhan University, Wuhan 430072, People's Republic of China
[45]Zhejiang University, Hangzhou 310027, People's Republic of China
[46]Zhengzhou University, Zhengzhou 450001, People's Republic of China
(Received 24 March 2013; published 17 June 2013)

We study the process $e^+e^- \to \pi^+\pi^- J/\psi$ at a center-of-mass energy of 4.260 GeV using a 525 pb^{-1} data sample collected with the BESIII detector operating at the Beijing Electron Positron Collider. The Born cross section is measured to be $(62.9 \pm 1.9 \pm 3.7)$ pb, consistent with the production of the $Y(4260)$. We observe a structure at around 3.9 GeV/c^2 in the $\pi^\pm J/\psi$ mass spectrum, which we refer to as the $Z_c(3900)$. If interpreted as a new particle, it is unusual in that it carries an electric charge and couples to charmonium. A fit to the $\pi^\pm J/\psi$ invariant mass spectrum, neglecting interference, results in a mass of $(3899.0 \pm 3.6 \pm 4.9)$ MeV/c^2 and a width of $(46 \pm 10 \pm 20)$ MeV. Its production ratio is measured to be $R = (\sigma(e^+e^- \to \pi^\pm Z_c(3900)^\mp \to \pi^+\pi^- J/\psi)/\sigma(e^+e^- \to \pi^+\pi^- J/\psi)) = (21.5 \pm 3.3 \pm 7.5)\%$. In all measurements the first errors are statistical and the second are systematic.

DOI: 10.1103/PhysRevLett.110.252001 PACS numbers: 14.40.Rt, 13.66.Bc, 14.40.Pq

Since its discovery in the initial-state-radiation (ISR) process $e^+e^- \to \gamma_{\mathrm{ISR}}\pi^+\pi^- J/\psi$ [1], and despite its subsequent observations [2–5], the nature of the $Y(4260)$ state has remained a mystery. Unlike other charmonium states with the same quantum numbers and in the same mass region, such as the $\psi(4040)$, $\psi(4160)$, and $\psi(4415)$, the

$Y(4260)$ state does not have a natural place within the quark model of charmonium [6]. Furthermore, while being well above the $D\bar{D}$ threshold, the $Y(4260)$ shows strong coupling to the $\pi^+\pi^- J/\psi$ final state [7], but relatively small coupling to open charm decay modes [8–12]. These properties perhaps indicate that the $Y(4260)$ state is not a conventional state of charmonium [13].

A similar situation has recently become apparent in the bottomonium system above the $B\bar{B}$ threshold, where there are indications of anomalously large couplings between the $\Upsilon(5S)$ state [or perhaps an unconventional bottomonium state with similar mass, the $Y_b(10890)$] and the $\pi^+\pi^-\Upsilon(1S, 2S, 3S)$ and $\pi^+\pi^- h_b(1P, 2P)$ final states [14,15]. More surprisingly, substructure in these $\pi^+\pi^-\Upsilon(1S, 2S, 3S)$ and $\pi^+\pi^- h_b(1P, 2P)$ decays indicates the possible existence of charged bottomoniumlike states [16], which must have at least four constituent quarks to have a nonzero electric charge, rather than the two in a conventional meson. By analogy, this suggests there may exist interesting substructure in the $Y(4260) \to \pi^+\pi^- J/\psi$ process in the charmonium region.

In this Letter, we present a study of the process $e^+e^- \to \pi^+\pi^- J/\psi$ at a center-of-mass (c.m.) energy of $\sqrt{s} = (4.260 \pm 0.001)$ GeV, which corresponds to the peak of the $Y(4260)$ cross section. We observe a charged structure in the $\pi^\pm J/\psi$ invariant mass spectrum, which we refer to as the $Z_c(3900)$. The analysis is performed with a 525 pb^{-1} data sample collected with the BESIII detector, which is described in detail in Ref. [17]. In the studies presented here, we rely only on charged particle tracking in the main drift chamber and energy deposition in the electromagnetic calorimeter (EMC).

The GEANT4-based Monte Carlo (MC) simulation software, which includes the geometric description of the BESIII detector and the detector response, is used to optimize the event selection criteria, determine the detection efficiency, and estimate backgrounds. For the signal process, we use a sample of $e^+e^- \to \pi^+\pi^- J/\psi$ MC events generated assuming the $\pi^+\pi^- J/\psi$ is produced via $Y(4260)$ decays, and using the $e^+e^- \to \pi^+\pi^- J/\psi$ cross sections measured by Belle [3] and *BABAR* [5]. The $\pi^+\pi^- J/\psi$ substructure is modelled according to the experimentally observed Dalitz plot distribution presented in this analysis. ISR is simulated with KKMC [18] with a maximum energy of 435 MeV for the ISR photon, corresponding to a $\pi^+\pi^- J/\psi$ mass of 3.8 GeV$/c^2$.

For $e^+e^- \to \pi^+\pi^- J/\psi$ events, the J/ψ candidate is reconstructed with lepton pairs (e^+e^- or $\mu^+\mu^-$). Since this decay results in a final state with four charged particles, we first select events with four good charged tracks with net charge zero. For each charged track, the polar angle in the main drift chamber must satisfy $|\cos\theta| < 0.93$, and the point of closest approach to the e^+e^- interaction point must be within ± 10 cm in the beam direction and within 1 cm in the plane perpendicular to the beam direction. Since pions and leptons are kinematically well separated in this decay, charged tracks with momenta larger than 1.0 GeV$/c$ in the lab frame are assumed to be leptons, and the others are assumed to be pions. We use the energy deposited in the EMC to separate electrons from muons. For muon candidates, the deposited energy in the EMC should be less than 0.35 GeV, while for electrons, it should be larger than 1.1 GeV. The efficiencies of these requirements are determined from MC simulation to be above 99% in the EMC sensitive region.

In order to reject radiative Bhabha and radiative dimuon ($\gamma e^+e^-/\gamma\mu^+\mu^-$) backgrounds associated with a photon-conversion, the cosine of the opening angle of the pion candidates, which are true e^+e^- pairs in the case of background, is required to be less than 0.98. In the e^+e^- mode, the same requirement is imposed on the $\pi^\pm e^\mp$ opening angles. This restriction removes less than 1% of the signal events.

The lepton pair and the two pions are subjected to a four-constraint (4C) kinematic fit to the total initial four-momentum of the colliding beams in order to improve the momentum resolution and reduce the background. The χ^2 of the kinematic fit is required to be less than 60.

After imposing these selection criteria, the invariant mass distributions of the lepton pairs are shown in Fig. 1. A clear J/ψ signal is observed in both the e^+e^- and $\mu^+\mu^-$ modes. There are still remaining $e^+e^- \to \pi^+\pi^-\pi^+\pi^-$, and other QED backgrounds, but these can be estimated using the events in the J/ψ mass sideband.

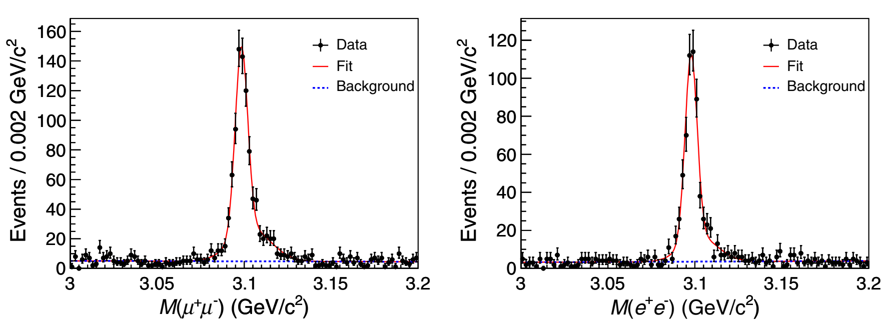

FIG. 1 (color online). The distributions of $M(\mu^+\mu^-)$ (left panel) and $M(e^+e^-)$ (right panel) after performing a 4C kinematic fit and imposing all selection criteria. Dots with error bars are data and the curves are the best fit described in the text.

The final selection efficiency is $(53.8 \pm 0.3)\%$ for $\mu^+\mu^-$ events and $(38.4 \pm 0.3)\%$ for e^+e^- events, where the errors are from the statistics of the MC sample. The main factors affecting the detection efficiencies include the detector acceptances for four charged tracks and the requirement on the quality of the kinematic fit adopted. The lower efficiency for e^+e^- events is due to final-state-radiation, bremsstrahlung energy loss of e^+e^- pairs, and the EMC deposit energy requirement.

To extract the number of $\pi^+\pi^-J/\psi$ signal events, invariant mass distributions of the lepton pairs are fit using the sum of two Gaussian functions with a linear background term. The fits yield $M(J/\psi) = (3098.4 \pm 0.2)\ \mathrm{MeV}/c^2$ with 882 ± 33 signal events in the $\mu^+\mu^-$ mode, and $M(J/\psi) = (3097.9 \pm 0.3)\ \mathrm{MeV}/c^2$ with 595 ± 28 signal events in the e^+e^- mode. Here the errors are statistical only. The mass resolution is $3.7\ \mathrm{MeV}/c^2$ in the $\mu^+\mu^-$ mode and $4.0\ \mathrm{MeV}/c^2$ in the e^+e^- mode.

The Born cross section is determined from the relation $\sigma^B = (N^{\mathrm{fit}}/\mathcal{L}_{\mathrm{int}}(1+\delta)\epsilon\mathcal{B})$, where N^{fit} is the number of signal events from the fit; $\mathcal{L}_{\mathrm{int}}$ is the integrated luminosity, ϵ is the selection efficiency obtained from a MC simulation, $\mathcal{B}$ is the branching fraction of $J/\psi \to \ell^+\ell^-$, and $(1+\delta)$ is the radiative correction factor, which is 0.818 according to a QED calculation [19]. The measured Born cross section for $e^+e^- \to \pi^+\pi^-J/\psi$ is (64.4 ± 2.4) pb in the $\mu^+\mu^-$ mode and (60.7 ± 2.9) pb in the e^+e^- mode. The combined measurement is $\sigma^B(e^+e^- \to \pi^+\pi^-J/\psi) = (62.9 \pm 1.9)$ pb.

Systematic errors in the cross section measurement come from the luminosity measurement, tracking efficiency, kinematic fit, background estimation, dilepton branching fractions of the J/ψ, and $Y(4260)$ decay dynamics.

The integrated luminosity of this data sample was measured using large angle Bhabha events, and has an estimated uncertainty of 1.0%. The tracking efficiency uncertainty is estimated to be 1% for each track from a study of the control samples $J/\psi \to \pi^+\pi^-\pi^0$ and $\psi(3686) \to \pi^+\pi^-J/\psi$. Since the luminosity is measured using Bhabha events, the tracking efficiency uncertainty of high momentum lepton pairs partly cancels in the calculation of the $\pi^+\pi^-J/\psi$ cross section. To be conservative, we take 4% for both the e^+e^- and $\mu^+\mu^-$ modes.

The uncertainty from the kinematic fit comes from the inconsistency between the data and MC simulation of the track helix parameters. Following the procedure described in Ref. [20], we take the difference between the efficiencies with and without the helix parameter correction as the systematic error, which is 2.2% in the $\mu^+\mu^-$ mode and 2.3% in the e^+e^- mode.

Uncertainties due to the choice of background shape and fit range are estimated by varying the background function from linear to a second-order polynomial and by extending the fit range.

Uncertainties in the $Y(4260)$ resonance parameters and possible distortions of the $Y(4260)$ line shape introduce small systematic uncertainties in the radiative correction factor and the efficiency. This is estimated using the different line shapes measured by Belle [3] and *BABAR* [5]. The difference in $(1+\delta)\epsilon$ is 0.6% in both the e^+e^- and $\mu^+\mu^-$ modes, and this is taken as a systematic error.

We use the observed Dalitz plot to generate $Y(4260) \to \pi^+\pi^-J/\psi$ events. To cover possible modelling inaccuracies, we conservatively take the difference between the efficiency using this model and the efficiency using a phase space model as a systematic error. The error is 3.1% in both the $\mu^+\mu^-$ and the e^+e^- modes.

The uncertainty in $\mathcal{B}(J/\psi \to \ell^+\ell^-)$ is 1% [21]. The trigger simulation, the event start time determination, and the final-state-radiation simulation are well understood; the total systematic error due to these sources is estimated to be less than 1%.

Assuming all of the sources are independent, the total systematic error in the $\pi^+\pi^-J/\psi$ cross section measurement is determined to be 5.9% for the $\mu^+\mu^-$ mode and 6.8% for the e^+e^- mode. Taking the correlations in errors between the two modes into account, the combined systematic error is slightly less than 5.9%.

Intermediate states are studied by examining the Dalitz plot of the selected $\pi^+\pi^-J/\psi$ candidate events. The J/ψ signal is selected using $3.08 < M(\ell^+\ell^-) < 3.12\ \mathrm{GeV}/c^2$ and the sideband using $3.00 < M(\ell^+\ell^-) < 3.06\ \mathrm{GeV}/c^2$ or $3.14 < M(\ell^+\ell^-) < 3.20\ \mathrm{GeV}/c^2$, which is three times the size of the signal region. In total, a sample of 1595 $\pi^+\pi^-J/\psi$ events with a purity of 90% is obtained.

Figure 2 shows the Dalitz plot of events in the J/ψ signal region, where there are structures in the $\pi^+\pi^-$ system and evidence for an exotic charmoniumlike structure in the $\pi^\pm J/\psi$ system. The inset shows background events from J/ψ mass sidebands (not normalized), where no obvious structures are observed.

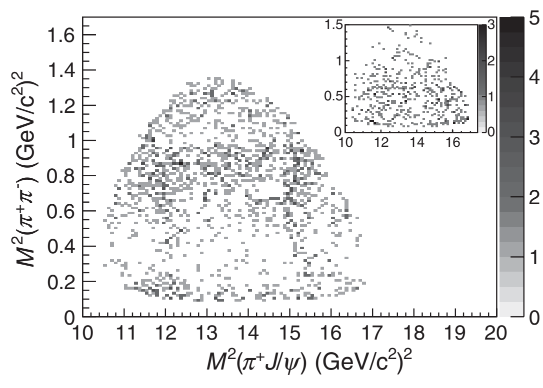

FIG. 2. Dalitz distributions of $M^2(\pi^+\pi^-)$ vs $M^2(\pi^+J/\psi)$ for selected $e^+e^- \to \pi^+\pi^-J/\psi$ events in the J/ψ signal region. The inset shows background events from the J/ψ mass sidebands (not normalized).

Figure 3 shows the projections of the $M(\pi^+ J/\psi)$, $M(\pi^- J/\psi)$, and $M(\pi^+\pi^-)$ distributions for the signal events, as well as the background events estimated from normalized J/ψ mass sidebands. In the $\pi^\pm J/\psi$ mass spectrum, there is a significant peak at around $3.9\ \mathrm{GeV}/c^2$ [referred to as the $Z_c(3900)$ hereafter]. The wider peak at low mass is a reflection of the $Z_c(3900)$ as indicated from MC simulation, and shown in Fig. 3. Similar structures are observed in the e^+e^- and $\mu^+\mu^-$ separated samples.

The $\pi^+\pi^-$ mass spectrum shows nontrivial structure. To test the possible effects of dynamics in the $\pi^+\pi^-$ mass spectrum on the $\pi^\pm J/\psi$ projection, we develop a parametrization for the $\pi^+\pi^-$ mass spectrum that includes a $f_0(980)$, $\sigma(500)$, and a nonresonant amplitude. An MC sample generated with this parametrization adequately describes the $\pi^+\pi^-$ spectrum, as shown in Fig. 3, but does not generate any peaking structure in the $\pi^\pm J/\psi$ projection consistent with the $Z_c(3900)$. We have also tested D-wave $\pi^+\pi^-$ amplitudes, which are not apparent in the data, and they, also, do not generate peaks in the $\pi^\pm J/\psi$ spectrum.

An unbinned maximum likelihood fit is applied to the distribution of $M_{\max}(\pi^\pm J/\psi)$, the larger one of the two mass combinations $M(\pi^+ J/\psi)$ and $M(\pi^- J/\psi)$ in each event. The signal shape is parametrized as an S-wave Breit-Wigner function convolved with a Gaussian with a mass resolution fixed at the MC simulated value ($4.2\ \mathrm{MeV}/c^2$). The phase space factor $p \cdot q$ is considered in the partial width, where p is the $Z_c(3900)$ momentum in the $Y(4260)$ c.m. frame and q is the J/ψ momentum in the $Z_c(3900)$ c.m. frame. The background shape is parametrized as $a/(x-3.6)^b + c + dx$, where a, b, c, and d are free parameters and $x = M_{\max}(\pi^\pm J/\psi)$. The efficiency curve is considered in the fit and the possible interference between the signal and background is neglected. Figure 4 shows the fit results; the fit yields a mass of $(3899.0 \pm 3.6)\ \mathrm{MeV}/c^2$, and a width of (46 ± 10) MeV. The goodness of the fit is found to be $\chi^2/\mathrm{ndf} = 32.6/37 = 0.9$.

The number of $Z_c(3900)$ events is determined to be $N[Z_c(3900)^\pm] = 307 \pm 48$. The production ratio is calculated to be $R = \sigma(e^+e^- \to \pi^\pm Z_c(3900)^\mp \to \pi^+\pi^- J/\psi)/\sigma(e^+e^- \to \pi^+\pi^- J/\psi) = (21.5 \pm 3.3)\%$, where the efficiency correction has been applied. The statistical significance is calculated by comparing the fit likelihoods with and without the signal. Besides the nominal fit, the fit is also performed by changing the fit range, the signal shape, or the background shape. In all cases, the significance is found to be greater than 8σ.

Fitting the $M(\pi^+ J/\psi)$ and $M(\pi^- J/\psi)$ distributions separately, one obtains masses, widths, and production rates of the $Z_c(3900)^+$ and $Z_c(3900)^-$ that agree with each other within statistical errors. Dividing the sample into two different $M(\pi^+\pi^-)$ regions [below and above $M^2(\pi^+\pi^-) = 0.7\ \mathrm{GeV}^2/c^4$] allows us to check the robustness of the $Z_c(3900)$ signal in the presence of two different sets of interfering $\pi^+\pi^- J/\psi$ amplitudes. In both samples, the $Z_c(3900)$ is significant and the observed mass can shift by as much as $14 \pm 5\ \mathrm{MeV}/c^2$ from the nominal fit, and the width can shift by (20 ± 11) MeV. We attribute the systematic shifts in mass and width to interference between the $Z_c(3900)\pi$ and $(\pi^+\pi^-)J/\psi$ amplitudes. In fitting the $\pi^\pm J/\psi$ projection of the Dalitz plot, our analysis averages over the entire $\pi^+\pi^-$ spectrum, and our measurement of the $Z_c(3900)$ mass, width, and production fraction neglects interference with other $\pi^+\pi^- J/\psi$ amplitudes.

The systematic errors for the resonance parameters of the $Z_c(3900)$ come from the mass calibration, parametrization of the signal and background shapes, and the mass resolution. The uncertainty from the mass calibration can be estimated using the difference between the measured and known J/ψ masses (reconstructed from e^+e^- and $\mu^+\mu^-$) and D^0 masses (reconstructed from $K^-\pi^+$). The differences are $(1.4 \pm 0.2)\ \mathrm{MeV}/c^2$ and $-(0.7 \pm 0.2)\ \mathrm{MeV}/c^2$, respectively. Since our signal topology has one low momentum pion, as in D^0 decay, and a pair of high momentum tracks from the J/ψ decay, we assume these differences added in quadrature is the systematic error of the $Z_c(3900)$ mass measurement due to tracking. Doing a fit by assuming a P wave between the $Z_c(3900)$ and the π, and between the J/ψ and π in the $Z_c(3900)$ system, yields

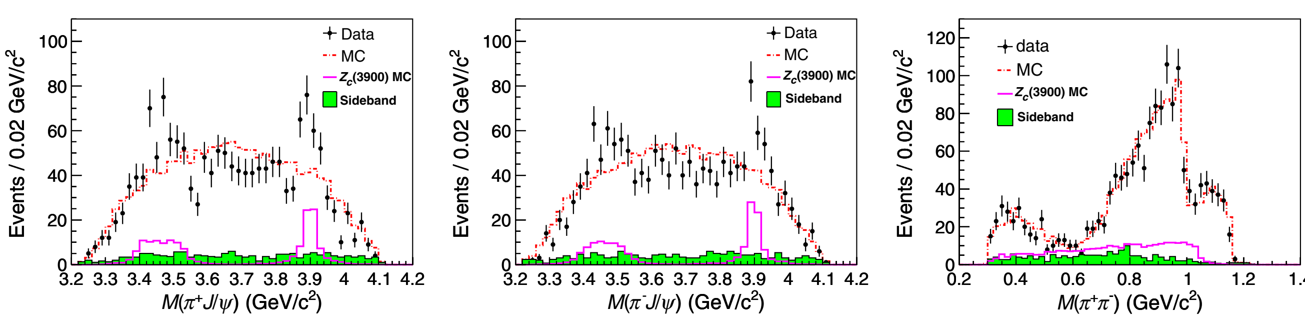

FIG. 3 (color online). One dimensional projections of the $M(\pi^+ J/\psi)$, $M(\pi^- J/\psi)$, and $M(\pi^+\pi^-)$ invariant mass distributions in $e^+e^- \to \pi^+\pi^- J/\psi$ for data in the J/ψ signal region (dots with error bars), data in the J/ψ sideband region (shaded histograms), and MC simulation results from $\sigma(500)$, $f_0(980)$, and nonresonant $\pi^+\pi^-$ amplitudes (red dotted-dashed histograms). The pink blank histograms show a MC simulation of the $Z_c(3900)$ signal with arbitrary normalization.

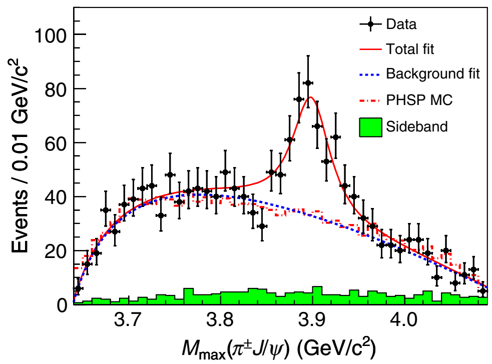

FIG. 4 (color online). Fit to the $M_{\max}(\pi^{\pm}J/\psi)$ distribution as described in the text. Dots with error bars are data; the red solid curve shows the total fit, and the blue dotted curve the background from the fit; the red dotted-dashed histogram shows the result of a phase space (PHSP) MC simulation; and the green shaded histogram shows the normalized J/ψ sideband events.

a mass difference of 2.1 MeV$/c^2$, a width difference of 3.7 MeV, and production ratio difference of 2.6% absolute. Assuming the $Z_c(3900)$ couples strongly with $D\bar{D}^*$ results in an energy dependence of the total width [22], and the fit yields a difference of 2.1 MeV$/c^2$ for mass, 15.4 MeV for width, and no change for the production ratio. We estimate the uncertainty due to the background shape by changing to a third-order polynomial or a phase space shape, varying the fit range, and varying the requirements on the χ^2 of the kinematic fit. We find differences of 3.5 MeV$/c^2$ for mass, 12.1 MeV for width, and 7.1% absolute for the production ratio. Uncertainties due to the mass resolution are estimated by increasing the resolution determined by MC simulations by 16%, which is the difference between the MC simulated and measured mass resolutions of the J/ψ and D^0 signals. We find the difference is 1.0 MeV in the width, and 0.2% absolute in the production ratio, which are taken as the systematic errors. Assuming all the sources of systematic uncertainty are independent, the total systematic error is 4.9 MeV$/c^2$ for mass, 20 MeV for width and 7.5% for the production ratio.

In Summary, we have studied $e^+e^- \to \pi^+\pi^- J/\psi$ at a c.m. energy of 4.26 GeV. The cross section is measured to be $(62.9 \pm 1.9 \pm 3.7)$ pb, which agrees with the existing results from the *BABAR* [5], Belle [3], and CLEO [4] experiments. In addition, a structure with a mass of $(3899.0 \pm 3.6 \pm 4.9)$ MeV$/c^2$ and a width of $(46 \pm 10 \pm 20)$ MeV is observed in the $\pi^{\pm}J/\psi$ mass spectrum. This structure couples to charmonium and has an electric charge, which is suggestive of a state containing more quarks than just a charm and anticharm quark. Similar studies were performed in B decays, with unconfirmed structures reported in the $\pi^{\pm}\psi(3686)$ and $\pi^{\pm}\chi_{c1}$ systems [23–26]. It is also noted that model-dependent calculations exist that attempt to explain the charged bottomonium-like structures which may also apply to the charmonium-like structures, and there were model predictions of charmoniumlike structures near the $D\bar{D}^*$ and $D^*\bar{D}^*$ thresholds [27].

The BESIII collaboration thanks the staff of BEPCII and the computing center for their hard efforts. This work is supported in part by the Ministry of Science and Technology of China under Contract No. 2009CB825200; National Natural Science Foundation of China (NSFC) under Contracts No. 10625524, No. 10821063, No. 10825524, No. 10835001, No. 10935007, No. 11125525, and No. 11235011; Joint Funds of the National Natural Science Foundation of China under Contracts No. 11079008, and No. 11179007; the Chinese Academy of Sciences (CAS) Large-Scale Scientific Facility Program; CAS under Contracts No. KJCX2-YW-N29, and No. KJCX2-YW-N45; 100 Talents Program of CAS; German Research Foundation DFG under Contract No. Collaborative Research Center CRC-1044; Istituto Nazionale di Fisica Nucleare, Italy; Ministry of Development of Turkey under Contract No. DPT2006K-120470; U. S. Department of Energy under Contracts No. DE-FG02-04ER41291, No. DE-FG02-05ER41374, and No. DE-FG02-94ER40823; U.S. National Science Foundation; University of Groningen (RuG) and the Helmholtzzentrum fuer Schwerionenforschung GmbH (GSI), Darmstadt; National Research Foundation of Korea Grant No. 2011-0029457 and WCU Grant No. R32-10155.

*Also at the Moscow Institute of Physics and Technology, Moscow 141700, Russia.
†On leave from the Bogolyubov Institute for Theoretical Physics, Kiev 03680, Ukraine.
‡Also at University of Texas at Dallas, Richardson, Texas 75083, USA.
§Also at the PNPI, Gatchina 188300, Russia.
‖Present address: Nagoya University, Nagoya 464-8601, Japan.

[1] B. Aubert *et al.* (*BABAR* Collaboration), Phys. Rev. Lett. **95**, 142001 (2005).
[2] Q. He *et al.* (CLEO Collaboration), Phys. Rev. D **74**, 091104(R) (2006).
[3] C. Z. Yuan *et al.* (Belle Collaboration), Phys. Rev. Lett. **99**, 182004 (2007).
[4] T. E. Coan *et al.* (CLEO Collaboration), Phys. Rev. Lett. **96**, 162003 (2006).
[5] J. P. Lees *et al.* (*BABAR* Collaboration), Phys. Rev. D **86**, 051102(R) (2012).
[6] T. Barnes, S. Godfrey, and E. S. Swanson, Phys. Rev. D **72**, 054026 (2005).
[7] X. H. Mo, G. Li, C. Z. Yuan, K. L. He, H. M. Hu, J. H. Hu, P. Wang, and Z. Y. Wang, Phys. Lett. B **640**, 182 (2006).
[8] D. Cronin-Hennessy *et al.* (CLEO Collaboration), Phys. Rev. D **80**, 072001 (2009).
[9] G. Pakhlova *et al.* (Belle Collaboration), Phys. Rev. Lett. **98**, 092001 (2007).

[10] B. Aubert *et al.* (*BABAR* Collaboration), Phys. Rev. D **76**, 111105 (2007).
[11] B. Aubert *et al.* (*BABAR* Collaboration), Phys. Rev. D **79**, 092001 (2009).
[12] P. del Amo Sanchez *et al.* (*BABAR* Collaboration), Phys. Rev. D **82**, 052004 (2010).
[13] For a recent review, see N. Brambilla *et al.*, Eur. Phys. J. C **71**, 1 (2011).
[14] K.-F Chen *et al.* (Belle Collaboration), Phys. Rev. Lett. **100**, 112001 (2008).
[15] I. Adachi *et al.* (Belle Collaboration), Phys. Rev. Lett. **108**, 032001 (2012).
[16] A. Bondar *et al.* (Belle Collaboration), Phys. Rev. Lett. **108**, 122001 (2012).
[17] M. Ablikim *et al.* (BESIII Collaboration), Nucl. Instrum. Methods Phys. Res., Sect. A **614**, 345 (2010).
[18] S. Jadach, B. F. L. Ward, and Z. Was, Comput. Phys. Commun. **130**, 260 (2000); Phys. Rev. D **63**, 113009 (2001).
[19] E. A. Kuraev and V. S. Fadin, Yad. Fiz. **41**, 733 (1985) [Sov. J. Nucl. Phys. **41**, 466 (1985)].
[20] M. Ablikim *et al.* (BESIII Collaboration), Phys. Rev. D **87**, 012002 (2013).
[21] J. Beringer *et al.* (Particle Data Group), Phys. Rev. D **86**, 010001 (2012).
[22] S. Flatté, Phys. Lett. **63B**, 224 (1976).
[23] S. K. Choi *et al.* (Belle Collaboration), Phys. Rev. Lett. **100**, 142001 (2008).
[24] B. Aubert *et al.* (*BABAR* Collaboration), Phys. Rev. D **79**, 112001 (2009).
[25] R. Mizuk *et al.* (Belle Collaboration), Phys. Rev. D **78**, 072004 (2008).
[26] J. P. Lees *et al.* (*BABAR* Collaboration), Phys. Rev. D **85**, 052003 (2012).
[27] L. Maiani, F. Piccinini, A. D. Polosa, and V. Riquer, Phys. Rev. D **71**, 014028 (2005); D.-Y. Chen, X. Liu, and T. Matsuki, arXiv:1208.2411; D.-Y. Chen and X. Liu, Phys. Rev. D **84**, 034032 (2011); Z.-F. Sun, J. He, X. Liu, Z.-G. Luo, and S.-L. Zhu, Phys. Rev. D **84**, 054002 (2011); Chinese Phys. C **36**, 194 (2012); A. Ali, C. Hambrock, and W. Wang, Phys. Rev. D **85**, 054011 (2012).

Observation of a Charged Charmoniumlike Structure $Z_c(4020)$ and Search for the $Z_c(3900)$ in $e^+e^- \to \pi^+\pi^- h_c$

M. Ablikim,[1] M. N. Achasov,[8,*] O. Albayrak,[4] D. J. Ambrose,[41] F. F. An,[1] Q. An,[42] J. Z. Bai,[1] R. Baldini Ferroli,[19a] Y. Ban,[28] J. Becker,[3] J. V. Bennett,[18] M. Bertani,[19a] J. M. Bian,[40] E. Boger,[21,†] O. Bondarenko,[22] I. Boyko,[21] S. Braun,[37] R. A. Briere,[4] V. Bytev,[21] H. Cai,[46] X. Cai,[1] O. Cakir,[36a] A. Calcaterra,[19a] G. F. Cao,[1] S. A. Cetin,[36b] J. F. Chang,[1] G. Chelkov,[21,†] G. Chen,[1] H. S. Chen,[1] J. C. Chen,[1] M. L. Chen,[1] S. J. Chen,[26] X. R. Chen,[23] Y. B. Chen,[1] H. P. Cheng,[16] X. K. Chu,[28] Y. P. Chu,[1] D. Cronin-Hennessy,[40] H. L. Dai,[1] J. P. Dai,[1] D. Dedovich,[21] Z. Y. Deng,[1] A. Denig,[20] I. Denysenko,[21] M. Destefanis,[45a,45c] W. M. Ding,[30] Y. Ding,[24] L. Y. Dong,[1] M. Y. Dong,[1] S. X. Du,[48] J. Fang,[1] S. S. Fang,[1] L. Fava,[45b,45c] C. Q. Feng,[42] P. Friedel,[3] C. D. Fu,[1] J. L. Fu,[26] O. Fuks,[21,†] Y. Gao,[35] C. Geng,[42] K. Goetzen,[9] W. X. Gong,[1] W. Gradl,[20] M. Greco,[45a,45c] M. H. Gu,[1] Y. T. Gu,[11] Y. H. Guan,[38] A. Q. Guo,[27] L. B. Guo,[25] T. Guo,[25] Y. P. Guo,[27,20] Y. L. Han,[1] F. A. Harris,[39] K. L. He,[1] M. He,[1] Z. Y. He,[27] T. Held,[3] Y. K. Heng,[1] Z. L. Hou,[1] C. Hu,[25] H. M. Hu,[1] J. F. Hu,[37] T. Hu,[1] G. M. Huang,[5] G. S. Huang,[42] J. S. Huang,[14] L. Huang,[1] X. T. Huang,[30] Y. Huang,[26] T. Hussain,[44] C. S. Ji,[42] Q. Ji,[1] Q. P. Ji,[27] X. B. Ji,[1] X. L. Ji,[1] L. L. Jiang,[1] X. S. Jiang,[1] J. B. Jiao,[30] Z. Jiao,[16] D. P. Jin,[1] S. Jin,[1] F. F. Jing,[35] N. Kalantar-Nayestanaki,[22] M. Kavatsyuk,[22] B. Kloss,[20] B. Kopf,[3] M. Kornicer,[39] W. Kuehn,[37] W. Lai,[1] J. S. Lange,[37] M. Lara,[18] P. Larin,[13] M. Leyhe,[3] C. H. Li,[1] Cheng Li,[42] Cui Li,[42] D. L. Li,[17] D. M. Li,[48] F. Li,[1] G. Li,[1] H. B. Li,[1] J. C. Li,[1] K. Li,[12] Lei Li,[1] N. Li,[11] P. R. Li,[38] Q. J. Li,[1] W. D. Li,[1] W. G. Li,[1] X. L. Li,[30] X. N. Li,[1] X. Q. Li,[27] X. R. Li,[29] Z. B. Li,[34] H. Liang,[42] Y. F. Liang,[32] Y. T. Liang,[37] G. R. Liao,[35] D. X. Lin,[13] B. J. Liu,[1] C. L. Liu,[4] C. X. Liu,[1] F. H. Liu,[31] Fang Liu,[1] Feng Liu,[5] H. B. Liu,[11] H. H. Liu,[15] H. M. Liu,[1] J. P. Liu,[46] K. Liu,[35] K. Y. Liu,[24] P. L. Liu,[30] Q. Liu,[38] S. B. Liu,[42] X. Liu,[23] Y. B. Liu,[27] Z. A. Liu,[1] Zhiqiang Liu,[1] Zhiqing Liu,[1] H. Loehner,[22] X. C. Lou,[1,‡] G. R. Lu,[14] H. J. Lu,[16] J. G. Lu,[1] X. R. Lu,[38] Y. P. Lu,[1] C. L. Luo,[25] M. X. Luo,[47] T. Luo,[39] X. L. Luo,[1] M. Lv,[1] F. C. Ma,[24] H. L. Ma,[1] Q. M. Ma,[1] S. Ma,[1] T. Ma,[1] X. Y. Ma,[1] F. E. Maas,[13] M. Maggiora,[45a,45c] Q. A. Malik,[44] Y. J. Mao,[28] Z. P. Mao,[1] J. G. Messchendorp,[22] J. Min,[1] T. J. Min,[1] R. E. Mitchell,[18] X. H. Mo,[1] H. Moeini,[22] C. Morales Morales,[13] K. Moriya,[18] N. Yu. Muchnoi,[8,*] H. Muramatsu,[41] Y. Nefedov,[21] I. B. Nikolaev,[8,*] Z. Ning,[1] S. Nisar,[7] S. L. Olsen,[29] Q. Ouyang,[1] S. Pacetti,[19b] J. W. Park,[39] M. Pelizaeus,[3] H. P. Peng,[42] K. Peters,[9] J. L. Ping,[25] R. G. Ping,[1] R. Poling,[40] E. Prencipe,[20] M. Qi,[26] S. Qian,[1] C. F. Qiao,[38] L. Q. Qin,[30] X. S. Qin,[1] Y. Qin,[28] Z. H. Qin,[1] J. F. Qiu,[1] K. H. Rashid,[44] C. F. Redmer,[20] M. Ripka,[20] G. Rong,[1] X. D. Ruan,[11] A. Sarantsev,[21,§] S. Schumann,[20] W. Shan,[28] M. Shao,[42] C. P. Shen,[2] X. Y. Shen,[1] H. Y. Sheng,[1] M. R. Shepherd,[18] W. M. Song,[1] X. Y. Song,[1] S. Spataro,[45a,45c] B. Spruck,[37] G. X. Sun,[1] J. F. Sun,[14] S. S. Sun,[1] Y. J. Sun,[42] Y. Z. Sun,[1] Z. J. Sun,[1] Z. T. Sun,[42] C. J. Tang,[32] X. Tang,[1] I. Tapan,[36c] E. H. Thorndike,[41] D. Toth,[40] M. Ullrich,[37] I. Uman,[36b] G. S. Varner,[39] B. Wang,[1] D. Wang,[28] D. Y. Wang,[28] K. Wang,[1] L. L. Wang,[1] L. S. Wang,[1] M. Wang,[30] P. Wang,[1] P. L. Wang,[1] Q. J. Wang,[1] S. G. Wang,[28] X. F. Wang,[35] X. L. Wang,[42] Y. D. Wang,[19a] Y. F. Wang,[1] Y. Q. Wang,[20] Z. Wang,[1] Z. G. Wang,[1] Z. H. Wang,[42] Z. Y. Wang,[1] D. H. Wei,[10] J. B. Wei,[28] P. Weidenkaff,[20] Q. G. Wen,[42] S. P. Wen,[1] M. Werner,[37] U. Wiedner,[3] L. H. Wu,[1] N. Wu,[1] S. X. Wu,[42] W. Wu,[27] Z. Wu,[1] L. G. Xia,[35] Y. X. Xia,[17] Z. J. Xiao,[25] Y. G. Xie,[1] Q. L. Xiu,[1] G. F. Xu,[1] Q. J. Xu,[12] Q. N. Xu,[38] X. P. Xu,[33] Z. R. Xu,[42] Z. Xue,[1] L. Yan,[42] W. B. Yan,[42] W. C. Yan,[42] Y. H. Yan,[17] H. X. Yang,[1] Y. Yang,[5] Y. X. Yang,[10] Y. Z. Yang,[11] H. Ye,[1] M. Ye,[1] M. H. Ye,[6] B. X. Yu,[1] C. X. Yu,[27] H. W. Yu,[28] J. S. Yu,[23] S. P. Yu,[30] C. Z. Yuan,[1] W. L. Yuan,[26] Y. Yuan,[1] A. A. Zafar,[44] A. Zallo,[19a] S. L. Zang,[26] Y. Zeng,[17] B. X. Zhang,[1] B. Y. Zhang,[1] C. Zhang,[26] C. B. Zhang,[17] C. C. Zhang,[1] D. H. Zhang,[1] H. H. Zhang,[34] H. Y. Zhang,[1] J. Q. Zhang,[1] J. W. Zhang,[1] J. Y. Zhang,[1] J. Z. Zhang,[1] LiLi Zhang,[17] S. H. Zhang,[1] X. J. Zhang,[1] X. Y. Zhang,[30] Y. Zhang,[1] Y. H. Zhang,[1] Z. P. Zhang,[42] Z. Y. Zhang,[46] Zhenghao Zhang,[5] G. Zhao,[1] J. W. Zhao,[1] Lei Zhao,[42] Ling Zhao,[1] M. G. Zhao,[27] Q. Zhao,[1] S. J. Zhao,[48] T. C. Zhao,[1] X. H. Zhao,[26] Y. B. Zhao,[1] Z. G. Zhao,[42] A. Zhemchugov,[21,†] B. Zheng,[43] J. P. Zheng,[1] Y. H. Zheng,[38] B. Zhong,[25] L. Zhou,[1] X. Zhou,[46] X. K. Zhou,[38] X. R. Zhou,[42] K. Zhu,[1] K. J. Zhu,[1] X. L. Zhu,[35] Y. C. Zhu,[42] Y. S. Zhu,[1] Z. A. Zhu,[1] J. Zhuang,[1] B. S. Zou,[1] and J. H. Zou[1]

(BESIII Collaboration)

[1]*Institute of High Energy Physics, Beijing 100049, People's Republic of China*
[2]*Beihang University, Beijing 100191, People's Republic of China*
[3]*Bochum Ruhr-University, D-44780 Bochum, Germany*
[4]*Carnegie Mellon University, Pittsburgh, Pennsylvania 15213, USA*

[5]Central China Normal University, Wuhan 430079, People's Republic of China
[6]China Center of Advanced Science and Technology, Beijing 100190, People's Republic of China
[7]COMSATS Institute of Information Technology, Lahore, Defence Road, Off Raiwind Road, 54000 Lahore, Pakistan
[8]G. I. Budker Institute of Nuclear Physics SB RAS (BINP), Novosibirsk 630090, Russia
[9]GSI Helmholtzcentre for Heavy Ion Research GmbH, D-64291 Darmstadt, Germany
[10]Guangxi Normal University, Guilin 541004, People's Republic of China
[11]GuangXi University, Nanning 530004, People's Republic of China
[12]Hangzhou Normal University, Hangzhou 310036, People's Republic of China
[13]Helmholtz Institute Mainz, Johann-Joachim-Becher-Weg 45, D-55099 Mainz, Germany
[14]Henan Normal University, Xinxiang 453007, People's Republic of China
[15]Henan University of Science and Technology, Luoyang 471003, People's Republic of China
[16]Huangshan College, Huangshan 245000, People's Republic of China
[17]Hunan University, Changsha 410082, People's Republic of China
[18]Indiana University, Bloomington, Indiana 47405, USA
[19a]INFN Laboratori Nazionali di Frascati, I-00044, Frascati, Italy
[19b]INFN and University of Perugia, I-06100, Perugia, Italy
[20]Johannes Gutenberg University of Mainz, Johann-Joachim-Becher-Weg 45, D-55099 Mainz, Germany
[21]Joint Institute for Nuclear Research, 141980 Dubna, Moscow region, Russia
[22]KVI, University of Groningen, NL-9747 AA Groningen, Netherlands
[23]Lanzhou University, Lanzhou 730000, People's Republic of China
[24]Liaoning University, Shenyang 110036, People's Republic of China
[25]Nanjing Normal University, Nanjing 210023, People's Republic of China
[26]Nanjing University, Nanjing 210093, People's Republic of China
[27]Nankai University, Tianjin 300071, People's Republic of China
[28]Peking University, Beijing 100871, People's Republic of China
[29]Seoul National University, Seoul, 151-747 Korea
[30]Shandong University, Jinan 250100, People's Republic of China
[31]Shanxi University, Taiyuan 030006, People's Republic of China
[32]Sichuan University, Chengdu 610064, People's Republic of China
[33]Soochow University, Suzhou 215006, People's Republic of China
[34]Sun Yat-Sen University, Guangzhou 510275, People's Republic of China
[35]Tsinghua University, Beijing 100084, People's Republic of China
[36a]Ankara University, Dogol Caddesi, 06100 Tandogan, Ankara, Turkey
[36b]Dogus University, 34722 Istanbul, Turkey
[36c]Uludag University, 16059 Bursa, Turkey
[37]Universitaet Giessen, D-35392 Giessen, Germany
[38]University of Chinese Academy of Sciences, Beijing 100049, People's Republic of China
[39]University of Hawaii, Honolulu, Hawaii 96822, USA
[40]University of Minnesota, Minneapolis, Minnesota 55455, USA
[41]University of Rochester, Rochester, New York 14627, USA
[42]University of Science and Technology of China, Hefei 230026, People's Republic of China
[43]University of South China, Hengyang 421001, People's Republic of China
[44]University of the Punjab, Lahore-54590, Pakistan
[45a]University of Turin, I-10125, Turin, Italy
[45b]University of Eastern Piedmont, I-15121 Alessandria, Italy
[45c]INFN, I-10125, Turin, Italy
[46]Wuhan University, Wuhan 430072, People's Republic of China
[47]Zhejiang University, Hangzhou 310027, People's Republic of China
[48]Zhengzhou University, Zhengzhou 450001, People's Republic of China

(Received 7 September 2013; published 10 December 2013)

We study $e^+e^- \to \pi^+\pi^- h_c$ at center-of-mass energies from 3.90 to 4.42 GeV by using data samples collected with the BESIII detector operating at the Beijing Electron Positron Collider. The Born cross sections are measured at 13 energies and are found to be of the same order of magnitude as those of $e^+e^- \to \pi^+\pi^- J/\psi$ but with a different line shape. In the $\pi^\pm h_c$ mass spectrum, a distinct structure, referred to as $Z_c(4020)$, is observed at $4.02\ \mathrm{GeV}/c^2$. The $Z_c(4020)$ carries an electric charge and couples to charmonium. A fit to the $\pi^\pm h_c$ invariant mass spectrum, neglecting possible interferences, results in a mass of $(4022.9 \pm 0.8 \pm 2.7)\ \mathrm{MeV}/c^2$ and a width of $(7.9 \pm 2.7 \pm 2.6)$ MeV for the $Z_c(4020)$, where the first errors are statistical and the second systematic. The difference between the parameters of this structure and the $Z_c(4025)$ observed in the $D^*\bar{D}^*$ final state is within 1.5σ, but whether they are the same state needs further investigation. No significant $Z_c(3900)$ signal is observed, and upper limits on the $Z_c(3900)$ production cross sections in $\pi^\pm h_c$ at center-of-mass energies of 4.23 and 4.26 GeV are set.

DOI: 10.1103/PhysRevLett.111.242001 PACS numbers: 14.40.Rt, 13.66.Bc, 14.40.Pq

In the study of the $e^+e^- \to \pi^+\pi^- J/\psi$ at center-of-mass (c.m.) energies around 4.26 GeV, the BESIII [1] and Belle [2] experiments observed a charged charmoniumlike state, the $Z_c(3900)$, which was confirmed shortly after with CLEO data at a c.m. energy of 4.17 GeV [3]. As there are at least four quarks within the $Z_c(3900)$, it is interpreted as either a tetraquark state, a $D\bar{D}^*$ molecule, hadroquarkonium, or other configurations [4]. More recently, BESIII has observed another charged $Z_c(4025)$ state in $e^+e^- \to \pi^\pm(D^*\bar{D}^*)^\mp$ [5]. These states together with similar states observed in the bottomonium system [6] would seem to indicate that a new class of hadrons has been observed.

Such a particle may couple to $\pi^\pm h_c$ [4] and thus can be searched for in $e^+e^- \to \pi^+\pi^- h_c$. This final state has been studied by CLEO [7], and a hint of a rising cross section at 4.26 GeV has been observed. An improved measurement may shed light on understanding the nature of the $Y(4260)$ as well [8,9].

In this Letter, we present a study of $e^+e^- \to \pi^+\pi^- h_c$ at 13 c.m. energies from 3.900 to 4.420 GeV. The data samples were collected with the BESIII detector [10] and are listed in Table I. The c.m. energies ($\sqrt{s}$) are measured with a beam energy measurement system [12] with an uncertainty of ± 1.0 MeV. A charged structure is observed in the $\pi^\pm h_c$ invariant mass spectrum at 4.02 GeV$/c^2$ [referred to as the $Z_c(4020)$ hereafter]. We also report on the search for $Z_c(3900)$ decays into the same final state. No significant signal is observed, and an upper limit on the production rate is determined. In the studies presented here, the h_c is reconstructed via its electric-dipole ($E1$) transition $h_c \to \gamma\eta_c$ with $\eta_c \to X_i$, where X_i signifies 16 exclusive hadronic final states: $p\bar{p}$, $2(\pi^+\pi^-)$, $2(K^+K^-)$, $K^+K^-\pi^+\pi^-$, $p\bar{p}\pi^+\pi^-$, $3(\pi^+\pi^-)$, $K^+K^-2(\pi^+\pi^-)$, $K_S^0K^\pm\pi^\mp$, $K_S^0K^\pm\pi^\mp\pi^\pm\pi^\mp$, $K^+K^-\pi^0$, $p\bar{p}\pi^0$, $\pi^+\pi^-\eta$, $K^+K^-\eta$, $2(\pi^+\pi^-)\eta$, $\pi^+\pi^-\pi^0\pi^0$, and $2(\pi^+\pi^-)\pi^0\pi^0$.

TABLE I. $e^+e^- \to \pi^+\pi^- h_c$ cross sections (or upper limits at the 90% confidence level). The third errors are from the uncertainty in $\mathcal{B}(h_c \to \gamma\eta_c)$ [11].

$\sqrt{s}$ (GeV)	$\mathcal{L}$ (pb^{-1})	$n_{h_c}^{\rm obs}$	$\sigma(e^+e^- \to \pi^+\pi^- h_c)$ (pb)
3.900	52.8	<2.3	<8.3
4.009	482.0	<13	<5.0
4.090	51.0	<6.0	<13
4.190	43.0	8.8 ± 4.9	$17.7 \pm 9.8 \pm 1.6 \pm 2.8$
4.210	54.7	21.7 ± 5.9	$34.8 \pm 9.5 \pm 3.2 \pm 5.5$
4.220	54.6	26.6 ± 6.8	$41.9 \pm 10.7 \pm 3.8 \pm 6.6$
4.230	1090.0	646 ± 33	$50.2 \pm 2.7 \pm 4.6 \pm 7.9$
4.245	56.0	22.6 ± 7.1	$32.7 \pm 10.3 \pm 3.0 \pm 5.1$
4.260	826.8	416 ± 28	$41.0 \pm 2.8 \pm 3.7 \pm 6.4$
4.310	44.9	34.6 ± 7.2	$61.9 \pm 12.9 \pm 5.6 \pm 9.7$
4.360	544.5	357 ± 25	$52.3 \pm 3.7 \pm 4.8 \pm 8.2$
4.390	55.1	30.0 ± 7.8	$41.8 \pm 10.8 \pm 3.8 \pm 6.6$
4.420	44.7	29.1 ± 7.3	$49.4 \pm 12.4 \pm 4.5 \pm 7.6$

We select charged tracks, photons, and $K_S^0 \to \pi^+\pi^-$ candidates as described in Ref. [13]. A candidate π^0 (η) is reconstructed from pairs of photons with an invariant mass in the range $|M_{\gamma\gamma} - m_{\pi^0}| < 15$ MeV$/c^2$ ($|M_{\gamma\gamma} - m_\eta| < 15$ MeV$/c^2$), where m_{π^0} (m_η) is the nominal π^0 (η) mass [14].

In selecting $e^+e^- \to \pi^+\pi^- h_c$, $h_c \to \gamma\eta_c$ candidates, all charged tracks are assumed to be pions, and events with at least one combination satisfying $M^{\rm recoil}_{\pi^+\pi^-} \in [3.45, 3.65]$ GeV$/c^2$ and $M^{\rm recoil}_{\gamma\pi^+\pi^-} \in [2.8, 3.2]$ GeV$/c^2$ are kept for further analysis. Here $M^{\rm recoil}_{\pi^+\pi^-}$ ($M^{\rm recoil}_{\gamma\pi^+\pi^-}$) is the mass recoiling from the $\pi^+\pi^-$ ($\gamma\pi^+\pi^-$) pair, which should be in the mass range of the h_c (η_c).

To determine the species of final state particles and to select the best photon when additional photons (and π^0 or η candidates) are found in an event, the combination with the minimum value of $\chi^2 = \chi^2_{4C} + \sum_{i=1}^N \chi^2_{\rm PID}(i) + \chi^2_{1C}$ is selected for further analysis, where χ^2_{4C} is the χ^2 from the initial-final four-momentum conservation (4C) kinematic fit and $\chi^2_{\rm PID}(i)$ is the χ^2 from particle identification (PID) using the energy loss in the main draft chamber and the time measured with the time-of-flight system. N is the number of the charged tracks in the final states, and χ^2_{1C} is the sum of the 1C (mass constraint of the two daughter photons) χ^2 of the π^0 and η in each final state. There is also a χ^2_{4C} requirement, which is optimized by using the figure of merit $S/\sqrt{S+B}$, where S and B are the numbers of Monte Carlo (MC) simulated signal and background events, respectively, and $\chi^2_{4C} < 35$ (efficiency is about 80% from MC simulation) is required for final states with only charged or K_S^0 particles, while $\chi^2_{4C} < 20$ (efficiency is about 70% from MC simulation) is required for those with π^0 or η [15]. A similar optimization procedure determines the η_c candidate mass window around the nominal η_c [14] mass to be ± 50 MeV$/c^2$ with efficiency about 85% from MC simulation ($\pm$ 45 MeV$/c^2$ with efficiency about 80% from MC simulation) for final states with only charged or K_S^0 particles (those with π^0 or η).

Figure 1 shows as an example the scatter plot of the mass of the η_c candidate versus that of the h_c candidate at the c.m. energy of 4.26 GeV, as well as the projection of the invariant mass distribution of $\gamma\eta_c$ in the η_c signal region,

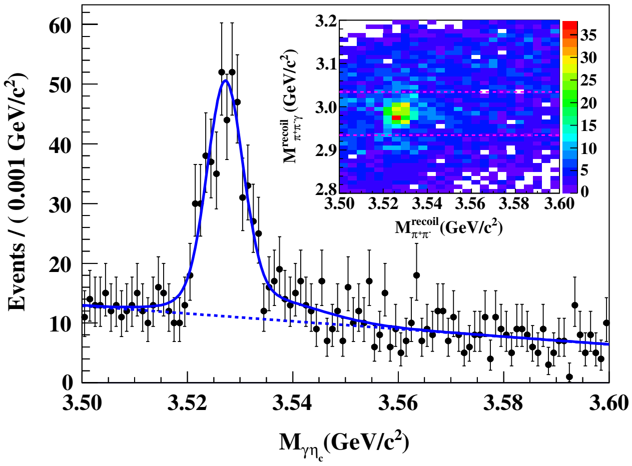

FIG. 1 (color online). The $M_{\gamma\eta_c}$ distribution after the η_c signal selection of 4.26 GeV data: dots with error bars are data, and the curves are the best fit described in the text. The inset is the scatter plot of the mass of the η_c candidate versus that of the h_c candidate.

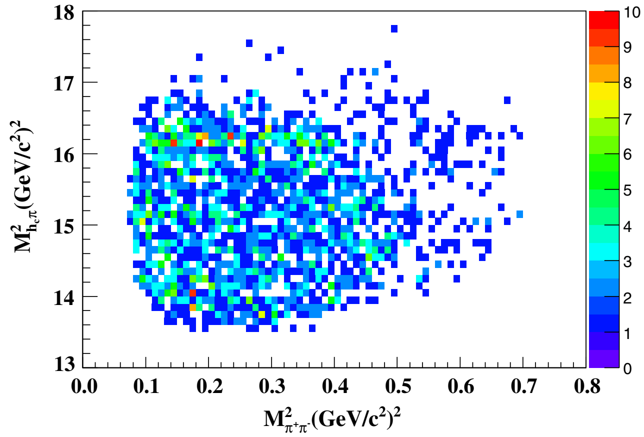

FIG. 2 (color online). Dalitz plot ($M^2_{\pi^+h_c}$ vs $M^2_{\pi^+\pi^-}$) for selected $e^+e^- \to \pi^+\pi^-h_c$ events, summed over all energy points.

where a clear $h_c \to \gamma\eta_c$ signal is observed. To extract the number of $\pi^+\pi^-h_c$ signal events, the $\gamma\eta_c$ mass spectrum is fitted by using the MC simulated signal shape convolved with a Gaussian function to reflect the mass resolution difference (around 10%) between the data and MC simulation, together with a linear background. The fit to the 4.26 GeV data is shown in Fig. 1. The tail in the high mass side is due to the events with initial state radiation (ISR), which is simulated well in MC, and its fraction is fixed in the fit. At the energy points with large statistics (4.23, 4.26, and 4.36 GeV), the fit is applied to the 16 η_c decay modes simultaneously, while, at the other energy points, we fit the mass spectrum summed over all the η_c decay modes. The number of signal events ($n^{obs}_{h_c}$) and the measured Born cross section at each energy are listed in Table I. The $\pi^+\pi^-h_c$ cross section appears to be constant above 4.2 GeV with a possible local maximum at around 4.23 GeV. This is in contrast to the observed energy dependence in the $e^+e^- \to \pi^+\pi^-J/\psi$ channel which revealed a decrease of cross sections at higher energies [2,17].

Systematic errors in the cross section measurement mainly come from the luminosity measurement, the branching fraction of $h_c \to \gamma\eta_c$, the branching fraction of $\eta_c \to X_i$, the detection efficiency, the ISR correction factor, and the fit. The integrated luminosity at each energy point is measured by using large angle Bhabha events, and it has an estimated uncertainty of 1.2%. The branching fractions of $h_c \to \gamma\eta_c$ and $\eta_c \to X_i$ are taken from Refs. [11,13]. The uncertainties in the detection efficiency are estimated in the same way as described in Refs. [13,16], and the error in the ISR correction is estimated as described in Ref. [1]. Uncertainties due to the choice of the signal shape, the background shape, the mass resolution, and the fit range are estimated by varying the h_c and η_c resonant parameters and line shapes in the MC simulation, varying the background function from linear to a second-order polynomial, varying the mass resolution difference between data and MC simulation by one standard deviation, and by extending the fit range. Assuming all of the sources are independent, the total systematic error in the $\pi^+\pi^-h_c$ cross section measurement is determined to be between 7% and 9% depending on the energy, and to be conservative we take 9% for all the energy points. The uncertainty in $\mathcal{B}(h_c \to \gamma\eta_c)$ is 15.7% [14], common to all energy points, and quoted separately in the cross section measurement. Altogether, about 95% of the total systematic errors are common to all the energy points.

Intermediate states are studied by examining the Dalitz plot of the selected $\pi^+\pi^-h_c$ candidate events. The h_c signal is selected by using $3.518 < M_{\gamma\eta_c} < 3.538$ GeV$/c^2$ and the sideband by using $3.490 < M_{\gamma\eta_c} < 3.510$ GeV$/c^2$ or $3.560 < M_{\gamma\eta_c} < 3.580$ GeV$/c^2$, which is twice as wide as the signal region. Figure 2 shows the Dalitz plot of the $\pi^+\pi^-h_c$ candidate events summed over all energies. While there are no clear structures in the $\pi^+\pi^-$ system, there is clear evidence for an exotic charmoniumlike structure in the $\pi^\pm h_c$ system. Figure 3 shows the projection of the $M_{\pi^\pm h_c}$ (two entries per event) distribution for the signal events, as well as the background events estimated from normalized h_c mass sidebands. There is a significant peak at around 4.02 GeV$/c^2$ [the $Z_c(4020)$], and the wider peak at low masses is the reflection of the $Z_c(4020)$. There are also some events at around 3.9 GeV$/c^2$, which could be the $Z_c(3900)$. The individual data sets at 4.23, 4.26, and 4.36 GeV show similar structures.

An unbinned maximum likelihood fit is applied to the $M_{\pi^\pm h_c}$ distribution summed over the 16 η_c decay modes. The data at 4.23, 4.26, and 4.36 GeV are fitted simultaneously with the same signal function with common mass and width. The signal shape is parametrized as a constant width relativistic Breit-Wigner function convolved with a

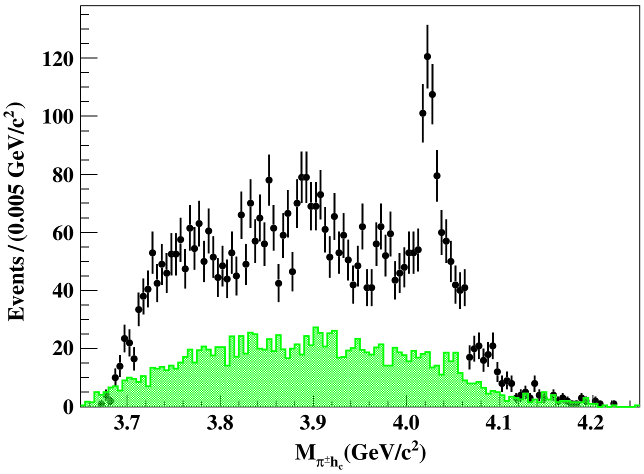

FIG. 3 (color online). $M_{\pi^\pm h_c}$ distribution of $e^+e^- \to \pi^+\pi^- h_c$ candidate events in the h_c signal region (dots with error bars) and the normalized h_c sideband region (shaded histogram), summed over data at all energy points.

Gaussian with a mass resolution determined from the data directly. Assuming the spin parity of the $Z_c(4020)$ $J^P = 1^+$, a phase space factor pq^3 is considered in the partial width, where p is the $Z_c(4020)$ momentum in the e^+e^- c.m. frame and q is the h_c momentum in the $Z_c(4020)$ c.m. frame. The background shape is parametrized as an ARGUS function [18]. The efficiency curve is considered in the fit, but possible interferences between the signal and background are neglected. Figure 4 shows the fit results; the fit yields a mass of (4022.9 ± 0.8) MeV$/c^2$ and a width of (7.9 ± 2.7) MeV. The goodness of fit is found to be $\chi^2/\text{n.d.f.} = 27.3/32 = 0.85$ by projecting the events into a histogram with 46 bins. The statistical significance of the $Z_c(4020)$ signal is calculated by comparing the fit likelihoods with and without the signal. Besides the nominal fit, the fit is also performed by changing the fit range, the signal shape, or the background shape. In all cases, the significance is found to be greater than 8.9σ.

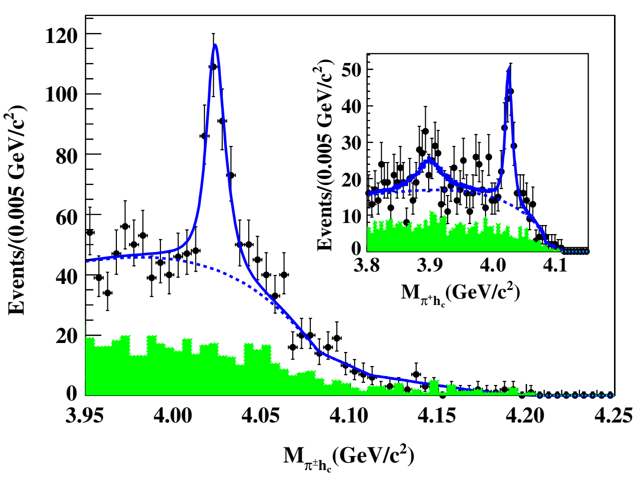

FIG. 4 (color online). Sum of the simultaneous fits to the $M_{\pi^\pm h_c}$ distributions at 4.23, 4.26, and 4.36 GeV as described in the text; the inset shows the sum of the simultaneous fit to the $M_{\pi^+ h_c}$ distributions at 4.23 and 4.26 GeV with $Z_c(3900)$ and $Z_c(4020)$. Dots with error bars are data; shaded histograms are the normalized sideband background; the solid curves show the total fit, and the dotted curves the backgrounds from the fit.

The numbers of $Z_c(4020)$ events are determined to be $N[Z_c(4020)^\pm] = 114 \pm 25$, 72 ± 17, and 67 ± 15 at 4.23, 4.26, and 4.36 GeV, respectively. The cross sections are calculated to be $\sigma[e^+e^- \to \pi^\pm Z_c(4020)^\mp \to \pi^+\pi^- h_c] = (8.7 \pm 1.9 \pm 2.8 \pm 1.4)$ pb at 4.23 GeV, $(7.4 \pm 1.7 \pm 2.1 \pm 1.2)$ pb at 4.26 GeV, and $(10.3 \pm 2.3 \pm 3.1 \pm 1.6)$ pb at 4.36 GeV, where the first errors are statistical, the second ones systematic (described in detail below), and the third ones from the uncertainty in $\mathcal{B}(h_c \to \gamma\eta_c)$ [14]. The $Z_c(4020)$ production rate is uniform at these three energy points.

Adding a $Z_c(3900)$ with the mass and width fixed to the BESIII measurement [1] in the fit results in a statistical significance of 2.1σ (see the inset in Fig. 4). We set upper limits on the production cross sections as $\sigma[e^+e^- \to \pi^\pm Z_c(3900)^\mp \to \pi^+\pi^- h_c] < 13$ pb at 4.23 GeV and <11 pb at 4.26 GeV, at the 90% confidence level (C.L.). The probability density function from the fit is smeared by a Gaussian function with a standard deviation of σ_{sys} to include the systematic error effect, where σ_{sys} is the relative systematic error in the cross section measurement described below. We do not fit the 4.36 GeV data, as the $Z_c(3900)$ signal overlaps with the reflection of the $Z_c(4020)$ signal.

The systematic errors for the resonance parameters of the $Z_c(4020)$ come from the mass calibration, parametrization of the signal and background shapes, possible existence of the $Z_c(3900)$ and interference with it, fitting range, efficiency curve, and mass resolution. The uncertainty from the mass calibration is estimated by using the difference between the measured and known h_c masses and D^0 masses (reconstructed from $K^-\pi^+$). The differences are (2.1 ± 0.4) and $-(0.7 \pm 0.2)$ MeV$/c^2$, respectively. Since our signal topology has one low momentum pion and many tracks from the h_c decay, we assume these differences added in quadrature, 2.6 MeV$/c^2$, is the systematic error due to the mass calibration. Spin parity conservation forbids a zero spin for the $Z_c(4020)$, and, assuming that contributions from D wave or higher are negligible, the only alternative is $J^P = 1^-$ for the $Z_c(4020)$. A fit under this scenario yields a mass difference of 0.2 MeV$/c^2$ and a width difference of 0.8 MeV. The uncertainty due to the background shape is determined by changing to a second-order polynomial and by varying the fit range. A difference of 0.1 MeV$/c^2$ for the mass is found from the former, and differences of 0.2 MeV$/c^2$ for mass and 1.1 MeV for width are found from the latter. Uncertainties due to the mass resolution are estimated by varying the resolution difference between the data and MC simulation by one standard

TABLE II. The percentage systematic errors in $\sigma[e^+e^- \to \pi^\pm Z_c(4020)^\mp \to \pi^+\pi^- h_c]$, in addition to those in the $\sigma(e^+e^- \to \pi^+\pi^- h_c)$ measurement.

$\sqrt{s}$ (GeV)	$Z_c(3900)$ signal	Interference	Fitting range	Signal shape	Background shape	h_c signal window	Mass resolution	Efficiency curve
4.230	18.3	20.0	13.2	4.5	3.5	1.7	1.8	0.9
4.260	16.2	20.0	8.3	4.2	2.8	1.7	1.8	0.0
4.360	18.3	20.0	4.5	6.0	6.0	1.4	1.5	0.0

deviation of the measured uncertainty in the mass resolution of the h_c signal; the difference is 0.5 MeV in the width, which is taken as the systematic error. The uncertainty in the efficiency curve results in 0.1 MeV$/c^2$ for mass and 0.1 MeV for width. Uncertainties due to the possible existence of the $Z_c(3900)$ and the interference with it are estimated by adding a $Z_c(3900)$ amplitude incoherently or coherently in the fit. The uncertainties due to $Z_c(3900)$ are 0.2 MeV$/c^2$ for mass and 2.1 MeV for width, while the uncertainties due to interference are 0.5 MeV$/c^2$ for the mass and 0.4 MeV for the width. Assuming all the sources of systematic uncertainty are independent, the total systematic error is 2.7 MeV$/c^2$ for the mass and 2.6 MeV for the width.

The systematic errors in $\sigma[e^+e^- \to \pi^\pm Z_c(4020)^\mp \to \pi^+\pi^- h_c]$ are estimated in the same way as for $\sigma(e^+e^- \to \pi^+\pi^- h_c)$. The systematic errors due to the inclusion of the $Z_c(3900)$ signal, the possible interference between $Z_c(4020)$ and $Z_c(3900)$, the fitting range, the signal and background parametrizations, the h_c signal window selection, the mass resolution, and the efficiency curve, in addition to those in the $\sigma(e^+e^- \to \pi^+\pi^- h_c)$ measurement, are considered and summarized in Table II. The systematic errors in $\sigma[e^+e^- \to \pi^\pm Z_c(3900)^\mp \to \pi^+\pi^- h_c]$ are determined similarly.

In summary, we measure $e^+e^- \to \pi^+\pi^- h_c$ cross sections at c.m. energies between 3.90 and 4.42 GeV for the first time. These cross sections are of the same order of magnitude as those of the $e^+e^- \to \pi^+\pi^- J/\psi$ measured by BESIII [1] and other experiments [2,17] but with a different line shape. There is a broad structure at high energy with a possible local maximum at around 4.23 GeV. A narrow structure very close to the $(D^*\bar{D}^*)^\pm$ threshold with a mass of $(4022.9 \pm 0.8 \pm 2.7)$ MeV$/c^2$ and a width of $(7.9 \pm 2.7 \pm 2.6)$ MeV is observed in the $\pi^\pm h_c$ mass spectrum. This structure couples to charmonium and has an electric charge, which is suggestive of a state containing more quarks than just a charm and an anticharm quark, as the $Z_c(3900)$ observed in the $\pi^\pm J/\psi$ system [1–3]. We do not find a significant signal for $Z_c(3900) \to \pi^\pm h_c$, and the production cross section is found to be smaller than 11 pb at the 90% C.L. at 4.26 GeV, which is lower than that of $Z_c(3900) \to \pi^\pm J/\psi$ [1]. The $Z_c(4020)$ parameters agree within 1.5σ of those of the $Z_c(4025)$, observed in $e^+e^- \to \pi^\pm(D^*\bar{D}^*)^\mp$ at a c.m. energy 4.26 GeV [5]. Results for the latter at 4.23 and 4.36 GeV may help us to understand whether they are the same state.

The BESIII Collaboration thanks the staff of BEPCII and the computing center for their strong support. This work is supported in part by the Ministry of Science and Technology of China under Contract No. 2009CB825200; National Natural Science Foundation of China (NSFC) under Contracts No. 10625524, No. 10821063, No. 10825524, No. 10835001, No. 10935007, No. 11125525, and No. 11235011; Joint Funds of the National Natural Science Foundation of China under Contracts No. 11079008, No. 11079023, No. 11179007, and No. U1332201; the Chinese Academy of Sciences (CAS) Large-Scale Scientific Facility Program; CAS under Contracts No. KJCX2-YW-N29 and No. KJCX2-YW-N45; 100 Talents Program of CAS; German Research Foundation DFG under Collaborative Research Center Contract No. CRC-1044; Istituto Nazionale di Fisica Nucleare, Italy; Ministry of Development of Turkey under Contract No. DPT2006K-120470; U.S. Department of Energy under Contracts No. DE-FG02-04ER41291, No. DE-FG02-05ER41374, and No. DE-FG02-94ER40823; U.S. National Science Foundation; University of Groningen (RuG) and the Helmholtzzentrum fuer Schwerionenforschung GmbH (GSI), Darmstadt; WCU Program of National Research Foundation of Korea under Contract No. R32-2008-000-10155-0.

*Also at the Novosibirsk State University, Novosibirsk, 630090, Russia.
†Also at the Moscow Institute of Physics and Technology, Moscow 141700, Russia.
‡Also at University of Texas at Dallas, Richardson, TX 75083, USA.
§Also at the PNPI, Gatchina 188300, Russia.

[1] M. Ablikim *et al.* (BESIII Collaboration), Phys. Rev. Lett. **110**, 252001 (2013).
[2] Z. Q. Liu *et al.* (Belle Collaboration), Phys. Rev. Lett. **110**, 252002 (2013).
[3] T. Xiao, S. Dobbs, A. Tomaradze, and K. K. Seth, arXiv:1304.3036.
[4] Q. Wang, C. Hanhart, and Q. Zhao, Phys. Rev. Lett. **111**, 132003 (2013); F.-K. Guo, C. Hidalgo-Duque, J. Nieves, and M. P. Valderrama, Phys. Rev. D **88**, 054007 (2013); G. Li, arXiv:1304.4458 [Eur. Phys. J. C (to be published)];

C.-Y. Cui, Y.-L. Liu, W.-B. Chen, and M.-Q. Huang, arXiv:1304.1850; J.-R. Zhang, Phys. Rev. D **87**, 116004 (2013); J. M. Dias, F. S. Navarra, M. Nielsen, and C. M. Zanetti, Phys. Rev. D **88**, 016004 (2013); M. B. Voloshin, Phys. Rev. D **87**, 091501 (2013); E. Braaten, Phys. Rev. Lett. **111**, 162003 (2013); E. Wilbring, H. W. Hammer, and U. G. Meißner, Phys. Lett. B **726**, 326 (2013); D.-Y. Chen, X. Liu, and T. Matsuki, Phys. Rev. D **88**, 036008 (2013); K. Terasaki, arXiv:1304.7080; Y.-R. Liu, Phys. Rev. D **88**, 074008 (2013); Q. Wang, C. Hanhart, and Q. Zhao, Phys. Lett. B **725**, 106 (2013); Y. Dong, A. Faessler, T. Gutsche, and V. E. Lyubovitskij, Phys. Rev. D **88**, 014030 (2013); X.-H. Liu and G. Li, Phys. Rev. D **88**, 014013 (2013); S. Prelovsek and L. Leskovec, arXiv:1308.2097 [Phys. Lett. B (to be published)].

[5] M. Ablikim *et al.* (BESIII Collaboration), arXiv:1308.2760.

[6] A. Bondar *et al.* (Belle Collaboration), Phys. Rev. Lett. **108**, 122001 (2012).

[7] T. K. Pedlar *et al.* (CLEO Collaboration), Phys. Rev. Lett. **107**, 041803 (2011).

[8] C. Z. Yuan *et al.* (Belle Collaboration), Phys. Rev. Lett. **99**, 182004 (2007).

[9] B. Aubert *et al.* (*BABAR* Collaboration), Phys. Rev. Lett. **95**, 142001 (2005).

[10] M. Ablikim *et al.* (BESIII Collaboration), Nucl. Instrum. Methods Phys. Res., Sect. A **614**, 345 (2010).

[11] M. Ablikim *et al.* (BESIII Collaboration), Phys. Rev. Lett. **104**, 132002 (2010).

[12] E. V. Abakumova *et al.*, Nucl. Instrum. Methods Phys. Res., Sect. A **659**, 21 (2011).

[13] M. Ablikim *et al.* (BESIII Collaboration), Phys. Rev. D **86**, 092009 (2012).

[14] J. Beringer *et al.* (Particle Data Group), Phys. Rev. D **86**, 010001 (2012).

[15] A track parameter correction procedure [16] is applied to the MC simulated charged tracks to improve the agreement between the data and MC simulation of the χ^2_{4C} distribution of the kinematic fit. The correction factors are obtained from a high purity control sample $J/\psi \to \phi f_0(980)$, with $\phi \to K^+K^-$ and $f_0(980) \to \pi^+\pi^-$. Reasonable agreement between the data and MC simulation is observed for the channels analyzed in this work. The systematic error of the χ^2_{4C} requirement is taken as half of the correction in the efficiency, which is much larger than the effect due to the uncertainties in the correction factors to cover possible unknown effects in the procedure.

[16] M. Ablikim *et al.* (BESIII Collaboration), Phys. Rev. D **87**, 012002 (2013).

[17] J. P. Lees *et al.* (*BABAR* Collaboration), Phys. Rev. D **86**, 051102(R) (2012).

[18] H. Albrecht *et al.* (ARGUS Collaboration), Phys. Lett. B **241**, 278 (1990).

Observation of $e^+e^- \to \gamma X(3872)$ at BESIII

M. Ablikim,[1] M. N. Achasov,[8,*] X. C. Ai,[1] O. Albayrak,[4] D. J. Ambrose,[41] F. F. An,[1] Q. An,[42] J. Z. Bai,[1] R. Baldini Ferroli,[19a] Y. Ban,[28] J. V. Bennett,[18] M. Bertani,[19a] J. M. Bian,[40] E. Boger,[21,†] O. Bondarenko,[22] I. Boyko,[21] S. Braun,[37] R. A. Briere,[4] H. Cai,[47] X. Cai,[1] O. Cakir,[36a] A. Calcaterra,[19a] G. F. Cao,[1] S. A. Cetin,[36b] J. F. Chang,[1] G. Chelkov,[21,†] G. Chen,[1] H. S. Chen,[1] J. C. Chen,[1] M. L. Chen,[1] S. J. Chen,[26] X. Chen,[1] X. R. Chen,[23] Y. B. Chen,[1] H. P. Cheng,[16] X. K. Chu,[28] Y. P. Chu,[1] D. Cronin-Hennessy,[40] H. L. Dai,[1] J. P. Dai,[1] D. Dedovich,[21] Z. Y. Deng,[1] A. Denig,[20] I. Denysenko,[21] M. Destefanis,[45a,45c] W. M. Ding,[30] Y. Ding,[24] C. Dong,[27] J. Dong,[1] L. Y. Dong,[1] M. Y. Dong,[1] S. X. Du,[49] J. Z. Fan,[35] J. Fang,[1] S. S. Fang,[1] Y. Fang,[1] L. Fava,[45b,45c] C. Q. Feng,[42] C. D. Fu,[1] J. L. Fu,[26] O. Fuks,[21,†] Q. Gao,[1] Y. Gao,[35] C. Geng,[42] K. Goetzen,[9] W. X. Gong,[1] W. Gradl,[20] M. Greco,[45a,45c] M. H. Gu,[1] Y. T. Gu,[11] Y. H. Guan,[1] A. Q. Guo,[27] L. B. Guo,[25] T. Guo,[25] Y. P. Guo,[20] Y. L. Han,[1] F. A. Harris,[39] K. L. He,[1] M. He,[1] Z. Y. He,[27] T. Held,[3] Y. K. Heng,[1] Z. L. Hou,[1] C. Hu,[25] H. M. Hu,[1] J. F. Hu,[37] T. Hu,[1] G. M. Huang,[5] G. S. Huang,[42] J. S. Huang,[14] L. Huang,[1] X. T. Huang,[30] Y. Huang,[26] T. Hussain,[44] C. S. Ji,[42] Q. Ji,[1] Q. P. Ji,[27] X. B. Ji,[1] X. L. Ji,[1] L. L. Jiang,[1] X. S. Jiang,[1] J. B. Jiao,[30] Z. Jiao,[16] D. P. Jin,[1] S. Jin,[1] T. Johansson,[46] N. Kalantar-Nayestanaki,[22] X. L. Kang,[1] X. S. Kang,[27] M. Kavatsyuk,[22] B. Kloss,[20] B. Kopf,[3] M. Kornicer,[39] W. Kuehn,[37] A. Kupsc,[46] W. Lai,[1] J. S. Lange,[37] M. Lara,[18] P. Larin,[13] M. Leyhe,[3] C. H. Li,[1] Cheng Li,[42] Cui Li,[42] D. Li,[17] D. M. Li,[49] F. Li,[1] G. Li,[1] H. B. Li,[1] J. C. Li,[1] K. Li,[30] K. Li,[12] Lei Li,[1] P. R. Li,[38] Q. J. Li,[1] T. Li,[30] W. D. Li,[1] W. G. Li,[1] X. L. Li,[30] X. N. Li,[1] X. Q. Li,[27] X. R. Li,[29] Z. B. Li,[34] H. Liang,[42] Y. F. Liang,[32] Y. T. Liang,[37] D. X. Lin,[13] B. J. Liu,[1] C. L. Liu,[4] C. X. Liu,[1] F. H. Liu,[31] Fang Liu,[1] Feng Liu,[5] H. B. Liu,[11] H. H. Liu,[15] H. M. Liu,[1] J. Liu,[1] J. P. Liu,[47] K. Liu,[35] K. Y. Liu,[24] P. L. Liu,[30] Q. Liu,[38] S. B. Liu,[42] X. Liu,[23] Y. B. Liu,[27] Z. A. Liu,[1] Zhiqiang Liu,[1] Zhiqing Liu,[20] H. Loehner,[22] X. C. Lou,[1,‡] G. R. Lu,[14] H. J. Lu,[16] H. L. Lu,[1] J. G. Lu,[1] X. R. Lu,[38] Y. Lu,[1] Y. P. Lu,[1] C. L. Luo,[25] M. X. Luo,[48] T. Luo,[39] X. L. Luo,[1] M. Lv,[1] F. C. Ma,[24] H. L. Ma,[1] Q. M. Ma,[1] S. Ma,[1] T. Ma,[1] X. Y. Ma,[1] F. E. Maas,[13] M. Maggiora,[45a,45c] Q. A. Malik,[44] Y. J. Mao,[28] Z. P. Mao,[1] J. G. Messchendorp,[22] J. Min,[1] T. J. Min,[1] R. E. Mitchell,[18] X. H. Mo,[1] Y. J. Mo,[5] H. Moeini,[22] C. Morales Morales,[13] K. Moriya,[18] N. Yu. Muchnoi,[8,*] H. Muramatsu,[40] Y. Nefedov,[21] I. B. Nikolaev,[8,*] Z. Ning,[1] S. Nisar,[7] X. Y. Niu,[1] S. L. Olsen,[29] Q. Ouyang,[1] S. Pacetti,[19b] M. Pelizaeus,[3] H. P. Peng,[42] K. Peters,[9] J. L. Ping,[25] R. G. Ping,[1] R. Poling,[40] E. Prencipe,[20] M. Qi,[26] S. Qian,[1] C. F. Qiao,[38] L. Q. Qin,[30] X. S. Qin,[1] Y. Qin,[28] Z. H. Qin,[1] J. F. Qiu,[1] K. H. Rashid,[44] C. F. Redmer,[20] M. Ripka,[20] G. Rong,[1] X. D. Ruan,[11] A. Sarantsev,[21,§] K. Schoenning,[46] S. Schumann,[20] W. Shan,[28] M. Shao,[42] C. P. Shen,[2] X. Y. Shen,[1] H. Y. Sheng,[1] M. R. Shepherd,[18] W. M. Song,[1] X. Y. Song,[1] S. Spataro,[45a,45c] B. Spruck,[37] G. X. Sun,[1] J. F. Sun,[14] S. S. Sun,[1] Y. J. Sun,[42] Y. Z. Sun,[1] Z. J. Sun,[1] Z. T. Sun,[42] C. J. Tang,[32] X. Tang,[1] I. Tapan,[36c] E. H. Thorndike,[41] D. Toth,[40] M. Ullrich,[37] I. Uman,[36b] G. S. Varner,[39] B. Wang,[27] D. Wang,[28] D. Y. Wang,[28] K. Wang,[1] L. L. Wang,[1] L. S. Wang,[1] M. Wang,[30] P. Wang,[1] P. L. Wang,[1] Q. J. Wang,[1] S. G. Wang,[28] W. Wang,[1] X. F. Wang,[35] Y. D. Wang,[19a] Y. F. Wang,[1] Y. Q. Wang,[20] Z. Wang,[1] Z. G. Wang,[1] Z. H. Wang,[42] Z. Y. Wang,[1] D. H. Wei,[10] J. B. Wei,[28] P. Weidenkaff,[20] S. P. Wen,[1] M. Werner,[37] U. Wiedner,[3] M. Wolke,[46] L. H. Wu,[1] N. Wu,[1] Z. Wu,[1] L. G. Xia,[35] Y. Xia,[17] D. Xiao,[1] Z. J. Xiao,[25] Y. G. Xie,[1] Q. L. Xiu,[1] G. F. Xu,[1] L. Xu,[1] Q. J. Xu,[12] Q. N. Xu,[38] X. P. Xu,[33] Z. Xue,[1] L. Yan,[42] W. B. Yan,[42] W. C. Yan,[42] Y. H. Yan,[17] H. X. Yang,[1] Y. Yang,[5] Y. X. Yang,[10] H. Ye,[1] M. Ye,[1] M. H. Ye,[6] B. X. Yu,[1] C. X. Yu,[27] H. W. Yu,[28] J. S. Yu,[23] S. P. Yu,[30] C. Z. Yuan,[1] W. L. Yuan,[26] Y. Yuan,[1] A. A. Zafar,[44] A. Zallo,[19a] S. L. Zang,[26] Y. Zeng,[17] B. X. Zhang,[1] B. Y. Zhang,[1] C. Zhang,[26] C. B. Zhang,[17] C. C. Zhang,[1] D. H. Zhang,[1] H. H. Zhang,[34] H. Y. Zhang,[1] J. J. Zhang,[1] J. Q. Zhang,[1] J. W. Zhang,[1] J. Y. Zhang,[1] J. Z. Zhang,[1] S. H. Zhang,[1] X. J. Zhang,[1] X. Y. Zhang,[30] Y. Zhang,[1] Y. H. Zhang,[1] Z. H. Zhang,[5] Z. P. Zhang,[42] Z. Y. Zhang,[47] G. Zhao,[1] J. W. Zhao,[1] Lei Zhao,[42] Ling Zhao,[1] M. G. Zhao,[27] Q. Zhao,[1] Q. W. Zhao,[1] S. J. Zhao,[49] T. C. Zhao,[1] X. H. Zhao,[26] Y. B. Zhao,[1] Z. G. Zhao,[42] A. Zhemchugov,[21,†] B. Zheng,[43] J. P. Zheng,[1] Y. H. Zheng,[38] B. Zhong,[25] L. Zhou,[1] Li Zhou,[27] X. Zhou,[47] X. K. Zhou,[38] X. R. Zhou,[42] X. Y. Zhou,[1] K. Zhu,[1] K. J. Zhu,[1] X. L. Zhu,[35] Y. C. Zhu,[42] Y. S. Zhu,[1] Z. A. Zhu,[1] J. Zhuang,[1] B. S. Zou,[1] J. H. Zou[1]

(BESIII Collaboration)

[1]*Institute of High Energy Physics, Beijing 100049, People's Republic of China*
[2]*Beihang University, Beijing 100191, People's Republic of China*
[3]*Bochum Ruhr-University, D-44780 Bochum, Germany*
[4]*Carnegie Mellon University, Pittsburgh, Pennsylvania 15213, USA*
[5]*Central China Normal University, Wuhan 430079, People's Republic of China*
[6]*China Center of Advanced Science and Technology, Beijing 100190, People's Republic of China*

[7]COMSATS Institute of Information Technology, Lahore, Defence Road, Off Raiwind Road, 54000 Lahore, Pakistan
[8]G.I. Budker Institute of Nuclear Physics SB RAS (BINP), Novosibirsk 630090, Russia
[9]GSI Helmholtzcentre for Heavy Ion Research GmbH, D-64291 Darmstadt, Germany
[10]Guangxi Normal University, Guilin 541004, People's Republic of China
[11]GuangXi University, Nanning 530004, People's Republic of China
[12]Hangzhou Normal University, Hangzhou 310036, People's Republic of China
[13]Helmholtz Institute Mainz, Johann-Joachim-Becher-Weg 45, D-55099 Mainz, Germany
[14]Henan Normal University, Xinxiang 453007, People's Republic of China
[15]Henan University of Science and Technology, Luoyang 471003, People's Republic of China
[16]Huangshan College, Huangshan 245000, People's Republic of China
[17]Hunan University, Changsha 410082, People's Republic of China
[18]Indiana University, Bloomington, Indiana 47405, USA
[19a]INFN Laboratori Nazionali di Frascati, I-00044 Frascati, Italy
[19b]INFN and University of Perugia, I-06100 Perugia, Italy
[20]Johannes Gutenberg University of Mainz, Johann-Joachim-Becher-Weg 45, D-55099 Mainz, Germany
[21]Joint Institute for Nuclear Research, 141980 Dubna, Moscow region, Russia
[22]KVI, University of Groningen, NL-9747 AA Groningen, The Netherlands
[23]Lanzhou University, Lanzhou 730000, People's Republic of China
[24]Liaoning University, Shenyang 110036, People's Republic of China
[25]Nanjing Normal University, Nanjing 210023, People's Republic of China
[26]Nanjing University, Nanjing 210093, People's Republic of China
[27]Nankai university, Tianjin 300071, People's Republic of China
[28]Peking University, Beijing 100871, People's Republic of China
[29]Seoul National University, Seoul 151-747, Korea
[30]Shandong University, Jinan 250100, People's Republic of China
[31]Shanxi University, Taiyuan 030006, People's Republic of China
[32]Sichuan University, Chengdu 610064, People's Republic of China
[33]Soochow University, Suzhou 215006, People's Republic of China
[34]Sun Yat-Sen University, Guangzhou 510275, People's Republic of China
[35]Tsinghua University, Beijing 100084, People's Republic of China
[36a]Ankara University, Dogol Caddesi, 06100 Tandogan, Ankara, Turkey;
[36b]Dogus University, 34722 Istanbul, Turkey
[36c]Uludag University, 16059 Bursa, Turkey
[37]Universitaet Giessen, D-35392 Giessen, Germany
[38]University of Chinese Academy of Sciences, Beijing 100049, People's Republic of China
[39]University of Hawaii, Honolulu, Hawaii 96822, USA
[40]University of Minnesota, Minneapolis, Minnesota 55455, USA
[41]University of Rochester, Rochester, New York 14627, USA
[42]University of Science and Technology of China, Hefei 230026, People's Republic of China
[43]University of South China, Hengyang 421001, People's Republic of China
[44]University of the Punjab, Lahore 54590, Pakistan
[45a]University of Turin, I-10125 Turin, Italy
[45b]University of Eastern Piedmont, I-15121 Alessandria, Italy
[45c]INFN, I-10125 Turin, Italy
[46]Uppsala University, Box 516, SE-75120 Uppsala, Sweden
[47]Wuhan University, Wuhan 430072, People's Republic of China
[48]Zhejiang University, Hangzhou 310027, People's Republic of China
[49]Zhengzhou University, Zhengzhou 450001, People's Republic of China

(Received 15 October 2013; revised manuscript received 16 December 2013; published 3 March 2014)

With data samples collected with the BESIII detector operating at the BEPCII storage ring at center-of-mass energies from 4.009 to 4.420 GeV, the process $e^+e^- \to \gamma X(3872)$ is observed for the first time with a statistical significance of 6.3σ. The measured mass of the $X(3872)$ is $(3871.9 \pm 0.7_{\rm stat} \pm 0.2_{\rm syst})$ MeV$/c^2$, in agreement with previous measurements. Measurements of the product of the cross section $\sigma[e^+e^- \to \gamma X(3872)]$ and the branching fraction $\mathcal{B}[X(3872) \to \pi^+\pi^- J/\psi]$ at center-of-mass energies 4.009, 4.229, 4.260, and 4.360 GeV are reported. Our measurements are consistent with expectations for the radiative transition process $Y(4260) \to \gamma X(3872)$.

DOI: 10.1103/PhysRevLett.112.092001 PACS numbers: 13.25.Gv, 13.40.Hq, 14.40.Pq

The $X(3872)$ was first observed 10 years ago by Belle [1] in $B^{\pm} \to K^{\pm}\pi^{+}\pi^{-}J/\psi$ decays; it was subsequently confirmed by several other experiments [2–4]. Since its discovery, the $X(3872)$ has stimulated considerable interest. Both *BABAR* and Belle observed the $X(3872) \to \gamma J/\psi$ decay process, which ensures that the $X(3872)$ is a C-even state [5,6]. The CDF and LHCb experiments determined the spin parity of the $X(3872)$ to be $J^{P} = 1^{+}$ [7,8], and CDF also found that the $\pi^{+}\pi^{-}$ system was dominated by the $\rho^{0}(770)$ resonance [9]. Because of the proximity of its mass to the $\bar{D}D^{*}$ mass threshold, the $X(3872)$ has been interpreted as a candidate for a hadronic molecule or a tetraquark state [10]. Until now, the $X(3872)$ was only observed in B meson decays and hadron collisions. Since the $X(3872)$ is a 1^{++} state, it should be able to be produced through the radiative transition of an excited vector charmonium or charmoniumlike states such as a ψ or a Y.

The puzzling $Y(4260)$ [11] and $Y(4360)$ [12] vector charmoniumlike states have only been observed in final states containing a charmonium meson and a $\pi^{+}\pi^{-}$ pair, in contrast to the $\psi(4040)$ and $\psi(4160)$ which dominantly couple to open charm final states [13]. The observation of the charged charmoniumlike state $Z_c(3900)$ [11,14], which is clearly not a conventional charmonium state and is produced recoiling against a $\pi^{\pm}$ at the c.m. energy of 4.26 GeV, indicates that these two "exotic" states seem to couple with each other. To better understand their nature, an investigation of other decay processes, such as the radiative transition of the $Y(4260)$ and $Y(4360)$ to lower lying charmonium or charmoniumlike states is important [15]. The process $Y(4260)/Y(4360) \to \gamma X(3872)$ is unique due to the exotic feature of both the $X(3872)$ and the $Y(4260)$ or $Y(4360)$ resonances.

In this Letter, we report the first observation of the process $e^{+}e^{-} \to \gamma X(3872) \to \gamma\pi^{+}\pi^{-}J/\psi$, $J/\psi \to \ell^{+}\ell^{-}$ ($\ell^{+}\ell^{-} = e^{+}e^{-}$ or $\mu^{+}\mu^{-}$) in an analysis of data collected with the BESIII detector operating at the BEPCII storage ring [16] at $e^{+}e^{-}$ center-of-mass (c.m.) energies from $\sqrt{s} = 4.009$ GeV to 4.420 GeV [17]. The c.m. energy is measured with a precision of ± 1.0 MeV [18]. A GEANT4-based Monte Carlo (MC) simulation software package that includes the geometric description of the BESIII detector and the detector response is used to optimize the event selection criteria, determine the detection efficiency, and estimate backgrounds. For the signal process, we generate $e^{+}e^{-} \to \gamma X(3872)$, with $X(3872) \to \pi^{+}\pi^{-}J/\psi$ at each c.m. energy. Initial state radiation (ISR) is simulated with KKMC [19], where the Born cross section of $e^{+}e^{-} \to \gamma X(3872)$ between 3.90 and 4.42 GeV is assumed to follow the $e^{+}e^{-} \to \pi^{+}\pi^{-}J/\psi$ line shape [11]. The maximum ISR photon energy corresponds to the 3.9 GeV$/c^{2}$ production threshold of the $\gamma X(3872)$ system. We generate $X(3872) \to \rho^{0}J/\psi$ MC events with $\rho^{0} \to \pi^{+}\pi^{-}$ to model the $\pi^{+}\pi^{-}$ system and determine the detection efficiency [9]. Here the ρ^{0} and J/ψ are assumed to be in a relative S wave. Final state radiation (FSR) is handled with PHOTOS [20].

Events with four good charged tracks with net charge zero are selected as described in Ref. [14]. Showers identified as photon candidates must satisfy fiducial and shower quality as well as timing requirement as described in Ref. [21]. When there is more than one photon candidate, the one with the largest energy is regarded as the radiative photon. In order to improve the momentum and energy resolution and reduce the background, the event is subjected to a four-constraint (4C) kinematic fit to the hypothesis $e^{+}e^{-} \to \gamma\pi^{+}\pi^{-}l^{+}l^{-}$, that constrains total four momentum of the measured particles to be equal to the initial four-momentum of the colliding beams. The χ^{2} of the kinematic fit is required to be less than 60. To reject radiative Bhabha and radiative dimuon ($\gamma e^{+}e^{-}/\gamma\mu^{+}\mu^{-}$) backgrounds associated with photon conversion, the cosine of the opening angle of the pion candidates, is required to be less than 0.98. This restriction removes almost all the background events with an efficiency loss for signal that is less than 1%. Background from $e^{+}e^{-} \to \eta J/\psi$ with $\eta \to \gamma\pi^{+}\pi^{-}/\pi^{+}\pi^{-}\pi^{0}$ is rejected by requiring $M(\gamma\pi^{+}\pi^{-}) > 0.6$ GeV$/c^{2}$, and its remaining contribution is negligible [21,22].

After imposing the above requirements, there are clear J/ψ peaks in the $\ell^{+}\ell^{-}$ invariant mass distribution at each c.m. energy data set. The J/ψ mass window to select signal events is $3.08 < M(\ell^{+}\ell^{-}) < 3.12$ GeV$/c^{2}$ (mass resolution is 6 MeV$/c^{2}$), while the sidebands are $3.0 < M(\ell^{+}\ell^{-}) < 3.06$ and $3.14 < M(\ell^{+}\ell^{-}) < 3.20$ GeV$/c^{2}$, which is three times as wide as the signal region.

The remaining backgrounds mainly come from $e^{+}e^{-} \to (\gamma_{\mathrm{ISR}})\pi^{+}\pi^{-}J/\psi$, $\eta' J/\psi$, and $\pi^{+}\pi^{-}\pi^{+}\pi^{-}\pi^{0}/\pi^{+}\pi^{-}\pi^{+}\pi^{-}\gamma$. MC simulation based on available measurements for $(\gamma_{\mathrm{ISR}})\pi^{+}\pi^{-}J/\psi$ [11], and cross sections measured from the same data samples for $\eta' J/\psi$ ($\eta' \to \gamma\pi^{+}\pi^{-}/\pi^{+}\pi^{-}\eta$) shows a smooth, nonpeaking $M(\pi^{+}\pi^{-}J/\psi)$ mass distribution in the $X(3872)$ signal region, and indicates that background from $e^{+}e^{-} \to \pi^{+}\pi^{-}\pi^{+}\pi^{-}(\pi^{0}/\gamma)$ is small and can be estimated from the J/ψ mass sideband data. Figure 1 shows the $\pi^{+}\pi^{-}J/\psi$ invariant mass distributions at $\sqrt{s} = 4.009$, 4.229, 4.260, and 4.360 GeV. Here $M(\pi^{+}\pi^{-}J/\psi) = M(\pi^{+}\pi^{-}\ell^{+}\ell^{-}) - M(\ell^{+}\ell^{-}) + m(J/\psi)$ is used to reduce the resolution effect of the lepton pairs, and $m(J/\psi)$ is the nominal mass of J/ψ [13]. There is a huge $e^{+}e^{-} \to \gamma_{\mathrm{ISR}}\psi(3686)$ signal at each c.m. energy data set. In addition, there is a narrow peak around 3872 MeV$/c^{2}$ in the 4.229 and 4.260 GeV data samples, while there is no significant signal at the other energies.

The $M(\pi^{+}\pi^{-}J/\psi)$ distribution (summed over all c.m. energy data sets) is fitted to determine the mass and $X(3872)$ yield. We use a MC simulated signal histogram convolved with a Gaussian function which represents the resolution difference between data and MC simulation as the signal shape, and a linear function for the background.

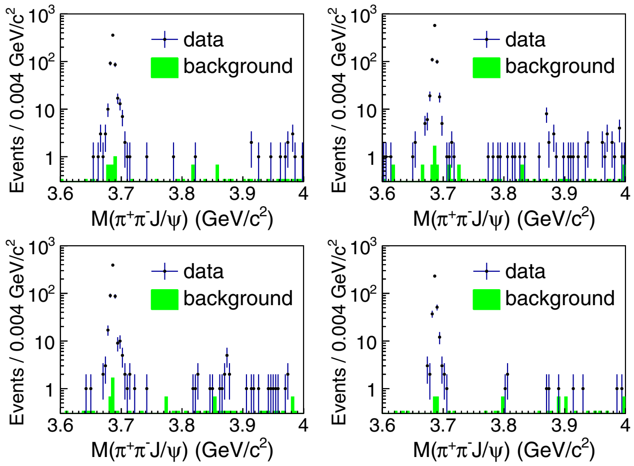

FIG. 1 (color online). The $\pi^+\pi^- J/\psi$ invariant mass distributions at $\sqrt{s} = 4.009$ (top left), 4.229 (top right), 4.260 (bottom left), and 4.360 GeV (bottom right). Dots with error bars are data, the green shaded histograms are normalized J/ψ sideband events.

The ISR $\psi(3686)$ signal is used to calibrate the absolute mass scale and to extract the resolution difference between data and MC simulation. The fit to the $\psi(3686)$ results in a mass shift of $\mu_{\psi(3686)} = -(0.34 \pm 0.04)$ MeV$/c^2$, and a standard deviation of the Gaussian resolution function of $\sigma = (1.14 \pm 0.07)$ MeV$/c^2$. The resolution parameter of the resolution Gaussian applied to the MC simulated signal shape is fixed at 1.14 MeV$/c^2$ in the fit to the $X(3872)$. Figure 2 shows the fit result (with $M[X(3872)]_{\text{input}} =$ 3871.7 MeV$/c^2$ as input in MC simulation), which gives $\mu_{X(3872)} = -(0.10 \pm 0.69)$ MeV$/c^2$ and $N[X(3872)] =$ 20.1 ± 4.5. So, the measured mass of $X(3872)$ is $M[X(3872)] = M[X(3872)]_{\text{input}} + \mu_{X(3872)} - \mu_{\psi(3686)} =$ (3871.9 ± 0.7) MeV$/c^2$, where the uncertainty includes

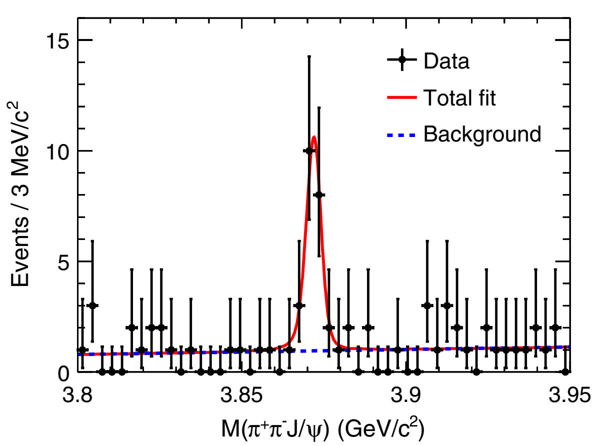

FIG. 2 (color online). Fit of the $M(\pi^+\pi^- J/\psi)$ distribution with a MC simulated histogram convolved with a Gaussian function for signal and a linear background function. Dots with error bars are data, the red curve shows the total fit result, while the blue dashed curve shows the background contribution.

the statistical uncertainties from the fit and the mass calibration. The limited statistics prevent us from measuring the intrinsic width of the $X(3872)$. From a fit with a floating width we obtain $\Gamma[X(3872)] = (0.0^{+1.7}_{-0.0})$ MeV, or less than 2.4 MeV at the 90% confidence level (C.L.). The statistical significance of $X(3872)$ is 6.3σ, estimated by comparing the difference of log-likelihood value $[\Delta(-2\ln\mathcal{L}) = 44.5]$ with and without the $X(3872)$ signal in the fit, and taking the change of the number of degrees of freedom (Δndf $= 2$) into consideration.

Figure 3 shows the angular distribution of the radiative photon in the e^+e^- c.m. frame and the $\pi^+\pi^-$ invariant mass distribution, for the $X(3872)$ signal events ($3.86 < M(\pi^+\pi^- J/\psi) < 3.88$ GeV$/c^2$) and normalized sideband events ($3.83 < M(\pi^+\pi^- J/\psi) < 3.86$ or $3.88 <$ $M(\pi^+\pi^- J/\psi) < 3.91$ GeV$/c^2$). The data agree with MC simulation assuming a pure $E1$-transition between the $Y(4260)$ and the $X(3872)$ for the polar angle distribution, and the $M(\pi^+\pi^-)$ distribution is consistent with the CDF observation [9] of a dominant $\rho^0(770)$ resonance contribution.

The product of the Born-order cross section times the branching fraction of $X(3872) \to \pi^+\pi^- J/\psi$ is calculated using $\sigma^B[e^+e^- \to \gamma X(3872)] \times \mathcal{B}[X(3872) \to \pi^+\pi^- J/\psi] = N^{\text{obs}}/\mathcal{L}_{\text{int}}(1+\delta)\epsilon\mathcal{B}$, where N^{obs} is the number of observed events obtained from the fit to the $M(\pi^+\pi^- J/\psi)$ distribution, $\mathcal{L}_{\text{int}}$ is integrated luminosity, ϵ is the detection efficiency, $\mathcal{B}$ is the branching fraction of $J/\psi \to \ell^+\ell^-$ and $(1+\delta)$ is the radiative correction factor, which depends on the line shape of $e^+e^- \to \gamma X(3872)$. Since we observe large cross sections at $\sqrt{s} = 4.229$ and 4.260 GeV, we assume the $e^+e^- \to \gamma X(3872)$ cross section follows that of $e^+e^- \to \pi^+\pi^- J/\psi$ over the full energy range of interest and use the $e^+e^- \to \pi^+\pi^- J/\psi$ line-shape from published results [11] as input in the calculation of the efficiency and radiative correction factor. The results of these studies at different energies ($\sqrt{s} = 4.009$, 4.229, 4.260, and 4.360 GeV) are listed in Table I. For the 4.009 and 4.360 GeV data, where the $X(3872)$ signal is not statistically significant, upper limits for production yield at 90% C.L. are also given. As a validation, the

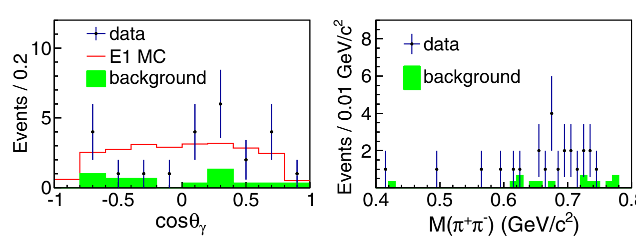

FIG. 3 (color online). The $\cos\theta$ distribution of the radiative photon in e^+e^- c.m. frame (left) and the $M(\pi^+\pi^-)$ distribution (right). Dots with error bars are data in the $X(3872)$ signal region, the green shaded histograms are normalized $X(3872)$ sideband events, and the red open histogram in the left panel is the result from a MC simulation that assumes a pure $E1$ transition.

TABLE I. The number of $X(3872)$ events ($N^{\rm obs}$), radiative correction factor $(1+\delta)$, detection efficiency (ϵ), measured Born cross section $\sigma^B[e^+e^- \to \gamma X(3872)]$ times $\mathcal{B}[X(3872) \to \pi^+\pi^- J/\psi]$ ($\sigma^B \cdot \mathcal{B}$, where the first uncertainties are statistical and the second systematic), measured ISR $\psi(3686)$ cross section ($\sigma^{\rm ISR}$, where the first uncertainties are statistical and the second systematic), and predicted ISR $\psi(3686)$ cross section ($\sigma^{\rm QED}$ with uncertainties from resonant parameters) from QED [23] using resonant parameters in PDG [13] as input at different energies. For 4.009 and 4.360 GeV, the upper limits of observed events ($N^{\rm up}$) and cross section times branching fraction ($\sigma^{\rm up} \cdot \mathcal{B}$) are given at the 90% C.L.

$\sqrt{s}$ (GeV)	$N^{\rm obs}$	$N^{\rm up}$	ε (%)	$1+\delta$	$\sigma^B \cdot \mathcal{B}$ (pb)	$\sigma^{\rm up} \cdot \mathcal{B}$ (pb)	$\sigma^{\rm ISR}$ (pb)	$\sigma^{\rm QED}$ (pb)
4.009	0.0 ± 0.5	< 1.4	28.7	0.861	$0.00 \pm 0.04 \pm 0.01$	< 0.11	$719 \pm 30 \pm 47$	735 ± 13
4.229	9.6 ± 3.1	...	34.4	0.799	$0.27 \pm 0.09 \pm 0.02$	...	$404 \pm 14 \pm 27$	408 ± 7
4.260	8.7 ± 3.0	...	33.1	0.814	$0.33 \pm 0.12 \pm 0.02$	...	$378 \pm 16 \pm 25$	382 ± 7
4.360	1.7 ± 1.4	< 5.1	23.2	1.023	$0.11 \pm 0.09 \pm 0.01$	< 0.36	$308 \pm 17 \pm 20$	316 ± 5

measured ISR $\psi(3686)$ cross section at each energy, together with the corresponding QED prediction [23] are also listed in Table I, where there is good agreement.

We fit the energy-dependent cross section with a $Y(4260)$ resonance (parameters fixed to PDG [13] values), a linear continuum, or a $E1$-transition phase space ($\propto E_\gamma^3$) term. Figure 4 shows all the fit results, which give $\chi^2/\mathrm{ndf} = 0.49/3$ (C.L. $= 92\%$), $5.5/2$ (C.L. $= 6\%$), and $8.7/3$ (C.L. $= 3\%$) for a $Y(4260)$ resonance, linear continuum, and phase space distribution, respectively. The $Y(4260)$ resonance describes the data better than the other two options.

The systematic uncertainty in the $X(3872)$ mass measurement include those from the absolute mass scale and the parametrization of the $X(3872)$ signal and background shapes. Since we use ISR $\psi(3686)$ events to calibrate the fit, the systematic uncertainty from the mass scale is estimated to be 0.1 MeV$/c^2$ (including statistical uncertainties of the MC samples used in the calibration procedure). In the $X(3872)$ mass fit, a MC simulated histogram with a zero width is used to parameterize the signal shape. We replace this histogram with a simulated $X(3872)$ resonance with a width of 1.2 MeV [13] (the upper limit of the $X(3872)$ width at 90% C.L.) and repeat the fit; the change in mass for this new fit is taken as the systematic uncertainty due to the signal parametrization, which is 0.1 MeV$/c^2$. Likewise, changes measured with a background shape from MC-simulated $(\gamma_{\rm ISR})\pi^+\pi^- J/\psi$ and $\eta' J/\psi$ events indicate a systematic uncertainty associated with the background shape of 0.1 MeV$/c^2$ in mass. By summing the contributions from all sources assuming that they are independent, we obtain a total systematic uncertainty of 0.2 MeV$/c^2$ for the $X(3872)$ mass measurement.

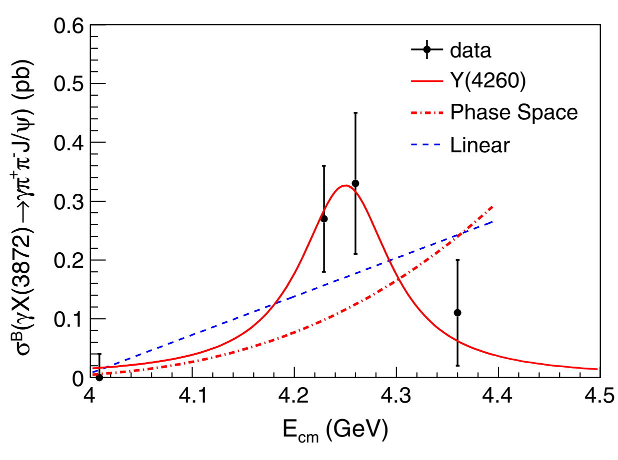

FIG. 4 (color online). The fit to $\sigma^B[e^+e^- \to \gamma X(3872)] \times \mathcal{B}[X(3872) \to \pi^+\pi^- J/\psi]$ with a $Y(4260)$ resonance (red solid curve), a linear continuum (blue dashed curve), or a $E1$-transition phase space term (red dotted-dashed curve). Dots with error bars are data.

The systematic uncertainty in the cross section measurement mainly comes from efficiencies, signal parametrization, background shape, radiative correction, and luminosity measurement. The luminosity is measured using Bhabha events, with an uncertainty of 1.0%. The uncertainty of tracking efficiency for high momenta leptons is 1.0% per track. Pions have momentum ranges from 0.1 to 0.6 GeV$/c$ at $\sqrt{s} = 4.260$ GeV, and with a small change with different c.m. energies. The momentum-weighted uncertainty is also estimated to be 1.0% per track. In this analysis, the radiative photons have energies that several hundreds of MeV. Studies with a sample of $J/\psi \to \rho\pi$ events show that the uncertainty in the reconstruction efficiency for photons in this energy range is less than 1.0%.

The number of $X(3872)$ signal events is obtained through a fit to the $M(\pi^+\pi^- J/\psi)$ distribution. In the nominal fit, a simulated histogram with zero width convolved with a Gaussian function is used to parameterize the $X(3872)$ signal. When a MC-simulated signal shape with $\Gamma[X(3872)] = 1.2$ MeV [13] is used, the difference in the $X(3872)$ signal yield, is 4.0%; this is taken as the systematic uncertainty due to signal parametrization. Changing the background shape from a linear term to the expected shape from the dominant background source $\eta' J/\psi$ results in a 0.2% difference in the $X(3872)$ yields. The $e^+e^- \to \pi^+\pi^- J/\psi$ line shape affects the radiative correction factor and detection efficiency. Using the measurements from BESIII, Belle, and *BABAR* [11] as inputs, the maximum difference in $(1+\delta)\epsilon$ is 0.6%, which is taken as the systematic uncertainty. The uncertainty from the kinematic fit is estimated with the very pure ISR $\psi(3686)$

sample, and the efficiency difference between data and MC simulation is found to be 1.5%. The systematic uncertainty for the J/ψ mass window is also estimated using the ISR $\psi(3686)$ events, and the efficiency difference between data and MC simulation is found to be $(0.8 \pm 0.8)\%$. We conservatively take 1.6% as the systematic uncertainty due to J/ψ mass window. The uncertainty in the branching fraction of $J/\psi \to \ell^+\ell^-$ is taken from Ref. [13]. The efficiencies for other selection criteria, the trigger simulation, the event start time determination, and the final-state-radiation simulation are quite high ($> 99\%$), and their systematic uncertainties are estimated to be less than 1%. Assuming all the systematic uncertainty sources are independent, we add all of them in quadrature, and the total systematic uncertainty is estimated to be 6.5%.

In summary, we report the first observation of the process $e^+e^- \to \gamma X(3872)$. The measured mass of the $X(3872)$, $M[X(3872)] = (3871.9 \pm 0.7 \pm 0.2)\ \mathrm{MeV}/c^2$, agrees well with previous measurements [13]. The production rate $\sigma^B[e^+e^- \to \gamma X(3872)]\mathcal{B}[X(3872) \to \pi^+\pi^- J/\psi]$ is measured to be $(0.27 \pm 0.09 \pm 0.02)$ pb at $\sqrt{s} = 4.229$ GeV, $(0.33 \pm 0.12 \pm 0.02)$ pb at $\sqrt{s} = 4.260$ GeV, less than 0.11 pb at $\sqrt{s} = 4.009$ GeV, and less than 0.36 pb at $\sqrt{s} = 4.360$ GeV at the 90% C.L. Here the first uncertainties are statistical and the second systematic. (For the upper limits, the efficiency has been lowered by a factor of $(1 - \sigma_{\mathrm{sys}})$).

These observations strongly support the existence of the radiative transition process $Y(4260) \to \gamma X(3872)$. While the measured cross sections at around 4.260 GeV are an order of magnitude higher than the NRQCD calculation of continuum production [24], the resonant contribution with $Y(4260)$ line shape provides a better description of the data than either a linear continuum or a $E1$-transition phase space distribution. The $Y(4260) \to \gamma X(3872)$ could be another previously unseen decay mode of the $Y(4260)$ resonance. This, together with the previously reported transitions to the charged charmoniumlike state $Z_c(3900)$ (which is manifestly exotic) [11,14], suggest that there might be some commonality in the nature of these three different states. This may be a clue that can facilitate a better theoretical interpretation of them. As an example, the measured relative large $\gamma X(3872)$ production rate near 4.260 GeV is similar to the model dependent calculations in Ref. [15] where the $Y(4260)$ is taken as a $\bar{D}D_1$ molecule.

Combining with the $e^+e^- \to \pi^+\pi^- J/\psi$ cross section measurement at $\sqrt{s} = 4.260$ GeV from BESIII [14], we obtain $\sigma^B[e^+e^- \to \gamma X(3872)]\mathcal{B}[X(3872) \to \pi^+\pi^- J/\psi]/\sigma^B(e^+e^- \to \pi^+\pi^- J/\psi) = (5.2 \pm 1.9) \times 10^{-3}$, under the assumption that the $X(3872)$ is produced only from the $Y(4260)$ radiative decays and the $\pi^+\pi^- J/\psi$ is only from the $Y(4260)$ hadronic decays. If we take $\mathcal{B}[X(3872) \to \pi^+\pi^- J/\psi] = 5\%$ [25], then $\mathcal{R} = (\sigma^B[e^+e^- \to \gamma X(3872)]/\sigma^B(e^+e^- \to \pi^+\pi^- J/\psi)) = 0.1$, or equivalently, $(\mathcal{B}[Y(4260) \to \gamma X(3872)]/\mathcal{B}(Y(4260) \to \pi^+\pi^- J/\psi)) = 0.1$.

The BESIII Collaboration thanks the staff of BEPCII and the computing center for their strong support. This work is supported in part by the Ministry of Science and Technology of China under Contract No. 2009CB825200; National Natural Science Foundation of China (NSFC) under Contracts No. 10625524, No. 10821063, No. 10825524, No. 10835001, No. 10935007, No. 11125525, No. 11235011; Joint Funds of the National Natural Science Foundation of China under Contracts No. 11079008, No. 11179007; the Chinese Academy of Sciences (CAS) Large-Scale Scientific Facility Program; CAS under Contracts No. KJCX2-YW-N29, No. KJCX2-YW-N45; 100 Talents Program of CAS; German Research Foundation DFG under Contract No. Collaborative Research Center CRC-1044; Seventh Framework Programme of the European Union under Marie Curie International Incoming Fellowship Grant Agreement No. 627240; Istituto Nazionale di Fisica Nucleare, Italy; Ministry of Development of Turkey under Contract No. DPT2006K-120470; U. S. Department of Energy under Contracts No. DE-FG02-04ER41291, No. DE-FG02-05ER41374, No. DE-FG02-94ER40823, No. DESC0010118; U.S. National Science Foundation; University of Groningen (RuG) and the Helmholtzzentrum fuer Schwerionenforschung GmbH (GSI), Darmstadt; and the WCU Program of the National Research Foundation of Korea under Contract No. R32-2008-000-10155-0.

[*]Also at the Novosibirsk State University, Novosibirsk 630090, Russia.
[†]Also at the Moscow Institute of Physics and Technology, Moscow 141700, Russia.
[‡]Also at University of Texas at Dallas, Richardson, Texas 75083, USA.
[§]Also at the PNPI, Gatchina 188300, Russia.

[1] S. K. Choi *et al.* (Belle Collaboration), Phys. Rev. Lett. **91**, 262001 (2003).
[2] D. Acosta *et al.* (CDF Collaboration), Phys. Rev. Lett. **93**, 072001 (2004).
[3] V. M. Abazov *et al.* (D0 Collaboration), Phys. Rev. Lett. **93**, 162002 (2004).
[4] B. Aubert *et al.* (*BABAR* Collaboration), Phys. Rev. D **71**, 071103 (2005).
[5] B. Aubert *et al.* (*BABAR* Collaboration), Phys. Rev. D **74**, 071101 (2006).
[6] V. Bhardwaj *et al.* (Belle Collaboration), Phys. Rev. Lett. **107**, 091803 (2011).
[7] A. Abulencia *et al.* (CDF Collaboration), Phys. Rev. Lett. **98**, 132002 (2007).
[8] R. Aaij *et al.* (LHCb Collaboration), Eur. Phys. J. C **72**, 1972 (2012); (LHCb Collaboration), Phys. Rev. Lett. **110**, 222001 (2013).
[9] A. Abulencia *et al.* (CDF Collaboration), Phys. Rev. Lett. **96**, 102002 (2006).
[10] For a recent review, see N. Brambilla *et al.*, Eur. Phys. J. C **71**, 1534 (2011).

[11] B. Aubert *et al.* (BABAR Collaboration), Phys. Rev. Lett. **95**, 142001 (2005); J. P. Lees *et al.* (*BABAR* Collaboration), Phys. Rev. D **86**, 051102(R) (2012); Z. Q. Liu *et al.* (Belle Collaboration), Phys. Rev. Lett. **110**, 252002 (2013).

[12] B. Aubert *et al.* (*BABAR* Collaboration), Phys. Rev. Lett. **98**, 212001 (2007); X. L. Wang *et al.* (Belle Collaboration), Phys. Rev. Lett. **99**, 142002 (2007); B. Aubert *et al.* (*BABAR* Collaboration), arXiv:1211.6271.

[13] J. Beringer *et al.* (Particle Data Group), Phys. Rev. D **86**, 010001 (2012).

[14] M. Ablikim *et al.* (BESIII Collaboration), Phys. Rev. Lett. **110**, 252001 (2013).

[15] F.-K. Guo, C. Hanhart, U.-G. Meissner, Q. Wang and Q. Zhao, Phys. Lett. B **725**, 127 (2013).

[16] M. Ablikim *et al.* (BESIII Collaboration), Nucl. Instrum. Methods Phys. Res., Sect. A **614**, 345 (2010).

[17] M. Ablikim *et al.* (BESIII Collaboration), Phys. Rev. Lett. **111**, 242001 (2013).

[18] E. V. Abakumova, M. N. Achasov, V. E. Blinov, X. Cai, H. Y. Dong, C. D. Fu, F. A. Harris and V. V. Kaminsky *et al.*, Nucl. Instrum. Methods Phys. Res., Sect. A **659**, 21 (2011).

[19] S. Jadach, B. F. L. Ward, and Z. Was, Comput. Phys. Commun. **130**, 260 (2000); Phys. Rev. D **63**, 113009 (2001).

[20] P. Golonka, and Z. Was, Eur. Phys. J. C **45**, 97 (2006).

[21] A. Ablikim *et al.* (BESIII Collaboration), Phys. Rev. D **86**, 071101(R) (2012).

[22] X. L. Wang *et al.* (Belle Collaboration), Phys. Rev. D **87**, 051101(R) (2013).

[23] E. A. Kuraev and V. S. Fadin, Yad. Fiz. **41**, 733 (1985) [Sov. J. Nucl. Phys. **41**, 466 (1985)].

[24] K.-T. Chao, Z.-G. He, D. Li, C. Meng, arXiv:1310.8597.

[25] C. Z. Yuan (for the Belle Collaboration), arXiv:0910.3138. We take 5% from the range presented in the paper of $2.3\% < \mathcal{B}[X(3872) \to \pi^+\pi^- J/\psi] < 6.6\%$ at 90% C.L.

Physics Letters B 753 (2016) 629–638

Contents lists available at ScienceDirect

Physics Letters B

www.elsevier.com/locate/physletb

Measurement of the $e^+e^- \to \pi^+\pi^-$ cross section between 600 and 900 MeV using initial state radiation

BESIII Collaboration

M. Ablikim [a], M.N. Achasov [i,6], X.C. Ai [a], O. Albayrak [e], M. Albrecht [d], D.J. Ambrose [av], A. Amoroso [ba,bc], F.F. An [a], Q. An [ax,1], J.Z. Bai [a], R. Baldini Ferroli [t], Y. Ban [ag], D.W. Bennett [s], J.V. Bennett [e], M. Bertani [t], D. Bettoni [v], J.M. Bian [au], F. Bianchi [ba,bc], E. Boger [y,4], I. Boyko [y], R.A. Briere [e], H. Cai [be], X. Cai [a,1], O. Cakir [ap,2], A. Calcaterra [t], G.F. Cao [a], S.A. Cetin [aq], J.F. Chang [a,1], G. Chelkov [y,4,5], G. Chen [a], H.S. Chen [a], H.Y. Chen [b], J.C. Chen [a], M.L. Chen [a,1], S.J. Chen [ae], X. Chen [a,1], X.R. Chen [ab], Y.B. Chen [a,1], H.P. Cheng [q], X.K. Chu [ag], G. Cibinetto [v], H.L. Dai [a,1], J.P. Dai [aj], A. Dbeyssi [n], D. Dedovich [y], Z.Y. Deng [a], A. Denig [x,*], I. Denysenko [y], M. Destefanis [ba,bc], F. De Mori [ba,bc], Y. Ding [ac], C. Dong [af], J. Dong [a,1], L.Y. Dong [a], M.Y. Dong [a,1], S.X. Du [bg], P.F. Duan [a], E.E. Eren [aq], J.Z. Fan [ao], J. Fang [a,1], S.S. Fang [a], X. Fang [ax,1], Y. Fang [a], L. Fava [bb,bc], F. Feldbauer [x], G. Felici [t], C.Q. Feng [ax,1], E. Fioravanti [v], M. Fritsch [n,x], C.D. Fu [a], Q. Gao [a], X.Y. Gao [b], Y. Gao [ao], Z. Gao [ax,1], I. Garzia [v], K. Goetzen [j], W.X. Gong [a,1], W. Gradl [x], M. Greco [ba,bc], M.H. Gu [a,1], Y.T. Gu [l], Y.H. Guan [a], A.Q. Guo [a], L.B. Guo [ad], Y. Guo [a], Y.P. Guo [x], Z. Haddadi [aa], A. Hafner [x], S. Han [be], X.Q. Hao [o], F.A. Harris [at], K.L. He [a], X.Q. He [aw], T. Held [d], Y.K. Heng [a,1], Z.L. Hou [a], C. Hu [ad], H.M. Hu [a], J.F. Hu [ba,bc], T. Hu [a,1], Y. Hu [a], G.M. Huang [f], G.S. Huang [ax,1], J.S. Huang [o], X.T. Huang [ai], Y. Huang [ae], T. Hussain [az], Q. Ji [a], Q.P. Ji [af], X.B. Ji [a], X.L. Ji [a,1], L.W. Jiang [be], X.S. Jiang [a,1], X.Y. Jiang [af], J.B. Jiao [ai], Z. Jiao [q], D.P. Jin [a,1], S. Jin [a], T. Johansson [bd], A. Julin [au], N. Kalantar-Nayestanaki [aa], X.L. Kang [a], X.S. Kang [af], M. Kavatsyuk [aa], B.C. Ke [e], P. Kiese [x], R. Kliemt [n], B. Kloss [x,*], O.B. Kolcu [aq,9], B. Kopf [d], M. Kornicer [at], W. Kühn [z], A. Kupsc [bd], J.S. Lange [z], M. Lara [s], P. Larin [n], C. Leng [bc], C. Li [bd], Cheng Li [ax,1], D.M. Li [bg], F. Li [a,1], F.Y. Li [ag], G. Li [a], H.B. Li [a], J.C. Li [a], Jin Li [ah], K. Li [ai], K. Li [m], Lei Li [c], P.R. Li [as], T. Li [ai], W.D. Li [a], W.G. Li [a], X.L. Li [ai], X.M. Li [l], X.N. Li [a,1], X.Q. Li [af], Z.B. Li [an], H. Liang [ax,1], Y.F. Liang [al], Y.T. Liang [z], G.R. Liao [k], D.X. Lin [n], B.J. Liu [a], C.X. Liu [a], F.H. Liu [ak], Fang Liu [a], Feng Liu [f], H.B. Liu [l], H.H. Liu [p], H.H. Liu [a], H.M. Liu [a], J. Liu [a], J.B. Liu [ax,1], J.P. Liu [be], J.Y. Liu [a], K. Liu [ao], K.Y. Liu [ac], L.D. Liu [ag], P.L. Liu [a,1], Q. Liu [as], S.B. Liu [ax,1], X. Liu [ab], Y.B. Liu [af], Z.A. Liu [a,1], Zhiqing Liu [x], H. Loehner [aa], X.C. Lou [a,1,8], H.J. Lu [q], J.G. Lu [a,1], Y. Lu [a], Y.P. Lu [a,1], C.L. Luo [ad], M.X. Luo [bf], T. Luo [at], X.L. Luo [a,1], X.R. Lyu [as], F.C. Ma [ac], H.L. Ma [a], L.L. Ma [ai], Q.M. Ma [a], T. Ma [a], X.N. Ma [af], X.Y. Ma [a,1], F.E. Maas [n], M. Maggiora [ba,bc], Y.J. Mao [ag], Z.P. Mao [a], S. Marcello [ba,bc], J.G. Messchendorp [aa], J. Min [a,1], R.E. Mitchell [s], X.H. Mo [a,1], Y.J. Mo [f], C. Morales Morales [n], K. Moriya [s], N.Yu. Muchnoi [i,6], H. Muramatsu [au], Y. Nefedov [y], F. Nerling [n], I.B. Nikolaev [i,6], Z. Ning [a,1], S. Nisar [h], S.L. Niu [a,1], X.Y. Niu [a], S.L. Olsen [ah], Q. Ouyang [a,1], S. Pacetti [u], P. Patteri [t], M. Pelizaeus [d], H.P. Peng [ax,1], K. Peters [j], J. Pettersson [bd], J.L. Ping [ad], R.G. Ping [a], R. Poling [au], V. Prasad [a], M. Qi [ae], S. Qian [a,1], C.F. Qiao [as], L.Q. Qin [ai], N. Qin [be], X.S. Qin [a], Z.H. Qin [a,1], J.F. Qiu [a], K.H. Rashid [az], C.F. Redmer [x], M. Ripka [x], G. Rong [a], Ch. Rosner [n], X.D. Ruan [l], V. Santoro [v], A. Sarantsev [y,7], M. Savrié [w], K. Schoenning [bd], S. Schumann [x], W. Shan [ag], M. Shao [ax,1], C.P. Shen [b], P.X. Shen [af], X.Y. Shen [a], H.Y. Sheng [a], W.M. Song [a],

http://dx.doi.org/10.1016/j.physletb.2015.11.043

M.R. Shepherd [s], X.Y. Song [a], S. Sosio [ba,bc], S. Spataro [ba,bc], G.X. Sun [a], J.F. Sun [o], S.S. Sun [a], Y.J. Sun [ax,1], Y.Z. Sun [a], Z.J. Sun [a,1], Z.T. Sun [s], C.J. Tang [al], X. Tang [a], I. Tapan [ar], E.H. Thorndike [av], M. Tiemens [aa], M. Ullrich [z], I. Uman [aq], G.S. Varner [at], B. Wang [af], D. Wang [ag], D.Y. Wang [ag], K. Wang [a,1], L.L. Wang [a], L.S. Wang [a], M. Wang [ai], P. Wang [a], P.L. Wang [a], S.G. Wang [ag], W. Wang [a,1], X.F. Wang [ao], Y.D. Wang [n], Y.F. Wang [a,1], Y.Q. Wang [x], Z. Wang [a,1], Z.G. Wang [a,1], Z.H. Wang [ax,1], Z.Y. Wang [a], T. Weber [x], D.H. Wei [k], J.B. Wei [ag], P. Weidenkaff [x], S.P. Wen [a], U. Wiedner [d], M. Wolke [bd], L.H. Wu [a], Z. Wu [a,1], L.G. Xia [ao], Y. Xia [r], D. Xiao [a], H. Xiao [ay], Z.J. Xiao [ad], Y.G. Xie [a,1], Q.L. Xiu [a,1], G.F. Xu [a], L. Xu [a], Q.J. Xu [m], X.P. Xu [am], L. Yan [ax,1], W.B. Yan [ax,1], W.C. Yan [ax,1], Y.H. Yan [r], H.J. Yang [aj], H.X. Yang [a], L. Yang [be], Y. Yang [f], Y.X. Yang [k], M. Ye [a,1], M.H. Ye [g], J.H. Yin [a], B.X. Yu [a,1], C.X. Yu [af], J.S. Yu [ab], C.Z. Yuan [a], W.L. Yuan [ae], Y. Yuan [a], A. Yuncu [aq,3], A.A. Zafar [az], A. Zallo [t], Y. Zeng [r], B.X. Zhang [a], B.Y. Zhang [a,1], C. Zhang [ae], C.C. Zhang [a], D.H. Zhang [a], H.H. Zhang [an], H.Y. Zhang [a,1], J.J. Zhang [a], J.L. Zhang [a], J.Q. Zhang [a], J.W. Zhang [a,1], J.Y. Zhang [a], J.Z. Zhang [a], K. Zhang [a], L. Zhang [a], X.Y. Zhang [ai], Y. Zhang [a], Y.N. Zhang [as], Y.H. Zhang [a,1], Y.T. Zhang [ax,1], Yu Zhang [as], Z.H. Zhang [f], Z.P. Zhang [ax], Z.Y. Zhang [be], G. Zhao [a], J.W. Zhao [a,1], J.Y. Zhao [a], J.Z. Zhao [a,1], Lei Zhao [ax,1], Ling Zhao [a], M.G. Zhao [af], Q. Zhao [a], Q.W. Zhao [a], S.J. Zhao [bg], T.C. Zhao [a], Y.B. Zhao [a,1], Z.G. Zhao [ax,1], A. Zhemchugov [y,4], B. Zheng [ay], J.P. Zheng [a,1], W.J. Zheng [ai], Y.H. Zheng [as], B. Zhong [ad], L. Zhou [a,1], X. Zhou [be], X.K. Zhou [ax,1], X.R. Zhou [ax,1], X.Y. Zhou [a], K. Zhu [a], K.J. Zhu [a,1], S. Zhu [a], S.H. Zhu [aw], X.L. Zhu [ao], Y.C. Zhu [ax,1], Y.S. Zhu [a], Z.A. Zhu [a], J. Zhuang [a,1], L. Zotti [ba,bc], B.S. Zou [a], J.H. Zou [a]

[a] Institute of High Energy Physics, Beijing 100049, People's Republic of China
[b] Beihang University, Beijing 100191, People's Republic of China
[c] Beijing Institute of Petrochemical Technology, Beijing 102617, People's Republic of China
[d] Bochum Ruhr-University, D-44780 Bochum, Germany
[e] Carnegie Mellon University, Pittsburgh, PA 15213, USA
[f] Central China Normal University, Wuhan 430079, People's Republic of China
[g] China Center of Advanced Science and Technology, Beijing 100190, People's Republic of China
[h] COMSATS Institute of Information Technology, Lahore, Defence Road, Off Raiwind Road, 54000 Lahore, Pakistan
[i] G.I. Budker Institute of Nuclear Physics SB RAS (BINP), Novosibirsk 630090, Russia
[j] GSI Helmholtzcentre for Heavy Ion Research GmbH, D-64291 Darmstadt, Germany
[k] Guangxi Normal University, Guilin 541004, People's Republic of China
[l] GuangXi University, Nanning 530004, People's Republic of China
[m] Hangzhou Normal University, Hangzhou 310036, People's Republic of China
[n] Helmholtz Institute Mainz, Johann-Joachim-Becher-Weg 45, D-55099 Mainz, Germany
[o] Henan Normal University, Xinxiang 453007, People's Republic of China
[p] Henan University of Science and Technology, Luoyang 471003, People's Republic of China
[q] Huangshan College, Huangshan 245000, People's Republic of China
[r] Hunan University, Changsha 410082, People's Republic of China
[s] Indiana University, Bloomington, IN 47405, USA
[t] INFN Laboratori Nazionali di Frascati, I-00044, Frascati, Italy
[u] INFN and University of Perugia, I-06100, Perugia, Italy
[v] INFN Sezione di Ferrara, I-44122, Ferrara, Italy
[w] University of Ferrara, I-44122, Ferrara, Italy
[x] Johannes Gutenberg University of Mainz, Johann-Joachim-Becher-Weg 45, D-55099 Mainz, Germany
[y] Joint Institute for Nuclear Research, 141980 Dubna, Moscow region, Russia
[z] Justus Liebig University Giessen, II. Physikalisches Institut, Heinrich-Buff-Ring 16, D-35392 Giessen, Germany
[aa] KVI-CART, University of Groningen, NL-9747 AA Groningen, The Netherlands
[ab] Lanzhou University, Lanzhou 730000, People's Republic of China
[ac] Liaoning University, Shenyang 110036, People's Republic of China
[ad] Nanjing Normal University, Nanjing 210023, People's Republic of China
[ae] Nanjing University, Nanjing 210093, People's Republic of China
[af] Nankai University, Tianjin 300071, People's Republic of China
[ag] Peking University, Beijing 100871, People's Republic of China
[ah] Seoul National University, Seoul, 151-747, Republic of Korea
[ai] Shandong University, Jinan 250100, People's Republic of China
[aj] Shanghai Jiao Tong University, Shanghai 200240, People's Republic of China
[ak] Shanxi University, Taiyuan 030006, People's Republic of China
[al] Sichuan University, Chengdu 610064, People's Republic of China
[am] Soochow University, Suzhou 215006, People's Republic of China
[an] Sun Yat-Sen University, Guangzhou 510275, People's Republic of China
[ao] Tsinghua University, Beijing 100084, People's Republic of China
[ap] Istanbul Aydin University, 34295 Sefakoy, Istanbul, Turkey
[aq] Dogus University, 34722 Istanbul, Turkey
[ar] Uludag University, 16059 Bursa, Turkey
[as] University of Chinese Academy of Sciences, Beijing 100049, People's Republic of China
[at] University of Hawaii, Honolulu, HI 96822, USA
[au] University of Minnesota, Minneapolis, MN 55455, USA
[av] University of Rochester, Rochester, NY 14627, USA

[aw] University of Science and Technology Liaoning, Anshan 114051, People's Republic of China
[ax] University of Science and Technology of China, Hefei 230026, People's Republic of China
[ay] University of South China, Hengyang 421001, People's Republic of China
[az] University of the Punjab, Lahore-54590, Pakistan
[ba] University of Turin, I-10125, Turin, Italy
[bb] University of Eastern Piedmont, I-15121, Alessandria, Italy
[bc] INFN, I-10125, Turin, Italy
[bd] Uppsala University, Box 516, SE-75120 Uppsala, Sweden
[be] Wuhan University, Wuhan 430072, People's Republic of China
[bf] Zhejiang University, Hangzhou 310027, People's Republic of China
[bg] Zhengzhou University, Zhengzhou 450001, People's Republic of China

A R T I C L E I N F O

Article history:
Received 30 July 2015
Received in revised form 28 October 2015
Accepted 14 November 2015
Available online 28 November 2015
Editor: V. Metag

Keywords:
Hadronic cross section
Muon anomaly
Initial state radiation
Pion form factor
BESIII

A B S T R A C T

We extract the $e^+e^- \to \pi^+\pi^-$ cross section in the energy range between 600 and 900 MeV, exploiting the method of initial state radiation. A data set with an integrated luminosity of 2.93 fb^{-1} taken at a center-of-mass energy of 3.773 GeV with the BESIII detector at the BEPCII collider is used. The cross section is measured with a systematic uncertainty of 0.9%. We extract the pion form factor $|F_\pi|^2$ as well as the contribution of the measured cross section to the leading-order hadronic vacuum polarization contribution to $(g-2)_\mu$. We find this value to be $a_\mu^{\pi\pi,\mathrm{LO}}(600\text{–}900\ \mathrm{MeV}) = (368.2 \pm 2.5_{\mathrm{stat}} \pm 3.3_{\mathrm{sys}}) \cdot 10^{-10}$, which is between the corresponding values using the BaBar or KLOE data.

1. Introduction

The cross section $\sigma_{\pi\pi} = \sigma(e^+e^- \to \pi^+\pi^-)$ has been measured in the past with ever increasing precision at accelerators in Novosibirsk [1–3], Orsay [4], Frascati [5–8], and SLAC [9,10]. More recently, the two most precise measurements have been performed by the KLOE Collaboration in Frascati [8] and the BaBar Collaboration at SLAC [9,10]. Both experiments claim a precision of better than 1% in the energy range below 1 GeV, in which the $\rho(770)$ resonance with its decay into pions dominates the total hadronic cross section. A discrepancy of approximately 3% on the peak of the $\rho(770)$ resonance is observed between the KLOE and BaBar spectra. The discrepancy is even increasing towards higher energies above the peak of the ρ resonance. Unfortunately, this discrepancy is limiting the current knowledge of the anomalous magnetic moment of the muon $a_\mu \equiv (g-2)_\mu/2$ [11], a precision observable of the Standard Model (SM). The accuracy of the SM prediction of $(g-2)_\mu$ is entirely limited by the knowledge of the hadronic vacuum polarization contribution, which is obtained in a dispersive framework by using experimental data on $\sigma(e^+e^- \to \text{hadrons})$ [11–13]. The cross section $\sigma(e^+e^- \to \pi^+\pi^-)$ contributes to more than 70% to this dispersion relation and, hence, is the most important exclusive hadronic channel of the total hadronic cross section. Currently, a discrepancy of 3.6 standard deviations [12] is found between the direct measurement of a_μ and its SM prediction. However, the discrepancy reduces to 2.4σ [14], when only BaBar data is used as input to the dispersion relation. In this letter we present a new measurement of the cross section $\sigma_{\pi\pi}$, obtained by the BESIII experiment at the BEPCII collider in Beijing.

The measurement exploits the method of initial state radiation (ISR), the same method as used by BaBar and KLOE. In the ISR method events are used in which one of the beam particles radiates a high-energy photon. In such a way, the available energy to produce a hadronic (or leptonic) final state is reduced, and the hadronic (or leptonic) mass range below the center-of-mass (cms) energy of the e^+e^- collider becomes available. In this paper, we restrict the studies to the mass range between 600 and 900 MeV/c^2, which corresponds to the ρ peak region.

The remainder of this letter is organized as follows: In section 2, the BESIII experiment is introduced. In section 3 we describe the data set used, the Monte Carlo (MC) simulation, the event selection of $e^+e^- \to \pi^+\pi^-\gamma$ events, and the data-MC efficiency corrections. The determination of the integrated luminosity of the data set is described in Section 4. A cross check of the used efficiency corrections using the well-known $e^+e^- \to \mu^+\mu^-\gamma$ QED process is performed in Section 5, before extracting the $\pi^+\pi^-$ cross section in Section 6.

2. The BESIII experiment

The BESIII detector is located at the double-ring Beijing electron–positron collider (BEPCII) [15].

The cylindrical BESIII detector covers 93% of the full solid angle. It consists of the following detector systems. (1) A Multilayer Drift Chamber (MDC), filled with helium gas, composed of 43 layers, which provides a spatial resolution of 135 μm, an ionization energy loss dE/dx resolution better than 6%, and a momentum resolution of 0.5% for charged tracks at 1 GeV/c. (2) A Time-of-Flight system (TOF), built with 176 plastic scintillator counters in the barrel part, and 96 counters in the endcaps. The time resolution is 80 ps in the barrel and 110 ps in the endcaps. For momenta

* Corresponding author.
E-mail addresses: denig@kph.uni-mainz.de (A. Denig), kloss@uni-mainz.de (B. Kloss), liu@kph.uni-mainz.de (Z. Liu).

[1] Also at State Key Laboratory of Particle Detection and Electronics, Beijing 100049, Hefei 230026, People's Republic of China.
[2] Also at Ankara University, 06100 Tandogan, Ankara, Turkey.
[3] Also at Bogazici University, 34342 Istanbul, Turkey.
[4] Also at the Moscow Institute of Physics and Technology, Moscow 141700, Russia.
[5] Also at the Functional Electronics Laboratory, Tomsk State University, Tomsk, 634050, Russia.
[6] Also at the Novosibirsk State University, Novosibirsk, 630090, Russia.
[7] Also at the NRC "Kurchatov Institute", PNPI, 188300, Gatchina, Russia.
[8] Also at the University of Texas at Dallas, Richardson, Texas 75083, USA.
[9] Also at Istanbul Arel University, 34295 Istanbul, Turkey.

up to 1 GeV/c, this provides a 2σ K/π separation. (3) A CsI(Tl) Electro-Magnetic Calorimeter (EMC), with an energy resolution of 2.5% in the barrel and 5% in the endcaps at an energy of 1 GeV. (4) A superconducting magnet producing a magnetic field of 1T. (5) A Muon Chamber (MUC) consisting of nine barrel and eight endcap resistive plate chamber layers with a 2 cm position resolution.

3. Data sample, event selection, and efficiency corrections

3.1. Data sample and MC simulations

We analyze 2.93 fb^{-1} (see Sect. 4) of data taken at a cms energy $\sqrt{s} = 3.773$ GeV, which were collected in two separate runs in 2010 and 2011. The Phokhara event generator [16,17] is used to simulate the signal process $e^+e^- \to \pi^+\pi^-\gamma$ and the dominant background channel $\mu^+\mu^-\gamma$. The generator includes ISR and final state radiation (FSR) corrections up to next-to-leading order (NLO). Effects of ISR–FSR interference are included as well. The continuum $q\bar{q}$ ($q = u, d, s$) MC sample is produced with the KKMC event generator [18]. Bhabha scattering events are simulated with BABAYAGA 3.5 [19]. The Bhabha process is also used for the luminosity measurement. All MC generators have been interfaced with the GEANT4-based detector simulation [20,21].

3.2. Event selection

Events of the type $e^+e^- \to \pi^+\pi^-\gamma$ are selected. Only a tagged ISR analysis is possible in the mass range $600 < m_{\pi\pi} < 900$ MeV/c^2, where $m_{\pi\pi}$ is the $\pi^+\pi^-$ invariant mass, *i.e.*, the radiated photon has to be explicitly detected in the detector. For untagged events, the photon escapes detection along the beam pipe; the hadronic system recoiling against the ISR photon is therefore also strongly boosted towards small polar angles, resulting in no geometrical acceptance in the investigated $m_{\pi\pi}$ range.

We require the presence of two charged tracks in the MDC with net charge zero. The points of closest approach to the interaction point (IP) of both tracks have to be within a cylinder with 1 cm radius in the transverse direction and ± 10 cm of length along the beam axis. For three-track events, we choose the combination with net charge zero for which the tracks are closest to the IP. The polar angle θ of the tracks is required to be found in the fiducial volume of the MDC, 0.4 rad $< \theta < \pi - 0.4$ rad, where θ is the polar angle of the track with respect to the beam axis. We require the transverse momentum p_t to be above 300 MeV/c for each track. In addition, we require the presence of at least one neutral cluster in the EMC without associated hits in the MDC. We require a deposited energy above 400 MeV. This cluster is then treated as the ISR photon candidate.

The radiative Bhabha process $e^+e^- \to e^+e^-\gamma(\gamma)$ has a cross section which is up to three orders of magnitude larger than the signal cross section. Electron tracks, therefore, need to be suppressed. An electron particle identification (PID) algorithm is used for this purpose, exploiting information from the MDC, TOF and EMC [22]. The probabilities for being a pion $P(\pi)$ and being an electron $P(e)$ are calculated, and $P(\pi) > P(e)$ is required for both charged tracks.

Using as input the momenta of the two selected track candidates, the energy of the photon candidate, as well as the four-momentum of the initial e^+e^- system, a four-constraint (4C) kinematic fit enforcing energy and momentum conservation is performed which tests the hypothesis $e^+e^- \to \pi^+\pi^-\gamma$. Events are considered to match the hypothesis if they fulfill the requirement $\chi^2_{4C} < 60$. It turns out that the $\mu^+\mu^-\gamma$ final state cannot be suppressed by means of kinematic fitting due to the limited momentum resolution of the MDC. An independent separation of pion and muon tracks is required.

We utilize a track-based muon–pion separation, which is based on the Artificial Neural Network (ANN) method, as provided by the TMVA package [23]. The following observables are exploited for the separation: the Zernicke moments of the EMC clusters [22], induced by pion or muon tracks, the ratio of the energy E of a track deposited in the EMC and its momentum p measured in the MDC, the ionization energy loss dE/dx in the MDC, and the depth of a track in the MUC. The ANN is trained using $\pi^+\pi^-\gamma$ and $\mu^+\mu^-\gamma$ MC samples. We choose the implementation of a Clermont-Ferrand Multilayer Perceptron (CFMlp) ANN as the method resulting in the best background rejection for a given signal efficiency. The output likelihood y_{ANN} is calculated after training the ANN for the signal pion tracks and background muon tracks. The response value y_{ANN} is required to be greater than 0.6 for each pion candidate in the event selection, yielding a background rejection of more than 90% and a signal loss of less than 30%.

3.3. Efficiency corrections

Given the accuracy of $\mathcal{O}(1\%)$ targeted for the cross section measurement, possible discrepancies between data and MC due to imperfections of the detector simulation need to be considered. We have investigated data and MC distributions concerning the tracking performance, the energy measurement, and the PID probabilities, both for the electron PID as well as the pion–muon separation. In order to produce test samples of muon and pion tracks over a wide range in momentum/energy and polar angle, we select samples of $\mu^+\mu^-\gamma$ and $\pi^+\pi^-\pi^+\pi^-\gamma$ events that have impurities at the per mille level. By comparing the efficiencies found in data with the corresponding results found in the MC samples, we determine possible discrepancies. Corresponding correction factors are computed in bins of the track momentum or energy and the track polar angle θ, and are applied to MC tracks to adjust the reconstructed number of events. While for the reconstruction of charged tracks and neutral clusters and for electron PID, the differences between data and MC are smaller than 1% on average, differences up to 10% occur in the ANN case. The corrections are applied separately for neutral clusters and for muon and pion tracks. Hence, we do not only obtain the corrections for the $\pi^+\pi^-\gamma$ signal events, but also for the dominating $\mu^+\mu^-\gamma$ background. The statistical errors of the correction factors are included in the statistical uncertainty of the measurement. Systematic uncertainties associated to the correction factors are presented in Sect. 6.5. The efficiency correction for the photon efficiency is obtained after the application of the kinematic fit procedure. The corresponding correction is therefore a combined correction of photon efficiency and differences between data and MC of the χ^2_{4C} distribution. The systematic uncertainty for the contribution of the photon efficiency and χ^2_{4C} distribution is, hence, incorporated in the systematic effects associated with the efficiency corrections. The systematic uncertainty connected with the p_t requirement is also associated with the corresponding efficiency correction.

3.4. Background subtraction

The $\mu^+\mu^-\gamma$ background remaining after the application of the ANN is still of the order of a few percent, compared to 5×10^5 signal events. It is, however, known with high accuracy, as will be shown in the next section, and is subtracted based on MC simulation. Additional background beyond $\mu^+\mu^-\gamma$ remains below the one per mille level. Table 1 lists the remaining MC events after applying all requirements and scaling to the luminosity of the used data set.

Table 1
Total number of remaining non-muon background events between $600 < m_{\pi\pi} < 900$ MeV/c^2 obtained with MC samples.

Final state	Background events
$e^+e^-(n\gamma)$	12.0 ± 3.5
$\pi^+\pi^-\pi^0\gamma$	3.3 ± 1.8
$\pi^+\pi^-\pi^0\pi^0\gamma$	negl.
$K^+K^-\gamma$	2.0 ± 1.5
$K^0\bar{K}^0\gamma$	0.4 ± 0.6
$p\bar{p}\gamma$	negl.
continuum	3.9 ± 1.9
$\psi(3770) \to D^+D^-$	negl.
$\psi(3770) \to D^0\bar{D}^0$	negl.
$\psi(3770) \to$ non $D\bar{D}$	3.1 ± 1.8
$\gamma\ \psi(2S)$	negl.
$\gamma\ J/\psi$	0.6 ± 0.8

4. Luminosity measurement using Bhabha events

The integrated luminosity of the data set used in this work was previously measured in Ref. [24] with a precision of 1.0% using Bhabha scattering events. In the course of this analysis, we re-measure the luminosity and decrease its systematic uncertainty by the following means: (1) Usage of the BABAYAGA@NLO [25] event generator with a theoretical uncertainty of 0.1%, instead of the previously used BABAYAGA 3.5 event generator with an uncertainty of 0.5% [19]. (2) Precise estimation of the signal selection efficiencies. In particular, the uncertainty estimate of the polar angle acceptance is evaluated by data-MC studies within the fiducial EMC detection volume, which is relevant for the luminosity study (0.13%). The very conservative estimate in [24] was based on acceptance comparisons with and without using the transition region between the EMC barrel and endcaps, leading to additional data-MC differences (0.75%). The other uncertainties of [24] remain unchanged and additional systematic uncertainties due to the uncertainty of $\sqrt{s}$ (0.2%) and the vacuum polarization correction (< 0.01%) are taken into account. Finally, the total integrated luminosity amounts to $\mathcal{L} = (2931.8 \pm 0.2_{\text{stat}} \pm 13.8_{\text{sys}})$ pb^{-1} with a relative uncertainty of 0.5%, which is consistent with the previous measurement [24].

5. QED test using $e^+e^- \to \mu^+\mu^-\gamma$ events

The yield of events of the channel $e^+e^- \to \mu^+\mu^-\gamma$ as a function of the two-muon invariant mass $m_{\mu\mu}$ can be compared to a precise prediction by QED, which is provided by the Phokhara generator. We select muon events according to the ANN method described previously and require $y_{\text{ANN}} < 0.4$ for both tracks, resulting in a background rejection of more than 90% and a signal loss of less than 20%. All other requirements in the selection are exactly the same as for the $\pi^+\pi^-\gamma$ analysis. The remaining pion background after the $\mu^+\mu^-\gamma$ selection is much reduced, reaching 10% in the ρ peak region. A comparison between data and MC is shown in Fig. 1. The same data sample as used in the main analysis is also used here, but we present a larger mass range than for the $\pi^+\pi^-\gamma$ case. The efficiency corrections described in the previous section have been applied to MC on a track and photon candidate basis. The lower panel of Fig. 1 shows the relative discrepancy between data and MC. A good agreement over the full $m_{\mu\mu}$ mass range at the level of $(1.0 \pm 0.3 \pm 0.9)$% and $\chi^2/\text{ndf} = 134/139$ is found, where the uncertainties are statistical and systematic, respectively. A difference in the mass resolution due to detector effects between data and MC is visible around the narrow J/ψ resonance. A fit in the mass range $600 < m_{\mu\mu} < 900$ MeV/c^2, which is the mass range studied in the main analysis, gives a relative discrepancy of $(2.0 \pm 1.7 \pm 0.9)$%; this is illustrated in the inset of the upper panel of Fig. 1. The theoretical uncertainty of the MC generator Phokhara is below 0.5% [16], while the systematic uncertainty of our measurement is 0.9%. The latter is dominated by the luminosity measurement, which is needed for the normalization of the data set. We consider the good agreement between the $\mu^+\mu^-\gamma$ QED prediction and data as a validation of the accuracy of our efficiency corrections. As a further cross check, we have applied the efficiency corrections also to a statistically independent $\mu^+\mu^-\gamma$ sample, resulting in a difference between data and MC of (0.7 ± 0.2)% over the full mass range, where the error is statistical only.

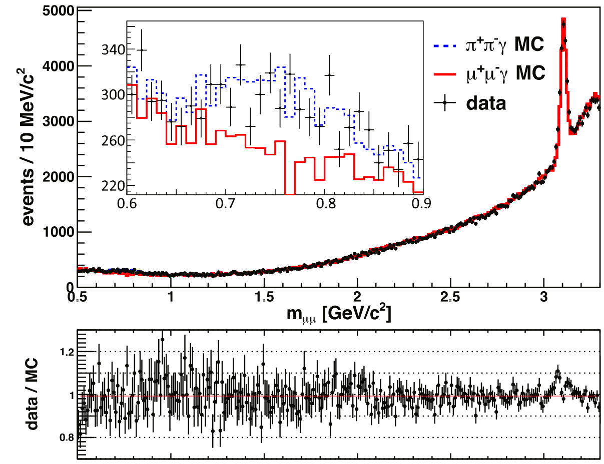

Fig. 1. Invariant $\mu^+\mu^-$ mass spectrum of data and $\mu^+\mu^-\gamma$ MC after using the ANN as muon selector and applying the efficiency corrections. The upper panel presents the absolute comparison of the number of events found in data and MC. The inset shows the zoom for invariant masses between 0.6 and 0.9 GeV/c^2. The MC sample is scaled to the luminosity of the data set. The lower plot shows the ratio of these two histograms. A linear fit is performed to quantify the data-MC difference, which gives a difference of $(1.0 \pm 0.3 \pm 0.9)$%. A difference in the mass resolution between data and MC is visible around the narrow J/ψ resonance.

6. Extraction of $\sigma(e^+e^- \to \pi^+\pi^-)$ and $|F_\pi^2|$

6.1. Methods

We finally extract $\sigma_{\pi\pi} = \sigma(e^+e^- \to \pi^+\pi^-)$ according to two independent normalization schemes. In the first method, we obtain the bare cross section, *i.e.*, the cross section corrected for vacuum polarization effects, according to the following formula:

$$\sigma^{\text{bare}}_{\pi\pi(\gamma_{\text{FSR}})} = \frac{N_{\pi\pi\gamma} \cdot (1 + \delta^{\pi\pi}_{\text{FSR}})}{\mathcal{L} \cdot \epsilon^{\pi\pi\gamma}_{\text{global}} \cdot H(s) \cdot \delta_{\text{vac}}}\ , \tag{1}$$

where $N_{\pi\pi\gamma}$ is the number of signal events found in data after applying all selection requirements described above and an unfolding procedure to correct for the mass resolution, $\mathcal{L}$ the luminosity of the data set, and H the radiator function. The global efficiency $\epsilon^{\pi\pi\gamma}_{\text{global}}$ is determined based on the signal MC by dividing the measured number of events after all selection requirements $N^{\text{true}}_{\text{measured}}$ by that of all generated events $N^{\text{true}}_{\text{generated}}$. The true MC sample is used, with the full θ_γ range, applying the efficiency corrections mentioned in Section 3.3 but without taking into account the detector resolution in the invariant mass m:

$$\epsilon_{\text{global}}(m) = \frac{N^{\text{true}}_{\text{measured}}(m)}{N^{\text{true}}_{\text{generated}}(m)}\ . \tag{2}$$

The efficiency is found to depend slightly on $m_{\pi\pi}$ and ranges from 2.8% to 3.0% from lowest to highest $m_{\pi\pi}$. An unfolding procedure, which eliminates the effect of the detector resolution, is described

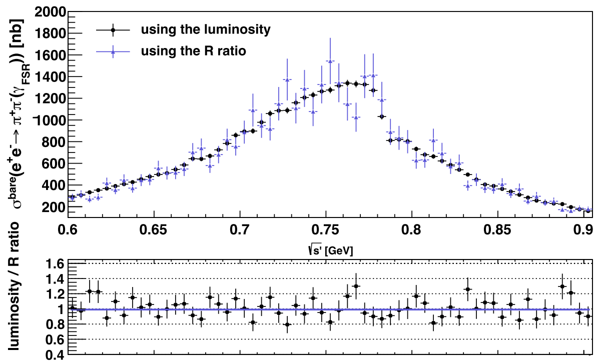

Fig. 2. Comparison between the methods to extract $\sigma_{\pi\pi}$ explained in the text – using the luminosity (black) and normalizing by $\sigma_{\mu\mu}$ (blue). The lower panel shows the ratio of these results together with a linear fit (blue line) to quantify their difference. (For interpretation of the references to color in this figure legend, the reader is referred to the web version of this article.)

in Sect. 6.2 and is applied before dividing by the global efficiency. The radiator function H is described in Sect. 6.4. As input for a_μ the bare cross section is needed. It can be obtained by dividing the cross section by the vacuum polarization correction δ_{vac}, which is also described in Sect. 6.4. As pointed out in Ref. [11], in order to consider radiative effects in the dispersion integral for a_μ, an FSR correction has to be performed. The determination of the correction factor $(1+\delta^{\pi\pi}_{\text{FSR}})$ is described in Sect. 6.3.

In the second method, we use a different normalization than in the first method and normalize $N_{\pi\pi\gamma}$ to the measured number of $\mu^+\mu^-\gamma$ events, $N_{\mu\mu\gamma}$. Since $\mathcal{L}$, H, and δ_{vac} cancel in this normalization, one finds the following formula:

$$\sigma^{\text{bare}}_{\pi\pi(\gamma_{\text{FSR}})} = \frac{N_{\pi\pi\gamma}}{N_{\mu\mu\gamma}} \cdot \frac{\epsilon^{\mu\mu\gamma}_{\text{global}}}{\epsilon^{\pi\pi\gamma}_{\text{global}}} \cdot \frac{1+\delta^{\mu\mu}_{\text{FSR}}}{1+\delta^{\pi\pi}_{\text{FSR}}} \cdot \sigma^{\text{bare}}_{\mu\mu}\,, \tag{3}$$

where $\epsilon^{\mu\mu\gamma}_{\text{global}}$ is the global efficiency of the dimuon selection, already described in Sect. 5, $\delta^{\mu\mu}_{\text{FSR}}$ is the FSR correction factor to the $\mu^+\mu^-$ final state, which can be obtained using the Phokhara event generator, $\sigma^{\text{bare}}_{\mu\mu}$ is the exact QED prediction of the dimuon cross section, given by [26, Eq. (5.13)]

$$\sigma^{\text{bare}}_{\mu\mu} = \frac{4\pi\alpha^2}{3s'} \cdot \frac{\beta_\mu(3-\beta_\mu^2)}{2}\,, \tag{4}$$

with the fine structure constant α, the cms energy $s' < s$ available for the creation of the final state, the muon velocity $\beta_\mu = \sqrt{1-4m_\mu^2/s'}$, and the muon mass m_μ. The contributions of radiator function, luminosity, and vacuum polarization to the systematic uncertainties of the bare cross section, cancel in the second method. The upper panel of Fig. 2 shows the comparison of the bare cross sections including FSR obtained with the first (black) and second method before unfolding (blue). The error bars are statistical only. They are much larger for the second method due to the limited $\mu^+\mu^-\gamma$ statistics in the mass range of interest. The lower panel shows the ratio of these cross sections. Again, a linear fit is performed to quantify the difference, which is found to be (0.85 ± 1.68)% and $\chi^2/\text{ndf} = 50/60$, where the error is statistical. Both methods agree within uncertainties. The first one is used in the analysis. Finally, the pion form factor as a function of s' can be calculated via

$$|F_\pi|^2(s') = \frac{3s'}{\pi\alpha^2\beta_\pi^3(s')}\sigma^{\text{dressed}}_{\pi\pi}(s')\,, \tag{5}$$

with the pion velocity $\beta_\pi(s') = \sqrt{1-4m_\pi^2/s'}$, the charged pion mass m_π, and the dressed cross section $\sigma^{\text{dressed}}_{\pi\pi}(s') = \sigma(e^+e^- \to \pi^+\pi^-)(s')$ containing vacuum polarization, but corrected for FSR effects. The result is presented in Sect. 7.

6.2. Unfolding

In order to obtain the final result for $\sigma_{\pi\pi}$, one has to rectify the detector resolution effects, *i.e.*, the mass spectrum needs to be unfolded. To this end, the Singular Value Decomposition (SVD) method [27] is used. It requires two input variables – the response matrix and the regularization parameter τ. The SVD algorithm calculates an operator which cancels the detector smearing by inverting the response matrix. We obtain the response matrix in the full mass range between threshold and 3.0 GeV, using a signal MC sample. The matrix corresponds to the correlation of the reconstructed $m_{\pi\pi}$ spectrum, and the originally generated $m_{\pi\pi}$ values. With the choice of a bin width of 5 MeV/c^2, about 43% of events are found to be on the diagonal axis.

To find the value of the regularization parameter τ, we compare two independent methods, as suggested in Ref. [27]. On the one hand, we perform a MC simulation where τ is optimized such that unfolded and true distributions have the best agreement. On the other hand, we process an algorithm, described in [27], exploiting the singular values of the response matrix. Both methods favor a similar regularization parameter of $\tau \cong 72$.

To estimate the systematic uncertainties and to test the stability of the SVD method, we perform two cross checks. In both cases we use a $\pi^+\pi^-\gamma$ MC sample which is independent of the one used to determine the response matrix. We modify and then unfold the spectra in both checks. In the first cross check, the reconstructed spectrum is smeared with an additional Gaussian error, which results in an about 20% larger detector smearing than expected from MC simulation. The resulting unfolded spectrum reproduces the true one on the sub- per mille level. In the second cross check, the mass of the ρ-resonance is varied systematically in the simulation in steps of 10 MeV/c^2 between 750 and 790 MeV/c^2. The response matrix is kept fixed and was determined with a ρ mass of 770 MeV/c^2. In all cases, the masses of the ρ peak after unfolding are found to be close to the initially simulated masses. From the comparisons of these checks, we take the maximum deviation of 0.2% as systematic uncertainty.

6.3. FSR correction

The correction factor δ_{FSR} is determined with the Phokhara generator in bins of $m_{\pi\pi}$. Two different correction methods are used on the data to cross check whether it is applied correctly.

(1) The whole FSR contribution of the $\pi^+\pi^-\gamma$ events is calculated with Phokhara, by dividing a true MC spectrum including FSR in NLO by the spectrum without any FSR contribution. The resulting distribution is used to correct data. As pointed out in Ref. [11], for the dispersion integral for a_μ, the FSR correction for the process $e^+e^- \to \pi^+\pi^-$ needs then to be added again. We use the calculation by Schwinger assuming point-like pions:

$$\sigma^{\text{dressed}}_{\pi\pi(\gamma)} = \sigma^{\text{dressed}}_{\pi\pi} \cdot \left[1+\eta(s)\frac{\alpha}{\pi}\right], \tag{6}$$

where $\eta(s)$ is the theoretical correction factor taken from [28]. In the ρ-peak region it is between 0.4% and 0.9%.

(2) A special version of the Phokhara generator is used [29], which, in contrast to the standard version of the generator, distinguishes whether a photon is emitted in the initial or the final state. In events in which photons have been radiated solely due to ISR, the momentum transfer of the virtual photon s_{γ^*} is equal to the invariant mass of the two pions $m^2_{\pi\pi}$. However, if an FSR

photon is emitted, the invariant mass is lowered due to this effect and hence $m^2_{\pi\pi} < s_{\gamma^*}$. The effect can be removed by applying an unfolding procedure, using again the SVD algorithm. Here, the response matrix is $m^2_{\pi\pi}$ vs. s_{γ^*}, obtained from a MC sample that includes FSR in NLO. The regularization parameter τ is determined as described in Sect. 6.2. After applying the corrections for the radiative $\pi^+\pi^-\gamma$ process, which are of the order of 2%, one obtains the $\pi^+\pi^-(\gamma_{\rm FSR})$ cross section directly.

The difference between both methods is found to be (0.18 ± 0.13)%. Both methods are complementary and agree with each other within errors. The difference is taken as systematic uncertainty. Finally, the correction obtained with method (1) is used in the analysis.

6.4. Radiator function and vacuum polarization correction

The radiator function is implemented within the Phokhara event generator with NLO precision. Hence, a very precise description is available with a claimed uncertainty of 0.5% [16].

To obtain the *bare* cross section, vacuum polarization effects $\delta_{\rm vac}$ must be taken into account. To this aim, the dressed cross section, including the vacuum polarization effects, is adjusted for the running of the coupling constant α [30]. Bare and dressed cross sections are related as follows:

$$\sigma^{\rm bare} = \frac{\sigma^{\rm dressed}}{\delta_{\rm vac}} = \sigma^{\rm dressed} \cdot \left(\frac{\alpha(0)}{\alpha(s)}\right)^2 . \quad (7)$$

The correction factors are taken from Ref. [31].

6.5. Summary of systematic uncertainties

Systematic uncertainties are studied within the investigated $m_{\pi\pi}$ range between 600 and 900 MeV/c^2. Sources are:

(1) Efficiency corrections: Each individual uncertainty is studied in bins of $m_{\pi\pi}$ with respect to three different sources. Firstly, the remaining background contaminations in the data samples are estimated with the corresponding MC simulation mentioned in Table 1. Their contribution is taken into account by multiplying the claimed uncertainties of the event generators and their fraction of the investigated signal events. Secondly, we vary the selection requirements (E/p, χ^2_{1C}, depth of a charged track in the MUC), which are used to select clean muon and pion samples for the efficiency studies, in a range of three times the resolution of the corresponding variable. The differences of the correction factors are calculated. Thirdly, the resolution of the correction factors, *i.e.*, the bin sizes of momentum and θ distributions, is varied by a factor two and the effects on the final correction factors are tested.

(2) Pion–muon separation: Additional uncertainties of using the ANN method for pion–muon separation are estimated by comparing the result from a different multivariate method, namely the Boosted Decision Tree (BDT) approach [23]. As a further cross check, the whole analysis is repeated without the use of a dedicated PID method.

(3) Residual background is subtracted using simulated events. The uncertainty is determined to be 0.1%.

(4) Angular acceptance: The knowledge of the angular acceptance of the tracks is studied by varying this requirement by more than three standard deviations of the angular resolution and studying the corresponding difference in the selected number of events. A difference of 0.1% in the result can be observed. The procedure is repeated for all other selection criteria. Their contribution to the total systematic uncertainty is found to be negligible.

(5) Unfolding: Uncertainties introduced by unfolding are smaller than 0.2%, as estimated by the two cross checks mentioned in Sect. 6.2.

Table 2
Summary of systematic uncertainties.

Source	Uncertainty (%)
Photon efficiency correction	0.2
Pion tracking efficiency correction	0.3
Pion ANN efficiency correction	0.2
Pion e-PID efficiency correction	0.2
ANN	negl.
Angular acceptance	0.1
Background subtraction	0.1
Unfolding	0.2
FSR correction $\delta_{\rm FSR}$	0.2
Vacuum polarization correction $\delta_{\rm vac}$	0.2
Radiator function	0.5
Luminosity $\mathcal{L}$	0.5
Sum	0.9

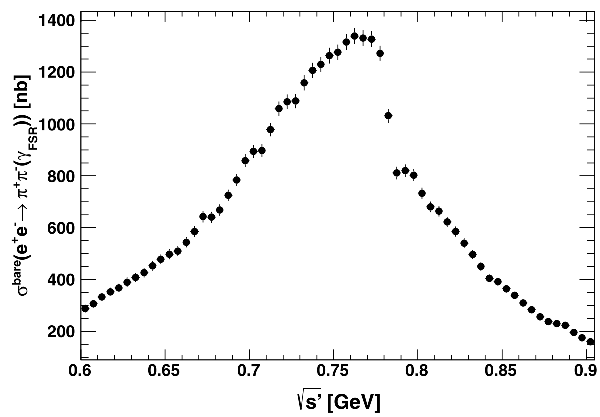

Fig. 3. The measured bare $e^+e^- \to \pi^+\pi^-(\gamma_{\rm FSR})$ cross section. Only the statistical errors are shown.

(6) FSR correction: The uncertainty due to the FSR correction is obtained by comparing two different approaches as described in Sect. 6.3. The uncertainty is found to be 0.2%.

(7) Vacuum Polarization: The uncertainty due to the vacuum polarization correction is conservatively estimated to be 0.2%.

(8) Radiator Function: The Radiator Function extracted from the Phokhara generator is implemented with a precision of 0.5%.

(9) Luminosity: The luminosity of the analyzed data set has been determined to a precision of 0.5%.

All systematic uncertainties are summarized in Table 2. They are added in quadrature, and a total systematic uncertainty for $\sigma^{\rm bare}(e^+e^- \to \pi^+\pi^-(\gamma_{\rm FSR}))$ of 0.9% is achieved, which is fully correlated amongst all data points.

7. Results

The result for $\sigma^{\rm bare}(e^+e^- \to \pi^+\pi^-(\gamma_{\rm FSR}))$ as a function of $\sqrt{s} = m_{\pi\pi}$ is illustrated in Fig. 3 and given numerically in Table 4. The cross section is corrected for vacuum polarization effects and includes final state radiation. Besides the dominant $\rho(770)$ peak, the well-known structure of the ρ–ω interference is observed. The result for the pion form factor $|F_\pi|^2$ is shown in Fig. 4 and given numerically in Table 4. It includes vacuum polarization corrections, but, differently from the cross section shown in Fig. 3, final state radiation effects are excluded here. The red line in Fig. 4 illustrates a fit to data according to a parametrization proposed by Gounaris and Sakurai [32]. Here, exactly the same fit formula and fit procedure are applied as described in detail in Ref. [10]. Free parameters of the fit are the mass and width Γ of the ρ meson, the mass of the ω meson, and the phase of the Breit–

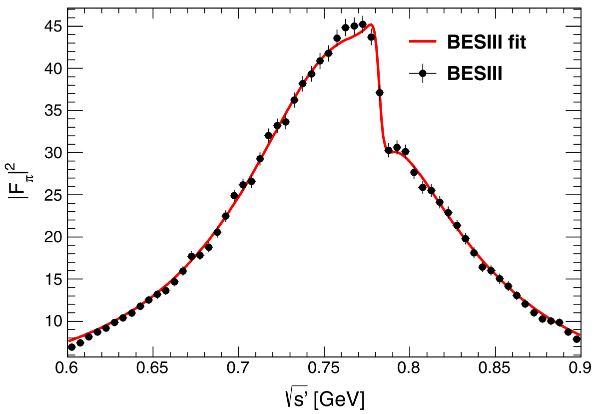

Fig. 4. The measured squared pion form factor $|F_\pi|^2$. Only statistical errors are shown. The solid line represents the fit using the Gounaris–Sakurai parametrization.

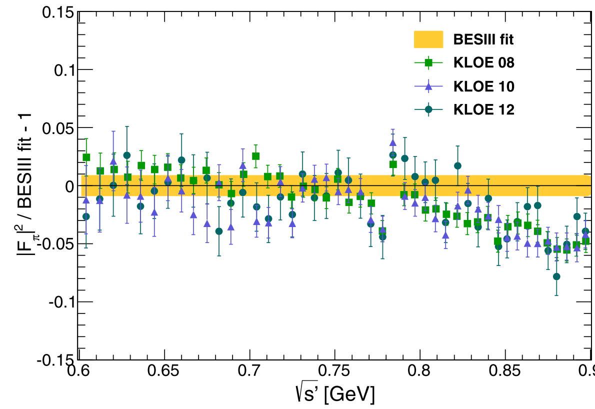

Fig. 6. Relative difference of the form factor squared from KLOE [6–8] and the BESIII fit. Statistical and systematic uncertainties are included in the data points. The width of the BESIII band shows the systematic uncertainty only.

Table 3
Fit parameters and statistical errors of the Gounaris–Sakurai fit of the pion form factor. Also shown are the PDG 2014 values [33].

Parameter	BESIII value	PDG 2014
m_ρ [MeV/c^2]	776.0 ± 0.4	775.26 ± 0.25
Γ_ρ [MeV]	151.7 ± 0.7	147.8± 0.9
m_ω [MeV/c^2]	782.2 ± 0.6	782.65 ± 0.12
Γ_ω [MeV]	fixed to PDG	8.49 ± 0.08
$\lvert c_\omega\rvert$ [10^{-3}]	1.7± 0.2	–
$\lvert\phi_\omega\rvert$ [rad]	0.04 ± 0.13	–

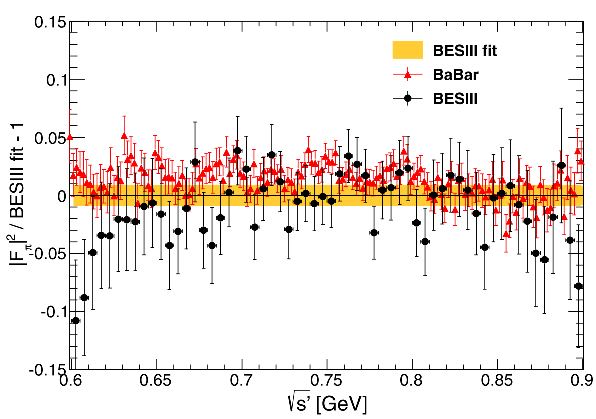

Fig. 5. Relative difference of the form factor squared from BaBar [10] and the BESIII fit. Statistical and systematic uncertainties are included in the data points. The width of the BESIII band shows the systematic uncertainty only.

Wigner function $c_\omega = |c_\omega|e^{i\phi_\omega}$. The width of the ω meson is fixed to the PDG value [33]. The resulting values are shown in Table 3. As can be seen, the resonance parameters are in agreement with the PDG values [33] within uncertainties, except for Γ_ρ, which shows a 3.4σ deviation. Corresponding amplitudes for the higher ρ states, $\rho(1450)$, $\rho(1700)$, and $\rho(2150)$, as well as the masses and widths of those states were taken from Ref. [10], and the systematic uncertainty in Γ_ρ due to these assumptions has not been quantitatively evaluated.

The Gounaris–Sakurai fit provides an excellent description of the BESIII data in the full mass range from 600 to 900 MeV/c^2, resulting in $\chi^2/\mathrm{ndf} = 49.1/56$. Fig. 5 shows the difference between fit and data. Here the data points show the statistical uncertainties only, while the shaded error band of the fit shows the systematic uncertainty only.

In order to compare the result with previous measurements, the relative difference of the BESIII fit and data from BaBar [10], KLOE [6–8], CMD2 [1,2], and SND [3] is investigated. Such a comparison is complicated by the fact, that previous measurements used different vacuum polarization corrections. Therefore, we consistently used the vacuum polarization correction from Ref. [31] for all the comparisons discussed in this section. The KLOE 08, 10, 12, and BaBar spectra have, hence, been modified accordingly. The individual comparisons are illustrated in Figs. 5 and 6. Here, the shaded error band of the fit includes the systematic error only, while the uncertainties of the data points include the sum of the statistical and systematic errors. We observe a very good agreement with the KLOE 08 and KLOE 12 data sets up to the mass range of the ρ–ω interference. In the same mass range the BaBar and KLOE 10 data sets show a systematic shift, however, the deviation is, not exceeding 1 to 2 standard deviations. At higher masses, the statistical error bars in the case of BESIII are relatively large, such that a comparison is not conclusive. There seem to be a good agreement with the BaBar data, while a large deviation with all three KLOE data sets is visible. There are indications that the BESIII data and BESIII fit show some disagreement in the low mass and very high mass tails as well. We have also compared our results in the ρ peak region with data from Novosibirsk. At lower and higher masses, the statistical uncertainties of the Novosibirsk results are too large to draw definite conclusions. The spectra from SND and from the 2006 publication of CMD-2 are found to be in very good agreement with BESIII in the ρ peak region, while the 2004 result of CMD-2 shows a systematic deviation of a few percent.

We also compute the contribution of our BESIII cross section measurement $\sigma^{\mathrm{bare}}(e^+e^- \to \pi^+\pi^-(\gamma_{\mathrm{FSR}}))$ to the hadronic contribution of $(g-2)_\mu$,

$$a_\mu^{\pi\pi,\mathrm{LO}}(0.6\text{–}0.9\,\mathrm{GeV}) = \frac{1}{4\pi^3}\int_{(0.6\mathrm{GeV})^2}^{(0.9\mathrm{GeV})^2} ds' K(s')\sigma^{\mathrm{bare}}_{\pi\pi(\gamma)}\,, \qquad (8)$$

where $K(s')$ is the kernel function [11, Eq. (5)]. As summarized in Fig. 7, the BESIII result, $a_\mu^{\pi\pi,\mathrm{LO}}(600\text{–}900\ \mathrm{MeV}) = (368.2 \pm 2.5_{\mathrm{stat}} \pm 3.3_{\mathrm{sys}}) \cdot 10^{-10}$, is found to be in good agreement with all three KLOE values. A difference of about 1.7σ with respect to the BaBar result is observed.

Table 4
Results of the BESIII measurement of the cross section $\sigma^{\text{bare}}_{\pi^+\pi^-(\gamma_{\text{FSR}})} \equiv \sigma^{\text{bare}}(e^+e^- \to \pi^+\pi^-(\gamma_{\text{FSR}}))$ and the squared pion form factor $|F_\pi|^2$. The errors are statistical only. The value of $\sqrt{s'}$ represents the bin center. The 0.9% systematic uncertainty is fully correlated between any two bins.

$\sqrt{s'}$ [MeV]	$\sigma^{\text{bare}}_{\pi^+\pi^-(\gamma_{\text{FSR}})}$ [nb]	$\lvert F_\pi\rvert^2$	$\sqrt{s'}$ [MeV]	$\sigma^{\text{bare}}_{\pi^+\pi^-(\gamma_{\text{FSR}})}$ [nb]	$\lvert F_\pi\rvert^2$
602.5	288.3 ± 15.2	6.9 ± 0.4	752.5	1276.1 ± 29.8	41.8 ± 1.0
607.5	306.6 ± 15.5	7.4 ± 0.4	757.5	1315.9 ± 31.3	43.6 ± 1.0
612.5	332.8 ± 16.3	8.2 ± 0.4	762.5	1339.3 ± 30.9	44.8 ± 1.0
617.5	352.5 ± 16.3	8.7 ± 0.4	767.5	1331.9 ± 30.8	45.0 ± 1.0
622.5	367.7 ± 16.6	9.2 ± 0.4	772.5	1327.0 ± 30.6	45.2 ± 1.0
627.5	390.1 ± 17.7	9.8 ± 0.4	777.5	1272.7 ± 29.2	43.7 ± 1.0
632.5	408.0 ± 18.0	10.4 ± 0.5	782.5	1031.5 ± 26.7	37.1 ± 0.9
637.5	426.6 ± 18.1	11.0 ± 0.5	787.5	810.7 ± 24.2	30.3 ± 0.8
642.5	453.5 ± 19.0	11.8 ± 0.5	792.5	819.7 ± 23.8	30.6 ± 0.8
647.5	477.7 ± 18.5	12.5 ± 0.5	797.5	803.1 ± 23.3	30.1 ± 0.8
652.5	497.4 ± 19.5	13.2 ± 0.5	802.5	732.4 ± 22.1	27.7 ± 0.8
657.5	509.2 ± 19.4	13.6 ± 0.5	807.5	679.9 ± 20.6	25.9 ± 0.7
662.5	543.4 ± 19.9	14.7 ± 0.5	812.5	663.6 ± 21.0	25.5 ± 0.8
667.5	585.0 ± 20.5	16.0 ± 0.6	817.5	622.2 ± 19.9	24.1 ± 0.7
672.5	642.7 ± 22.2	17.7 ± 0.6	822.5	585.0 ± 19.5	22.9 ± 0.7
677.5	640.5 ± 21.0	17.8 ± 0.6	827.5	540.8 ± 18.1	21.4 ± 0.7
682.5	668.0 ± 21.9	18.8 ± 0.6	832.5	496.4 ± 17.7	19.8 ± 0.7
687.5	724.4 ± 22.9	20.6 ± 0.6	837.5	450.4 ± 16.8	18.1 ± 0.6
692.5	783.5 ± 23.2	22.5 ± 0.7	842.5	404.7 ± 15.2	16.4 ± 0.6
697.5	858.6 ± 25.3	24.9 ± 0.7	847.5	391.3 ± 15.4	16.0 ± 0.6
702.5	893.8 ± 25.4	26.2 ± 0.7	852.5	364.0 ± 15.0	15.0 ± 0.6
707.5	897.8 ± 25.0	26.6 ± 0.7	857.5	339.6 ± 14.0	14.2 ± 0.6
712.5	978.6 ± 26.6	29.3 ± 0.8	862.5	310.0 ± 13.7	13.0 ± 0.6
717.5	1059.1 ± 27.9	32.0 ± 0.8	867.5	283.8 ± 13.0	12.1 ± 0.5
722.5	1086.0 ± 28.3	33.2 ± 0.9	872.5	256.5 ± 12.4	11.0 ± 0.5
727.5	1088.4 ± 27.7	33.6 ± 0.9	877.5	237.3 ± 11.4	10.3 ± 0.5
732.5	1158.8 ± 29.2	36.2 ± 0.9	882.5	229.7 ± 11.6	10.0 ± 0.5
737.5	1206.5 ± 29.6	38.2 ± 0.9	887.5	224.0 ± 11.6	9.9 ± 0.5
742.5	1229.9 ± 29.0	39.3 ± 0.9	892.5	196.1 ± 10.5	8.7 ± 0.4
747.5	1263.3 ± 30.3	40.9 ± 1.0	897.5	175.9 ± 9.7	7.9 ± 0.4

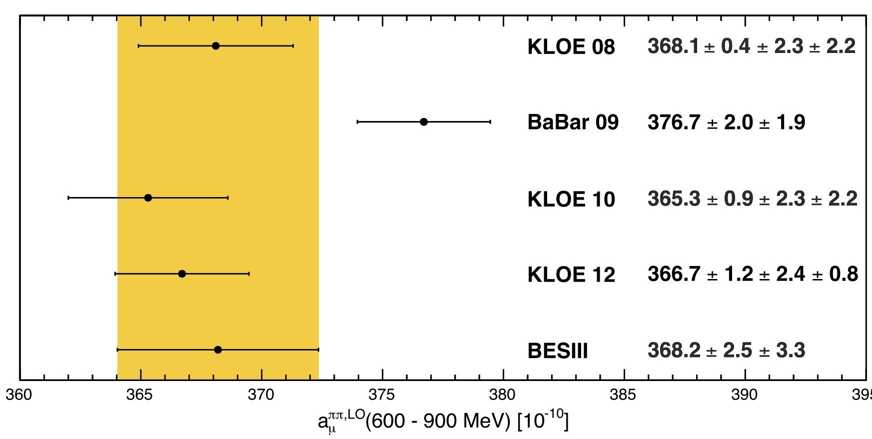

Fig. 7. Our calculation of the leading-order (LO) hadronic vacuum polarization 2π contributions to $(g-2)_\mu$ in the energy range 600–900 MeV from BESIII and based on the data from KLOE 08 [6], 10 [7], 12 [8], and BaBar [10], with the statistical and systematic errors. The statistical and systematic errors are added quadratically. The band shows the 1σ range of the BESIII result.

8. Conclusion

A new measurement of the cross section $\sigma^{\text{bare}}(e^+e^- \to \pi^+\pi^-(\gamma_{\text{FSR}}))$ has been performed with an accuracy of 0.9% in the dominant $\rho(770)$ mass region between 600 and 900 MeV/c^2, using the ISR method at BESIII. The energy dependence of the cross section appears compatible with corresponding measurements from KLOE and BaBar within approximately one standard deviation. The two-pion contribution to the hadronic vacuum polarization contribution to $(g-2)_\mu$ has been determined from the BESIII data to be $a_\mu^{\pi\pi,\text{LO}}(600\text{–}900\ \text{MeV}) = (368.2 \pm 2.5_{\text{stat}} \pm 3.3_{\text{sys}}) \cdot 10^{-10}$. By averaging the KLOE, BaBar, and BESIII values of $a_\mu^{\pi\pi,\text{LO}}$ and assuming that the five data sets are independent, a deviation of more than 3σ between the SM prediction of $(g-2)_\mu$ and its direct measurement is confirmed. For the low mass region < 600 MeV/c^2 and the high mass region > 900 MeV/c^2, the BaBar data was used in this calculation.

Acknowledgements

The BESIII Collaboration thanks the staff of BEPCII and the IHEP computing center for their strong support. We thank Thomas Teubner for the recalculation of $a_\mu^{\pi\pi,\text{LO}}$(600–900 MeV) and Fedor Ignatov for the useful discussions. This work is supported in part by National Key Basic Research Program of China under Contract No. 2015CB856700; National Natural Science Foundation of China (NSFC) under Contract Nos. 11125525, 11235011, 11322544, 11335008, 11425524; the Chinese Academy of Sciences (CAS) Large-Scale Scientific Facility Program; the CAS Center for Excellence in Particle Physics (CCEPP); the Collaborative Innovation Center for Particles and Interactions (CICPI); Joint Large-Scale Scientific Facility Funds of the NSFC and CAS under Contract Nos. 11179007, U1232201, U1332201; CAS under Contract Nos. KJCX2-YW-N29, KJCX2-YW-N45; 100 Talents Program of CAS; National 1000 Talents Program of China; INPAC and Shanghai Key Laboratory for Particle Physics and Cosmology; German Research Foundation DFG under Contract No. Collaborative Research Center CRC-1044; Istituto Nazionale di Fisica Nucleare, Italy; Ministry of Development of Turkey under Contract No. DPT2006K-120470; Russian Foundation for Basic Research under Contract No. 14-07-91152; The Swedish Resarch Council; U.S. Department of Energy under Contract Nos. DE-FG02-04ER41291, DE-FG02-05ER41374, DE-FG02-94ER40823, DESC0010118; U.S. National Science Foundation; University of Groningen (RuG) and the Helmholtzzentrum für Schwerionenforschung GmbH (GSI), Darmstadt; WCU Program of National Research Foundation of Korea under Contract No. R32-2008-000-10155-0.

Appendix A. Supplementary material

Supplementary material related to this article can be found online at http://dx.doi.org/10.1016/j.physletb.2015.11.043.

References

[1] R.R. Akhmetshin, et al., CMD2 Collaboration, Phys. Lett. B 578 (2004) 285.
[2] R.R. Akhmetshin, et al., CMD2 Collaboration, Phys. Lett. B 648 (2007) 28.
[3] M.N. Achasov, et al., SND Collaboration, J. Exp. Theor. Phys. 101 (2005) 1053.
[4] J.E. Augustin, et al., Phys. Rev. Lett. 20 (1968) 126.
[5] A. Aloisio, et al., KLOE Collaboration, Phys. Lett. B 606 (2005) 12.
[6] F. Ambrosio, et al., KLOE Collaboration, Phys. Lett. B 670 (2009) 285.
[7] F. Ambrosino, et al., KLOE Collaboration, Phys. Lett. B 700 (2011) 102.
[8] D. Babusci, et al., KLOE Collaboration, Phys. Lett. B 720 (2013) 336.
[9] B. Aubert, et al., BABAR Collaboration, Phys. Rev. Lett. 103 (2009) 231801.
[10] J.P. Lees, et al., BABAR Collaboration, Phys. Rev. D 86 (2012) 032013.
[11] S. Eidelman, F. Jegerlehner, Z. Phys. C 67 (1995) 585.
[12] M. Davier, A. Hoecker, B. Malescu, Z. Zhang, Eur. Phys. J. C 71 (2011) 1515.
[13] K. Hagiwara, R. Liao, A.D. Martin, Daisuke Nomura, T. Teubner, J. Phys. G 38 (2011) 085003.
[14] M. Davier, A. Hoecker, B. Malescu, C.Z. Yuan, Z. Zhang, Eur. Phys. J. C 66 (2010) 1.
[15] M. Ablikim, et al., BESIII Collaboration, Nucl. Instrum. Methods, Sect. A 614 (2010) 345.
[16] G. Rodrigo, H. Czyż, J.H. Kuhn, M. Szopa, Eur. Phys. J. C 24 (2002) 71.
[17] H. Czyż, J.H. Kuhn, A. Wapienik, Phys. Rev. D 77 (2008) 114005.
[18] S. Jadach, B.F.L. Ward, Z. Was, Comput. Phys. Commun. 130 (2000) 260.
[19] G. Balossini, C.M.C. Calame, G. Montagna, O. Nicrosini, F. Piccinini, Nucl. Phys. B 758 (2006) 227.
[20] J. Allison, et al., GEANT4 Collaboration, IEEE Trans. Nucl. Sci. 53 (2006) 270.
[21] S. Agostinelli, et al., GEANT4 Collaboration, Nucl. Instrum. Methods, Sect. A 506 (2003) 250.
[22] D.M. Asner, et al., Int. J. Mod. Phys. A 24 (2009) 1.
[23] A. Hoecker, P. Speckmayer, J. Stelzer, J. Therhaag, E. Von Toerne, H. Voss, PoS ACAT 040 (2007).
[24] M. Ablikim, et al., BESIII Collaboration, Chin. Phys. C 37 (2013) 123001.
[25] G. Balossini, C. Bignamini, C.M. Carloni Calame, G. Montagna, F. Piccinini, O. Nicrosini, Phys. Lett. B 663 (2008) 209.
[26] M.E. Peskin, D.V. Schroeder, An Introduction to Quantum Field Theory, vol. 2, Addison–Wesley, USA, 1995, p. 135.
[27] A. Hoecker, V. Kartvelishvili, Nucl. Instrum. Methods, Sect. A 372 (1996) 469.
[28] J.S. Schwinger, Particles, Sources and Fields, vol. 3, Addison–Wesley, Redwood City, USA, 1989, p. 99 ff.
[29] Private communication with H. Czyz.
[30] A. Höfer, J. Gluza, F. Jegerlehner, Eur. Phys. J. C 24 (2002) 51.
[31] F. Jegerlehner, Nucl. Phys. Proc. Suppl. 181–182 (2008) 135;
F. Jegerlehner, Z. Phys. C 32 (1986) 195;
F. Jegerlehner, www-com.physik.hu-berlin.de/~fjeger/alphaQED.tar.gz, 2015.
[32] G.J. Gounaris, J.J. Sakurai, Phys. Rev. Lett. 21 (1968) 244.
[33] K.A. Olive, et al., Particle Data Group, Chin. Phys. C 38 (2014) 090001.

Observation of an Anomalous Line Shape of the $\eta'\pi^+\pi^-$ Mass Spectrum near the $p\bar{p}$ Mass Threshold in $J/\psi \to \gamma\eta'\pi^+\pi^-$

M. Ablikim,[1] M. N. Achasov,[9e] S. Ahmed,[14] X. C. Ai,[1] O. Albayrak,[5] M. Albrecht,[4] D. J. Ambrose,[44] A. Amoroso,[49a,49c] F. F. An,[1] Q. An,[46a] J. Z. Bai,[1] R. Baldini Ferroli,[20a] Y. Ban,[31] D. W. Bennett,[19] J. V. Bennett,[5] N. Berger,[22] M. Bertani,[20a] D. Bettoni,[21a] J. M. Bian,[43] F. Bianchi,[49a,49c] E. Boger,[23c] I. Boyko,[23] R. A. Briere,[5] H. Cai,[51] X. Cai,[1a] O. Cakir,[40a] A. Calcaterra,[20a] G. F. Cao,[1] S. A. Cetin,[40b] J. F. Chang,[1a] G. Chelkov,[23c,d] G. Chen,[1] H. S. Chen,[1] H. Y. Chen,[2] J. C. Chen,[1] M. L. Chen,[1a] S. Chen,[41] S. J. Chen,[29] X. Chen,[1a] X. R. Chen,[26] Y. B. Chen,[1a] H. P. Cheng,[17] X. K. Chu,[31] G. Cibinetto,[21a] H. L. Dai,[1a] J. P. Dai,[34] A. Dbeyssi,[14] D. Dedovich,[23] Z. Y. Deng,[1] A. Denig,[22] I. Denysenko,[23] M. Destefanis,[49a,49c] F. De Mori,[49a,49c] Y. Ding,[27] C. Dong,[30] J. Dong,[1a] L. Y. Dong,[1] M. Y. Dong,[1a] Z. L. Dou,[29] S. X. Du,[53] P. F. Duan,[1] J. Z. Fan,[39] J. Fang,[1a] S. S. Fang,[1] X. Fang,[46a] Y. Fang,[1] R. Farinelli,[21a,21b] L. Fava,[49b,49c] O. Fedorov,[23] F. Feldbauer,[22] G. Felici,[20a] C. Q. Feng,[46a] E. Fioravanti,[21a] M. Fritsch,[14,22] C. D. Fu,[1] Q. Gao,[1] X. L. Gao,[46a] X. Y. Gao,[2] Y. Gao,[39] Z. Gao,[46a] I. Garzia,[21a] K. Goetzen,[10] L. Gong,[30] W. X. Gong,[1a] W. Gradl,[22] M. Greco,[49a,49c] M. H. Gu,[1a] Y. T. Gu,[12] Y. H. Guan,[1] A. Q. Guo,[1] L. B. Guo,[28] R. P. Guo,[1] Y. Guo,[1] Y. P. Guo,[22] Z. Haddadi,[25] A. Hafner,[22] S. Han,[51] X. Q. Hao,[15] F. A. Harris,[42] K. L. He,[1] F. H. Heinsius,[4] T. Held,[4] Y. K. Heng,[1a] T. Holtmann,[4] Z. L. Hou,[1] C. Hu,[28] H. M. Hu,[1] J. F. Hu,[49a,49c] T. Hu,[1a] Y. Hu,[1] G. S. Huang,[46a] Y. P. Huang,[1i] J. S. Huang,[15] X. T. Huang,[33] X. Z. Huang,[29] Y. Huang,[29] Z. L. Huang,[27] T. Hussain,[48] Q. Ji,[1] Q. P. Ji,[30] X. B. Ji,[1] X. L. Ji,[1a] L. W. Jiang,[51] X. S. Jiang,[1a] X. Y. Jiang,[30] J. B. Jiao,[33] Z. Jiao,[17] D. P. Jin,[1a] S. Jin,[1] T. Johansson,[50] A. Julin,[43] N. Kalantar-Nayestanaki,[25] X. L. Kang,[1] X. S. Kang,[30] M. Kavatsyuk,[25] B. C. Ke,[5] P. Kiese,[22] R. Kliemt,[14] B. Kloss,[22] O. B. Kolcu,[40bh] B. Kopf,[4] M. Kornicer,[42] A. Kupsc,[50] W. Kühn,[24] J. S. Lange,[24] M. Lara,[19] P. Larin,[14] H. Leithoff,[22] C. Leng,[49c] C. Li,[50] Cheng Li,[46a] D. M. Li,[53] F. Li,[1a] F. Y. Li,[31] G. Li,[1] H. B. Li,[1] H. J. Li,[1] J. C. Li,[1] Jin Li,[32] K. Li,[13] K. Li,[33] Lei Li,[3] P. R. Li,[41] Q. Y. Li,[33] T. Li,[33] W. D. Li,[1] W. G. Li,[1] X. L. Li,[33] X. N. Li,[1a] X. Q. Li,[30] Y. B. Li,[2] Z. B. Li,[38] H. Liang,[46a] Y. F. Liang,[36] Y. T. Liang,[24] G. R. Liao,[11] D. X. Lin,[14] B. Liu,[34] B. J. Liu,[1] C. X. Liu,[1] D. Liu,[46a] F. H. Liu,[35] Fang Liu,[1] Feng Liu,[6] H. B. Liu,[12] H. H. Liu,[1] H. H. Liu,[16] H. M. Liu,[1] J. Liu,[1] J. B. Liu,[46a] J. P. Liu,[51] J. Y. Liu,[1] K. Liu,[39] K. Y. Liu,[27] L. D. Liu,[31] P. L. Liu,[1a] Q. Liu,[41] S. B. Liu,[46a] X. Liu,[26] Y. B. Liu,[30] Y. Y. Liu,[30] Z. A. Liu,[1a] Zhiqing Liu,[22] H. Loehner,[25] X. C. Lou,[1a,g] H. J. Lu,[17] J. G. Lu,[1a] Y. Lu,[1] Y. P. Lu,[1a] C. L. Luo,[28] M. X. Luo,[52] T. Luo,[42] X. L. Luo,[1a] X. R. Lyu,[41] F. C. Ma,[27] H. L. Ma,[1] L. L. Ma,[33] M. M. Ma,[1] Q. M. Ma,[1] T. Ma,[1] X. N. Ma,[30] X. Y. Ma,[1a] Y. M. Ma,[33] F. E. Maas,[14] M. Maggiora,[49a,49c] Q. A. Malik,[48] Y. J. Mao,[31] Z. P. Mao,[1] S. Marcello,[49a,49c] J. G. Messchendorp,[25] G. Mezzadri,[21b] J. Min,[1a] T. J. Min,[1,41] R. E. Mitchell,[19] X. H. Mo,[1a] Y. J. Mo,[6] C. Morales Morales,[14] N. Yu. Muchnoi,[9e] H. Muramatsu,[43] P. Musiol,[4] Y. Nefedov,[23] F. Nerling,[14] I. B. Nikolaev,[9e] Z. Ning,[1a] S. Nisar,[8] S. L. Niu,[1a] X. Y. Niu,[1] S. L. Olsen,[32] Q. Ouyang,[1a] S. Pacetti,[20b] Y. Pan,[46a] P. Patteri,[20a] M. Pelizaeus,[4] H. P. Peng,[46a] K. Peters,[10] J. Pettersson,[50] J. L. Ping,[28] R. G. Ping,[1] R. Poling,[43] V. Prasad,[1] H. R. Qi,[2] M. Qi,[29] S. Qian,[1a] C. F. Qiao,[41] L. Q. Qin,[33] N. Qin,[51] X. S. Qin,[1] Z. H. Qin,[1a] J. F. Qiu,[1] K. H. Rashid,[48] C. F. Redmer,[22] M. Ripka,[22] G. Rong,[1] Ch. Rosner,[14] X. D. Ruan,[12] A. Sarantsev,[23f] M. Savrié,[21b] C. Schnier,[4] K. Schoenning,[50] S. Schumann,[22] W. Shan,[31] M. Shao,[46a] C. P. Shen,[2] P. X. Shen,[30] X. Y. Shen,[1] H. Y. Sheng,[1] M. Shi,[1] W. M. Song,[1] X. Y. Song,[1] S. Sosio,[49a,49c] S. Spataro,[49a,49c] G. X. Sun,[1] J. F. Sun,[15] S. S. Sun,[1] X. H. Sun,[1] Y. J. Sun,[46a] Y. Z. Sun,[1] Z. J. Sun,[1a] Z. T. Sun,[19] C. J. Tang,[36] X. Tang,[1] I. Tapan,[40c] E. H. Thorndike,[44] M. Tiemens,[25] I. Uman,[40d] G. S. Varner,[42] B. Wang,[30] B. L. Wang,[41] D. Wang,[31] D. Y. Wang,[31] K. Wang,[1a] L. L. Wang,[1] L. S. Wang,[1] M. Wang,[33] P. Wang,[1] P. L. Wang,[1] S. G. Wang,[31] W. Wang,[1a] W. P. Wang,[46a] X. F. Wang,[39] Y. Wang,[37] Y. D. Wang,[14] Y. F. Wang,[1a] Y. Q. Wang,[22] Z. Wang,[1a] Z. G. Wang,[1a] Z. H. Wang,[46a] Z. Y. Wang,[1] Z. Y. Wang,[1] T. Weber,[22] D. H. Wei,[11] J. B. Wei,[31] P. Weidenkaff,[22] S. P. Wen,[1] U. Wiedner,[4] M. Wolke,[50] L. H. Wu,[1] L. J. Wu,[1] Z. Wu,[1a] L. Xia,[46a] L. G. Xia,[39] Y. Xia,[18] D. Xiao,[1] H. Xiao,[47] Z. J. Xiao,[28] Y. G. Xie,[1a] Q. L. Xiu,[1a] G. F. Xu,[1] J. J. Xu,[1] L. Xu,[1] Q. J. Xu,[13] Q. N. Xu,[41] X. P. Xu,[37] L. Yan,[49a,49c] W. B. Yan,[46a] W. C. Yan,[46a] Y. H. Yan,[18] H. J. Yang,[34] H. X. Yang,[1] L. Yang,[51] Y. X. Yang,[11] M. Ye,[1a] M. H. Ye,[7] J. H. Yin,[1] B. X. Yu,[1a] C. X. Yu,[30] J. S. Yu,[26] C. Z. Yuan,[1] W. L. Yuan,[29] Y. Yuan,[1] A. Yuncu,[40bb] A. A. Zafar,[48] A. Zallo,[20a] Y. Zeng,[18] Z. Zeng,[46a] B. X. Zhang,[1] B. Y. Zhang,[1a] C. Zhang,[29] C. C. Zhang,[1] D. H. Zhang,[1] H. H. Zhang,[38] H. Y. Zhang,[1a] J. Zhang,[1] J. J. Zhang,[1] J. L. Zhang,[1] J. Q. Zhang,[1] J. W. Zhang,[1a] J. Y. Zhang,[1] J. Z. Zhang,[1] K. Zhang,[1] L. Zhang,[1] S. Q. Zhang,[30] X. Y. Zhang,[33] Y. Zhang,[1] Y. H. Zhang,[1a] Y. N. Zhang,[41] Y. T. Zhang,[46a] Yu Zhang,[41] Z. H. Zhang,[6] Z. P. Zhang,[46] Z. Y. Zhang,[51] G. Zhao,[1] J. W. Zhao,[1a] J. Y. Zhao,[1] J. Z. Zhao,[1a] Lei Zhao,[46a] Ling Zhao,[1] M. G. Zhao,[30] Q. Zhao,[1] Q. W. Zhao,[1] S. J. Zhao,[53] T. C. Zhao,[1] Y. B. Zhao,[1a] Z. G. Zhao,[46a] A. Zhemchugov,[23c] B. Zheng,[47] J. P. Zheng,[1a] W. J. Zheng,[33] Y. H. Zheng,[41] B. Zhong,[28] L. Zhou,[1a] X. Zhou,[51] X. K. Zhou,[46a] X. R. Zhou,[46a] X. Y. Zhou,[1] K. Zhu,[1] K. J. Zhu,[1a] S. Zhu,[1] S. H. Zhu,[45] X. L. Zhu,[39] Y. C. Zhu,[46a] Y. S. Zhu,[1] Z. A. Zhu,[1] J. Zhuang,[1a] L. Zotti,[49a,49c] B. S. Zou,[1] and J. H. Zou[1]

(BESIII Collaboration)

[1]*Institute of High Energy Physics, Beijing 100049, People's Republic of China*
[2]*Beihang University, Beijing 100191, People's Republic of China*
[3]*Beijing Institute of Petrochemical Technology, Beijing 102617, People's Republic of China*
[4]*Bochum Ruhr-University, D-44780 Bochum, Germany*
[5]*Carnegie Mellon University, Pittsburgh, Pennsylvania 15213, USA*
[6]*Central China Normal University, Wuhan 430079, People's Republic of China*
[7]*China Center of Advanced Science and Technology, Beijing 100190, People's Republic of China*
[8]*COMSATS Institute of Information Technology, Lahore, Defence Road, Off Raiwind Road, 54000 Lahore, Pakistan*
[9]*G.I. Budker Institute of Nuclear Physics SB RAS (BINP), Novosibirsk 630090, Russia*
[10]*GSI Helmholtzcentre for Heavy Ion Research GmbH, D-64291 Darmstadt, Germany*
[11]*Guangxi Normal University, Guilin 541004, People's Republic of China*
[12]*GuangXi University, Nanning 530004, People's Republic of China*
[13]*Hangzhou Normal University, Hangzhou 310036, People's Republic of China*
[14]*Helmholtz Institute Mainz, Johann-Joachim-Becher-Weg 45, D-55099 Mainz, Germany*
[15]*Henan Normal University, Xinxiang 453007, People's Republic of China*
[16]*Henan University of Science and Technology, Luoyang 471003, People's Republic of China*
[17]*Huangshan College, Huangshan 245000, People's Republic of China*
[18]*Hunan University, Changsha 410082, People's Republic of China*
[19]*Indiana University, Bloomington, Indiana 47405, USA*
[20a]*INFN Laboratori Nazionali di Frascati, I-00044 Frascati, Italy*
[20b]*INFN and University of Perugia, I-06100 Perugia, Italy*
[21a]*INFN Sezione di Ferrara, I-44122 Ferrara, Italy*
[21b]*University of Ferrara, I-44122 Ferrara, Italy*
[22]*Johannes Gutenberg University of Mainz, Johann-Joachim-Becher-Weg 45, D-55099 Mainz, Germany*
[23]*Joint Institute for Nuclear Research, 141980 Dubna, Moscow region, Russia*
[24]*Justus-Liebig-Universitaet Giessen, II. Physikalisches Institut, Heinrich-Buff-Ring 16, D-35392 Giessen, Germany*
[25]*KVI-CART, University of Groningen, NL-9747 AA Groningen, The Netherlands*
[26]*Lanzhou University, Lanzhou 730000, People's Republic of China*
[27]*Liaoning University, Shenyang 110036, People's Republic of China*
[28]*Nanjing Normal University, Nanjing 210023, People's Republic of China*
[29]*Nanjing University, Nanjing 210093, People's Republic of China*
[30]*Nankai University, Tianjin 300071, People's Republic of China*
[31]*Peking University, Beijing 100871, People's Republic of China*
[32]*Seoul National University, Seoul 151-747, Korea*
[33]*Shandong University, Jinan 250100, People's Republic of China*
[34]*Shanghai Jiao Tong University, Shanghai 200240, People's Republic of China*
[35]*Shanxi University, Taiyuan 030006, People's Republic of China*
[36]*Sichuan University, Chengdu 610064, People's Republic of China*
[37]*Soochow University, Suzhou 215006, People's Republic of China*
[38]*Sun Yat-Sen University, Guangzhou 510275, People's Republic of China*
[39]*Tsinghua University, Beijing 100084, People's Republic of China*
[40a]*Ankara University, 06100 Tandogan, Ankara, Turkey*
[40b]*Istanbul Bilgi University, 34060 Eyup, Istanbul, Turkey*
[40c]*Uludag University, 16059 Bursa, Turkey*
[40d]*Near East University, Nicosia, North Cyprus, Mersin 10, Turkey*
[41]*University of Chinese Academy of Sciences, Beijing 100049, People's Republic of China*
[42]*University of Hawaii, Honolulu, Hawaii 96822, USA*
[43]*University of Minnesota, Minneapolis, Minnesota 55455, USA*
[44]*University of Rochester, Rochester, New York 14627, USA*
[45]*University of Science and Technology Liaoning, Anshan 114051, People's Republic of China*
[46]*University of Science and Technology of China, Hefei 230026, People's Republic of China*
[47]*University of South China, Hengyang 421001, People's Republic of China*
[48]*University of the Punjab, Lahore-54590, Pakistan*
[49a]*University of Turin, I-10125 Turin, Italy*
[49b]*University of Eastern Piedmont, I-15121 Alessandria, Italy*
[49c]*INFN, I-10125 Turin, Italy*
[50]*Uppsala University, Box 516, SE-75120 Uppsala, Sweden*

[51]Wuhan University, Wuhan 430072, People's Republic of China
[52]Zhejiang University, Hangzhou 310027, People's Republic of China
[53]Zhengzhou University, Zhengzhou 450001, People's Republic of China
(Received 1 April 2016; published 21 July 2016)

Using 1.09×10^9 J/ψ events collected by the BESIII experiment in 2012, we study the $J/\psi \to \gamma\eta'\pi^+\pi^-$ process and observe a significant abrupt change in the slope of the $\eta'\pi^+\pi^-$ invariant mass distribution at the proton-antiproton ($p\bar{p}$) mass threshold. We use two models to characterize the $\eta'\pi^+\pi^-$ line shape around 1.85 GeV$/c^2$: one that explicitly incorporates the opening of a decay threshold in the mass spectrum (Flatté formula), and another that is the coherent sum of two resonant amplitudes. Both fits show almost equally good agreement with data, and suggest the existence of either a broad state around 1.85 GeV$/c^2$ with strong couplings to the $p\bar{p}$ final states or a narrow state just below the $p\bar{p}$ mass threshold. Although we cannot distinguish between the fits, either one supports the existence of a $p\bar{p}$ moleculelike state or bound state with greater than 7σ significance.

DOI: 10.1103/PhysRevLett.117.042002

The state $X(1835)$ was first observed by the BESII experiment as a peak in the $\eta'\pi^+\pi^-$ invariant mass distribution in $J/\psi \to \gamma\eta'\pi^+\pi^-$ decays [1]. This observation was later confirmed by BESIII studies of the same process [2] with the mass and width measured to be $M = 1836.5 \pm 3^{+5.6}_{-2.1}$ MeV$/c^2$ and $\Gamma = 190 \pm 9^{+38}_{-36}$ MeV$/c^2$; the $X(1835)$ was also observed in the $\eta K^0_S K^0_S$ channel in $J/\psi \to \gamma\eta K^0_S K^0_S$ decays, where its spin parity was determined to be $J^P = 0^-$ by a partial wave analysis [3]. An anomalously strong enhancement at the proton-antiproton ($p\bar{p}$) mass threshold, dubbed $X(p\bar{p})$, was first observed by BESII in $J/\psi \to \gamma p\bar{p}$ decays [4]; this observation was confirmed by BESIII [5] and CLEO [6]. This enhancement structure was subsequently determined to have spin parity $J^P = 0^-$ by BESIII [7]. Among the various theoretical interpretations on the nature of the $X(1835)$ and $X(p\bar{p})$ [8–12], a particularly intriguing one suggests that the two structures originate from a $p\bar{p}$ bound state [13–17]. If the $X(1835)$ is really a $p\bar{p}$ bound state, it should have a strong coupling to 0^- $p\bar{p}$ systems, in which case the line shape of $X(1835)$ at the $p\bar{p}$ mass threshold would be affected by the opening of the $X(1835) \to p\bar{p}$ decay mode. A study of the $\eta'\pi^+\pi^-$ line shape of $X(1835)$ with high statistical precision therefore provides valuable information that helps clarify the nature of the $X(1835)$ and $X(p\bar{p})$.

In this Letter, we report the observation of a significant abrupt change in slope of the $X(1835) \to \eta'\pi^+\pi^-$ line shape at the $p\bar{p}$ mass threshold in a sample of $J/\psi \to \gamma\eta'\pi^+\pi^-$ events collected in the BESIII detector at the BEPCII e^+e^- storage ring. The η' is reconstructed in its two major decay modes: $\eta' \to \gamma\pi^+\pi^-$ and $\eta' \to \eta\pi^+\pi^-$, $\eta \to \gamma\gamma$. The data sample used in this analysis contains a total of 1.09×10^9 J/ψ decay events [18] accumulated by the BESIII experiment in 2012.

The BESIII detector [19] is a magnetic spectrometer operating at BEPCII [20], a double-ring e^+e^- collider with center of mass energies between 2.0 and 4.6 GeV. The cylindrical core of the BESIII detector consists of a helium-based main drift chamber, a plastic scintillator time-of-flight system, and a CsI(Tl) electromagnetic calorimeter that are all enclosed in a superconducting solenoidal magnet providing a 0.9 T magnetic field. The solenoid is supported by an octagonal flux-return yoke with resistive plate counter muon identifier modules interleaved with steel. The acceptance of charged particles and photons is 93% of the 4π solid angle. The charged-particle momentum resolution at 1 GeV$/c$ is 0.5%; the electromagnetic calorimeter measures 1 GeV photons with an energy resolution of 2.5% (5%) in the barrel (end cap) regions. A GEANT4-based [21] Monte Carlo (MC) simulation software package is used to optimize the event selection criteria, estimate backgrounds, and determine the detection efficiency. The KKMC [22] generator is used to simulate J/ψ production.

The event selection criteria are identical to the previous publication on $J/\psi \to \gamma\eta'\pi^+\pi^-$ at BESIII [2] except for one cut in the $J/\psi \to \gamma\eta'(\to \gamma\pi^+\pi^-)\pi^+\pi^-$ channel: in the previous study, events with $|M_{\gamma\pi^+\pi^-} - m_\eta| < 7$ MeV$/c^2$ are rejected to suppress background from $J/\psi \to \gamma\eta(\to \gamma\pi^+\pi^-)\pi^+\pi^-$; in this analysis, a tighter cut that rejects events with $400\,\mathrm{MeV}/c^2 < M_{\gamma\pi^+\pi^-} < 563\,\mathrm{MeV}/c^2$ is required to suppress background from $J/\psi \to \gamma\eta(\to \pi^0\pi^+\pi^-)\pi^+\pi^-$ as well as background from $J/\psi \to \gamma\eta(\to \gamma\pi^+\pi^-)\pi^+\pi^-$.

The $\eta'\pi^+\pi^-$ invariant mass spectra of the surviving events are shown in Fig. 1, where peaks corresponding to the $X(1835)$, $X(2120)$, $X(2370)$, and η_c [2], and a structure near 2.6 GeV$/c^2$ that has not been seen before are evident for both η' decays. Thanks to the high statistical precision, an abrupt change in slope of the $X(1835)$ line shape at the $p\bar{p}$ mass threshold is evident in both event samples.

An inclusive sample of 10^9 J/ψ decay events that are generated according to the Lund-Charm model [23] and Particle Data Group [24] decay tables is used to study potential background processes. These include events with no real η''s in the final state (non η') and those from $J/\psi \to \pi^0\eta'\pi^+\pi^-$. We use η' mass sideband events to estimate the non-η' background contribution to the

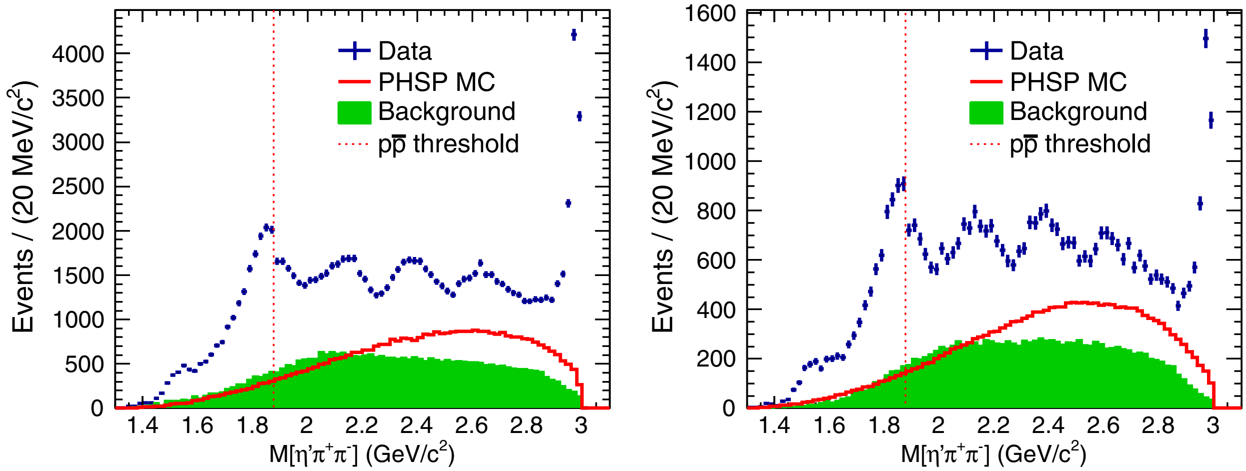

FIG. 1. The $\eta'\pi^+\pi^-$ invariant mass spectra after the application of all selection criteria. The plot on the left side shows the spectrum for events with the $\eta' \to \gamma\pi^+\pi^-$ channel, and that on the right shows the spectrum for the $\eta' \to \eta(\to \gamma\gamma)\pi^+\pi^-$ channel. In both plots, the dots with error bars are data, the shaded histograms are the background, the solid histograms are phase space (PHSP) MC events of $J/\psi \to \gamma\eta'\pi^+\pi^-$ (arbitrary normalization), and the dotted vertical line shows the position of the $p\bar{p}$ mass threshold.

$\eta'\pi^+\pi^-$ invariant mass distribution. For the $J/\psi \to \pi^0\eta'\pi^+\pi^-$ background, we use a one-dimensional data-driven method that first selects $J/\psi \to \pi^0\eta'\pi^+\pi^-$ events from the data to determine the shape of their contribution to the selected $\eta'\pi^+\pi^-$ mass spectrum and reweight this shape by the ratio of MC-determined efficiencies for $J/\psi \to \gamma\eta'\pi^+\pi^-$ and $J/\psi \to \pi^0\eta'\pi^+\pi^-$ events; the total weight after reweighting is the estimated number of $J/\psi \to \pi^0\eta'\pi^+\pi^-$ background events. Our studies of background processes show that neither the four peaks mentioned above nor the abrupt change in the line shape at $2m_p$ is caused by background processes.

We perform simultaneous fits to the $\eta'\pi^+\pi^-$ invariant mass distributions between 1.3 and 2.25 GeV$/c^2$ for both selected event samples with the $f_1(1510)$, $X(1835)$, and $X(2120)$ peaks represented by three efficiency-corrected Breit-Wigner functions convolved with a Gaussian function to account for the mass resolution, where the Breit-Wigner masses and widths are free parameters. The nonresonant $\eta'\pi^+\pi^-$ contribution is obtained from Monte Carlo simulation; the non-η' and $J/\psi \to \pi^0\eta'\pi^+\pi^-$ background contributions are obtained as discussed above. For resonances and the nonresonant $\eta'\pi^+\pi^-$ contribution, the phase space for $J/\psi \to \gamma\eta'\pi^+\pi^-$ is considered: according to the J^P of $f_1(1510)$ and $X(1835)$, $J/\psi \to \gamma f_1(1510)$ and $J/\psi \to \gamma X(1835)$ are S-wave and P-wave processes, respectively; all other processes are assumed to be S-wave processes. Without explicit mention, all components are treated as incoherent contributions. In the simultaneous fits, the masses and widths of resonances, as well as the branching fraction for J/ψ radiative decays to $\eta'\pi^+\pi^-$ final states (including resonances and nonresonant $\eta'\pi^+\pi^-$) are constrained to be the same for both η' decay channels. The fit results are shown in Fig. 2, where it is evident that using a simple Breit-Wigner function to describe the $X(1835)$ line shape fails near the $p\bar{p}$ mass threshold. The log $\mathcal{L}$ ($\mathcal{L}$ is the combined likelihood of simultaneous fits) of this fit is 630 503.3. Typically, there are two circumstances where an abrupt distortion of a resonance's line shape shows up: a threshold effect caused by the opening of an additional

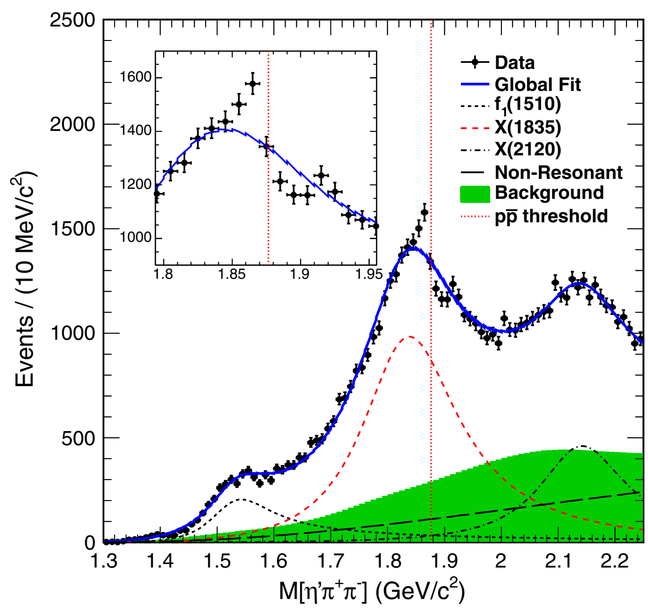

FIG. 2. Fit results with simple Breit-Wigner formulas. The dashed dotted vertical line shows the position of the $p\bar{p}$ mass threshold, the dots with error bars are data, the solid curves are total fit results, the dashed curves are the $X(1835)$, the short-dashed curves are the $f_1(1510)$, the dash-dot curves are the $X(2120)$, and the long-dashed curves are the nonresonant $\eta'\pi^+\pi^-$ fit results; the shaded histograms are background events. The inset shows the data and the global fit between 1.8 and 1.95 GeV$/c^2$.

decay mode, or interference between two resonances. We tried to fit the data for both of these possibilities.

In the first model, we assume the state around $1.85\ \mathrm{GeV}/c^2$ couples to the $p\bar{p}$. The line shape of $\eta'\pi^+\pi^-$ above the $p\bar{p}$ threshold is therefore affected by the opening of the $X(1835) \to p\bar{p}$ decay channel, similar to the distortion of the $f_0(980) \to \pi^+\pi^-$ line shape at the $K\bar{K}$ threshold. To study this, the Flatté formula [25] is used for the $X(1835)$ line shape:

$$T = \frac{\sqrt{\rho_{\mathrm{out}}}}{\mathcal{M}^2 - s - i\sum_k g_k^2 \rho_k}. \tag{1}$$

Here, T is the decay amplitude, ρ_{out} is the phase space for $J/\psi \to \gamma\eta'\pi^+\pi^-$, $\mathcal{M}$ is a parameter with the dimension of mass, s is the square of the $\eta'\pi^+\pi^-$ system's mass, ρ_k is the phase space for decay mode k, and g_k^2 is the corresponding coupling strength. The term $\sum_k g_k^2 \rho_k$ describes how the decay width varies with s. Approximately,

$$\sum_k g_k^2 \rho_k \approx g_0^2 \left(\rho_0 + \frac{g_{p\bar{p}}^2}{g_0^2} \rho_{p\bar{p}} \right), \tag{2}$$

where g_0^2 is the sum of g^2 of all decay modes other than the $X(1835) \to p\bar{p}$, ρ_0 is the maximum two-body decay phase space volume [24], and $g_{p\bar{p}}^2/g_0^2$ is the ratio between the coupling strength to the $p\bar{p}$ channel and the sum of all other channels.

The fit results for this model are shown in Fig. 3. The Flatté model fit has a $\log\mathcal{L} = 630549.5$ that is improved over the simple Breit-Wigner one by 46, so the significance of $g_{p\bar{p}}^2/g_0^2$ being nonzero is 9.6σ. In the fit, an additional Breit-Wigner resonance [denoted as "$X(1920)$" in Fig. 3] is needed with a mass of $1918.6 \pm 3.0\ \mathrm{MeV}/c^2$ and a width of $50.6 \pm 20.9\ \mathrm{MeV}/c^2$; the statistical significance of this peak is 5.7σ. In the simple Breit-Wigner fit, the significance of $X(1920)$ is negligible. The fit yields $\mathcal{M} = 1638.0 \pm 121.9\ \mathrm{MeV}/c^2$, $g_0^2 = 93.7 \pm 35.4 (\mathrm{GeV}/c^2)^2$, $g_{p\bar{p}}^2/g_0^2 = 2.31 \pm 0.37$, and a product branching fraction of $\mathcal{B}(J/\psi \to \gamma X)\mathcal{B}(X \to \eta'\pi^+\pi^-) = (3.93 \pm 0.38) \times 10^{-4}$. The value of $g_{p\bar{p}}^2/g_0^2$ implies that the couplings between the state around $1.85\ \mathrm{GeV}/c^2$ and the $p\bar{p}$ final states is very large. Following the definitions given in Ref. [26], the pole position is determined by requiring the denominator in Eq. (1) to be zero. The pole nearest to the $p\bar{p}$ mass threshold is found to be $M_{\mathrm{pole}} = 1909.5 \pm 15.9\ \mathrm{MeV}/c^2$ and $\Gamma_{\mathrm{pole}} = 273.5 \pm 21.4\ \mathrm{MeV}/c^2$. Taking the systematic uncertainties (see below) into account, the significance of $g_{p\bar{p}}^2/g_0^2$ being nonzero is larger than 7σ.

In the second model, we assume the existence of a narrow resonance near the $p\bar{p}$ threshold and that the interference between this resonance and the $X(1835)$ produces the line shape distortion. Here, we denote this narrow resonance as "$X(1870)$." For this case we represent the line shape in the vicinity of $1835\ \mathrm{MeV}/c^2$ by the square of T, where

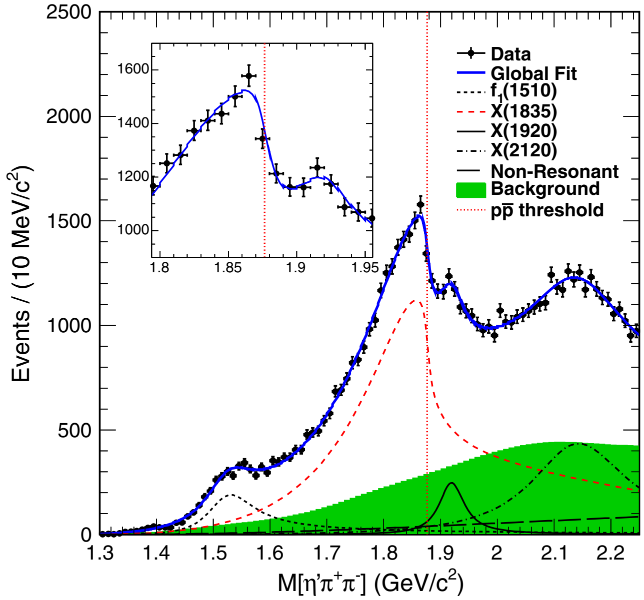

FIG. 3. Fit results of using the Flatté formula. The dashed dotted vertical line shows the position of the $p\bar{p}$ mass threshold, the dots with error bars are data, the solid curves are total fit results, the dashed curves are the state around $1.85\ \mathrm{GeV}/c^2$, the short-dashed curves are the $f_1(1510)$, the dash-dotted curves are the $X(2120)$, the dash-dot-dot-dotted curves are the $X(1920)$, and the long-dashed curves are nonresonant $\eta'\pi^+\pi^-$ fit results; the shaded histograms are background events. The inset shows the data and the global fit between 1.8 and $1.95\ \mathrm{GeV}/c^2$.

$$T = \left(\frac{\sqrt{\rho_{\mathrm{out}}}}{M_1^2 - s - iM_1\Gamma_1} + \frac{\beta e^{i\theta}\sqrt{\rho_{\mathrm{out}}}}{M_2^2 - s - iM_2\Gamma_2} \right). \tag{3}$$

Here, ρ_{out} and s have the same meaning as they had in Eq. (1); M_1, Γ_1, M_2, and Γ_2 represent the masses and widths of the $X(1835)$ and $X(1870)$ resonances, respectively; and β and θ are the relative $\eta'\pi^+\pi^-$ coupling strengths and the phase between the two resonances.

The fit results for the second model are shown in Fig. 4. The $\log\mathcal{L}$ of this fit is 630 540.3, which is improved by 37 with four additional parameters over that for the fit using one simple Breit-Wigner function. The $X(1835)$ mass is $1825.3 \pm 2.4\ \mathrm{MeV}/c^2$ and the width is $245.2 \pm 13.1\ \mathrm{MeV}/c^2$; the $X(1870)$ mass is $1870.2 \pm 2.2\ \mathrm{MeV}/c^2$ and the width is $13.0 \pm 6.1\ \mathrm{MeV}/c^2$, with a statistical significance that is 7.9σ. It is known that there are two nontrivial solutions in a fit using a coherent sum of two Breit-Wigner functions [27]. In the parametrization of Eq. (3), the two solutions share the same M_1, Γ_1, M_2, and Γ_2, but have different values of β and θ, which means that the only observable difference between the solutions are branching fractions of the two Breit-Wigner functions. The product branching fractions with constructive interference are $\mathcal{B}[J/\psi \to \gamma X(1835)]\mathcal{B}[X(1835) \to \eta'\pi^+\pi^-] = (3.01 \pm 0.17) \times 10^{-4}$ and $\mathcal{B}[J/\psi \to \gamma X(1870)]\mathcal{B}[X(1870) \to \eta'\pi^+\pi^-] = (2.03 \pm 0.12) \times 10^{-7}$, while the solution with destructive interference

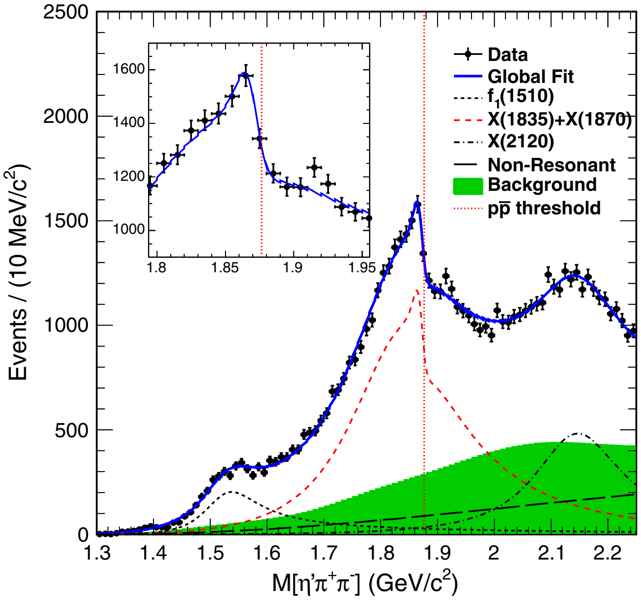

FIG. 4. Fit results of using a coherent sum of two Breit-Wigner amplitudes. The dashed dotted vertical line shows the position of the $p\bar{p}$ mass threshold, the dots with error bars are data, the solid curves are total fit results, the dashed curves are the sum of $X(1835)$ and $X(1870)$, the short-dashed curves are the $f_1(1510)$, the dash-dotted curves are the $X(2120)$, the long-dashed curves are nonresonant $\eta'\pi^+\pi^-$ fit results, and the shaded histograms are background events. The inset shows the data and the global fit between 1.8 and 1.95 GeV$/c^2$.

gives $\mathcal{B}[J/\psi\to\gamma X(1835)]\mathcal{B}[X(1835)\to\eta'\pi^+\pi^-]=(3.72\pm 0.21)\times10^{-4}$, and $\mathcal{B}[J/\psi\to\gamma X(1870)]\mathcal{B}[X(1870)\to\eta'\pi^+\pi^-]=(1.57\pm0.09)\times10^{-5}$. In this model, the $X(1920)$ is not included in the fit because its significance is just 3.9σ. Considering systematic uncertainties (see below), the significance of $X(1870)$ is larger than 7σ.

The systematic uncertainties come from data-MC differences in the tracking, photon detection and particle identification efficiencies, the kinematic fit, requirements on the invariant mass distribution of $\gamma\gamma$, signal selection of ρ^0, η, and η', total number of J/ψ events, branching fractions for intermediate states decays, fit ranges, background descriptions, mass resolutions, and the intermediate structure of $\pi^+\pi^-$. In the first model, the dominant terms are the fit range, the background description, and the intermediate structure of $\pi^+\pi^-$. Considering all systematic uncertainties, the final result is shown in Table I. For the second model, the dominant two systematic sources are the background description and the intermediate structure of $\pi^+\pi^-$. Considering all systematic uncertainties, the final result is shown in Table II.

In summary, the $J/\psi\to\gamma\eta'\pi^+\pi^-$ process is studied with 1.09×10^9 J/ψ events collected at the BESIII experiment in 2012. We observed a significant distortion of the $\eta'\pi^+\pi^-$ line shape near the $p\bar{p}$ mass threshold that cannot be accommodated by an ordinary Breit-Wigner resonance function. Two typical models for such a line shape are used to fit the data. The first model assumes the state around 1.85 GeV$/c^2$ couples with the $p\bar{p}$ and the distortion reflects the opening of the $p\bar{p}$ decay channel. The fit result for this model yields a strong coupling between the broad structure and the $p\bar{p}$ of $g^2_{p\bar{p}}/g^2_0 = 2.31\pm0.37^{+0.83}_{-0.60}$, with a statistical significance larger than 7σ for being nonzero. The pole nearest to the $p\bar{p}$ mass threshold of this state is located at $M_{\rm pole} = 1909.5\pm15.9({\rm stat})^{+9.4}_{-27.5}({\rm syst})$ MeV$/c^2$ and $\Gamma_{\rm pole} = 273.5\pm21.4({\rm stat})^{+6.1}_{-64.0}({\rm syst})$ MeV$/c^2$. The second model assumes the distortion reflects interference between the $X(1835)$ and another resonance with mass close to the $p\bar{p}$ mass threshold. A fit with this model uses a coherent sum of two interfering Breit-Wigner amplitudes to describe the $\eta'\pi^+\pi^-$ mass spectrum around 1.85 GeV$/c^2$. This fit yields a narrow resonance below the $p\bar{p}$ mass threshold with $M=1870.2\pm2.2({\rm stat})^{+2.3}_{-0.7}({\rm syst})$ MeV$/c^2$ and $\Gamma=13.0\pm 6.1({\rm stat})^{+2.1}_{-3.8}({\rm syst})$ MeV$/c^2$, with a statistical significance larger than 7σ. With current data, both models fit the data well with fit qualities, and both suggest the existence of a state, either a broad state with strong couplings to the $p\bar{p}$, or a narrow state just below the $p\bar{p}$ mass threshold. For the broad state above the $p\bar{p}$ mass threshold, its strong

TABLE I. Fit results of using the Flatté formula. The first errors are statistical errors, and the second errors are systematic errors; the branching ratio is the product of $\mathcal{B}(J/\psi\to\gamma X)$ and $\mathcal{B}(X\to\eta'\pi^+\pi^-)$.

The state around 1.85 GeV$/c^2$	
$\mathcal{M}$ (MeV$/c^2$)	$1638.0\pm121.9^{+127.8}_{-254.3}$
g_0^2 [(GeV$/c^2)^2$]	$93.7\pm35.4^{+47.6}_{-43.9}$
$g^2_{p\bar{p}}/g^2_0$	$2.31\pm0.37^{+0.83}_{-0.60}$
$M_{\rm pole}$ (MeV$/c^2$)	$1909.5\pm15.9^{+9.4}_{-27.5}$
$\Gamma_{\rm pole}$ (MeV$/c^2$)	$273.5\pm21.4^{+6.1}_{-64.0}$
Branching ratio	$(3.93\pm0.38^{+0.31}_{-0.84})\times10^{-4}$

TABLE II. Fit results using a coherent sum of two Breit-Wigner amplitudes. The first errors are statistical errors, and the second errors are systematic errors; the branching ratio (B.R.) is the product of $\mathcal{B}(J/\psi\to\gamma X)$ and $\mathcal{B}(X\to\eta'\pi^+\pi^-)$.

$X(1835)$	
Mass (MeV$/c^2$)	$1825.3\pm2.4^{+17.3}_{-2.4}$
Width (MeV$/c^2$)	$245.2\pm13.1^{+4.6}_{-9.6}$
B.R. (constructive interference)	$(3.01\pm0.17^{+0.26}_{-0.28})\times10^{-4}$
B.R. (destructive interference)	$(3.72\pm0.21^{+0.18}_{-0.35})\times10^{-4}$
$X(1870)$	
Mass (MeV$/c^2$)	$1870.2\pm2.2^{+2.3}_{-0.7}$
Width (MeV$/c^2$)	$13.0\pm6.1^{+2.1}_{-3.8}$
B.R. (constructive interference)	$(2.03\pm0.12^{+0.43}_{-0.70})\times10^{-7}$
B.R. (destructive interference)	$(1.57\pm0.09^{+0.49}_{-0.86})\times10^{-5}$

couplings to the $p\bar{p}$ suggest the existence of a $p\bar{p}$ moleculelike state. For the narrow state just below the $p\bar{p}$ mass threshold, its very narrow width suggests that it is an unconventional meson, most likely a $p\bar{p}$ bound state. So both fits support the existence of a $p\bar{p}$ moleculelike or bound state. With current statistics, more sophisticated models such as a mixture of above two models cannot be ruled out. In order to elucidate further the nature of the states around 1.85 GeV$/c^2$, more data are needed to further study the $J/\psi \to \gamma\eta'\pi^+\pi^-$ process. Also, line shapes for other decay modes should be studied near the $p\bar{p}$ mass threshold, including further studies of $J/\psi \to \gamma p\bar{p}$ and $J/\psi \to \gamma\eta K_S^0 K_S^0$.

BESIII Collaboration thanks the staff of BEPCII and the IHEP computing center for their strong support. This work is supported in part by the National Key Basic Research Program of China under Contract No. 2015CB856700; the National Natural Science Foundation of China (NSFC) under Contracts No. 11235011, No. 11322544, No. 11335008, and No. 11425524; the Chinese Academy of Sciences (CAS) Large-Scale Scientific Facility Program; the CAS Center for Excellence in Particle Physics (CCEPP); the Collaborative Innovation Center for Particles and Interactions (CICPI); the Joint Large-Scale Scientific Facility Funds of the NSFC and CAS under Contracts No. U1232201 and No. U1332201; the CAS under Contracts No. KJCX2-YW-N29 and No. KJCX2-YW-N45; the 100 Talents Program of the CAS; the National 1000 Talents Program of China; INPAC and Shanghai Key Laboratory for Particle Physics and Cosmology; Istituto Nazionale di Fisica Nucleare, Italy; the Joint Large-Scale Scientific Facility Funds of the NSFC and the CAS under Contract No. U1532257; the Joint Large-Scale Scientific Facility Funds of the NSFC and the CAS under Contract No. U1532258; Koninklijke Nederlandse Akademie van Wetenschappen (KNAW) under Contract No. 530-4CDP03; the Ministry of Development of Turkey under Contract No. DPT2006K-120470; the Swedish Research Council; the U.S. Department of Energy under Contracts No. DE-FG02-05ER41374, No. DE-SC-0010504, and No. DE-SC0012069; the U.S. National Science Foundation; the University of Groningen (RuG) and the Helmholtzzentrum fuer Schwerionenforschung GmbH (GSI), Darmstadt; the WCU Program of the National Research Foundation of Korea under Contract No. R32-2008-000-10155-0.

[a]Also at State Key Laboratory of Particle Detection and Electronics, Beijing 100049, Hefei 230026, People's Republic of China.
[b]Also at Bogazici University, 34342 Istanbul, Turkey.
[c]Also at the Moscow Institute of Physics and Technology, Moscow 141700, Russia.
[d]Also at the Functional Electronics Laboratory, Tomsk State University, Tomsk, 634050, Russia.
[e]Also at the Novosibirsk State University, Novosibirsk, 630090, Russia.
[f]Also at the NRC "Kurchatov Institute", PNPI, 188300, Gatchina, Russia.
[g]Also at University of Texas at Dallas, Richardson, Texas 75083, USA.
[h]Also at Istanbul Arel University, 34295 Istanbul, Turkey.
[i]Present address: Currently at DESY, 22607 Hamburg, Germany.

[1] M. Ablikim *et al.* (BES Collaboration), Phys. Rev. Lett. **95**, 262001 (2005).
[2] M. Ablikim *et al.* (BESIII Collaboration), Phys. Rev. Lett. **106**, 072002 (2011).
[3] M. Ablikim *et al.* (BESIII Collaboration), Phys. Rev. Lett. **115**, 091803 (2015).
[4] J. Z. Bai *et al.* (BES Collaboration), Phys. Rev. Lett. **91**, 022001 (2003).
[5] M. Ablikim *et al.* (BESIII Collaboration), Chin. Phys. C **34**, 421 (2010).
[6] J. P. Alexander *et al.* (CLEO Collaboration), Phys. Rev. D **82**, 092002 (2010).
[7] M. Ablikim *et al.* (BESIII Collaboration), Phys. Rev. Lett. **108**, 112003 (2012).
[8] T. Huang and S. L. Zhu, Phys. Rev. D **73**, 014023 (2006).
[9] N. Kochelev and D. P. Min, Phys. Lett. B **633**, 283 (2006).
[10] G. Hao, C. F. Qiao, and A. Zhang, Phys. Lett. B **642**, 53 (2006).
[11] B. A. Li, Phys. Rev. D **74**, 034019 (2006).
[12] X. H. Liu, Y. J. Zhang, and Q. Zhao, Phys. Rev. D **80**, 034032 (2009).
[13] S. L. Zhu and C. S. Gao, Commun. Theor. Phys. **46**, 291 (2006).
[14] J. P. Dedonder, B. Loiseau, B. El-Bennich, and S. Wycech, Phys. Rev. C **80**, 045207 (2009).
[15] G. J. Ding, R. G. Ping, and M. L. Yan, Eur. Phys. J. A **28**, 351 (2006).
[16] C. Liu, Eur. Phys. J. C **53**, 413 (2008).
[17] Z. G. Wang and S. L. Wan, J. Phys. G **34**, 505 (2007).
[18] M. Ablikim *et al.* (BESIII Collaboration), Chin. Phys. C **36**, 915 (2012).
[19] M. Ablikim *et al.* (BESIII Collaboration), Nucl. Instrum. Methods Phys. Res., Sect. A **614**, 345 (2010).
[20] J. Z. Bai *et al.* (BES Collaboration), Nucl. Instrum. Methods Phys. Res., Sect. A **344**, 319 (1994); **458**, 627 (2001).
[21] S. Agostinelli *et al.* (GEANT4 Collaboration), Nucl. Instrum. Methods Phys. Res., Sect. A **506**, 250 (2003).
[22] S. Jadach, B. F. L. Ward, and Z. Was, Comput. Phys. Commun. **130**, 260 (2000); Phys. Rev. D **63**, 113009 (2001).
[23] J. C. Chen, G. S. Huang, X. R. Qi, D. H. Zhang, and Y. S. Zhu, Phys. Rev. D **62**, 034003 (2000).
[24] K. A. Olive *et al.* (Particle Data Group), Chin. Phys. C **38**, 090001 (2014).
[25] S. M. Flatté, Phys. Lett. B **63**, 224 (1976).
[26] B. S. Zou and D. V. Bugg, Phys. Rev. D **48**, R3948 (1993).
[27] K. Zhu, X. H. Mo, C. Z. Yuan, and P. Wang, Int. J. Mod. Phys. A **26**, 4511 (2011).

Precise Measurement of the $e^+e^- \to \pi^+\pi^- J/\psi$ Cross Section at Center-of-Mass Energies from 3.77 to 4.60 GeV

M. Ablikim,[1] M. N. Achasov,[9,e] S. Ahmed,[14] X. C. Ai,[1] O. Albayrak,[5] M. Albrecht,[4] D. J. Ambrose,[44] A. Amoroso,[49a,49c] F. F. An,[1] Q. An,[46,a] J. Z. Bai,[1] O. Bakina,[23] R. Baldini Ferroli,[20] Y. Ban,[31] D. W. Bennett,[19] J. V. Bennett,[5] N. Berger,[22] M. Bertani,[20] D. Bettoni,[21] J. M. Bian,[43] F. Bianchi,[49a,49c] E. Boger,[23,c] I. Boyko,[23] R. A. Briere,[5] H. Cai,[51] X. Cai,[1,a] O. Cakir,[40] A. Calcaterra,[20] G. F. Cao,[1] S. A. Cetin,[40] J. Chai,[49] J. F. Chang,[1,a] G. Chelkov,[23,c,d] G. Chen,[1] H. S. Chen,[1] J. C. Chen,[1] M. L. Chen,[1,a] S. Chen,[41] S. J. Chen,[29] X. Chen,[1,a] X. R. Chen,[26] Y. B. Chen,[1,a] X. K. Chu,[31] G. Cibinetto,[21] H. L. Dai,[1,a] J. P. Dai,[34] A. Dbeyssi,[14] D. Dedovich,[23] Z. Y. Deng,[1] A. Denig,[22] I. Denysenko,[23] M. Destefanis,[49a,49c] F. De Mori,[49a,49c] Y. Ding,[27] C. Dong,[30] J. Dong,[1,a] L. Y. Dong,[1] M. Y. Dong,[1,a] Z. L. Dou,[29] S. X. Du,[53] P. F. Duan,[1] J. Z. Fan,[39] J. Fang,[1,a] S. S. Fang,[1] X. Fang,[46,a] Y. Fang,[1] R. Farinelli,[21a,21b] L. Fava,[49b,49c] F. Feldbauer,[22] G. Felici,[20] C. Q. Feng,[46,a] E. Fioravanti,[21] M. Fritsch,[14,22] C. D. Fu,[1] Q. Gao,[1] X. L. Gao,[46,a] Y. Gao,[39] Z. Gao,[46,a] I. Garzia,[21] K. Goetzen,[10] L. Gong,[30] W. X. Gong,[1,a] W. Gradl,[22] M. Greco,[49a,49c] M. H. Gu,[1,a] Y. T. Gu,[12] Y. H. Guan,[1] A. Q. Guo,[1] L. B. Guo,[28] R. P. Guo,[1] Y. Guo,[1] Y. P. Guo,[22] Z. Haddadi,[25] A. Hafner,[22] S. Han,[51] X. Q. Hao,[15] F. A. Harris,[42] K. L. He,[1] F. H. Heinsius,[4] T. Held,[4] Y. K. Heng,[1,a] T. Holtmann,[4] Z. L. Hou,[1] C. Hu,[28] H. M. Hu,[1] J. F. Hu,[49a,49c] T. Hu,[1,a] Y. Hu,[1] G. S. Huang,[46,a] J. S. Huang,[15] X. T. Huang,[33] X. Z. Huang,[29] Z. L. Huang,[27] T. Hussain,[48] W. Ikegami Andersson,[50] Q. Ji,[1] Q. P. Ji,[15] X. B. Ji,[1] X. L. Ji,[1,a] L. W. Jiang,[51] X. S. Jiang,[1,a] X. Y. Jiang,[30] J. B. Jiao,[33] Z. Jiao,[17] D. P. Jin,[1,a] S. Jin,[1] T. Johansson,[50] A. Julin,[43] N. Kalantar-Nayestanaki,[25] X. L. Kang,[1] X. S. Kang,[30] M. Kavatsyuk,[25] B. C. Ke,[5] P. Kiese,[22] R. Kliemt,[10] B. Kloss,[22] O. B. Kolcu,[40b,h] B. Kopf,[4] M. Kornicer,[42] A. Kupsc,[50] W. Kühn,[24] J. S. Lange,[24] M. Lara,[19] P. Larin,[14] L. Lavezzi,[49c,1] H. Leithoff,[22] C. Leng,[49] C. Li,[50] Cheng Li,[46,a] D. M. Li,[53] F. Li,[1,a] F. Y. Li,[31] G. Li,[1] H. B. Li,[1] H. J. Li,[1] J. C. Li,[1] Jin Li,[32] K. Li,[13] K. Li,[33] Lei Li,[3] P. R. Li,[7,41] Q. Y. Li,[33] T. Li,[33] W. D. Li,[1] W. G. Li,[1] X. L. Li,[33] X. N. Li,[1,a] X. Q. Li,[30] Y. B. Li,[2] Z. B. Li,[38] H. Liang,[46,a] Y. F. Liang,[36] Y. T. Liang,[24] G. R. Liao,[11] D. X. Lin,[14] B. Liu,[34] B. J. Liu,[1] C. X. Liu,[1] D. Liu,[46,a] F. H. Liu,[35] Fang Liu,[1] Feng Liu,[6] H. B. Liu,[12] H. H. Liu,[1] H. H. Liu,[16] H. M. Liu,[1] J. Liu,[1] J. B. Liu,[46,a] J. P. Liu,[51] J. Y. Liu,[1] K. Liu,[39] K. Y. Liu,[27] L. D. Liu,[31] P. L. Liu,[1,a] Q. Liu,[41] S. B. Liu,[46,a] X. Liu,[26] Y. B. Liu,[30] Y. Y. Liu,[30] Z. A. Liu,[1,a] Zhiqing Liu,[22,*] H. Loehner,[25] X. C. Lou,[1,a,g] H. J. Lu,[17] J. G. Lu,[1,a] Y. Lu,[1] Y. P. Lu,[1,a] C. L. Luo,[28] M. X. Luo,[52] T. Luo,[42] X. L. Luo,[1,a] X. R. Lyu,[41] F. C. Ma,[27] H. L. Ma,[1] L. L. Ma,[33] M. M. Ma,[1] Q. M. Ma,[1] T. Ma,[1] X. N. Ma,[30] X. Y. Ma,[1,a] Y. M. Ma,[33] F. E. Maas,[14] M. Maggiora,[49a,49c] Q. A. Malik,[48] Y. J. Mao,[31] Z. P. Mao,[1] S. Marcello,[49a,49c] J. G. Messchendorp,[25] G. Mezzadri,[21] J. Min,[1,a] T. J. Min,[1] R. E. Mitchell,[19] X. H. Mo,[1,a] Y. J. Mo,[6] C. Morales Morales,[14] N. Yu. Muchnoi,[9,e] H. Muramatsu,[43] P. Musiol,[4] Y. Nefedov,[23] F. Nerling,[10] I. B. Nikolaev,[9,e] Z. Ning,[1,a] S. Nisar,[8] S. L. Niu,[1,a] X. Y. Niu,[1] S. L. Olsen,[32] Q. Ouyang,[1,a] S. Pacetti,[20] Y. Pan,[46,a] P. Patteri,[20] M. Pelizaeus,[4] H. P. Peng,[46,a] K. Peters,[10,i] J. Pettersson,[50] J. L. Ping,[28] R. G. Ping,[1] R. Poling,[43] V. Prasad,[1] H. R. Qi,[2] M. Qi,[29] S. Qian,[1,a] C. F. Qiao,[41] L. Q. Qin,[33] N. Qin,[51] X. S. Qin,[1] Z. H. Qin,[1,a] J. F. Qiu,[1] K. H. Rashid,[48] C. F. Redmer,[22] M. Ripka,[22] G. Rong,[1] Ch. Rosner,[14] X. D. Ruan,[12] A. Sarantsev,[23,f] M. Savrié,[21] C. Schnier,[4] K. Schoenning,[50] W. Shan,[31] M. Shao,[46,a] C. P. Shen,[2] P. X. Shen,[30] X. Y. Shen,[1] H. Y. Sheng,[1] W. M. Song,[1] X. Y. Song,[1] S. Sosio,[49a,49c] S. Spataro,[49a,49c] G. X. Sun,[1] J. F. Sun,[15] S. S. Sun,[1] X. H. Sun,[1] Y. J. Sun,[46,a] Y. Z. Sun,[1] Z. J. Sun,[1,a] Z. T. Sun,[19] C. J. Tang,[36] X. Tang,[1] I. Tapan,[40] E. H. Thorndike,[44] M. Tiemens,[25] I. Uman,[40] G. S. Varner,[42] B. Wang,[30] B. L. Wang,[41] D. Wang,[31] D. Y. Wang,[31] K. Wang,[1,a] L. L. Wang,[1] L. S. Wang,[1] M. Wang,[33] P. Wang,[1] P. L. Wang,[1] W. Wang,[1,a] W. P. Wang,[46,a] X. F. Wang,[39] Y. Wang,[37] Y. D. Wang,[14] Y. F. Wang,[1,a] Y. Q. Wang,[22] Z. Wang,[1,a] Z. G. Wang,[1,a] Z. H. Wang,[46,a] Z. Y. Wang,[1] Z. Y. Wang,[1] T. Weber,[22] D. H. Wei,[11] P. Weidenkaff,[22] S. P. Wen,[1] U. Wiedner,[4] M. Wolke,[50] L. H. Wu,[1] L. J. Wu,[1] Z. Wu,[1,a] L. Xia,[46,a] L. G. Xia,[39] Y. Xia,[18] D. Xiao,[1] H. Xiao,[47] Z. J. Xiao,[28] Y. G. Xie,[1,a] Yuehong Xie,[6] Q. L. Xiu,[1,a] G. F. Xu,[1] J. J. Xu,[1] L. Xu,[1] Q. J. Xu,[13] Q. N. Xu,[41] X. P. Xu,[37] L. Yan,[49a,49c] W. B. Yan,[46,a] W. C. Yan,[46,a] Y. H. Yan,[18] H. J. Yang,[34,j] H. X. Yang,[1] L. Yang,[51] Y. X. Yang,[11] M. Ye,[1,a] M. H. Ye,[7] J. H. Yin,[1] Z. Y. You,[38] B. X. Yu,[1,a] C. X. Yu,[30] J. S. Yu,[26] C. Z. Yuan,[1] Y. Yuan,[1] A. Yuncu,[40b,b] A. A. Zafar,[48] Y. Zeng,[18] Z. Zeng,[46,a] B. X. Zhang,[1] B. Y. Zhang,[1,a] C. C. Zhang,[1] D. H. Zhang,[1] H. H. Zhang,[38] H. Y. Zhang,[1,a] J. Zhang,[1] J. J. Zhang,[1] J. L. Zhang,[1] J. Q. Zhang,[1] J. W. Zhang,[1,a] J. Y. Zhang,[1] J. Z. Zhang,[1] K. Zhang,[1] L. Zhang,[1] S. Q. Zhang,[30] X. Y. Zhang,[33] Y. Zhang,[1] Y. Zhang,[1] Y. H. Zhang,[1,a] Y. N. Zhang,[41] Y. T. Zhang,[46,a] Yu Zhang,[41] Z. H. Zhang,[6] Z. P. Zhang,[46] Z. Y. Zhang,[51] G. Zhao,[1] J. W. Zhao,[1,a] J. Y. Zhao,[1] J. Z. Zhao,[1,a] Lei Zhao,[46,a] Ling Zhao,[1]

M. G. Zhao,[30] Q. Zhao,[1] Q. W. Zhao,[1] S. J. Zhao,[53] T. C. Zhao,[1] Y. B. Zhao,[1,a] Z. G. Zhao,[46,a] A. Zhemchugov,[23,c] B. Zheng,[47] J. P. Zheng,[1,a] W. J. Zheng,[33] Y. H. Zheng,[41] B. Zhong,[28] L. Zhou,[1,a] X. Zhou,[51] X. K. Zhou,[46,a] X. R. Zhou,[46,a] X. Y. Zhou,[1] K. Zhu,[1] K. J. Zhu,[1,a] S. Zhu,[1] S. H. Zhu,[45] X. L. Zhu,[39] Y. C. Zhu,[46,a] Y. S. Zhu,[1] Z. A. Zhu,[1] J. Zhuang,[1,a] L. Zotti,[49a,49c] B. S. Zou,[1] and J. H. Zou[1]

(BESIII Collaboration)

[1]*Institute of High Energy Physics, Beijing 100049, People's Republic of China*
[2]*Beihang University, Beijing 100191, People's Republic of China*
[3]*Beijing Institute of Petrochemical Technology, Beijing 102617, People's Republic of China*
[4]*Bochum Ruhr-University, D-44780 Bochum, Germany*
[5]*Carnegie Mellon University, Pittsburgh, Pennsylvania 15213, USA*
[6]*Central China Normal University, Wuhan 430079, People's Republic of China*
[7]*China Center of Advanced Science and Technology, Beijing 100190, People's Republic of China*
[8]*COMSATS Institute of Information Technology, Lahore, Defence Road, Off Raiwind Road, 54000 Lahore, Pakistan*
[9]*G.I. Budker Institute of Nuclear Physics SB RAS (BINP), Novosibirsk 630090, Russia*
[10]*GSI Helmholtzcentre for Heavy Ion Research GmbH, D-64291 Darmstadt, Germany*
[11]*Guangxi Normal University, Guilin 541004, People's Republic of China*
[12]*Guangxi University, Nanning 530004, People's Republic of China*
[13]*Hangzhou Normal University, Hangzhou 310036, People's Republic of China*
[14]*Helmholtz Institute Mainz, Johann-Joachim-Becher-Weg 45, D-55099 Mainz, Germany*
[15]*Henan Normal University, Xinxiang 453007, People's Republic of China*
[16]*Henan University of Science and Technology, Luoyang 471003, People's Republic of China*
[17]*Huangshan College, Huangshan 245000, People's Republic of China*
[18]*Hunan University, Changsha 410082, People's Republic of China*
[19]*Indiana University, Bloomington, Indiana 47405, USA*
[20a]*INFN Laboratori Nazionali di Frascati, I-00044, Frascati, Italy;*
[20b]*INFN and University of Perugia, I-06100, Perugia, Italy*
[21a]*INFN Sezione di Ferrara, I-44122, Ferrara, Italy;*
[21b]*University of Ferrara, I-44122, Ferrara, Italy*
[22]*Johannes Gutenberg University of Mainz, Johann-Joachim-Becher-Weg 45, D-55099 Mainz, Germany*
[23]*Joint Institute for Nuclear Research, 141980 Dubna, Moscow region, Russia*
[24]*Justus-Liebig-Universitaet Giessen, II. Physikalisches Institut, Heinrich-Buff-Ring 16, D-35392 Giessen, Germany*
[25]*KVI-CART, University of Groningen, NL-9747 AA Groningen, The Netherlands*
[26]*Lanzhou University, Lanzhou 730000, People's Republic of China*
[27]*Liaoning University, Shenyang 110036, People's Republic of China*
[28]*Nanjing Normal University, Nanjing 210023, People's Republic of China*
[29]*Nanjing University, Nanjing 210093, People's Republic of China*
[30]*Nankai University, Tianjin 300071, People's Republic of China*
[31]*Peking University, Beijing 100871, People's Republic of China*
[32]*Seoul National University, Seoul, 151-747 Korea*
[33]*Shandong University, Jinan 250100, People's Republic of China*
[34]*Shanghai Jiao Tong University, Shanghai 200240, People's Republic of China*
[35]*Shanxi University, Taiyuan 030006, People's Republic of China*
[36]*Sichuan University, Chengdu 610064, People's Republic of China*
[37]*Soochow University, Suzhou 215006, People's Republic of China*
[38]*Sun Yat-Sen University, Guangzhou 510275, People's Republic of China*
[39]*Tsinghua University, Beijing 100084, People's Republic of China*
[40a]*Ankara University, 06100 Tandogan, Ankara, Turkey;*
[40b]*Istanbul Bilgi University, 34060 Eyup, Istanbul, Turkey;*
[40c]*Uludag University, 16059 Bursa, Turkey;*
[40d]*Near East University, Nicosia, North Cyprus, Mersin 10, Turkey*
[41]*University of Chinese Academy of Sciences, Beijing 100049, People's Republic of China*
[42]*University of Hawaii, Honolulu, Hawaii 96822, USA*
[43]*University of Minnesota, Minneapolis, Minnesota 55455, USA*
[44]*University of Rochester, Rochester, New York 14627, USA*
[45]*University of Science and Technology Liaoning, Anshan 114051, People's Republic of China*
[46]*University of Science and Technology of China, Hefei 230026, People's Republic of China*
[47]*University of South China, Hengyang 421001, People's Republic of China*

[48]University of the Punjab, Lahore-54590, Pakistan
[49a]University of Turin, I-10125 Turin, Italy;
[49b]University of Eastern Piedmont, I-15121 Alessandria, Italy;
[49c]INFN, I-10125 Turin, Italy
[50]Uppsala University, Box 516, SE-75120 Uppsala, Sweden
[51]Wuhan University, Wuhan 430072, People's Republic of China
[52]Zhejiang University, Hangzhou 310027, People's Republic of China
[53]Zhengzhou University, Zhengzhou 450001, People's Republic of China

(Received 4 November 2016; revised manuscript received 11 January 2017; published 1 March 2017)

The cross section for the process $e^+e^- \to \pi^+\pi^- J/\psi$ is measured precisely at center-of-mass energies from 3.77 to 4.60 GeV using 9 fb^{-1} of data collected with the BESIII detector operating at the BEPCII storage ring. Two resonant structures are observed in a fit to the cross section. The first resonance has a mass of $(4222.0 \pm 3.1 \pm 1.4)\ \mathrm{MeV}/c^2$ and a width of $(44.1 \pm 4.3 \pm 2.0)$ MeV, while the second one has a mass of $(4320.0 \pm 10.4 \pm 7.0)\ \mathrm{MeV}/c^2$ and a width of $(101.4^{+25.3}_{-19.7} \pm 10.2)$ MeV, where the first errors are statistical and second ones are systematic. The first resonance agrees with the $Y(4260)$ resonance reported by previous experiments. The precision of its resonant parameters is improved significantly. The second resonance is observed in $e^+e^- \to \pi^+\pi^- J/\psi$ for the first time. The statistical significance of this resonance is estimated to be larger than 7.6σ. The mass and width of the second resonance agree with the $Y(4360)$ resonance reported by the *BABAR* and Belle experiments within errors. Finally, the $Y(4008)$ resonance previously observed by the Belle experiment is not confirmed in the description of the BESIII data.

DOI: 10.1103/PhysRevLett.118.092001

The process $e^+e^- \to \pi^+\pi^- J/\psi$ at center-of-mass (c.m.) energies between 3.8 and 5.0 GeV was first studied by the *BABAR* experiment using an initial-state-radiation (ISR) technique [1], and a new structure, the $Y(4260)$, was reported with a mass around 4.26 GeV/c^2. This observation was immediately confirmed by the CLEO [2] and Belle experiments [3] in the same process. In addition, the Belle experiment reported an accumulation of events at around 4 GeV, which was called $Y(4008)$ later. Although the $Y(4008)$ state is still controversial—a new measurement by the *BABAR* experiment does not confirm it [4], while an updated measurement by the Belle experiment still supports its existence [5]—the observation of the Y states has stimulated substantial theoretical discussions on their nature [6,7].

Being produced in e^+e^- annihilation, the Y states have quantum numbers $J^{PC} = 1^{--}$. However, unlike the known 1^{--} charmonium states in the same mass range, such as $\psi(4040)$, $\psi(4160)$, and $\psi(4415)$ [8], which decay predominantly into open charm final states [$D^{(*)}\bar{D}^{(*)}$], the Y states show strong coupling to hidden-charm final states [9]. Furthermore, the observation of the states $Y(4360)$ and $Y(4660)$ in $e^+e^- \to \pi^+\pi^-\psi(2S)$ [10], together with the newly observed resonant structures in $e^+e^- \to \omega\chi_{c0}$ [11] and $e^+e^- \to \pi^+\pi^- h_c$ [12], overpopulates the vector charmonium spectrum predicted by potential models [13]. All of this indicates that the Y states may not be conventional charmonium states, and they are good candidates for new types of exotic particles, such as hybrids, tetraquarks, or meson molecules [6,7].

The $Y(4260)$ state was once considered a good hybrid candidate [14], since its mass is close to the value predicted by the flux tube model for the lightest hybrid charmonium [15]. Recent lattice calculations also show a 1^{--} hybrid charmonium could have a mass of $4285 \pm 14\ \mathrm{MeV}/c^2$ [16] or $4.33(2)\ \mathrm{GeV}/c^2$ [17]. Meanwhile, the diquark-antidiquark tetraquark model predicts a wide spectrum of states which can also accommodate the $Y(4260)$ [18]. Moreover, the mass of $Y(4260)$ is near the mass threshold of $D_s^{*+}D_s^{*-}$, $\bar{D}D_1$, $D_0\bar{D}^*$, and $f_0(980)J/\psi$, and $Y(4260)$ was supposed to be a meson molecule candidate of these meson pairs [19,20]. A recent observation of a charged charmoniumlike state $Z_c(3900)$ by BESIII [21], Belle [5], and with CLEO data [22] seems to favor the $\bar{D}D_1$ meson pair option [19]. Another possible interpretation describes the $Y(4260)$ as a heavy charmonium (J/ψ) being bound inside light hadronic matter—hadrocharmonium [23]. To better identify the nature of the Y states and distinguish various models, more precise experimental measurements, including the production cross section and the mass and width of the Y states, are essential.

In this Letter, we report a precise measurement of the $e^+e^- \to \pi^+\pi^- J/\psi$ cross section at e^+e^- c.m. energies from 3.77 to 4.60 GeV, using a data sample with an integrated luminosity of 9.05 fb^{-1} [24] collected with the BESIII detector operating at the BEPCII storage ring [25]. The J/ψ candidate is reconstructed with its leptonic decay modes ($\mu^+\mu^-$ and e^+e^-). The data sample used in this measurement includes two independent data sets. A high luminosity data set (dubbed "XYZ data") contains more than 40 pb^{-1} at each c.m. energy with a total integrated luminosity of 8.2 fb^{-1}, which dominates the precision of this measurement, and a low luminosity data set (dubbed "scan data") contains about 7–9 pb^{-1} at each c.m. energy with a total integrated luminosity of 0.8 fb^{-1}.

The integrated luminosities are measured with Bhabha events with an uncertainty of 1% [24]. The c.m. energy of each data set is measured using dimuon events, with an uncertainty of ± 0.8 MeV [26].

The BESIII detector is described in detail elsewhere [25]. The GEANT4-based [27] Monte Carlo (MC) simulation software package BOOST [28], which includes the geometric description of the BESIII detector and the detector response, is used to optimize event selection criteria, determine the detection efficiency, and estimate the backgrounds. For the signal process, we generate 60 000 $e^+e^- \to \pi^+\pi^- J/\psi$ events at each c.m. energy of the XYZ data, and an extrapolation is performed to the scan data with nearby c.m. energies. At e^+e^- c.m. energies between 4.189 and 4.358 GeV, the signal events are generated according to the Dalitz plot distributions obtained from the data set at corresponding c.m. energy, since there is significant $Z_c(3900)$ production [5,21,22]. At other c.m. energies, signal events are generated using an EVTGEN [29] phase space model. The J/ψ decays into $\mu^+\mu^-$ and e^+e^- with the same branching fractions [8]. The ISR is simulated with KKMC [30], and the maximum ISR photon energy is set to correspond to a 3.72 GeV$/c^2$ production threshold of the $\pi^+\pi^- J/\psi$ system. Final-state radiation (FSR) is simulated with PHOTOS [31]. Possible background contributions are estimated with KKMC-generated inclusive MC samples [$e^+e^- \to e^+e^-$, $\mu^+\mu^-$, $\tau^+\tau^-$, $\gamma\gamma$, $\gamma_{\rm ISR} J/\psi$, $\gamma_{\rm ISR}\psi(2S)$, and $q\bar{q}$ with $q = u$, d, s, c] with comparable integrated luminosities to the XYZ data.

Events with four charged tracks with zero net charge are selected. For each charged track, the polar angle in the drift chamber must satisfy $|\cos\theta| < 0.93$, and the point of closest approach to the e^+e^- interaction point must be within ± 10 cm in the beam direction and within 1 cm in the plane perpendicular to the beam direction. Taking advantage of the fact that pions and leptons are kinematically well separated in the signal decay, charged tracks with momenta larger than 1.06 GeV$/c$ in the laboratory frame are assumed to be leptons, and the others are assumed to be pions. We use the energy deposited in the electromagnetic calorimeter (EMC) to separate electrons from muons. For both muon candidates, the deposited energy in the EMC is required to be less than 0.35 GeV, while for both electrons, it is required to be larger than 1.1 GeV. To avoid systematic errors due to unstable operation, the muon system is not used here. Each event is required to have one $\pi^+\pi^-\ell^+\ell^-$ ($\ell = e$ or μ) combination.

To improve the momentum and energy resolution and to reduce the background, a four-constraint kinematic fit is applied to the event with the hypothesis $e^+e^- \to \pi^+\pi^-\ell^+\ell^-$, which constrains the total four-momentum of the final state particles to that of the initial colliding beams. The χ^2/n.d.f. of the kinematic fit is required to be less than 60/4.

To suppress radiative Bhabha and radiative dimuon ($e^+e^- \to \gamma e^+e^-/\gamma\mu^+\mu^-$) backgrounds associated with photon conversion to an e^+e^- pair which subsequently is misidentified as a $\pi^+\pi^-$ pair, the cosine of the opening angle of the pion-pair ($\cos\theta_{\pi^+\pi^-}$) candidates is required to be less than 0.98 for both $J/\psi \to \mu^+\mu^-$ and e^+e^- events. For $J/\psi \to e^+e^-$ events, since there are more abundant photon sources from radiative Bhabha events, we further require the cosine of the opening angles of both pion-electron pairs ($\cos\theta_{\pi^\pm e^\mp}$) to be less than 0.98. These requirements remove almost all of the Bhabha and dimuon background events, with an efficiency loss of less than 1% for signal events.

After imposing the above selection criteria, a clear J/ψ signal is observed in the invariant mass distribution of the lepton pairs [$M(\ell^+\ell^-)$]. The mass resolution of the $M(\ell^+\ell^-)$ distribution is estimated to be (3.7 ± 0.2) MeV$/c^2$ for $J/\psi \to \mu^+\mu^-$ and (3.9 ± 0.3) MeV$/c^2$ for $J/\psi \to e^+e^-$ in data for the range of c.m. energies investigated in this study. The J/ψ mass window is defined as $3.08 < M(\ell^+\ell^-) < 3.12$ GeV$/c^2$. In order to estimate the non-J/ψ background contribution, we also define the J/ψ mass sideband as $3.00 < M(\ell^+\ell^-) < 3.06$ GeV$/c^2$ and $3.14 < M(\ell^+\ell^-) < 3.20$ GeV$/c^2$, which is 3 times as wide as the signal region. The dominant background comes from $e^+e^- \to q\bar{q}$ ($q = u$, d, s) processes, such as $e^+e^- \to \pi^+\pi^-\pi^+\pi^-$. Since $q\bar{q}$ events form a smooth distribution in the J/ψ signal region, their contribution is estimated by the J/ψ mass sideband. Contributions from backgrounds related with charm quark production, such as $e^+e^- \to \eta J/\psi$ [32], $D^{(*)}\bar{D}^{(*)}$, and other open-charm mesons, are estimated to be negligible according to MC simulation studies.

In order to determine the signal yields, we make use of both fitting and counting methods on the $M(\ell^+\ell^-)$ distribution. In the XYZ data, each data set contains many signal events, and an unbinned maximum likelihood fit to the $M(\ell^+\ell^-)$ distribution is performed. We use a MC simulated signal shape convolved with a Gaussian function (with standard deviation 1.9 MeV, which represents the resolution difference between the data and the MC simulation) as the signal probability density function (PDF) and a linear term for the background. For the scan data, due to the low statistics, we directly count the number of events in the J/ψ signal region and that of the normalized background events in the J/ψ mass sideband and take the difference as the signal yields.

The cross section of $e^+e^- \to \pi^+\pi^- J/\psi$ at a certain e^+e^- c.m. energy $\sqrt{s}$ is calculated using

$$\sigma(\sqrt{s}) = \frac{N^{\rm sig}}{\mathcal{L}_{\rm int}(1+\delta)\epsilon\mathcal{B}}, \tag{1}$$

where $N^{\rm sig}$ is the number of signal events, $\mathcal{L}_{\rm int}$ is the integrated luminosity of data, $1+\delta$ is the ISR correction factor, ϵ is the detection efficiency, and $\mathcal{B}$ is the branching fraction of $J/\psi \to \ell^+\ell^-$ [8]. The ISR correction factor is

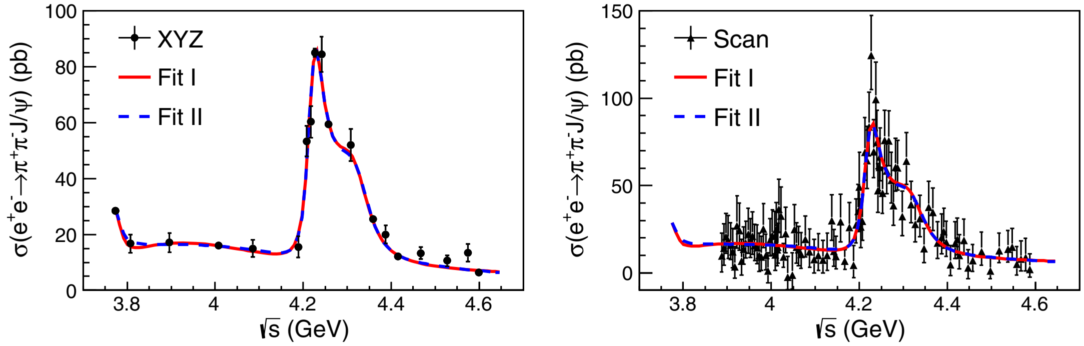

FIG. 1. Measured cross section $\sigma(e^+e^- \to \pi^+\pi^- J/\psi)$ and simultaneous fit to the XYZ data (left) and scan data (right) with the coherent sum of three Breit-Wigner functions (red solid curves) and the coherent sum of an exponential continuum and two Breit-Wigner functions (blue dashed curves). Dots with error bars are data.

calculated using the KKMC [30] program. To get the correct ISR photon energy distribution, we use the $\sqrt{s}$-dependent cross section line shape of the $e^+e^- \to \pi^+\pi^- J/\psi$ process, i.e., $\sigma(\sqrt{s})$, to replace the default one of KKMC. Since $\sigma(\sqrt{s})$ is what we measure in this study, the ISR correction procedure needs to be iterated, and the final results are obtained when the iteration converges. Figure 1 shows the measured cross section $\sigma(\sqrt{s})$ from both the XYZ data and scan data (numerical results are listed in Supplemental Material [33]).

To study the possible resonant structures in the $e^+e^- \to \pi^+\pi^- J/\psi$ process, a binned maximum likelihood fit is performed simultaneously to the measured cross section $\sigma(\sqrt{s})$ of the XYZ data with Gaussian uncertainties and the scan data with Poisson uncertainties. The PDF is parameterized as the coherent sum of three Breit-Wigner functions, together with an incoherent $\psi(3770)$ component which accounts for the decay of $\psi(3770) \to \pi^+\pi^- J/\psi$, with $\psi(3770)$ mass and width fixed to PDG [8] values. Because of the lack of data near the $\psi(3770)$ resonance, it is impossible to determine the relative phase between the $\psi(3770)$ amplitude and the other amplitudes. The amplitude to describe a resonance R is written as

$$\mathcal{A}(\sqrt{s}) = \frac{M}{\sqrt{s}} \frac{\sqrt{12\pi\Gamma_{e^+e^-}\Gamma_{\rm tot}\mathcal{B}_R}}{s - M^2 + iM\Gamma_{\rm tot}} \sqrt{\frac{\Phi(\sqrt{s})}{\Phi(M)}} e^{i\phi}, \qquad (2)$$

where M, $\Gamma_{\rm tot}$, and $\Gamma_{e^+e^-}$ are the mass, full width, and electronic width of the resonance R, respectively; $\mathcal{B}_R$ is the branching fraction of the decay $R \to \pi^+\pi^- J/\psi$; $\Phi(\sqrt{s})$ is the phase space factor of the three-body decay $R \to \pi^+\pi^- J/\psi$ [8]; and ϕ is the phase of the amplitude. The fit has four solutions with equally good fit quality [34] and identical masses and widths of the resonances (listed in Table I), while the phases and the product of the electronic widths with the branching fractions are different (listed in Table II). Figure 1 shows the fit results. The resonance R_1 has a mass and width consistent with that of $Y(4008)$ observed by Belle [5] within 1.0σ and 2.9σ, respectively. The resonance R_2 has a mass $4222.0 \pm 3.1\ \mathrm{MeV}/c^2$, which agrees with the average mass, $4251 \pm 9\ \mathrm{MeV}/c^2$ [8], of the $Y(4260)$ peak [1–5] within 3.0σ. However, its measured width is much narrower than the average width, 120 ± 12 MeV [8], of the $Y(4260)$. We also observe a new resonance R_3. The statistical significance of R_3 is estimated to be 7.9σ (including systematic uncertainties) by comparing the change of $\Delta(-2\ln\mathcal{L}) = 74.9$ with and without the R_3 amplitude in the fit and taking the change of number of degree of freedom Δn.d.f. $= 4$ into account. The fit quality is estimated using a χ^2-test method, with χ^2/n.d.f. $= 93.6/110$. Fit models taken from previous experiments [1–5] are also investigated and are ruled out with a confidence level equivalent to more than 5.4σ.

As an alternative description of the data, we use an exponential [35] to model the cross section near 4 GeV as in Ref. [4] instead of the resonance R_1. The fit results are shown as dashed lines in Fig. 1. This model also describes the data very well. A χ^2 test to the fit quality gives χ^2/n.d.f. $= 93.2/111$. Thus, the existence of a resonance near 4 GeV, such as the resonance R_1 or the $Y(4008)$ resonance [3], is not necessary to explain the data. The fit has four solutions with equally good fit quality [34] and

TABLE I. The measured masses and widths of the resonances from the fit to the $e^+e^- \to \pi^+\pi^- J/\psi$ cross section with three coherent Breit-Wigner functions. The numbers in the brackets correspond to a fit by replacing R_1 with an exponential describing the continuum. The errors are statistical only.

Parameters	Fit result
$M(R_1)$	$3812.6^{+61.9}_{-96.6}$ $(\cdots)$
$\Gamma_{\rm tot}(R_1)$	$476.9^{+78.4}_{-64.8}$ $(\cdots)$
$M(R_2)$	4222.0 ± 3.1 (4220.9 ± 2.9)
$\Gamma_{\rm tot}(R_2)$	44.1 ± 4.3 (44.1 ± 3.8)
$M(R_3)$	4320.0 ± 10.4 (4326.8 ± 10.0)
$\Gamma_{\rm tot}(R_3)$	$101.4^{+25.3}_{-19.7}$ $(98.2^{+25.4}_{-19.6})$

TABLE II. The values of $\Gamma_{e^+e^-}\mathcal{B}(R \to \pi^+\pi^- J/\psi)$ (in eV) from a fit to the $e^+e^- \to \pi^+\pi^- J/\psi$ cross section. ϕ_1 and ϕ_2 (in degrees) are the phase of the resonance R_2 and R_3, and the phase of resonance R_1 (or continuum) is set to 0. The numbers in the brackets correspond to the fit by replacing resonance R_1 with an exponential to describe the continuum. The errors are statistical only.

Parameters	Solution I	Solution II	Solution III	Solution IV
$\Gamma_{e^+e^-}\mathcal{B}[\psi(3770) \to \pi^+\pi^- J/\psi]$	0.5 ± 0.1 (0.4 ± 0.1)			
$\Gamma_{e^+e^-}\mathcal{B}(R_1 \to \pi^+\pi^- J/\psi)$	$8.8^{+1.5}_{-2.2}$ $(\cdots)$	$6.8^{+1.1}_{-1.5}$ $(\cdots)$	$7.2^{+0.9}_{-1.5}$ $(\cdots)$	$5.6^{+0.6}_{-1.0}$ $(\cdots)$
$\Gamma_{e^+e^-}\mathcal{B}(R_2 \to \pi^+\pi^- J/\psi)$	13.3 ± 1.4 (12.0 ± 1.0)	9.2 ± 0.7 (8.9 ± 0.6)	2.3 ± 0.6 (2.1 ± 0.4)	1.6 ± 0.4 (1.5 ± 0.3)
$\Gamma_{e^+e^-}\mathcal{B}(R_3 \to \pi^+\pi^- J/\psi)$	21.1 ± 3.9 (17.9 ± 3.3)	$1.7^{+0.8}_{-0.6}$ $(1.1^{+0.5}_{-0.4})$	$13.3^{+2.3}_{-1.8}$ $(12.4^{+1.9}_{-1.7})$	$1.1^{+0.4}_{-0.3}$ (0.8 ± 0.3)
ϕ_1	-58 ± 11 (-33 ± 8)	-116^{+9}_{-10} (-81^{+7}_{-8})	65^{+24}_{-20} (81^{+16}_{-14})	8 ± 13 (33 ± 9)
ϕ_2	-156 ± 5 (-132 ± 3)	68 ± 24 (107 ± 20)	-115^{+11}_{-9} (-95^{+6}_{-5})	110 ± 16 (144 ± 14)

identical masses and widths of the resonances (listed in Table I), while the phases and the product of the electronic widths with the branching fractions are different (listed in Table II). We observe the resonance R_2 and the resonance R_3 again. The statistical significance of resonance R_3 in this model is estimated to be 7.6σ (including systematic uncertainties) $[\Delta(-2\ln\mathcal{L}) = 70.7,\ \Delta\text{n.d.f.} = 4]$ using the same method as above.

The systematic uncertainty for the cross section measurement mainly comes from uncertainties in the luminosity, efficiencies, radiative correction, background shape, and branching fraction of $J/\psi \to \ell^+\ell^-$. The integrated luminosities of all the data sets are measured using large angle Bhabha scattering events, with an uncertainty of 1% [24]. The uncertainty in the tracking efficiency for high momentum leptons is 1% per track. Pions have momenta that range from 0.1 to 1.06 GeV/c, and their momentum-weighted tracking efficiency uncertainty is also 1% per track. For the kinematic fit, we use a similar method as in Ref. [36] to improve the agreement of the χ^2 distribution between the data and MC simulation, and the systematic uncertainty for the kinematic fit is estimated to be 0.6% (1.1%) for $\mu^+\mu^-$ (e^+e^-) events. For the MC simulation of signal events, we use both the $\pi^\pm Z_c(3900)^\mp$ model [5,21,22] and the phase space model to describe the $e^+e^- \to \pi^+\pi^- J/\psi$ process. The efficiency difference between these two models is 3.1%, which is taken as systematic uncertainty due to the decay model.

The efficiencies for the other selection criteria, the trigger simulation, the event start time determination, and the FSR simulation, are quite high (>99%), and their systematic errors are estimated to be less than 1%. In the ISR correction procedure, we iterate the cross section measurement until $(1+\delta)\epsilon$ converges. The convergence criterion is taken as the systematic uncertainty due to the ISR correction, which is 1%. We obtain the number of signal events by either fitting or counting events in the $M(\ell^+\ell^-)$ distribution. The background shape is described by a linear distribution. Varying the background shape from a linear shape to a second-order polynomial causes a 1.6% (2.1%) difference for the J/ψ signal yield for the $\mu^+\mu^-$ (e^+e^-) mode, which is taken as the systematic uncertainty for the background shape. The branching fraction of $J/\psi \to \ell^+\ell^-$ is taken from PDG [8], and the errors are 0.6% for both J/ψ decay modes. Assuming all the sources of systematic uncertainty are independent, the total systematic uncertainties are obtained by adding them in quadrature, resulting in 5.7% for the $\mu^+\mu^-$ mode and 5.9% for the e^+e^- mode.

In both fit scenarios to the $e^+e^- \to \pi^+\pi^- J/\psi$ cross section, we observe the resonance R_2 and R_3. Since we cannot distinguish the two scenarios from the data, we take the difference in mass and width as the systematic uncertainties, i.e., 1.1 (6.8) MeV/c^2 for the mass and 0.0 (3.2) MeV for the width of $R_2(R_3)$. The absolute c.m. energies of all the data sets were measured with dimuon events, with an uncertainty of ± 0.8 MeV. Such a kind of common uncertainty will propagate only to the masses of the resonances with the same amount, i.e., ± 0.8 MeV/c^2. In both fits, the $\psi(3770)$ amplitude was added incoherently. The possible interference effect of the $\psi(3770)$ component was investigated by adding it coherently in the fit with various phases. The largest deviation of the resonant parameters between the fits with and without interference for the $\psi(3770)$ amplitude is taken as a systematic error, which is 0.3 (1.3) MeV/c^2 for the mass and 2.0 (9.7) MeV for the width of the $R_2(R_3)$ resonance. Assuming all the systematic uncertainties are independent, we get the total systematic uncertainties by adding them in quadrature, which is 1.4 (7.0) MeV/c^2 for the mass and 2.0 (10.2) MeV for the width of $R_2(R_3)$, respectively.

In summary, we perform a precise cross section measurement of $e^+e^- \to \pi^+\pi^- J/\psi$ for c.m. energies from $\sqrt{s} =$ 3.77 to 4.60 GeV. Two resonant structures are observed, one with a mass of $(4222.0 \pm 3.1 \pm 1.4)$ MeV/c^2 and a width of $(44.1 \pm 4.3 \pm 2.0)$ MeV and the other with a mass of $(4320.0 \pm 10.4 \pm 7.0)$ MeV/c^2 and a width of $(101.4^{+25.3}_{-19.7} \pm 10.2)$ MeV, where the first errors are statistical and the second ones are systematic. The first resonance agrees with the $Y(4260)$ resonance reported by *BABAR*, CLEO, and Belle [1–5]. However, our measured width is much narrower than the $Y(4260)$ average width [8] reported by previous experiments. This is thanks to the much more precise data from BESIII, which results in the observation of the second resonance. The second resonance is observed for the first time in the process $e^+e^- \to \pi^+\pi^- J/\psi$. Its statistical significance is estimated to be larger than 7.6σ. The second resonance has a mass and width comparable to the $Y(4360)$ resonance reported by Belle and *BABAR* in $e^+e^- \to \pi^+\pi^-\psi(2S)$ [10]. If we assume it is the same resonance as the $Y(4360)$, we observe a new decay channel of $Y(4360) \to \pi^+\pi^- J/\psi$ for the first time. Finally, we cannot confirm the existence of the $Y(4008)$ resonance [3,5] from our data, since a continuum term also describes the cross section near 4 GeV equally well.

The BESIII Collaboration thanks the staff of BEPCII and the IHEP computing center for their strong support. This work is supported in part by National Key Basic Research Program of China under Contract No. 2015CB856700; National Natural Science Foundation of China (NSFC) under Contracts No. 11235011, No. 11322544, No. 11335008, and No. 11425524; the Chinese Academy of Sciences (CAS) Large-Scale Scientific Facility Program; the CAS Center for Excellence in Particle Physics (CCEPP); the Collaborative Innovation Center for Particles and Interactions (CICPI); Joint Large-Scale Scientific Facility Funds of the NSFC and CAS under Contracts No. U1232201 and No. U1332201; CAS under Contracts No. KJCX2-YW-N29 and No. KJCX2-YW-N45; 100 Talents Program of CAS; National 1000 Talents Program of China; INPAC and Shanghai Key Laboratory for Particle Physics and Cosmology; German Research Foundation DFG under Collaborative Research Center Contracts No. CRC 1044 and No. FOR 2359; Seventh Framework Programme of the European Commission under Marie Curie International Incoming Fellowship Grant Agreement No. 627240; Istituto Nazionale di Fisica Nucleare, Italy; Joint Large-Scale Scientific Facility Funds of the NSFC and CAS under Contract No. U1532257; Joint Large-Scale Scientific Facility Funds of the NSFC and CAS under Contract No. U1532258; Koninklijke Nederlandse Akademie van Wetenschappen (KNAW) under Contract No. 530-4CDP03; Ministry of Development of Turkey under Contract No. DPT2006K-120470; NSFC under Contract No. 11275266; The Swedish Resarch Council; U.S. Department of Energy under Contracts No. DE-FG02-05ER41374, No. DE-SC-0010504, No. DE-SC0012069, and No. DESC0010118; U.S. National Science Foundation; University of Groningen (RuG) and the Helmholtzzentrum fuer Schwerionenforschung GmbH (GSI), Darmstadt; WCU Program of National Research Foundation of Korea under Contract No. R32-2008-000-10155-0.

[*]Corresponding author.
zqliu@ihep.ac.cn

[a]Also at State Key Laboratory of Particle Detection and Electronics, Beijing 100049, Hefei 230026, People's Republic of China.

[b]Also at Bogazici University, 34342 Istanbul, Turkey.

[c]Also at the Moscow Institute of Physics and Technology, Moscow 141700, Russia.

[d]Also at the Functional Electronics Laboratory, Tomsk State University, Tomsk, 634050, Russia.

[e]Also at the Novosibirsk State University, Novosibirsk, 630090, Russia.

[f]Also at the NRC "Kurchatov Institute," PNPI, 188300, Gatchina, Russia.

[g]Also at University of Texas at Dallas, Richardson, TX 75083, USA.

[h]Also at Istanbul Arel University, 34295 Istanbul, Turkey.

[i]Also at Goethe University Frankfurt, 60323 Frankfurt am Main, Germany.

[j]Also at Institute of Nuclear and Particle Physics, Shanghai Key Laboratory for Particle Physics and Cosmology, Shanghai 200240, People's Republic of China.

[1] B. Aubert *et al.* (*BABAR* Collaboration), Phys. Rev. Lett. **95**, 142001 (2005).

[2] Q. He *et al.* (CLEO Collaboration), Phys. Rev. D **74**, 091104(R) (2006).

[3] C. Z. Yuan *et al.* (Belle Collaboration), Phys. Rev. Lett. **99**, 182004 (2007).

[4] J. P. Lees *et al.* (*BABAR* Collaboration), Phys. Rev. D **86**, 051102(R) (2012).

[5] Z. Q. Liu *et al.* (Belle Collaboration), Phys. Rev. Lett. **110**, 252002 (2013).

[6] N. Brambilla *et al.*, Eur. Phys. J. C **71**, 1534 (2011).

[7] H. X. Chen, W. Chen, X. Liu, and S. L. Zhu, Phys. Rep. **639**, 1 (2016).

[8] K. A. Olive *et al.* (Particle Data Group), Chin. Phys. C **38**, 090001 (2014).

[9] X. H. Mo, G. Li, C. Z. Yuan, K. L. He, H. M. Hu, J. H. Hu, P. Wang, and Z. Y. Wang, Phys. Lett. B **640**, 182 (2006).

[10] B. Aubert *et al.* (*BABAR* Collaboration), Phys. Rev. Lett. **98**, 212001 (2007); X. L. Wang *et al.* (Belle Collaboration), Phys. Rev. Lett. **99**, 142002 (2007); B. Aubert *et al.* (*BABAR* Collaboration), Phys. Rev. D **89**, 111103 (2014); X. L. Wang *et al.* (Belle Collaboration), Phys. Rev. D **91**, 112007 (2015).

[11] M. Ablikim *et al.* (BESIII Collaboration), Phys. Rev. Lett. **114**, 092003 (2015); Phys. Rev. D **93**, 011102(R) (2016).

[12] C.-Z. Yuan, Chin. Phys. C **38** (2014) 043001; M. Ablikim *et al.* (BESIII Collaboration), following Letter, Phys. Rev. Lett. **118**, 092002 (2017).

[13] E. Eichten, K. Gottfried, T. Kinoshita, K. D. Lane, and T. M. Yan, Phys. Rev. D **17**, 3090 (1978); **21**, 203 (1980); S. Godfrey and N. Isgur, Phys. Rev. D **32**, 189 (1985).

[14] F. E. Close and P. R. Page, Phys. Lett. B **628**, 215 (2005); S. L. Zhu, Phys. Lett. B **625**, 212 (2005).

[15] T. Barnes, F. E. Close, and E. S. Swanson, Phys. Rev. D **52**, 5242 (1995).

[16] L. Liu, G. Moir, M. Peardon, S. M. Ryan, C. E. Thomas, P. Vilaseca, J. J. Dudek, R. G. Edwards, B. Joó, and D. G. Richards (Hadron Spectrum Collaboration), J. High Energy Phys. 07 (2012) 126.

[17] Y. Chen, W.-F. Chiu, M. Gong, L.-C. Gui, and Z.-F. Liu, Chin. Phys. C **40**, 081002 (2016).

[18] L. Maiani, V. Riquer, F. Piccinini, and A. D. Polosa, Phys. Rev. D **72**, 031502 (2005); D. Ebert, R. N. Faustov, and V. O. Galkin, Eur. Phys. J. C **58**, 399 (2008).

[19] Q. Wang, C. Hanhart, and Q. Zhao, Phys. Rev. Lett. **111**, 132003 (2013); M. Cleven, Q. Wang, F. K. Guo, C. Hanhart, Ulf-G. Meissner, and Q. Zhao, Phys. Rev. D **90**, 074039 (2014).

[20] A. Martinez Torres, K. P. Khemchandani, D. Gamermann, and E. Oset, Phys. Rev. D **80**, 094012 (2009); R. M. Albuquerque and M. Nielsen, Nucl. Phys. **A815**, 53 (2009).

[21] M. Ablikim *et al.* (BESIII Collaboration), Phys. Rev. Lett. **110**, 252001 (2013).

[22] T. Xiao, S. Dobbs, A. Tomaradze, and K. K. Seth, Phys. Lett. B **727**, 366 (2013).

[23] S. Dubynskiy and M. B. Voloshin, Phys. Lett. B **666**, 344 (2008); Xin Li and M. B. Voloshin, Mod. Phys. Lett. A **29**, 1450060 (2014).

[24] M. Ablikim *et al.* (BESIII Collaboration), Chin. Phys. C **39**, 093001 (2015); **37**, 123001 (2013).

[25] M. Ablikim *et al.* (BESIII Collaboration), Nucl. Instrum. Methods Phys. Res., Sect. A **614**, 345 (2010).

[26] M. Ablikim *et al.* (BESIII Collaboration), Chin. Phys. C **40**, 063001 (2016).

[27] S. Agostinelli *et al.* (GEANT4 Collaboration), Nucl. Instrum. Methods Phys. Res., Sect. A **506**, 250 (2003).

[28] Z. Y. Deng *et al.*, Chin. Phys. C **30**, 371 (2006).

[29] D. J. Lange, Nucl. Instrum. Methods Phys. Res., Sect. A **462**, 152 (2001).

[30] S. Jadach, B. F. L. Ward, and Z. Was, Comput. Phys. Commun. **130**, 260 (2000); Phys. Rev. D **63**, 113009 (2001).

[31] P. Golonka and Z. Was, Eur. Phys. J. C **45**, 97 (2006).

[32] M. Ablikim *et al.* (BESIII Collaboration), Phys. Rev. D **86**, 071101(R) (2012); X. L. Wang *et al.* (Belle Collaboration), Phys. Rev. D **87**, 051101(R) (2013); M. Ablikim *et al.* (BESIII Collaboration), Phys. Rev. D **91**, 112005 (2015).

[33] See Supplemental Material at http://link.aps.org/supplemental/10.1103/PhysRevLett.118.092001 for a summary of the number of signal events, luminosity, and cross section at each energy.

[34] K. Zhu, X. H. Mo, C. Z. Yuan, and P. Wang, Int. J. Mod. Phys. A **26**, 4511 (2011); A. D. Bukin, arXiv:0710.5627.

[35] $p_0 e^{-p_1(\sqrt{s}-M_{\rm th})}\Phi(\sqrt{s})$, where p_0 and p_1 are free parameters, $M_{\rm th} = 2m_\pi + m_{J/\psi}$ is the mass threshold of the $\pi^+\pi^- J/\psi$ system, and $\Phi(\sqrt{s})$ is the phase space factor.

[36] M. Ablikim *et al.* (BESIII Collaboration), Phys. Rev. D **87**, 012002 (2013).

nature physics

LETTERS

https://doi.org/10.1038/s41567-019-0494-8

Polarization and entanglement in baryon–antibaryon pair production in electron–positron annihilation

The BESIII Collaboration*

Particles directly produced at electron–positron colliders, such as the J/ψ meson, decay with relatively high probability into a baryon–antibaryon pair[1]. For spin-1/2 baryons, the pair can have the same or opposite helicites. A non-vanishing phase $\Delta\Phi$ between the transition amplitudes to these helicity states results in a transverse polarization of the baryons[2-4]. From the joint angular distribution of the decay products of the baryons, this phase as well as the parameters characterizing the baryon and the antibaryon decays can be determined. Here, we report the measurement of $\Delta\Phi = 42.4 \pm 0.6 \pm 0.5°$ using $\Lambda \to p\pi^-$ and $\bar{\Lambda} \to \bar{p}\pi^+, \bar{n}\pi^0$ decays at BESIII. We find a value for the $\Lambda \to p\pi^-$ decay parameter of $\alpha_- = 0.750 \pm 0.009 \pm 0.004$, 17 ± 3% higher than the current world average, which has been used as input for all Λ polarization measurements since 1978[5,6]. For $\bar{\Lambda} \to \bar{p}\pi^+$ we find $\alpha_+ = -0.758 \pm 0.010 \pm 0.007$, giving $A_{CP} = (\alpha_- + \alpha_+)/(\alpha_- - \alpha_+) = -0.006 \pm 0.012 \pm 0.007$, a precise direct test of charge–parity symmetry (CP) violation in Λ decays.

At the Beijing Electron–Positron Collider II (BEPC II), electrons and positrons annihilate, creating a resonance. Here, we study entangled pairs of baryons and antibaryons produced in the process $e^+e^- \to J/\psi \to \Lambda\bar{\Lambda}$, as illustrated in Fig. 1. The J/ψ resonance, a spin-1 meson with mass 3096.900(6) MeV c^{-2} and decay width 92.9(28) keV (ref. [6]), is produced at rest in a single photon annihilation process, which subsequently decays into a $\Lambda\bar{\Lambda}$ pair. The transition between the initial electron–positron pair and the final baryon–antibaryon pair includes helicity conserving and helicity-flip amplitudes[7–11]. Because the electron mass is negligible in comparison to the J/ψ mass, the initial electron and positron helicities have to be opposite. This implies that the angular distribution and polarization of the produced Λ and $\bar{\Lambda}$ particles can be described uniquely by only two quantities: the $J/\psi \to \Lambda\bar{\Lambda}$ angular distribution parameter α_ψ and the helicity phase $\Delta\Phi$. The value of the parameter α_ψ is well known[12–14], but the parameter $\Delta\Phi$ has never been measured before. If the phase difference $\Delta\Phi$ is non-vanishing, Λ and $\bar{\Lambda}$ will be polarized in the direction perpendicular to the production plane, and the magnitude of the polarization depends on the angle θ_Λ between the Λ momentum and the electron beam direction in the J/ψ rest frame (Fig. 1).

The polarization of weakly decaying particles, such as the Λ hyperons, can be inferred from the angular distribution of the daughter particles. In the case of decay $\Lambda \to p\pi^-$ and with the Λ hyperon polarization given by the vector $\mathbf{P}_\Lambda$, the angular distribution of the daughter protons is $\frac{1}{4\pi}(1 + \alpha_- \mathbf{P}_\Lambda \cdot \mathbf{n})$, where $\mathbf{n}$ is the unit vector along the proton momentum in the Λ rest frame. The asymmetry parameter α_- of the decay is bounded by $-1 \le \alpha_- \le 1$ and characterizes the degree of mixing of parity-conserving and parity-violating amplitudes in the process[15]. The corresponding asymmetry parameters α_+ for $\bar{\Lambda} \to \bar{p}\pi^+$, α_0 for $\Lambda \to n\pi^0$ and $\bar{\alpha}_0$ for $\bar{\Lambda} \to \bar{n}\pi^0$ are defined in the same way[6]. The joint angular distribution of $J/\psi \to \Lambda\bar{\Lambda}$ ($\Lambda \to f$ and $\bar{\Lambda} \to \bar{f}$, $f = p\pi^-$ or $n\pi^0$) depends on the Λ and $\bar{\Lambda}$ polarization and the spin correlation of the $\Lambda\bar{\Lambda}$ pair via the parameters α_ψ and $\Delta\Phi$. The spin correlation implies a correlation between the directions of the detected (anti-)nucleons. Together with the long lifetime of Λ and $\bar{\Lambda}$, this provides an example of a quantum entangled system as defined in refs. [16,17]. The joint angular distribution of the decay chain $J/\psi \to (\Lambda \to p\pi^-)(\bar{\Lambda} \to \bar{p}\pi^+)$ can be expressed as[4]

$$
\begin{aligned}
&\mathcal{W}(\boldsymbol{\xi}; \alpha_\psi, \Delta\Phi, \alpha_-, \alpha_+) \\
&= 1 + \alpha_\psi \cos^2\theta_\Lambda + \alpha_-\alpha_+ [\sin^2\theta_\Lambda (n_{1,x}n_{2,x} - \alpha_\psi n_{1,y}n_{2,y}) \\
&+ (\cos^2\theta_\Lambda + \alpha_\psi) n_{1,z}n_{2,z}] \\
&+ \alpha_-\alpha_+ \sqrt{1-\alpha_\psi^2} \cos(\Delta\Phi) \sin\theta_\Lambda \cos\theta_\Lambda (n_{1,x}n_{2,z} + n_{1,z}n_{2,x}) \\
&+ \sqrt{1-\alpha_\psi^2} \sin(\Delta\Phi) \sin\theta_\Lambda \cos\theta_\Lambda (\alpha_- n_{1,y} + \alpha_+ n_{2,y})
\end{aligned} \tag{1}
$$

where $\hat{\mathbf{n}}_1$ ($\hat{\mathbf{n}}_2$) is the unit vector in the direction of the nucleon (antinucleon) in the rest frame of Λ ($\bar{\Lambda}$). The components of these vectors are expressed using a coordinate system $(\hat{x}, \hat{y}, \hat{z})$ with the orientation shown in Fig. 1. The $\hat{z}$ axis of both Λ and $\bar{\Lambda}$ rest frames is oriented along the Λ momentum $\mathbf{p}_\Lambda$ in the J/ψ rest system. The $\hat{y}$ axis is perpendicular to the production plane and oriented along the vector $\mathbf{k}_- \times \mathbf{p}_\Lambda$, where $\mathbf{k}_-$ is the electron beam momentum in the J/ψ rest system. The variable ξ denotes the set of kinematic variables $(\theta_\Lambda, \hat{\mathbf{n}}_1, \hat{\mathbf{n}}_2)$, which uniquely specifies an event configuration. The terms multiplied by $\alpha_-\alpha_+$ in equation (1) represent the contribution from $\Lambda\bar{\Lambda}$ spin correlations, while the terms multiplied by α_- and α_+ separately represent the contribution from the polarization, P_y:

$$
P_y(\cos\theta_\Lambda) = \frac{\sqrt{1-\alpha_\psi^2} \sin(\Delta\Phi) \cos\theta_\Lambda \sin\theta_\Lambda}{1 + \alpha_\psi \cos^2\theta_\Lambda} \tag{2}
$$

The presence of all three contributions in equation (1) enables an unambiguous determination of the parameters α_ψ and $\Delta\Phi$ and the decay asymmetries α_-, α_+. If $\bar{\Lambda}$ is reconstructed via its $\bar{n}\pi^0$ decay, the parameters α_ψ, $\Delta\Phi$ and the decay asymmetries α_- and $\bar{\alpha}_0$ can be determined independently, because the corresponding angular distribution is obtained by replacing α_+ by $\bar{\alpha}_0$ and interpreting n_2 as the antineutron direction in equation (1). The case where Λ decays into $n\pi^0$ is not included in the present analysis because it suffers

*A full list of authors and affiliations appears in the online version of this paper.

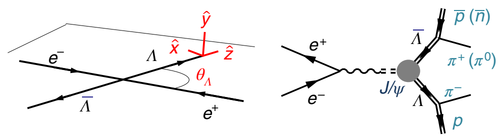

Fig. 1 | Illustration of the $e^+e^- \to J/\psi \to \Lambda\bar{\Lambda}$ process. Left: in the collision of the e^+ and e^- beams with opposite momenta the J/ψ particle is created and decays into a $\Lambda\bar{\Lambda}$ pair. The Λ particle is emitted in the $\hat{z}$ direction at an angle θ_Λ with respect to the e^- beam direction, and the $\bar{\Lambda}$ is emitted in the opposite direction. The hyperons are polarized in the direction perpendicular to the production plane ($\hat{y}$). The hyperons are reconstructed, and the polarization is determined by measuring their decay products: (anti-)nucleons and pions. Right: a Feynman diagram of $\Lambda\bar{\Lambda}$ pair production in e^+e^- annihilation with subsequent weak decays of Λ and $\bar{\Lambda}$.

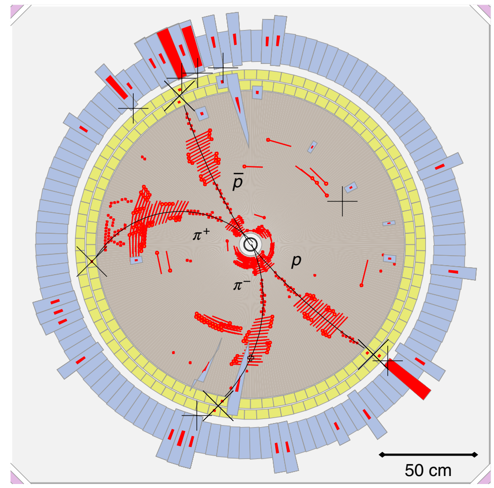

Fig. 2 | An example $J/\psi \to (\Lambda \to p\pi^-)(\bar{\Lambda} \to \bar{p}\pi^+)$ event in the BESIII detector. Cross-section of the detector in the plane perpendicular to the colliding electron–positron beams and a schematic representation of the information collected for the event. The mean decay length of the neutral $\Lambda(\bar{\Lambda})$ is 5 cm. The curved tracks of the charged particles from the subsequent $\Lambda(\bar{\Lambda})$ decays are registered in the drift chamber, indicated by the brown region of the display. The momenta of (anti-)baryons are greater than 750 MeV c^{-1} and pions are less than 300 MeV c^{-1}.

from low efficiency due to a selection criterion designed to suppress the combinatorial background.

The BESIII experiment[18] is located at the Beijing Electron–Positron Collider (BEPCII), where the centre-of-mass energy can be varied between 2 GeV and 4.6 GeV. The experiment is well known for the recent discoveries of exotic four-quark hadrons[19,20]. The cross-section of the BESIII detector in the plane perpendicular to the colliding beams is shown in Fig. 2. The inner part of the detector is a cylindrical tracking system that allows the determination of the momenta of charged particles from the track curvature in the magnetic field of a superconducting solenoid. An electromagnetic calorimeter outside the tracker measures energies deposited by particles. The signals from one $J/\psi \to (\Lambda \to p\pi^-)(\bar{\Lambda} \to \bar{p}\pi^+)$ event are shown in Fig. 2. A data sample of 1.31×10^9 J/ψ events is used in the analysis. The Λ hyperons are reconstructed using their $p\pi^-$ decays and the $\bar{\Lambda}$ hyperons using their $\bar{p}\pi^+$ or $\bar{n}\pi^0$ decays. The event reconstruction and selection procedures are described in the Methods. The resulting data samples are essentially background-free, as shown in Supplementary Figs. 1 and 2. A sample of Monte Carlo (MC) simulated events including all known J/ψ decays is used to determine the background contribution. The sizes of the final data samples are 420,593 and 47,009 events, with an estimated background of 399 ± 20 and 66.0 ± 8.2 events for the $p\pi^-\bar{p}\pi^+$ and $p\pi^-\bar{n}\pi^0$ final states, respectively. For each event the full set of the kinematic variables $\boldsymbol{\xi}$ is reconstructed.

The free parameters describing the angular distributions for the two data sets—α_ψ, $\Delta\Phi$, α_-, α_+ and $\bar{\alpha}_0$—are determined from a simultaneous unbinned maximum likelihood fit. In the fit, the likelihood function is constructed from the probability density function for an event characterized by the vector $\boldsymbol{\xi}^{(i)}$:

$$\mathcal{P}(\boldsymbol{\xi}^{(i)};\alpha_\psi,\Delta\Phi,\alpha_-,\alpha_2)=\mathcal{C}\mathcal{W}(\boldsymbol{\xi}^{(i)};\alpha_\psi,\Delta\Phi,\alpha_-,\alpha_2)\epsilon(\boldsymbol{\xi}^{(i)}) \qquad (3)$$

with $\alpha_2=\alpha_+$ and $\alpha_2=\bar{\alpha}_0$ for the $p\pi^-\bar{p}\pi^+$ and $p\pi^-\bar{n}\pi^0$ data sets, respectively. The joint angular distribution $\mathcal{W}(\boldsymbol{\xi};\alpha_\psi,\Delta\Phi,\alpha_-,\alpha_2)$ is given by equation (1), and $\epsilon(\boldsymbol{\xi})$ is the detection efficiency. The normalization factor $\mathcal{C}^{-1}=\int\mathcal{W}(\boldsymbol{\xi};\alpha_\psi,\Delta\Phi,\alpha_-,\alpha_2)\epsilon(\boldsymbol{\xi})\mathrm{d}\boldsymbol{\xi}$ has to be evaluated for each choice of parameters (α_ψ, $\Delta\Phi$, α_-, α_2). The maximum log likelihood fit including the normalization procedure is described in the Methods. The resulting global fit describes the multidimensional angular distributions very well, as illustrated in Supplementary Figs. 3 and 4. For a crosscheck, the fit was applied to the two data sets separately, and the obtained values of the parameters agree within statistical uncertainties as shown in Supplementary Table 1. The details of the fit as well the evaluation of the systematic uncertainties are discussed in the Methods, and the contributions to the systematic uncertainty are listed in Supplementary Table 2.

A clear polarization signal, strongly dependent on the Λ direction, $\cos\theta_\Lambda$, is observed for Λ and $\bar{\Lambda}$. In Fig. 3, the moment

$$\mu(\cos\theta_\Lambda)=\frac{m}{N}\sum_{i=1}^{N_k}(n_{1,y}^{(i)}-n_{2,y}^{(i)}) \qquad (4)$$

related to the polarization, is calculated for $m=50$ bins in $\cos\theta_\Lambda$. N is the total number of events in the data sample and N_k is the number of events in the kth $\cos\theta_\Lambda$ bin. The expected angular dependence of the moment is

$$\mu(\cos\theta_\Lambda)=\frac{\alpha_--\alpha_2}{2}\frac{1+\alpha_\psi\cos^2\theta_\Lambda}{3+\alpha_\psi}P_y(\theta_\Lambda) \qquad (5)$$

for the acceptance corrected data. The helicity phase is determined to be $\Delta\Phi=(42.4\pm0.6\pm0.5)°$, where the first uncertainty is statistical and the second systematic. This corresponds to the Λ and $\bar{\Lambda}$ transverse polarization dependence on $\cos\theta_\Lambda$ as shown in Supplementary Fig. 5 with the maximum polarization of 24.8% (ref. [3]). This large value of $\Delta\Phi$ enables a simultaneous determination of the decay asymmetry parameters for $\Lambda\to p\pi^-$, $\bar{\Lambda}\to\bar{p}\pi^+$ and $\bar{\Lambda}\to\bar{n}\pi^0$, as shown in Table 1. The value of $\alpha_-=0.750\pm0.009\pm0.004$ differs by more than 5 s.d. from the world average of $\alpha_-^{\mathrm{PDG}}=0.642\pm0.013$ established in 1978 (PDG, Particle Data Group)[5]. We note that the two most precise results[21,22] included in the average were obtained by measuring the asymmetry in the secondary scattering of the polarized protons from Λ decays on a Carbon target. The α_- value was then determined using a compilation of the polarized proton scattering data on Carbon[23], which is no longer in use (data sets[24–26] are used instead). In addition, the average value α_-^{PDG} does not include a systematical uncertainty of 5% mentioned in ref. [21], which points to the need for a critical reevaluation of the α_-^{PDG} value. Considering the caveats concerning the current world average α_-^{PDG}, our new result implies that all published measurements on $\Lambda/\bar{\Lambda}$ polarization derived using α_-^{PDG} are 17 ± 3% too large. The value obtained for

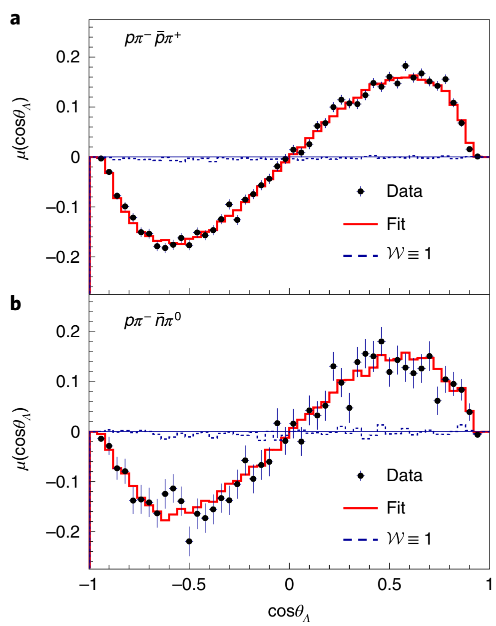

Fig. 3 | The polarization signal for $\Lambda(\bar{\Lambda})$ in $e^+e^- \to J/\psi \to \Lambda\bar{\Lambda}$. a,b, For each event, the weight $(n_{1,y}^{(i)} - n_{2,y}^{(i)})$ is calculated and the average weight $\mu(\cos\theta_\Lambda)$ is obtained using equation (4) for $m=50$ bins in $\cos\theta_\Lambda$. The moments $\mu(\cos\theta_\Lambda)$ are plotted as a function of $\cos\theta_\Lambda$ for $p\pi^-\bar{p}\pi^+$ (**a**) and $p\pi^-\bar{n}\pi^0$ (**b**) data sets. Filled circles indicate BESIII data and solid red lines show the result of the global fit based on equation (3). The dashed line represents the expected distribution without polarization $\mathcal{W}(\boldsymbol{\xi}; 0, 0, 0, 0) \equiv 1$ in equation (3). The errors are 1 s.d. statistical and calculated by error propagation of equation (4).

Table 1 | Summary of the results

Parameters	This work	Previous results
α_ψ	$0.461 \pm 0.006 \pm 0.007$	0.469 ± 0.027 (ref. [14])
$\Delta\Phi$	$42.4 \pm 0.6 \pm 0.5°$	-
α_-	$0.750 \pm 0.009 \pm 0.004$	0.642 ± 0.013 (ref. [6])
α_+	$-0.758 \pm 0.010 \pm 0.007$	-0.71 ± 0.08 (ref. [6])
$\bar{\alpha}_0$	$-0.692 \pm 0.016 \pm 0.006$	-
A_{CP}	$-0.006 \pm 0.012 \pm 0.007$	0.006 ± 0.021 (ref. [6])
$\bar{\alpha}_0/\alpha_+$	$0.913 \pm 0.028 \pm 0.012$	-

Parameters: $J/\psi \to \Lambda\bar{\Lambda}$ angular distribution parameter α_ψ, helicity phase $\Delta\Phi$, asymmetry parameters for the $\Lambda \to p\pi^-$ (α_-), $\bar{\Lambda} \to \bar{p}\pi^+$ (α_+) and $\bar{\Lambda} \to \bar{n}\pi^0$ ($\bar{\alpha}_0$) decays, CP asymmetry A_{CP} and ratio $\bar{\alpha}_0/\alpha_+$. The first uncertainty is 1 s.d. statistical, and the second is systematic, calculated as described in the Methods.

the ratio $\bar{\alpha}_0/\alpha_+$ is 3σ smaller than unity, indicating an isospin three-half contribution to the final state[27–29]. The reported values of α_- and α_+, along with the covariance (reported in the Methods), enable a calculation of the CP odd observable $A_{CP} = (\alpha_- + \alpha_+)/(\alpha_- - \alpha_+) = -0.006 \pm 0.012 \pm 0.007$, where the uncertainties refer to statistical and systematic, respectively. This is the most sensitive test of CP violation for Λ baryons with a substantially improved precision over previous measurements[30] (Table 1) using a direct method. The Standard Model calculations predict $A_{CP} \approx 10^{-4}$ (ref. [31]), while larger values are expected in various extensions of the Standard Model aiming to explain the observed baryon–antibaryon asymmetry in the universe[32]. This new method to test for CP violation in baryon decays is expected to reach sensitivities comparable to theoretical predictions when larger data sets of foreseen experiments become available.

Online content

Any methods, additional references, Nature Research reporting summaries, source data, statements of code and data availability and associated accession codes are available at https://doi.org/10.1038/s41567-019-0494-8.

Received: 30 May 2018; Accepted: 11 March 2019;
Published online: 6 May 2019

References

1. Kopke, L. & Wermes, N. *J/ψ* decays. *Phys. Rep.* **174**, 67–227 (1989).
2. Cabibbo, N. & Gatto, R. Electron positron colliding beam experiments. *Phys. Rev.* **124**, 1577–1595 (1961).
3. Brodsky, S. J., Carlson, C. E., Hiller, J. R. & Hwang, D. S. Single spin polarization effects and the determination of time-like proton form-factors. *Phys. Rev. D* **69**, 054022 (2004).
4. Fäldt, G. & Kupsc, A. Hadronic structure functions in the $e^+e^- \to \bar{\Lambda}\Lambda$ reaction. *Phys. Lett. B* **772**, 16–20 (2017).
5. Bricman, C. et al. Review of particle properties. *Phys. Lett. B* **75**, 1–250 (1978).
6. Tanabashi, M. et al. Review of particle physics. *Phys. Rev. D* **98**, 030001 (2018).
7. Dubnickova, A. Z., Dubnicka, S. & Rekalo, M. P. Investigation of the nucleon electromagnetic structure by polarization effects in $e^+e^- \to N\bar{N}$ processes. *Nuovo Cim. A* **109**, 241–256 (1996).
8. Gakh, G. I. & Tomasi-Gustafsson, E. General analysis of polarization phenomena in $e^+ + e^- \to N + \bar{N}$ for axial parametrization of two-photon exchange. *Nucl. Phys. A* **771**, 169–183 (2006).
9. Czyz, H., Grzelinska, A. & Kuhn, J. H. Spin asymmetries and correlations in lambda-pair production through the radiative return method. *Phys. Rev. D* **75**, 074026 (2007).
10. Fäldt, G. Entanglement in joint $\Lambda\bar{\Lambda}$ decay. *Eur. Phys. J. A* **51**, 74 (2015).
11. Fäldt, G. Polarization observables in the $e^+e^- \to \bar{\Lambda}\Lambda$ reaction. *Eur. Phys. J. A* **52**, 141 (2016).
12. Bai, J. Z. et al. Decays of the *J/ψ* to $\Lambda\bar{\Lambda}$, $\Lambda\bar{\Lambda}\gamma$ and $\Lambda\bar{\Lambda}$, $\Lambda\bar{\Lambda}\gamma$ final states. *Phys. Lett. B* **424**, 213–218 (1998). Erratum **438**, 447 (1998).
13. Ablikim, M. et al. Measurement of *J/ψ* decays into $\Lambda\bar{\Lambda}\pi^+\pi^-$. *Chin. Phys. C* **36**, 1031–1039 (2012).
14. Ablikim, M. et al. Study of *J/ψ* and *ψ*(3686) decay to $\Lambda\bar{\Lambda}$ and $\Lambda\bar{\Lambda}$ final states. *Phys. Rev. D* **95**, 052003 (2017).
15. Lee, T. D. & Yang, C.-N. General partial wave analysis of the decay of a hyperon of spin 1/2. *Phys. Rev.* **108**, 1645–1647 (1957).
16. Tornqvist, N. A. Suggestion for Einstein–Podolsky–Rosen experiments using reactions like $e^+e^- \to \Lambda\bar{\Lambda} \to \pi^-p\pi^+\bar{p}$. *Found. Phys.* **11**, 171–177 (1981).
17. Hiesmayr, B. C. Limits of quantum information in weak interaction processes of hyperons. *Sci. Rep.* **5**, 11591 (2015).
18. Ablikim, M. et al. Design and construction of the BESIII detector. *Nucl. Instrum. Methods* **A614**, 345–399 (2010).
19. Ablikim, M. et al. Observation of a charged charmonium like structure in $e^+e^- \to \pi^+\pi^-J/\psi$ at $\sqrt{s} = 4.26$ GeV. *Phys. Rev. Lett.* **110**, 252001 (2013).
20. Shepherd, M. R., Dudek, J. J. & Mitchell, R. E. Searching for the rules that govern hadron construction. *Nature* **534**, 487–493 (2016).
21. Overseth, O. E. & Roth, R. F. Time reversal invariance in Λ^0 decay. *Phys. Rev. Lett.* **19**, 391–393 (1967).
22. Cleland, W. E. et al. A measurement of the beta-parameter in the charged nonleptonic decay of the Λ^0 hyperon. *Nucl. Phys.* **B40**, 221–254 (1972).
23. Peterson, V. Z. *Analyzing Power of Carbon for High-Energy Polarized Protons* Report No. LRL-UCRL-10622 https://escholarship.org/uc/item/7777n2h0 (1963).
24. Besset, D. et al. Proton Carbon analyzing power between 300 MeV and 560 MeV. *Nucl. Instrum. Methods* **166**, 379–389 (1979).
25. Aprile-Giboni, E. et al. Proton carbon effective analyzing power between 95 MeV and 570 MeV. *Nucl. Instrum. Methods* **215**, 147–157 (1983).
26. Mcnaughton, M. W. et al. The p-C analyzing power between 100 MeV and 750 MeV. *Nucl. Instrum. Methods* **A241**, 435–440 (1985).
27. Overseth, O. E. & Pakvasa, S. Final-state interactions in nonleptonic hyperon decay. *Phys. Rev.* **184**, 1663–1667 (1969).
28. Olsen, S. et al. Asymmetry parameter for $\Lambda^0 \to n\pi^0$. *Phys. Rev. Lett.* **24**, 843–847 (1970).
29. Cheng, H.-Y. Status of the $\Delta I = 1/2$ rule in kaon decay. *Int. J. Mod. Phys.* **A4**, 495 (1989).
30. Barnes, P. D. et al. Observables in high statistics measurements of the reaction $\bar{p}p \to \bar{\Lambda}\Lambda$. *Phys. Rev. C* **54**, 1877–1886 (1996).

31. Donoghue, J. F., He, X.-G. & Pakvasa, S. Hyperon decays and CP nonconservation. *Phys. Rev. D* **34**, 833–842 (1986).
32. Bigi, I. I., Kang, X.-W. & Li, H.-B. CP asymmetries in strange baryon decays. *Chin. Phys. C* **42**, 013101 (2018).

Acknowledgements

The BESIII collaboration thanks the staff of BEPCII and the IHEP computing centre for their support. This work is supported in part by the National Key Basic Research Program of China under contract no. 2015CB856700; the National Natural Science Foundation of China (NSFC) under contract nos. 11335008, 11375205, 11425524, 11625523, 11635010, 11735014, 11835012 and 11875054; the Chinese Academy of Sciences (CAS) Large-Scale Scientific Facility Program; the CAS Center for Excellence in Particle Physics (CCEPP); Joint Large-Scale Scientific Facility Funds of the NSFC and CAS under contract nos. U1532257, U1532258, U1732102, U1732263 and U1832207; CAS Key Research Program of Frontier Sciences under contract nos. QYZDJ-SSW-SLH003 and QYZDJ-SSW-SLH040; 100 Talents Program of CAS; the CAS President's International Fellowship Initiative; INPAC and Shanghai Key Laboratory for Particle Physics and Cosmology; German Research Foundation DFG under the contracts Collaborative Research Center CRC 1044 and FOR 2359; Istituto Nazionale di Fisica Nucleare, Italy; Koninklijke Nederlandse Akademie van Wetenschappen (KNAW) under contract no. 530-4CDP03; Ministry of Development of Turkey under contract no. DPT2006K-120470; National Science and Technology fund; The Swedish Research Council; the Knut and Alice Wallenberg Foundation; US Department of Energy under contract nos. DE-FG02-05ER41374, DE-SC-0010118, DE-SC-0010504 and DE-SC-0012069; University of Groningen (RuG); Helmholtzzentrum fuer Schwerionenforschung GmbH (GSI), Darmstadt. All consortium work was carried out at affiliations 1–67.

Author contributions

All authors have contributed to this publication, being variously involved in the design and construction of the detectors, writing software, calibrating sub-systems, operating the detectors, acquiring data and analysing the processed data.

Competing interests

The authors declare no competing interests.

Additional information

Supplementary information is available for this paper at https://doi.org/10.1038/s41567-019-0494-8.

Reprints and permissions information is available at www.nature.com/reprints.

Correspondence and requests for materials should be addressed to A.Kupsc.

Journal peer review information: *Nature Physics* thanks Anna Zuzana Dubnickova, Ulrik Egede and Ilya Selyuzhenkov for their contribution to the peer review of this work.

Publisher's note: Springer Nature remains neutral with regard to jurisdictional claims in published maps and institutional affiliations.

Methods

Monte Carlo simulation. The optimization of event selection criteria and the estimation of backgrounds are based on Monte Carlo (MC) simulations. The Geant4-based simulation software includes the geometry and the material description of the BESIII spectrometer, the detector response and the digitization models, as well as the database of the running conditions and detector performance. Production of the J/ψ resonance is simulated by the MC event generator kkmc[33]; the known decays are generated by Besevtgen[34,35] with branching ratios set to the world average values[6], and missing decays are generated by the Lundcharm[36] model with optimized parameters[37]. Signal and background events are generated using helicity amplitudes. For the signal process $J/\psi \to \Lambda\bar{\Lambda}$, the angular distribution of equation (1) is used. For the backgrounds, $J/\psi \to \Sigma^0\bar{\Sigma}^0$, $\Sigma^+\bar{\Sigma}^-$ and $\Lambda\bar{\Sigma}^0$ + c.c. decays, the helicity amplitudes are taken from ref. [38] and the angular distribution parameters are fixed to −0.24 (ref. [39]) for $J/\psi \to \Sigma^0\bar{\Sigma}^0$ and $J/\psi \to \Sigma^+\bar{\Sigma}^-$ and to 0.38 (ref. [40]) for $J/\psi \to \Lambda\bar{\Sigma}^0$ + c.c.

General selection criteria. Charged tracks detected in the main drift chamber (MDC) must satisfy $|\cos\theta| < 0.93$, where θ is the polar angle with respect to the positron beam direction. No additional particle identification requirements are applied to select the tracks. Showers in the electromagnetic calorimeter (EMC) not associated with any charged track are identified as photon candidates if they fulfil the following requirements: the deposited energy is required to be larger than 25 MeV and 50 MeV for clusters reconstructed in the barrel ($|\cos\theta| < 0.8$) and end cap ($0.86 < |\cos\theta| < 0.92$), respectively. To suppress electronic noise and showers unrelated to the event, the EMC time difference from the event start time is required to be within [0, 700] ns. To remove showers originating from charged particles, the angle between the shower position and charged tracks extrapolated to the EMC must be greater than 10°.

Selection of $J/\psi \to \Lambda\bar{\Lambda}, \Lambda \to p\pi^-, \bar{\Lambda} \to \bar{p}\pi^+$. Events with at least four charged tracks are selected. Fits of the Λ and $\bar{\Lambda}$ vertices are performed using all pairs of positive and negative charged tracks. There should be at least one $\Lambda\bar{\Lambda}$ pair in an event. If more than one set of $\Lambda\bar{\Lambda}$ pairs is found (the fraction of such events is 1.18%), the one with the smallest value of $(M_{p\pi^-} - M_\Lambda)^2 + (M_{\bar{p}\pi^+} - M_\Lambda)^2$, where M_Λ is the nominal Λ mass, is retained for further analysis. A four-constraint kinematic fit imposing overall energy–momentum conservation (4C-fit) is performed with the $\Lambda \to p\pi^-$ and $\bar{\Lambda} \to \bar{p}\pi^+$ hypothesis, and events with $\chi^2 < 60$ are retained. The invariant masses of $p\pi^-$ and $\bar{p}\pi^+$ are required to be within $|M_{p\pi^-} - M_\Lambda| < 5\,\mathrm{MeV}\,c^{-2}$ and $|M_{\bar{p}\pi^+} - M_\Lambda| < 5\,\mathrm{MeV}\,c^{-2}$. The $p\pi^-$ and $\bar{p}\pi^+$ invariant mass spectra and the selection windows are shown in Supplementary Fig. 1.

Selection of $J/\psi \to \Lambda\bar{\Lambda}, \Lambda \to p\pi^-, \bar{\Lambda} \to \bar{n}\pi^0$. Events with at least two charged tracks and at least three showers are selected. Two showers, consistent with being photons, are used to reconstruct the π^0 candidates, and the invariant mass of the photon pair is required to be in the interval [0.12, 0.15] GeV c^{-2}. To improve the momentum resolution, a mass-constrained fit to the π^0 nominal mass is applied to the photon pairs, and the resulting energy and momentum of the π^0 are used for further analysis. Candidates for Λ are formed by combining two oppositely charged tracks into the final states $p\pi^-$. The two daughter tracks are constrained to originate from a common decay vertex by requiring the χ^2 of the vertex fit to be less than 100. The maximum energy for the photons from π^0 decays in these events is 300 MeV. Therefore, showers produced by $\bar{n}$ can be uniquely identified by selecting the cluster with an energy deposit larger than 350 MeV. In addition, the second moment of the cluster is required to be larger than 20 cm². The moment is defined as $\sum_i E_i r_i^2 / \sum_i E_i$, where E_i is the deposited energy in the ith crystal, and r_i is the radial distance of the crystal i from the cluster centre. To select the $J/\psi \to \Lambda(p\pi^-)\bar{\Lambda}(\bar{n}\pi^0)$ candidate events, a one-constraint (1C) kinematic fit is performed, where the momentum of the anti-neutron is unmeasured. The selected events are required to have a $\chi^2_{1C-\bar{n}}$ of the 1C kinematic fit less than 10, and if there is more than one combination, the one with the smallest $\chi^2_{1C-\bar{n}}$ value is chosen. To further suppress background contributions, we require $|M_{p\pi^-} - M_\Lambda| < 5\,\mathrm{MeV}\,c^{-2}$, where M_Λ is the nominal Λ mass. Supplementary Fig. 2 shows the invariant mass ($M_{\bar{n}\pi^0}$) of the $\bar{n}\pi^0$ pair and the mass $M^{\mathrm{Recoiling}}_{\Lambda\pi^0}$ recoiling against the $\Lambda\pi^0$, where $M_{\bar{n}\pi^0} = \sqrt{(E_{\bar{n}} + E_{\pi^0})^2 - (\vec{P}_{\bar{n}} + \vec{P}_{\pi^0})^2}$, $\vec{P}_{\bar{n}} = -(\vec{P}_{\Lambda} + \vec{P}_{\pi^0})$ is evaluated in the rest frame of J/ψ, and $E_{\bar{n}} = \sqrt{|\vec{P}_{\bar{n}}|^2 + M_n^2}$ (with M_n the nominal neutron mass). The signal regions are defined as $|M_{\bar{n}\pi^0} - M_\Lambda| < 23\,\mathrm{MeV}\,c^{-2}$ and $|M^{\mathrm{Recoiling}}_{\Lambda\pi^0} - M_n| < 7\,\mathrm{MeV}\,c^{-2}$ as shown in Supplementary Fig. 2. The above selection strategy is not suitable for the channel $J/\psi \to \Lambda\bar{\Lambda}, \Lambda \to n\pi^0, \bar{\Lambda} \to \bar{p}\pi^+$. The reason for this is the requirement of the energy deposit of 350 MeV used to identify the neutron cluster. We estimate that the overall efficiency would be lower by at least a factor of four with respect to the $J/\psi \to \Lambda\bar{\Lambda}, \Lambda \to p\pi^-, \bar{\Lambda} \to \bar{n}\pi^0$ channel.

Background analysis. The potential backgrounds are studied using the inclusive MC sample for J/ψ decays. After applying the same selection criteria as for the signal, the main backgrounds for the $\bar{\Lambda} \to \bar{p}\pi^+$ final state are from $J/\psi \to \gamma\Lambda\bar{\Lambda}$, $\Lambda\bar{\Sigma}^0$ + c.c., $\Sigma^0\bar{\Sigma}^0$, $\Delta^{++}\bar{p}\pi^-$ + c.c., $\Delta^{++}\bar{\Delta}^{--}$ and $p\pi^-\bar{p}\pi^+$ decays. Decays of $J/\psi \to \Lambda\bar{\Sigma}^0$ + c.c. and $\Sigma^0\bar{\Sigma}^0$ are generated using the helicity amplitudes and include subsequent Λ and $\bar{\Lambda}$ decays. The remaining decay modes are generated according to the phase space model, and the contribution is shown in Supplementary Fig. 1. For the $\bar{\Lambda} \to \bar{n}\pi^0$ final state, the dominant background processes are from the decay modes $J/\psi \to \gamma\Lambda\bar{\Lambda}$, $\Lambda\bar{\Sigma}^0$ + c.c., $\Sigma^0(\gamma\Lambda)\bar{\Sigma}^0(\gamma\bar{\Lambda})$, $\Sigma^+(p\pi^0)\bar{\Sigma}^-(\bar{n}\pi^-)$ and $\Lambda(p\pi^-)\bar{\Lambda}(\bar{p}\pi^+)$. Exclusive MC samples for these background channels are generated and used to estimate the background contamination shown in Supplementary Fig. 2.

The global fit. Based on the joint angular distribution shown in equation (1), a simultaneous fit is performed to the two data sets according to the decay modes:

$$\mathrm{I}: J/\psi \to \Lambda\bar{\Lambda}, \Lambda \to p\pi^- \text{ and } \bar{\Lambda} \to \bar{p}\pi^+$$
$$\mathrm{II}: J/\psi \to \Lambda\bar{\Lambda}, \Lambda \to p\pi^- \text{ and } \bar{\Lambda} \to \bar{n}\pi^0$$

There are three common parameters (α_ψ, $\Delta\Phi$ and α_-) and two separate parameters (α_+ and $\bar{\alpha}_0$) for the $\bar{\Lambda}$ decays to $\bar{p}\pi^+$ and $\bar{n}\pi^0$, respectively. For data set I, the joint likelihood function is defined as[38]

$$\begin{aligned}\mathcal{L}^{\mathrm{I}} &= \prod_{i=1}^{N^{\mathrm{I}}} \mathcal{P}(\xi_{\mathrm{I}}^{(i)}; \alpha_\psi, \Delta\Phi, \alpha_-, \alpha_+) \\ &= (\mathcal{C}^{\mathrm{I}})^{N^{\mathrm{I}}} \prod_{i=1}^{N^{\mathrm{I}}} \mathcal{W}(\xi_{\mathrm{I}}^{(i)}; \alpha_\psi, \Delta\Phi, \alpha_-, \alpha_+)\epsilon(\boldsymbol{\xi}_{\mathrm{I}}^{(i)})\end{aligned} \tag{6}$$

where $\mathcal{P}(\xi_{\mathrm{I}}^{(i)}; \alpha_\psi, \Delta\Phi, \alpha_-, \alpha_+)$ is the probability density function defined in equation (3) and evaluated for the kinematic variables $\xi_{\mathrm{I}}^{(i)}$ of event i, and $\mathcal{W}(\xi_{\mathrm{I}}^{(i)}; \alpha_\psi, \Delta\Phi, \alpha_-, \alpha_+)$ is defined in equation (1). The detection efficiency terms, $\epsilon(\boldsymbol{\xi}_{\mathrm{I}}^{(i)})$, can be set arbitrarily to one because they do not influence the minimization of the function $-\ln\mathcal{L}^{\mathrm{I}}$ with respect to the parameters α_ψ, $\Delta\Phi$, α_- and α_+. The normalization factor $(\mathcal{C}^{\mathrm{I}})^{-1} = \frac{1}{N_{\mathrm{MC}}}\sum_{j=1}^{N_{\mathrm{MC}}} \mathcal{W}(\xi^{(j)}I; \alpha_\psi, \Delta\Phi, \alpha_-, \alpha_+)$ is estimated with the accepted N_{MC} events, which are generated with the phase space model, undergo detector simulation and are selected with the same event criteria as for data. To ensure an accurate value for the normalization factor, N_{MC} is 7,850,525 for $p\bar{p}\pi^+\pi^-$ and 907,253 for $p\bar{n}\pi^+\pi^0$. The definition of the likelihood function for data set II, $\mathcal{L}^{\mathrm{II}}$, is the same except for its calculation with different parameters and data set. To determine the parameters, we use the package MINUIT from the CERN library[41] to minimize the function defined as

$$S = -\ln\mathcal{L}^{\mathrm{I}}_{\mathrm{data}} - \ln\mathcal{L}^{\mathrm{II}}_{\mathrm{data}} + \ln\mathcal{L}^{\mathrm{I}}_{\mathrm{bg.}} + \ln\mathcal{L}^{\mathrm{II}}_{\mathrm{bg.}} \tag{7}$$

where $\ln\mathcal{L}^{\mathrm{I(II)}}_{\mathrm{data}}$ and $\ln\mathcal{L}^{\mathrm{I(II)}}_{\mathrm{bg.}}$ are the likelihood functions for the two data sets and the background events taken from simulation, respectively. The results of the separate fits for the two data sets are given in Supplementary Table 1. We compare the fit with the data using moments $T_1, \ldots, T_5$ directly related to the terms in equation (1). The moments are calculated for 100 bins in $\cos\theta_\Lambda$ and are explicitly given by

$$\begin{aligned}T_1 &= \sum_{i=1}^{N_k} (\sin^2\theta_\Lambda n_{1,x}^{(i)} n_{2,x}^{(i)} + \cos^2\theta_\Lambda n_{1,z}^{(i)} n_{2,z}^{(i)}) \\ T_2 &= -\sum_{i=1}^{N_k} \sin\theta_\Lambda \cos\theta_\Lambda (n_{1,x}^{(i)} n_{2,z}^{(i)} + n_{1,z}^{(i)} n_{2,x}^{(i)}) \\ T_3 &= -\sum_{i=1}^{N_k} \sin\theta_\Lambda \cos\theta_\Lambda n_{1,y}^{(i)} \\ T_4 &= -\sum_{i=1}^{N_k} \sin\theta_\Lambda \cos\theta_\Lambda n_{2,y}^{(i)} \\ T_5 &= \sum_{i=1}^{N_k} (n_{1,z}^{(i)} n_{2,z}^{(i)} - \sin^2\theta_\Lambda n_{1,y}^{(i)} n_{2,y}^{(i)})\end{aligned} \tag{8}$$

where N_k is the number of events in the kth $\cos\theta_\Lambda$ bin. Supplementary Figs. 3 and 4 show the moments and the Λ angular distribution for data compared to those calculated using the probability density function $\mathcal{P}(\xi; \alpha_\psi, \Delta\Phi, \alpha_-, \alpha_2)$ with the parameters set to the values from the global fit. The unsymmetric distributions of T_3 and T_4 indicate that significant transverse polarization of Λ and $\bar{\Lambda}$ hyperons is observed. The simultaneous fit results for α_ψ, α_-, α_+, $\Delta\Phi$ and $\bar{\alpha}_0$ parameters are given in Supplementary Table 1. Based on these parameters, the observables $\bar{\alpha}_0/\alpha_+$ and $A_{\mathrm{CP}} = (\alpha_- + \alpha_+)/(\alpha_- - \alpha_+)$ are calculated, and their statistical uncertainties are evaluated taking into account the correlation coefficients $\rho(\alpha_+, \alpha_0) = 0.42$ and $\rho(\alpha_+, \alpha_-) = 0.82$, respectively. As a cross-check, separate fits to data sets I and II are performed, and the results are consistent with the simultaneous fit within statistical uncertainties, as shown in Supplementary Table 1.

Systematic uncertainty. The systematic uncertainties can be divided into two categories. The first category is from the event selection, including the uncertainties on MDC tracking efficiency, the kinematic fit, π^0 and $\bar{n}$ efficiencies,

Λ and $\bar{\Lambda}$ reconstruction, background estimation and the Λ, $\bar{\Lambda}$ and $M^{\mathrm{Recoiling}}_{\Lambda\pi^0}$ mass window requirements. The second category includes uncertainties associated with the fit procedure based on equations (1) and (3).

(1) The uncertainty due to the efficiency of charged particle tracking has been investigated with control samples of $J/\psi \to \Lambda\bar{\Lambda} \to p\pi^-\bar{p}\pi^+$ (ref. [42]), taking into consideration the correlation between the magnitude of charged particle momentum and its polar angle acceptances. Corrections are made based on the two-dimensional distribution of track momentum versus polar angle. The difference between the fit results with and without the tracking correction is taken as a systematic uncertainty.

(2) The uncertainty due to the π^0 reconstruction is estimated from the difference between data and MC simulation using a $J/\psi \to \pi^+\pi^-\pi^0$ control sample. The uncertainty due to the $\bar{n}$ shower requirement is estimated with a $J/\psi \to p\pi^-\bar{n}$ control sample, and the correction factors between data and MC simulations are determined. The differences in the fit results with and without corrections to the efficiencies of the π^0 and $\bar{n}$ reconstructions are taken as systematic uncertainties.

(3) The systematic uncertainties for the determination of the physics parameters in the fits due to the Λ and $\bar{\Lambda}$ vertex reconstructions are found to be negligible.

(4) The systematic uncertainties due to kinematic fits are determined by making corrections to the track parameters distributions in the MC simulations to better match the data. The corrections are done with the five-dimensional distributions over the θ_Λ, $\hat{\mathbf{n}}_1$, $\hat{\mathbf{n}}_2$ variables, where $\hat{\mathbf{n}}_1$ and $\hat{\mathbf{n}}_2$ are expressed using spherical coordinates. The fit to data with the corrected MC sample yields $\alpha_\psi = 0.462 \pm 0.006$, $\alpha_- = 0.749 \pm 0.009$, $\alpha_+ = -0.752 \pm 0.009$ and $\bar{\alpha}_0 = -0.688 \pm 0.017$. The differences between the fit with corrections and the nominal fit are considered as the systematic uncertainties. For α_ψ, the difference between the fit results with and without this correction is negligible.

(5) A possible bias and uncertainty due to the fit procedure is estimated using MC simulation, where the parameters in the joint angular distribution equation (1) are set to the central values of Table 1 and the number of generated events is the same as for the data. This procedure tests also if the number of MC events used for normalization of the probability density function in equation (6) is sufficient.

(6) The systematic uncertainty caused by the background estimation is studied by fitting the data with and without considering background subtraction. The differences in the parameters are taken as the systematic uncertainties. The contamination rate of background events in this analysis is less than 0.1% according to the full MC simulations, and the uncertainty due to the background estimation is negligible.

The total systematic uncertainty for the parameters is obtained by summing the individual systematic uncertainties in quadrature (summarized in Supplementary Table 2).

Data availability

The data that support the plots within this paper and other findings of this study are available from the corresponding author upon reasonable request.

References

33. Jadach, S., Ward, B. F. L. & Was, Z. The precision Monte Carlo event generator *KK* for two fermion final states in e^+e^- collisions. *Comput. Phys. Commun.* **130**, 260–325 (2000).
34. Lange, D. J. The EvtGen particle decay simulation package. *Nucl. Instrum. Methods* **A462**, 152–155 (2001).
35. Ping, R.-G. Event generators at BESIII. *Chin. Phys. C* **32**, 599 (2008).
36. Chen, J. C., Huang, G. S., Qi, X. R., Zhang, D. H. & Zhu, Y. S. Event generator for J/ψ and $\psi(2S)$ decay. *Phys. Rev. D* **62**, 034003 (2000).
37. Yang, R.-L., Ping, R.-G. & Chen, H. Tuning and validation of the Lundcharm model with J/ψ decays. *Chin. Phys. Lett.* **31**, 061301 (2014).
38. Zhong, B., Ping, R.-G. & Xiao, Z.-J. Study of $\bar{\Lambda}$ decay parameter in $\bar{\Lambda}$ decay. *Chin. Phys. C* **32**, 692 (2008).
39. Ablikim, M. et al. Study of J/ψ decays to $\Lambda\bar{\Lambda}$ and $\Lambda\bar{\Lambda}$. *Phys. Lett. B* **632**, 181–186 (2006).
40. Ablikim, M. et al. First observation of the isospin violating decay $J/\psi \to \Lambda\bar{\Sigma}^0 + c.c.$ *Phys. Rev. D* **86**, 032008 (2012).
41. James, F. & Roos, M. Minuit: a system for function minimization and analysis of the parameter errors and correlations. *Comput. Phys. Commun.* **10**, 343–367 (1975).
42. Ablikim, M. et al. Amplitude analysis of the $D^+ \to K^0_S\pi^+\pi^0$ Dalitz plot. *Phys. Rev. D* **89**, 052001 (2014).

The BESIII Collaboration

M. Ablikim[1], M. N. Achasov[2,68], S. Ahmed[3], M. Albrecht[4], M. Alekseev[5,6], A. Amoroso[5,6], F. F. An[1], Q. An[7,8], Y. Bai[9], O. Bakina[10], R. Baldini Ferroli[11], Y. Ban[12], K. Begzsuren[13], D. W. Bennett[14], J. V. Bennett[15], N. Berger[16], M. Bertani[11], D. Bettoni[17], F. Bianchi[5,6], E. Boger[10,69], I. Boyko[10], R. A. Briere[15], H. Cai[18], X. Cai[1,7], A. Calcaterra[11], G. F. Cao[1,19], S. A. Cetin[20,21,22], J. Chai[6], J. F. Chang[1,7], W. L. Chang[1,19], G. Chelkov[10,69,70], G. Chen[1], H. S. Chen[1,19], J. C. Chen[1], M. L. Chen[1,7], P. L. Chen[23], S. J. Chen[24], X. R. Chen[25], Y. B. Chen[1,7], W. Cheng[6], X. K. Chu[12], G. Cibinetto[17], F. Cossio[6], H. L. Dai[1,7], J. P. Dai[26,71], A. Dbeyssi[3], D. Dedovich[10], Z. Y. Deng[1], A. Denig[16], I. Denysenko[10], M. Destefanis[5,6], F. De Mori[5,6], Y. Ding[27], C. Dong[28], J. Dong[1,7], L. Y. Dong[1,19], M. Y. Dong[1,7,19], Z. L. Dou[24], S. X. Du[29], P. F. Duan[1], J. Z. Fan[30], J. Fang[1,7], S. S. Fang[1,19], Y. Fang[1], R. Farinelli[17,31], L. Fava[6,32], S. Fegan[16], F. Feldbauer[4], G. Felici[11], C. Q. Feng[7,8], E. Fioravanti[17], M. Fritsch[4], C. D. Fu[1], Q. Gao[1], X. L. Gao[7,8], Y. Gao[30], Y. G. Gao[33], Z. Gao[7,8], B. Garillon[16], I. Garzia[17], A. Gilman[34], K. Goetzen[35], L. Gong[28], W. X. Gong[1,7], W. Gradl[16], M. Greco[5,6], L. M. Gu[24], M. H. Gu[1,7], Y. T. Gu[36], A. Q. Guo[1], L. B. Guo[37], R. P. Guo[1,19], Y. P. Guo[16], A. Guskov[10], Z. Haddadi[38], S. Han[18], X. Q. Hao[39], F. A. Harris[40], K. L. He[1,19], F. H. Heinsius[4], T. Held[4], Y. K. Heng[1,7,19], Z. L. Hou[1], H. M. Hu[1,19], J. F. Hu[26,71], T. Hu[1,7,19], Y. Hu[1], G. S. Huang[7,8], J. S. Huang[39], X. T. Huang[41], X. Z. Huang[24], Z. L. Huang[27], T. Hussain[42], W. Ikegami Andersson[43], M. Irshad[7,8], Q. Ji[1], Q. P. Ji[39], X. B. Ji[1,19], X. L. Ji[1,7], H. L. Jiang[41], X. S. Jiang[1,7,19], X. Y. Jiang[28], J. B. Jiao[41], Z. Jiao[44], D. P. Jin[1,7,19], S. Jin[24], Y. Jin[45], T. Johansson[43], A. Julin[34], N. Kalantar-Nayestanaki[38], X. S. Kang[28], M. Kavatsyuk[38], B. C. Ke[1], I. K. Keshk[4], T. Khan[7,8], A. Khoukaz[46], P. Kiese[16], R. Kiuchi[1], R. Kliemt[35], L. Koch[47], O. B. Kolcu[21,72], B. Kopf[4], M. Kornicer[40], M. Kuemmel[4], M. Kuessner[4], A. Kupsc[43]*, M. Kurth[1], W. Kühn[47], J. S. Lange[47],

P. Larin[3], L. Lavezzi[6], S. Leiber[4], H. Leithoff[16], C. Li[43], Cheng Li[7,8], D. M. Li[29], F. Li[1,7], F. Y. Li[12], G. Li[1], H. B. Li[1,19], H. J. Li[1,19], J. C. Li[1], J. W. Li[48], K. J. Li[49], Kang Li[50], Ke Li[1], Lei Li[51], P. L. Li[7,8], P. R. Li[19,52], Q. Y. Li[41], T. Li[41], W. D. Li[1,19], W. G. Li[1], X. L. Li[41], X. N. Li[1,7], X. Q. Li[28], Z. B. Li[49], H. Liang[7,8], Y. F. Liang[53], Y. T. Liang[47], G. R. Liao[54], L. Z. Liao[1,19], J. Libby[55], C. X. Lin[49], D. X. Lin[3], B. Liu[26,71], B. J. Liu[1], C. X. Liu[1], D. Liu[7,8], D. Y. Liu[26,71], F. H. Liu[56], Fang Liu[1], Feng Liu[33], H. B. Liu[36], H. L Liu[9], H. M. Liu[1,19], Huanhuan Liu[1], Huihui Liu[57], J. Liu[1], J. B. Liu[7,8], J. Y. Liu[1,19], K. Y. Liu[27], Ke Liu[33], L. D. Liu[12], Q. Liu[19], S. B. Liu[7,8], X. Liu[25], Y. B. Liu[28], Z. A. Liu[1,7,19], Zhiqing Liu[16], Y. F. Long[12], X. C. Lou[1,7,19], H. J. Lu[44], J. G. Lu[1,7], Y. Lu[1], Y. P. Lu[1,7], C. L. Luo[37], M. X. Luo[58], P. W. Luo[49], T. Luo[59,73], X. L. Luo[1,7], S. Lusso[6], X. R. Lyu[19], F. C. Ma[27], H. L. Ma[1], L. L. Ma[41], M. M. Ma[1,19], Q. M. Ma[1], X. N. Ma[28], X. Y. Ma[1,7], X. X. Ma[1,19], Y. M. Ma[41], F. E. Maas[3], M. Maggiora[5,6], S. Maldaner[16], Q. A. Malik[42], A. Mangoni[60], Y. J. Mao[12], Z. P. Mao[1], S. Marcello[5,6], Z. X. Meng[45], J. G. Messchendorp[38], G. Mezzadri[17], J. Min[1,7], T. J. Min[24], R. E. Mitchell[14], X. H. Mo[1,7,19], Y. J. Mo[33], C. Morales Morales[3], N. Yu. Muchnoi[2,68], H. Muramatsu[34], A. Mustafa[4], S. Nakhoul[35,74], Y. Nefedov[10], F. Nerling[35,74], I. B. Nikolaev[2,68], Z. Ning[1,7], S. Nisar[61], S. L. Niu[1,7], X. Y. Niu[1,19], S. L. Olsen[19], Q. Ouyang[1,7,19], S. Pacetti[60], Y. Pan[7,8], M. Papenbrock[43], P. Patteri[11], M. Pelizaeus[4], J. Pellegrino[5,6], H. P. Peng[7,8], Z. Y. Peng[36], K. Peters[35,74], J. Pettersson[43], J. L. Ping[37], R. G. Ping[1,19], A. Pitka[4], R. Poling[34], V. Prasad[7,8], H. R. Qi[62], M. Qi[24], T. Y. Qi[62], S. Qian[1,7], C. F. Qiao[19], N. Qin[18], X. S. Qin[4], Z. H. Qin[1,7], J. F. Qiu[1], S. Q. Qu[28], K. H. Rashid[42,75], C. F. Redmer[16], M. Richter[4], M. Ripka[16], A. Rivetti[6], M. Rolo[6], G. Rong[1,19], Ch. Rosner[3], M. Rump[46], A. Sarantsev[10,76], M. Savrié[31], K. Schoenning[43], W. Shan[63], X. Y. Shan[7,8], M. Shao[7,8], C. P. Shen[62], P. X. Shen[28], X. Y. Shen[1,19], H. Y. Sheng[1], X. Shi[1,7], J. J. Song[41], W. M. Song[41], X. Y. Song[1], S. Sosio[5,6], C. Sowa[4], S. Spataro[5,6], F. F. Sui[41], G. X. Sun[1], J. F. Sun[39], L. Sun[18], S. S. Sun[1,19], X. H. Sun[1], Y. J. Sun[7,8], Y. K Sun[7,8], Y. Z. Sun[1], Z. J. Sun[1,7], Z. T. Sun[1], Y. T Tan[7,8], C. J. Tang[53], G. Y. Tang[1], X. Tang[1], M. Tiemens[38], B. Tsednee[13], I. Uman[64], B. Wang[1], B. L. Wang[19], C. W. Wang[24], D. Wang[12], D. Y. Wang[12], Dan Wang[19], H. H. Wang[41], K. Wang[1,7], L. L. Wang[1], L. S. Wang[1], M. Wang[41], Meng Wang[1,19], P. Wang[1], P. L. Wang[1], W. P. Wang[7,8], X. F. Wang[1], Y. Wang[7,8], Y. F. Wang[1,7,19], Z. Wang[1,7], Z. G. Wang[1,7], Z. Y. Wang[1], Zongyuan Wang[1,19], T. Weber[4], D. H. Wei[54], P. Weidenkaff[16], S. P. Wen[1], U. Wiedner[4], M. Wolke[43], L. H. Wu[1], L. J. Wu[1,19], Z. Wu[1,7], L. Xia[7,8], X. Xia[41], Y. Xia[65], D. Xiao[1], Y. J. Xiao[1,19], Z. J. Xiao[37], Y. G. Xie[1,7], Y. H. Xie[33], X. A. Xiong[1,19], Q. L. Xiu[1,7], G. F. Xu[1], J. J. Xu[1,19], L. Xu[1], Q. J. Xu[50], X. P. Xu[48], F. Yan[23], L. Yan[5,6], W. B. Yan[7,8], W. C. Yan[62], Y. H. Yan[65], H. J. Yang[26,71], H. X. Yang[1], L. Yang[18], R. X. Yang[7,8], S. L. Yang[1,19], Y. H. Yang[24], Y. X. Yang[54], Yifan Yang[1,19], Z. Q. Yang[65], M. Ye[1,7], M. H. Ye[52], J. H. Yin[1], Z. Y. You[49], B. X. Yu[1,7,19], C. X. Yu[28], J. S. Yu[65], C. Z. Yuan[1,19], Y. Yuan[1], A. Yuncu[21,77], A. A. Zafar[42], Y. Zeng[65], B. X. Zhang[1], B. Y. Zhang[1,7], C. C. Zhang[1], D. H. Zhang[1], H. H. Zhang[49], H. Y. Zhang[1,7], J. Zhang[1,19], J. L. Zhang[66], J. Q. Zhang[4], J. W. Zhang[1,7,19], J. Y. Zhang[1], J. Z. Zhang[1,19], K. Zhang[1,19], L. Zhang[30], S. F. Zhang[24], T. J. Zhang[26,71], X. Y. Zhang[41], Y. Zhang[7,8], Y. H. Zhang[1,7], Y. T. Zhang[7,8], Yang Zhang[1], Yao Zhang[1], Yu Zhang[19], Z. H. Zhang[33], Z. P. Zhang[8], Z. Y. Zhang[18], G. Zhao[1], J. W. Zhao[1,7], J. Y. Zhao[1,19], J. Z. Zhao[1,7], Lei Zhao[7,8], Ling Zhao[1], M. G. Zhao[28], Q. Zhao[1], S. J. Zhao[29], T. C. Zhao[1], Y. B. Zhao[1,7], Z. G. Zhao[7,8], A. Zhemchugov[10,69], B. Zheng[23], J. P. Zheng[1,7], W. J. Zheng[41], Y. H. Zheng[19], B. Zhong[37], L. Zhou[1,7], Q. Zhou[1,19], X. Zhou[18], X. K. Zhou[7,8], X. R. Zhou[7,8], X. Y. Zhou[1], Xiaoyu Zhou[65], Xu Zhou[65], A. N. Zhu[1,19], J. Zhu[28], J. Zhu[49], K. Zhu[1], K. J. Zhu[1,7,19], S. Zhu[1], S. H. Zhu[67], X. L. Zhu[30], Y. C. Zhu[7,8], Y. S. Zhu[1,19], Z. A. Zhu[1,19], J. Zhuang[1,7], B. S. Zou[1] and J. H. Zou[1]

[1]Institute of High Energy Physics, Beijing, China. [2]G.I. Budker Institute of Nuclear Physics SB RAS (BINP), Novosibirsk, Russia. [3]Helmholtz Institute Mainz, Mainz, Germany. [4]Bochum Ruhr-University, Bochum, Germany. [5]University of Turin, Turin, Italy. [6]INFN, Turin, Italy. [7]State Key Laboratory of Particle Detection and Electronics, Beijing, Hefei, China. [8]University of Science and Technology of China, Hefei, China. [9]Southeast University, Nanjing, China. [10]Joint Institute for Nuclear Research, Dubna, Moscow, Russia. [11]INFN Laboratori Nazionali di Frascati, Frascati, Italy. [12]Peking University, Beijing, China. [13]Institute of Physics and Technology, Ulaanbaatar, Mongolia. [14]Indiana University, Bloomington, IN, USA. [15]Carnegie Mellon University, Pittsburgh, PA, USA.

[16]Johannes Gutenberg University of Mainz, Mainz, Germany. [17]INFN Sezione di Ferrara, Ferrara, Italy. [18]Wuhan University, Wuhan, China. [19]University of Chinese Academy of Sciences, Beijing, China. [20]Ankara University, Tandogan, Ankara, Turkey. [21]Istanbul Bilgi University, Eyup, Istanbul, Turkey. [22]Uludag University, Bursa, Turkey. [23]University of South China, Hengyang, China. [24]Nanjing University, Nanjing, China. [25]Lanzhou University, Lanzhou, China. [26]Shanghai Jiao Tong University, Shanghai, China. [27]Liaoning University, Shenyang, China. [28]Nankai University, Tianjin, China. [29]Zhengzhou University, Zhengzhou, China. [30]Tsinghua University, Beijing, China. [31]University of Ferrara, Ferrara, Italy. [32]University of Eastern Piedmont, Alessandria, Italy. [33]Central China Normal University, Wuhan, China. [34]University of Minnesota, Minneapolis, MN, USA. [35]GSI Helmholtzcentre for Heavy Ion Research GmbH, Darmstadt, Germany. [36]Guangxi University, Nanning, China. [37]Nanjing Normal University, Nanjing, China. [38]KVI-CART, University of Groningen, Groningen, The Netherlands. [39]Henan Normal University, Xinxiang, China. [40]University of Hawaii, Honolulu, HI, USA. [41]Shandong University, Jinan, China. [42]University of the Punjab, Lahore, Pakistan. [43]Uppsala University, Uppsala, Sweden. [44]Huangshan College, Huangshan, China. [45]University of Jinan, Jinan, China. [46]University of Muenster, Muenster, Germany. [47]Justus-Liebig-Universitaet Giessen, II Physikalisches Institut, Giessen, Germany. [48]Soochow University, Suzhou, China. [49]Sun Yat-Sen University, Guangzhou, China. [50]Hangzhou Normal University, Hangzhou, China. [51]Beijing Institute of Petrochemical Technology, Beijing, China. [52]China Center of Advanced Science and Technology, Beijing, China. [53]Sichuan University, Chengdu, China. [54]Guangxi Normal University, Guilin, China. [55]Indian Institute of Technology Madras, Chennai, India. [56]Shanxi University, Taiyuan, China. [57]Henan University of Science and Technology, Luoyang, China. [58]Zhejiang University, Hangzhou, China. [59]Fudan University, Shanghai, China. [60]INFN and University of Perugia, Perugia, Italy. [61]COMSATS Institute of Information Technology, Lahore, Pakistan. [62]Beihang University, Beijing, China. [63]Hunan Normal University, Changsha, China. [64]Near East University, Nicosia, North Cyprus, Turkey. [65]Hunan University, Changsha, China. [66]Xinyang Normal University, Xinyang, China. [67]University of Science and Technology Liaoning, Anshan, China. [68]The Novosibirsk State University, Novosibirsk, Russia. [69]The Moscow Institute of Physics and Technology, Moscow, Russia. [70]The Functional Electronics Laboratory, Tomsk State University, Tomsk, Russia. [71]Key Laboratory for Particle Physics, Astrophysics and Cosmology, Ministry of Education; Shanghai Key Laboratory for Particle Physics and Cosmology, Institute of Nuclear and Particle Physics, Shanghai, China. [72]Istanbul Arel University, Istanbul, Turkey. [73]Key Laboratory of Nuclear Physics and Ion-beam Application (MOE) and Institute of Modern Physics, Fudan University, Shanghai, China. [74]Goethe University Frankfurt, Frankfurt, Germany. [75]Government College Women University, Sialkot, Punjab, Pakistan. [76]The NRC 'Kurchatov Institute', PNPI, Gatchina, Russia. [77]Bogazici University, Istanbul, Turkey. *e-mail: andrzej.kupsc@physics.uu.se

Study of the $D^0 \to K^- \mu^+ \nu_\mu$ Dynamics and Test of Lepton Flavor Universality with $D^0 \to K^- \ell^+ \nu_\ell$ Decays

M. Ablikim,[1] M. N. Achasov,[9,d] S. Ahmed,[14] M. Albrecht,[4] M. Alekseev,[55a,55c] A. Amoroso,[55a,55c] F. F. An,[1] Q. An,[52,42] J. Z. Bai,[1] Y. Bai,[41] O. Bakina,[26] R. Baldini Ferroli,[22a] Y. Ban,[34] K. Begzsuren,[24] D. W. Bennett,[21] J. V. Bennett,[5] N. Berger,[25] M. Bertani,[22a] D. Bettoni,[23a] F. Bianchi,[55a,55c] E. Boger,[26,b] I. Boyko,[26] R. A. Briere,[5] H. Cai,[57] X. Cai,[1,42] O. Cakir,[45a] A. Calcaterra,[22a] G. F. Cao,[1,46] S. A. Cetin,[45b] J. Chai,[55c] J. F. Chang,[1,42] G. Chelkov,[26,b,c] G. Chen,[1] H. S. Chen,[1,46] J. C. Chen,[1] M. L. Chen,[1,42] P. L. Chen,[53] S. J. Chen,[32] X. R. Chen,[29] Y. B. Chen,[1,42] W. Cheng,[55c] X. K. Chu,[34] G. Cibinetto,[23a] F. Cossio,[55c] H. L. Dai,[1,42] J. P. Dai,[37,h] A. Dbeyssi,[14] D. Dedovich,[26] Z. Y. Deng,[1] A. Denig,[25] I. Denysenko,[26] M. Destefanis,[55a,55c] F. De Mori,[55a,55c] Y. Ding,[30] C. Dong,[33] J. Dong,[1,42] L. Y. Dong,[1,46] M. Y. Dong,[1,42,46] Z. L. Dou,[32] S. X. Du,[60] P. F. Duan,[1] J. Fang,[1,42] S. S. Fang,[1,46] Y. Fang,[1] R. Farinelli,[23a,23b] L. Fava,[55b,55c] S. Fegan,[25] F. Feldbauer,[4] G. Felici,[22a] C. Q. Feng,[52,42] E. Fioravanti,[23a] M. Fritsch,[4] C. D. Fu,[1] Q. Gao,[1] X. L. Gao,[52,42] Y. Gao,[44] Y. G. Gao,[6] Z. Gao,[52,42] B. Garillon,[25] I. Garzia,[23a] A. Gilman,[49] K. Goetzen,[10] L. Gong,[33] W. X. Gong,[1,42] W. Gradl,[25] M. Greco,[55a,55c] M. H. Gu,[1,42] Y. T. Gu,[12] A. Q. Guo,[1] R. P. Guo,[1,46] Y. P. Guo,[25] A. Guskov,[26] Z. Haddadi,[28] S. Han,[57] X. Q. Hao,[15] F. A. Harris,[47] K. L. He,[1,46] X. Q. He,[51] F. H. Heinsius,[4] T. Held,[4] Y. K. Heng,[1,42,46] T. Holtmann,[4] Z. L. Hou,[1] H. M. Hu,[1,46] J. F. Hu,[37,h] T. Hu,[1,42,46] Y. Hu,[1] G. S. Huang,[52,42] J. S. Huang,[15] X. T. Huang,[36] X. Z. Huang,[32] Z. L. Huang,[30] T. Hussain,[54] W. Ikegami Andersson,[56] M. Irshad,[52,42] Q. Ji,[1] Q. P. Ji,[15] X. B. Ji,[1,46] X. L. Ji,[1,42] X. S. Jiang,[1,42,46] X. Y. Jiang,[33] J. B. Jiao,[36] Z. Jiao,[17] D. P. Jin,[1,42,46] S. Jin,[1,46] Y. Jin,[48] T. Johansson,[56] A. Julin,[49] N. Kalantar-Nayestanaki,[28] X. S. Kang,[33] M. Kavatsyuk,[28] B. C. Ke,[1] T. Khan,[52,42] A. Khoukaz,[50] P. Kiese,[25] R. Kiuchi,[1] R. Kliemt,[10] L. Koch,[27] O. B. Kolcu,[45b,f] B. Kopf,[4] M. Kornicer,[47] M. Kuemmel,[4] M. Kuessner,[4] A. Kupsc,[56] M. Kurth,[1] W. Kühn,[27] J. S. Lange,[27] M. Lara,[21] P. Larin,[14] L. Lavezzi,[55c] H. Leithoff,[25] C. Li,[56] Cheng Li,[52,42] D. M. Li,[60] F. Li,[1,42] F. Y. Li,[34] G. Li,[1] H. B. Li,[1,46] H. J. Li,[1,46] J. C. Li,[1] J. W. Li,[40] Jin Li,[35] K. J. Li,[43] Kang Li,[13] Ke Li,[1] Lei Li,[3] P. L. Li,[52,42] P. R. Li,[46,7] Q. Y. Li,[36] W. D. Li,[1,46] W. G. Li,[1] X. L. Li,[36] X. N. Li,[1,42] X. Q. Li,[33] Z. B. Li,[43] H. Liang,[52,42] Y. F. Liang,[39] Y. T. Liang,[27] G. R. Liao,[11] L. Z. Liao,[1,46] J. Libby,[20] C. X. Lin,[43] D. X. Lin,[14] B. Liu,[37,h] B. J. Liu,[1] C. X. Liu,[1] D. Liu,[52,42] D. Y. Liu,[37,h] F. H. Liu,[38] Fang Liu,[1] Feng Liu,[6] H. B. Liu,[12] H. L. Liu,[41] H. M. Liu,[1,46] Huanhuan Liu,[1] Huihui Liu,[16] J. B. Liu,[52,42] J. Y. Liu,[1,46] K. Liu,[44] K. Y. Liu,[30] Ke Liu,[6] L. D. Liu,[34] Q. Liu,[46] S. B. Liu,[52,42] X. Liu,[29] Y. B. Liu,[33] Z. A. Liu,[1,42,46] Zhiqing Liu,[25] Y. F. Long,[34] X. C. Lou,[1,42,46] H. J. Lu,[17] J. G. Lu,[1,42] Y. Lu,[1] Y. P. Lu,[1,42] C. L. Luo,[31] M. X. Luo,[59] X. L. Luo,[1,42] S. Lusso,[55c] X. R. Lyu,[46] F. C. Ma,[30] H. L. Ma,[1] L. L. Ma,[36] M. M. Ma,[1,46] Q. M. Ma,[1] T. Ma,[1] X. N. Ma,[33] X. Y. Ma,[1,42] Y. M. Ma,[36] F. E. Maas,[14] M. Maggiora,[55a,55c] Q. A. Malik,[54] A. Mangoni,[22b] Y. J. Mao,[34] Z. P. Mao,[1] S. Marcello,[55a,55c] Z. X. Meng,[48] J. G. Messchendorp,[28] G. Mezzadri,[23b] J. Min,[1,42] R. E. Mitchell,[21] X. H. Mo,[1,42,46] Y. J. Mo,[6] C. Morales Morales,[14] N. Yu. Muchnoi,[9,d] H. Muramatsu,[49] A. Mustafa,[4] Y. Nefedov,[26] F. Nerling,[10] I. B. Nikolaev,[9,d] Z. Ning,[1,42] S. Nisar,[8] S. L. Niu,[1,42] X. Y. Niu,[1,46] S. L. Olsen,[35,j] Q. Ouyang,[1,42,46] S. Pacetti,[22b] Y. Pan,[52,42] M. Papenbrock,[56] P. Patteri,[22a] M. Pelizaeus,[4] J. Pellegrino,[55a,55c] H. P. Peng,[52,42] Z. Y. Peng,[12] K. Peters,[10,g] J. Pettersson,[56] J. L. Ping,[31] R. G. Ping,[1,46] A. Pitka,[4] R. Poling,[49] V. Prasad,[52,42] H. R. Qi,[2] M. Qi,[32] T. Y. Qi,[2] S. Qian,[1,42] C. F. Qiao,[46] N. Qin,[57] X. S. Qin,[4] Z. H. Qin,[1,42] J. F. Qiu,[1] K. H. Rashid,[54,i] C. F. Redmer,[25] M. Richter,[4] M. Ripka,[25] A. Rivetti,[55c] M. Rolo,[55c] G. Rong,[1,46] Ch. Rosner,[14] A. Sarantsev,[26,e] M. Savrié,[23b] C. Schnier,[4] K. Schoenning,[56] W. Shan,[18] X. Y. Shan,[52,42] M. Shao,[52,42] C. P. Shen,[2] P. X. Shen,[33] X. Y. Shen,[1,46] H. Y. Sheng,[1] X. Shi,[1,42] J. J. Song,[36] W. M. Song,[36] X. Y. Song,[1] S. Sosio,[55a,55c] C. Sowa,[4] S. Spataro,[55a,55c] G. X. Sun,[1] J. F. Sun,[15] L. Sun,[57] S. S. Sun,[1,46] X. H. Sun,[1] Y. J. Sun,[52,42] Y. K. Sun,[52,42] Y. Z. Sun,[1] Z. J. Sun,[1,42] Z. T. Sun,[21] Y. T. Tan,[52,42] C. J. Tang,[39] G. Y. Tang,[1] X. Tang,[1] I. Tapan,[45c] M. Tiemens,[28] B. Tsednee,[24] I. Uman,[45d] G. S. Varner,[47] B. Wang,[1] B. L. Wang,[46] D. Wang,[34] D. Y. Wang,[34] Dan Wang,[46] K. Wang,[1,42] L. L. Wang,[1] L. S. Wang,[1] M. Wang,[36] Meng Wang,[1,46] P. Wang,[1] P. L. Wang,[1] W. P. Wang,[52,42] X. F. Wang,[44] Y. Wang,[52,42] Y. F. Wang,[1,42,46] Y. Q. Wang,[25] Z. Wang,[1,42] Z. G. Wang,[1,42] Z. Y. Wang,[1] Zongyuan Wang,[1,46] T. Weber,[4] D. H. Wei,[11] P. Weidenkaff,[25] S. P. Wen,[1] U. Wiedner,[4] M. Wolke,[56] L. H. Wu,[1] L. J. Wu,[1,46] Z. Wu,[1,42] L. Xia,[52,42] Y. Xia,[19] D. Xiao,[1] Y. J. Xiao,[1,46] Z. J. Xiao,[31] Y. G. Xie,[1,42] Y. H. Xie,[6] X. A. Xiong,[1,46] Q. L. Xiu,[1,42] G. F. Xu,[1] J. J. Xu,[1,46] L. Xu,[1] Q. J. Xu,[13] Q. N. Xu,[46] X. P. Xu,[40] F. Yan,[53] L. Yan,[55a,55c] W. B. Yan,[52,42] W. C. Yan,[2] Y. H. Yan,[19] H. J. Yang,[37,h] H. X. Yang,[1] L. Yang,[57] Y. H. Yang,[32] Y. X. Yang,[11] Yifan Yang,[1,46] Z. Q. Yang,[19] M. Ye,[1,42] M. H. Ye,[7] J. H. Yin,[1] Z. Y. You,[43] B. X. Yu,[1,42,46] C. X. Yu,[33] J. S. Yu,[19] J. S. Yu,[29] C. Z. Yuan,[1,46] Y. Yuan,[1] A. Yuncu,[45b,a] A. A. Zafar,[54] Y. Zeng,[19] Z. Zeng,[52,42] B. X. Zhang,[1] B. Y. Zhang,[1,42] C. C. Zhang,[1] D. H. Zhang,[1] H. H. Zhang,[43] H. Y. Zhang,[1,42] J. Zhang,[1,46] J. L. Zhang,[58] J. Q. Zhang,[4] J. W. Zhang,[1,42,46] J. Y. Zhang,[1] J. Z. Zhang,[1,46] K. Zhang,[1,46]

L. Zhang,[44] S. F. Zhang,[32] T. J. Zhang,[37,h] X. Y. Zhang,[36] Y. Zhang,[52,42] Y. H. Zhang,[1,42] Y. T. Zhang,[52,42] Yang Zhang,[1] Yao Zhang,[1] Yu Zhang,[46] Z. H. Zhang,[6] Z. P. Zhang,[52] Z. Y. Zhang,[57] G. Zhao,[1] J. W. Zhao,[1,42] J. Y. Zhao,[1,46] J. Z. Zhao,[1,42] Lei Zhao,[52,42] Ling Zhao,[1] M. G. Zhao,[33] Q. Zhao,[1] S. J. Zhao,[60] T. C. Zhao,[1] Y. B. Zhao,[1,42] Z. G. Zhao,[52,42] A. Zhemchugov,[26,b] B. Zheng,[53] J. P. Zheng,[1,42] W. J. Zheng,[36] Y. H. Zheng,[46] B. Zhong,[31] L. Zhou,[1,42] Q. Zhou,[1,46] X. Zhou,[57] X. K. Zhou,[52,42] X. R. Zhou,[52,42] X. Y. Zhou,[1] Xiaoyu Zhou,[19] Xu Zhou,[19] A. N. Zhu,[1,46] J. Zhu,[33] J. Zhu,[43] K. Zhu,[1] K. J. Zhu,[1,42,46] S. Zhu,[1] S. H. Zhu,[51] X. L. Zhu,[44] Y. C. Zhu,[52,42] Y. S. Zhu,[1,46] Z. A. Zhu,[1,46] J. Zhuang,[1,42] B. S. Zou,[1] and J. H. Zou[1]

(BESIII Collaboration)

[1]*Institute of High Energy Physics, Beijing 100049, People's Republic of China*
[2]*Beihang University, Beijing 100191, People's Republic of China*
[3]*Beijing Institute of Petrochemical Technology, Beijing 102617, People's Republic of China*
[4]*Bochum Ruhr-University, D-44780 Bochum, Germany*
[5]*Carnegie Mellon University, Pittsburgh, Pennsylvania 15213, USA*
[6]*Central China Normal University, Wuhan 430079, People's Republic of China*
[7]*China Center of Advanced Science and Technology, Beijing 100190, People's Republic of China*
[8]*COMSATS Institute of Information Technology, Lahore, Defence Road, Off Raiwind Road, 54000 Lahore, Pakistan*
[9]*G.I. Budker Institute of Nuclear Physics SB RAS (BINP), Novosibirsk 630090, Russia*
[10]*GSI Helmholtzcentre for Heavy Ion Research GmbH, D-64291 Darmstadt, Germany*
[11]*Guangxi Normal University, Guilin 541004, People's Republic of China*
[12]*Guangxi University, Nanning 530004, People's Republic of China*
[13]*Hangzhou Normal University, Hangzhou 310036, People's Republic of China*
[14]*Helmholtz Institute Mainz, Johann-Joachim-Becher-Weg 45, D-55099 Mainz, Germany*
[15]*Henan Normal University, Xinxiang 453007, People's Republic of China*
[16]*Henan University of Science and Technology, Luoyang 471003, People's Republic of China*
[17]*Huangshan College, Huangshan 245000, People's Republic of China*
[18]*Hunan Normal University, Changsha 410081, People's Republic of China*
[19]*Hunan University, Changsha 410082, People's Republic of China*
[20]*Indian Institute of Technology Madras, Chennai 600036, India*
[21]*Indiana University, Bloomington, Indiana 47405, USA*
[22a]*INFN Laboratori Nazionali di Frascati, I-00044 Frascati, Italy*
[22b]*INFN and University of Perugia, I-06100 Perugia, Italy*
[23a]*INFN Sezione di Ferrara, I-44122 Ferrara, Italy*
[23b]*University of Ferrara, I-44122 Ferrara, Italy*
[24]*Institute of Physics and Technology, Peace Ave. 54B, Ulaanbaatar 13330, Mongolia*
[25]*Johannes Gutenberg University of Mainz, Johann-Joachim-Becher-Weg 45, D-55099 Mainz, Germany*
[26]*Joint Institute for Nuclear Research, 141980 Dubna, Moscow region, Russia*
[27]*Justus-Liebig-Universitaet Giessen, II. Physikalisches Institut, Heinrich-Buff-Ring 16, D-35392 Giessen, Germany*
[28]*KVI-CART, University of Groningen, NL-9747 AA Groningen, The Netherlands*
[29]*Lanzhou University, Lanzhou 730000, People's Republic of China*
[30]*Liaoning University, Shenyang 110036, People's Republic of China*
[31]*Nanjing Normal University, Nanjing 210023, People's Republic of China*
[32]*Nanjing University, Nanjing 210093, People's Republic of China*
[33]*Nankai University, Tianjin 300071, People's Republic of China*
[34]*Peking University, Beijing 100871, People's Republic of China*
[35]*Seoul National University, Seoul 151-747 Korea*
[36]*Shandong University, Jinan 250100, People's Republic of China*
[37]*Shanghai Jiao Tong University, Shanghai 200240, People's Republic of China*
[38]*Shanxi University, Taiyuan 030006, People's Republic of China*
[39]*Sichuan University, Chengdu 610064, People's Republic of China*
[40]*Soochow University, Suzhou 215006, People's Republic of China*
[41]*Southeast University, Nanjing 211100, People's Republic of China*
[42]*State Key Laboratory of Particle Detection and Electronics, Beijing 100049, Hefei 230026, People's Republic of China*
[43]*Sun Yat-Sen University, Guangzhou 510275, People's Republic of China*
[44]*Tsinghua University, Beijing 100084, People's Republic of China*
[45a]*Ankara University, 06100 Tandogan, Ankara, Turkey*
[45b]*Istanbul Bilgi University, 34060 Eyup, Istanbul, Turkey*
[45c]*Uludag University, 16059 Bursa, Turkey*

[45d]Near East University, Nicosia, North Cyprus, Mersin 10, Turkey
[46]University of Chinese Academy of Sciences, Beijing 100049, People's Republic of China
[47]University of Hawaii, Honolulu, Hawaii 96822, USA
[48]University of Jinan, Jinan 250022, People's Republic of China
[49]University of Minnesota, Minneapolis, Minnesota 55455, USA
[50]University of Muenster, Wilhelm-Klemm-Str. 9, 48149 Muenster, Germany
[51]University of Science and Technology Liaoning, Anshan 114051, People's Republic of China
[52]University of Science and Technology of China, Hefei 230026, People's Republic of China
[53]University of South China, Hengyang 421001, People's Republic of China
[54]University of the Punjab, Lahore-54590, Pakistan
[55a]University of Turin, I-10125 Turin, Italy
[55b]University of Eastern Piedmont, I-15121 Alessandria, Italy
[55c]INFN, I-10125 Turin, Italy
[56]Uppsala University, Box 516, SE-75120 Uppsala, Sweden
[57]Wuhan University, Wuhan 430072, People's Republic of China
[58]Xinyang Normal University, Xinyang 464000, People's Republic of China
[59]Zhejiang University, Hangzhou 310027, People's Republic of China
[60]Zhengzhou University, Zhengzhou 450001, People's Republic of China

(Received 7 October 2018; revised manuscript received 30 November 2018; published 10 January 2019)

Using e^+e^- annihilation data of 2.93 fb^{-1} collected at center-of-mass energy $\sqrt{s} = 3.773$ GeV with the BESIII detector, we measure the absolute branching fraction of $D^0 \to K^-\mu^+\nu_\mu$ with significantly improved precision: $\mathcal{B}_{D^0\to K^-\mu^+\nu_\mu} = (3.413 \pm 0.019_{\rm stat} \pm 0.035_{\rm syst})\%$. Combining with our previous measurement of $\mathcal{B}_{D^0\to K^-e^+\nu_e}$, the ratio of the two branching fractions is determined to be $\mathcal{B}_{D^0\to K^-\mu^+\nu_\mu}/\mathcal{B}_{D^0\to K^-e^+\nu_e} = 0.974 \pm 0.007_{\rm stat} \pm 0.012_{\rm syst}$, which agrees with the theoretical expectation of lepton flavor universality within the uncertainty. A study of the ratio of the two branching fractions in different four-momentum transfer regions is also performed, and no evidence for lepton flavor universality violation is found with current statistics. Taking inputs from global fit in the standard model and lattice quantum chromodynamics separately, we determine $f_+^K(0) = 0.7327 \pm 0.0039_{\rm stat} \pm 0.0030_{\rm syst}$ and $|V_{cs}| = 0.955 \pm 0.005_{\rm stat} \pm 0.004_{\rm syst} \pm 0.024_{\rm LQCD}$.

DOI: 10.1103/PhysRevLett.122.011804

In the standard model (SM), lepton flavor universality (LFU) requires equality of couplings between three families of leptons and gauge bosons. Semileptonic (SL) decays of pseudoscalar mesons, well understood in the SM, offer an excellent opportunity to test LFU and search for new physics effects. Recently, various LFU tests in SL B decays were reported at *BABAR*, Belle, and LHCb. The measured branching fraction (BF) ratios $\mathcal{R}^{\tau/\ell}_{D^{(*)}} = \mathcal{B}_{B\to\bar{D}^{(*)}\tau^+\nu_\tau}/\mathcal{B}_{B\to\bar{D}^{(*)}\ell^+\nu_\ell}$ ($\ell = \mu,\ e$) [1–5] and $\mathcal{R}^{\mu\mu/ee}_{K^{(*)}} = \mathcal{B}_{B\to K^{(*)}\mu^+\mu^-}/\mathcal{B}_{B\to K^{(*)}e^+e^-}$ [6,7] deviate from SM predictions by 3.9σ [8] and 2.1–2.5σ, respectively. Various models [9–14] were proposed to explain these tensions. Precision measurements of SL D decays provide critical and complementary tests of LFU. Reference [15] states that observable LFU violations may exist in $D^0 \to K^-\ell^+\nu_\ell$ decays. In the SM, Ref. [16] predicts $\mathcal{R}_{\mu/e} = \mathcal{B}_{D^0\to K^-\mu^+\nu_\mu}/\mathcal{B}_{D^0\to K^-e^+\nu_e} = 0.975 \pm 0.001$. Above $q^2 = 0.1\ \mathrm{GeV}^2/c^4$ (q is the total four momentum of $\ell^+\nu_\ell$), one expects $\mathcal{R}_{\mu/e}$ close to 1 with negligible uncertainty [17]. This Letter presents an improved measurement of $D^0 \to K^-\mu^+\nu_\mu$ [18], and LFU test with $D^0 \to K^-\ell^+\nu_\ell$ decays in the full kinematic range and various separate q^2 intervals.

Moreover, experimental studies of the $D^0 \to K^-\ell^+\nu_\ell$ dynamics help to determine the $c \to s$ quark mixing matrix element $|V_{cs}|$ and the hadronic form factors (FFs) $f_\pm^K(0)$ [16,19,20]. The $D^0 \to K^-e^+\nu_e$ dynamics was well studied by CLEO-c, Belle, *BABAR*, and BESIII [21–24]. However, the $D^0 \to K^-\mu^+\nu_\mu$ dynamics was only investigated by Belle and FOCUS [21,25], with relatively poor precision. By analyzing the $D^0 \to K^-\mu^+\nu_\mu$ dynamics, we determine $|V_{cs}|$ and $f_+^K(0)$ incorporating the inputs from global fit in the SM [26] and lattice quantum chromodynamics (LQCD) [27]. These are critical to test quark mixing matrix unitarity and validate LQCD calculations on FFs. This analysis is performed using 2.93 fb^{-1} of data taken at center-of-mass energy $\sqrt{s} = 3.773$ GeV with the BESIII detector.

Details about the design and performance of the BESIII detector are given in Ref. [28]. The Monte Carlo (MC) simulated events are generated with a GEANT4-based [29] detector simulation software package, BOOST. An inclusive MC sample, which includes the $D^0\bar{D}^0$, D^+D^-, and non-$D\bar{D}$ decays of $\psi(3770)$, the initial state radiation (ISR) production of $\psi(3686)$ and J/ψ, and the $q\bar{q}$ ($q = u, d, s$) continuum process, along with Bhabha scattering, $\mu^+\mu^-$ and $\tau^+\tau^-$ events, is produced at $\sqrt{s} = 3.773$ GeV to determine the detection efficiencies and to estimate the potential backgrounds. The production of the charmonium states is simulated by the MC generator KKMC [30]. The measured decay modes of the charmonium states are generated using EVTGEN [31] with BFs from the Particle Data Group (PDG) [26], and the remaining unknown decay modes are generated by LUNDCHARM [32]. The $D^0 \to K^-\mu^+\nu_\mu$ decay is simulated with the modified pole model [33].

At $\sqrt{s} = 3.773$ GeV, the $\psi(3770)$ resonance decays predominately into $D^0\bar{D}^0$ or D^+D^- meson pairs. If a $\bar{D}^0$ meson is fully reconstructed by $\bar{D}^0 \to K^+\pi^-$, $K^+\pi^-\pi^0$ or $K^+\pi^-\pi^-\pi^+$, a D^0 meson must exist in the recoiling system of the reconstructed $\bar{D}^0$ [called the single-tag (ST) $\bar{D}^0$]. In the presence of the ST $\bar{D}^0$, we select and study $D^0 \to K^-\mu^+\nu_\mu$ decay [called the double-tag (DT) events]. The BF of the SL decay is given by

$$\mathcal{B}_{D^0\to K^-\mu^+\nu_\mu} = N_{\rm DT}/(N_{\rm ST}^{\rm tot} \times \varepsilon_{\rm SL}), \tag{1}$$

where $N_{\rm ST}^{\rm tot}$ and $N_{\rm DT}$ are the ST and DT yields, $\varepsilon_{\rm SL} = \varepsilon_{\rm DT}/\varepsilon_{\rm ST}$ is the efficiency of reconstructing $D^0 \to K^-\mu^+\nu_\mu$ in the presence of the ST $\bar{D}^0$, and $\varepsilon_{\rm ST}$ and $\varepsilon_{\rm DT}$ are the efficiencies of selecting ST and DT events.

All charged tracks must originate from the interaction point with a distance of closest approach less than 1 cm in the transverse plane and less than 10 cm along the z axis. Their polar angles (θ) are required to satisfy $|\cos\theta| < 0.93$. Charged particle identification (PID) is performed by combining the time-of-flight information and the specific ionization energy loss measured in the main drift chamber. The information of the electromagnetic calorimeter (EMC) is also included to identify muon candidates. Combined confidence levels for electron, muon, pion and kaon hypotheses (CL_e, CL_μ, CL_π, and CL_K) are calculated individually. Kaon (pion) and muon candidates must satisfy $\mathrm{CL}_{K(\pi)} > \mathrm{CL}_{\pi(K)}$ and $\mathrm{CL}_\mu > 0.001$, CL_e, and CL_K, respectively. In addition, the deposited energy in the EMC of the muon is required to be within (0.02, 0.29) GeV. The π^0 meson is reconstructed via $\pi^0 \to \gamma\gamma$ decay. The energy deposited in the EMC of each photon is required to be greater than 0.025 GeV in the barrel ($|\cos\theta| < 0.80$) region or 0.050 GeV in the end cap ($0.86 < |\cos\theta| < 0.92$) region, and the shower time has to be within 700 ns of the event start time. The π^0 candidates with both photons

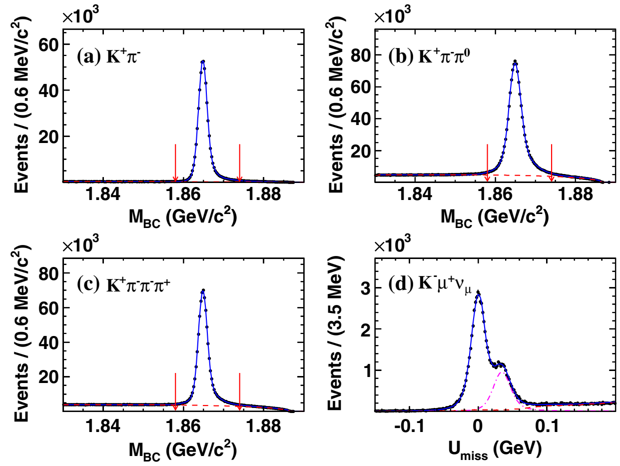

FIG. 1. Fits to [(a)–(c)] the $M_{\rm BC}$ distributions for the three ST modes, and (d) the $U_{\rm miss}$ distribution for $D^0 \to K^-\mu^+\nu_\mu$ candidates. Dots with error bars are data, solid curves show the fit results, dashed curves show the fitted non-peaking background shapes, the dash-dotted curve in (d) is the peaking background shape of $D^0 \to K^-\pi^+\pi^0$ and the red arrows in (a)–(c) give the $M_{\rm BC}$ windows.

from the end cap are rejected because of poor resolution. The $\gamma\gamma$ combination with an invariant mass ($M_{\gamma\gamma}$) in the range $(0.115, 0.150)$ GeV$/c^2$ is regarded as a π^0 candidate, and a kinematic fit by constraining the $M_{\gamma\gamma}$ to the π^0 nominal mass [26] is performed to improve the mass resolution. For $\bar{D}^0 \to K^+\pi^-$, the backgrounds from cosmic ray events, radiative Bhabha scattering and dimuon events are suppressed with the same requirements as used in Ref. [34].

The ST $\bar{D}^0$ mesons are identified by the energy difference $\Delta E \equiv E_{\bar{D}^0} - E_{\rm beam}$ and the beam-constrained mass $M_{\rm BC} \equiv \sqrt{E_{\rm beam}^2 - |\vec{p}_{\bar{D}^0}|^2}$, where $E_{\rm beam}$ is the beam energy, and $E_{\bar{D}^0}$ and $\vec{p}_{\bar{D}^0}$ are the total energy and momentum of the ST $\bar{D}^0$ in the e^+e^- rest frame. If there are multiple combinations in an event, the combination with the smallest $|\Delta E|$ is chosen for each tag mode and for D^0 and $\bar{D}^0$. For one event, there may be up to six ST D candidates selected. To determine the ST yield, we fit the $M_{\rm BC}$ distributions of the accepted candidates after imposing mode dependent ΔE requirements. The signal is described by the MC-simulated shape convolved with a double-Gaussian function accounting for the resolution difference between data and MC simulation, and the background is modeled by an ARGUS function [35]. Fit results are shown in Figs. 1(a)–1(c). The corresponding ΔE and $M_{\rm BC}$ requirements, ST yields and efficiencies for various ST modes are summarized in Table I. The total ST yield is $N_{\rm ST}^{\rm tot} = 2341408 \pm 2056$.

Candidates for $D^0 \to K^-\mu^+\nu_\mu$ must contain two oppositely charged tracks which are identified as a kaon and a muon, respectively. The muon must have the same charge as the kaon on the ST side. To suppress the peaking

TABLE I. ΔE and $M_{\rm BC}$ requirements, ST yields $N_{\rm ST}$, ST efficiencies $\varepsilon_{\rm ST}$ and signal efficiencies $\varepsilon_{\rm SL}$ for different ST modes. Uncertainties are statistical only.

ST mode	ΔE (MeV)	$M_{\rm BC}$ (GeV/c^2)	$N_{\rm ST}$	$\varepsilon_{\rm ST}$ (%)	$\varepsilon_{\rm SL}$ (%)
$K^+\pi^-$	$(-29, 27)$	(1.858,1.874)	538865 ± 785	65.37 ± 0.09	57.74 ± 0.09
$K^+\pi^-\pi^0$	$(-69, 38)$	(1.858,1.874)	1080050 ± 1532	34.67 ± 0.04	61.23 ± 0.09
$K^+\pi^-\pi^-\pi^+$	$(-31, 28)$	(1.858,1.874)	722493 ± 1126	38.20 ± 0.06	56.42 ± 0.09

backgrounds from $D^0 \to K^-\pi^+(\pi^0)$, the $K^-\mu^+$ invariant mass ($M_{K^-\mu^+}$) is required to be less than 1.56 GeV/c^2, and the maximum energy of any photon that is not used in the ST selection ($E^{\rm max}_{{\rm extra}\gamma}$) must be less than 0.25 GeV.

The kinematic quantity $U_{\rm miss} \equiv E_{\rm miss} - |\vec{p}_{\rm miss}|$ is calculated for each event, where $E_{\rm miss}$ and $\vec{p}_{\rm miss}$ are the energy and momentum of the missing particle, which can be calculated by $E_{\rm miss} \equiv E_{\rm beam} - E_{K^-} - E_{\mu^+}$ and $\vec{p}_{\rm miss} \equiv \vec{p}_{D^0} - \vec{p}_{K^-} - \vec{p}_{\mu^+}$ in the e^+e^- center-of-mass frame, where $E_{K^-(\mu^+)}$ and $\vec{p}_{K^-(\mu^+)}$ are the energy and momentum of the kaon (muon) candidates. To improve the $U_{\rm miss}$ resolution, the D^0 energy is constrained to the beam energy and $\vec{p}_{D^0} \equiv -\hat{p}_{\bar{D}^0}\sqrt{E^2_{\rm beam} - m^2_{\bar{D}^0}}$, where $\hat{p}_{\bar{D}^0}$ is the unit vector in the momentum direction of the ST $\bar{D}^0$ and $m_{\bar{D}^0}$ is the $\bar{D}^0$ nominal mass [26].

The SL decay yield is obtained from an unbinned fit to the $U_{\rm miss}$ distribution of the accepted events of data, as shown in Fig. 1(d). In the fit, the signal, the peaking background of $D^0 \to K^-\pi^+\pi^0$ decay and other backgrounds are described by the corresponding MC-simulated shapes. The former two are convolved with the same Gaussian function to account for the resolution difference between data and MC simulation. All parameters are left free. The fitted signal yield is $N_{\rm DT} = 47100 \pm 259$.

The efficiencies of finding $D^0 \to K^-\mu^+\nu_\mu$ for different ST modes are summarized in Table I. They are weighted by the ST yields and give the average efficiency $\varepsilon_{\rm SL} = (58.93 \pm 0.07)\%$. To verify the reliability of the efficiency, typical distributions of the SL decay, e.g., momenta and $\cos\theta$ of K^- and μ^+, are checked and good consistency between data and MC simulation has been found (see Fig. 1 of Ref. [36]).

By inserting $N_{\rm DT}$, $\varepsilon_{\rm SL}$ and $N^{\rm tot}_{\rm ST}$ into Eq. (1), one obtains

$$\mathcal{B}_{D^0\to K^-\mu^+\nu_\mu} = (3.413 \pm 0.019_{\rm stat} \pm 0.035_{\rm syst})\%.$$

The systematic uncertainties in the BF measurement are described as follows. The uncertainty in $N^{\rm tot}_{\rm ST}$ is taken as 0.5% by examining the changes of the fitted yields by varying the fit range, the signal shape, and the endpoint of the ARGUS function. The efficiencies of muon and kaon tracking (PID) are studied with $e^+e^- \to \gamma\mu^+\mu^-$ events and DT hadronic events, respectively. The uncertainties of tracking and PID efficiencies each are assigned as 0.3% per kaon or muon. The differences of the momentum and $\cos\theta$ distributions between $D^0 \to K^-\mu^+\nu_\mu$ and the control samples have been considered. The uncertainty of the $E^{\rm max}_{{\rm extra}\gamma}$ requirement is estimated to be 0.1% by analyzing the DT hadronic events. The uncertainty in the $M_{K^-\mu^+}$ requirement is estimated with the alternative $M_{K^-\mu^+}$ requirements of 1.51 or 1.61 GeV/c^2, and the larger change on the BF 0.4% is taken as the systematic uncertainty. The uncertainty of the $U_{\rm miss}$ fit is estimated to be 0.5% by applying different fit ranges, and signal and background shapes. The uncertainty of the limited MC size is 0.1%. The uncertainty in the MC model is estimated to be 0.1%, which is the difference between our nominal DT efficiency and that determined by reweighting the q^2 distribution of the signal MC events to data with the obtained FF parameters (see below). The total uncertainty is 1.02%, which is obtained by adding these uncertainties in quadrature.

The BFs of $D^0 \to K^-\mu^+\nu_\mu$ and $\bar{D}^0 \to K^+\mu^-\bar{\nu}_\mu$ are measured separately. The results are $\mathcal{B}_{D^0\to K^-\mu^+\nu_\mu} = (3.433 \pm 0.026_{\rm stat} \pm 0.039_{\rm syst})\%$ and $\mathcal{B}_{\bar{D}^0\to K^+\mu^-\bar{\nu}_\mu} = (3.392 \pm 0.027_{\rm stat} \pm 0.034_{\rm syst})\%$. The BF asymmetry is determined to be $\mathcal{A} = [(\mathcal{B}_{D^0\to K^-\mu^+\nu_\mu} - \mathcal{B}_{\bar{D}^0\to K^+\mu^-\bar{\nu}_\mu})/(\mathcal{B}_{D^0\to K^-\mu^+\nu_\mu} + \mathcal{B}_{\bar{D}^0\to K^+\mu^-\bar{\nu}_\mu})] = (0.6 \pm 0.6_{\rm stat} \pm 0.8_{\rm syst})\%$, and no asymmetry in the BFs of $D^0 \to K^-\mu^+\nu_\mu$ and $\bar{D}^0 \to K^+\mu^-\bar{\nu}_\mu$ decays is found. All the systematic uncertainties except for those in the $E^{\rm max}_{{\rm extra}\gamma}$ requirement and MC model are studied separately and are not canceled out in the BF asymmetry calculation.

The $D^0 \to K^-\mu^+\nu_\mu$ dynamics is studied by dividing the SL candidate events into various q^2 intervals. The measured partial decay rate (PDR) in the ith q^2 interval, $\Delta\Gamma^i_{\rm msr}$, is determined by

$$\Delta\Gamma^i_{\rm msr} \equiv \int_i (d\Gamma/dq^2)dq^2 = N^i_{\rm pro}/(\tau_{D^0} \times N^{\rm tot}_{\rm ST}), \quad (2)$$

where $N^i_{\rm pro}$ is the SL decay signal yield produced in the ith q^2 interval, τ_{D^0} is the D^0 lifetime and $N^{\rm tot}_{\rm ST}$ is the ST yield. The signal yield produced in the ith q^2 interval in data is calculated by

$$N^i_{\rm pro} = \sum_j^{N_{\rm intervals}} (\varepsilon^{-1})_{ij} N^j_{\rm obs}, \quad (3)$$

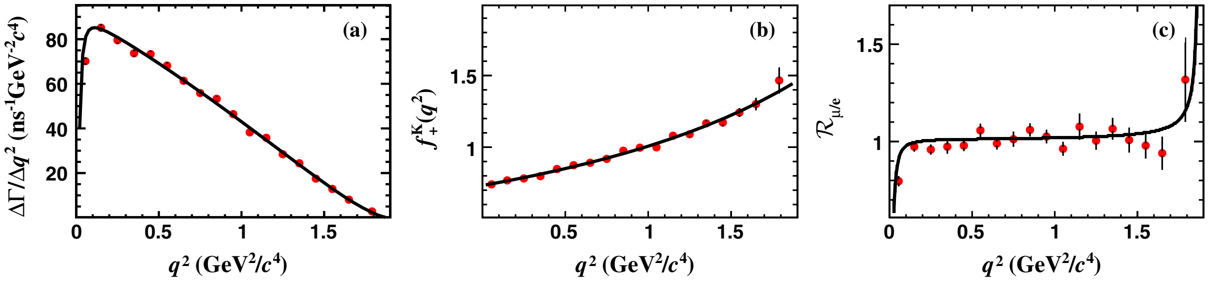

FIG. 2. (a) Fit to the PDRs, (b) projection to $f_+^K(q^2)$ for $D^0 \to K^-\mu^+\nu_\mu$, and (c) the measured $\mathcal{R}_{\mu/e}$ in each q^2 interval. Dots with error bars are data. Solid curves are the fit, the projection or the $\mathcal{R}_{\mu/e}$ expected with the parameters in Ref. [17] where the uncertainty is negligible due to strong correlations in hadronic FFs.

where the observed DT yield in the jth q^2 interval $N^j_{\rm obs}$ is obtained from the similar fit to the corresponding $U_{\rm miss}$ distribution of data (see Fig. 2 of Ref. [36]). ε is the efficiency matrix (Table I of Ref. [36]), which is obtained by analyzing the signal MC events and is given by

$$\varepsilon_{ij} = \sum_k (1/N^{\rm tot}_{\rm ST}) \times [(N^{ij}_{\rm rec} \times N_{\rm ST})/(N^j_{\rm gen} \times \varepsilon_{\rm ST})]_k, \quad (4)$$

where $N^{ij}_{\rm rec}$ is the DT yield generated in the jth q^2 interval and reconstructed in the ith q^2 interval, $N^j_{\rm gen}$ is the total signal yield generated in the jth q^2 interval, and the index k denotes the kth ST mode. The measured PDRs are shown in Fig. 2(a) and details can be found in Table II of Ref. [36].

The FF is parametrized as the series expansion parameterization [37] (SEP), which has been shown to be consistent with constraints from QCD [22,24,38]. The 2-parameter SEP is chosen and is given by

$$f_+^K(t) = \frac{1}{P(t)\Phi(t,t_0)} \frac{f_+^K(0)P(0)\Phi(0,t_0)}{1+r_1(t_0)z(0,t_0)} \times \{1 + r_1(t_0)[z(t,t_0)]\}. \quad (5)$$

Here, $P(t) = z(t, m^2_{D_s^*})$ and Φ is given by

$$\Phi(t,t_0) = \sqrt{\frac{1}{24\pi\chi_V}} \left(\frac{t_+ - t}{t_+ - t_0}\right)^{1/4} (\sqrt{t_+ - t} + \sqrt{t_+})^{-5} \times (\sqrt{t_+ - t} + \sqrt{t_+ - t_0})(\sqrt{t_+ - t} + \sqrt{t_+ - t_-})^{3/2} \times (t_+ - t)^{3/4}, \quad (6)$$

where $z(t,t_0) = [(\sqrt{t_+ - t} - \sqrt{t_+ - t_0})/(\sqrt{t_+ - t} + \sqrt{t_+ - t_0})]$, $t_\pm = (m_D \pm m_K)^2$, $t_0 = t_+(1 - \sqrt{1 - t_-/t_+})$, m_D and m_K are the masses of D and K particles, $m_{D_s^*}$ is the pole mass of the vector FF accounting for the strong interaction between D and K mesons and usually taken as the mass of the lowest lying $c\bar{s}$ vector meson D_s^* [26], and χ_V can be obtained from dispersion relations using perturbative QCD [39].

The PDRs are fitted by assuming the ratio $f_+^K(q^2)/f_-^K(q^2)$ to be independent of q^2, and minimizing the χ^2 constructed as

$$\chi^2 = \sum_{i,j=1}^{N_{\rm intervals}} (\Delta\Gamma^i_{\rm msr} - \Delta\Gamma^i_{\rm exp}) C^{-1}_{ij} (\Delta\Gamma^j_{\rm msr} - \Delta\Gamma^j_{\rm exp}), \quad (7)$$

where $\Delta\Gamma^i_{\rm exp}$ is the expected PDR in the ith q^2 interval given by [40,41]

$$\Delta\Gamma^i_{\rm exp} = \int_i \frac{G_F^2|V_{cs}|^2}{8\pi^3 m_D} |\vec{p}_K||f_+^K(q^2)|^2 \left(\frac{W_0 - E_K}{F_0}\right)^2 \times \left\{\frac{1}{3} m_D|\vec{p}_K|^2 + \frac{m_\ell^2}{8m_D}(m_D^2 + m_K^2 + 2m_D E_K) + \frac{1}{3} m_\ell^2 \frac{|\vec{p}_K|^2}{F_0} + \frac{1}{4} m_\ell^2 \frac{m_D^2 - m_K^2}{m_D} {\rm Re}\left[\frac{f_-^K(q^2)}{f_+^K(q^2)}\right] + \frac{1}{4} m_\ell^2 F_0 \left|\frac{f_-^K(q^2)}{f_+^K(q^2)}\right|^2\right\} dq^2, \quad (8)$$

and $C_{ij} = C^{\rm stat}_{ij} + C^{\rm syst}_{ij}$ is the covariance matrix of the measured PDRs among q^2 intervals. In Eq. (8), G_F is the Fermi coupling constant, m_ℓ is the mass of the lepton, $|\vec{p}_K|$ and E_K are the momentum and energy of the kaon in the D rest frame, $W_0 = (m_D^2 + m_K^2 - m_\ell^2)/(2m_D)$ is the maximum energy of the kaon in the D rest frame, and $F_0 = W_0 - E_K + m_\ell^2/(2m_D) = q^2/(2m_D)$. The statistical covariance matrix (Table III of Ref. [36]) is constructed as

$$C^{\rm stat}_{ij} = \left(\frac{1}{\tau_{D^0} N^{\rm tot}_{\rm ST}}\right)^2 \sum_\alpha \varepsilon^{-1}_{i\alpha} \varepsilon^{-1}_{j\alpha} [\sigma(N^\alpha_{\rm obs})]^2. \quad (9)$$

The systematic covariance matrix (Table IV of Ref. [36]) is obtained by summing all the covariance matrices for each source of systematic uncertainty. In general, it has the form

$$C^{\rm syst}_{ij} = \delta(\Delta\Gamma^i_{\rm msr})\delta(\Delta\Gamma^j_{\rm msr}), \quad (10)$$

where $\delta(\Delta\Gamma^i_{\rm msr})$ is the systematic uncertainty of the PDR in the ith q^2 interval. The systematic uncertainties in $N^{\rm tot}_{\rm ST}$, τ_{D^0}

and $E^{\max}_{\mathrm{extra}\gamma}$ requirement are considered to be fully correlated across q^2 intervals while others are studied separately in each q^2 interval with the same method used in the BF measurement.

Figures 2(a) and 2(b) show the fit to the PDRs of $D^0 \to K^-\mu^+\nu_\mu$ and the projection to $f^K_+(q^2)$. The goodness of fit is $\chi^2/\mathrm{NDOF} = 15.0/15$, where NDOF is the number of degrees of freedom. From the fit, we obtain the product of $f^K_+(0)|V_{cs}| = 0.7133 \pm 0.0038_{\mathrm{stat}} \pm 0.0030_{\mathrm{syst}}$, the first order coefficient $r_1 = -1.90 \pm 0.21_{\mathrm{stat}} \pm 0.07_{\mathrm{syst}}$, and the FF ratio $f^K_-/f^K_+ = -0.6 \pm 0.8_{\mathrm{stat}} \pm 0.2_{\mathrm{syst}}$. The nominal fit parameters are taken from the results obtained by fitting with the combined statistical and systematic covariance matrix, and the statistical uncertainties of the fit parameters are taken from the fit with only the statistical covariance matrix. For each parameter, the systematic uncertainty is obtained by calculating the quadratic difference of uncertainties between these two fits.

Combining $\mathcal{B}_{D^0\to K^-\mu^+\nu_\mu}$ with our previous measurement $\mathcal{B}_{D^0\to K^-e^+\nu_e} = (3.505 \pm 0.014_{\mathrm{stat}} \pm 0.033_{\mathrm{syst}})\%$ [24] gives $\mathcal{R}_{\mu/e} = 0.974 \pm 0.007_{\mathrm{stat}} \pm 0.012_{\mathrm{syst}}$, which agrees with the theoretical calculations with LQCD [16,17] and an SM quark model [42]. Additionally, we determine $\mathcal{R}_{\mu/e}$ in each q^2 interval, as shown in Fig. 2(c), where the error bars include both statistical and the uncanceled systematic uncertainties. In the $\mathcal{R}_{\mu/e}$ calculation, the uncertainties in $N^{\mathrm{tot}}_{\mathrm{ST}}$, τ_{D^0} as well as the tracking and PID efficiencies of the kaon cancel. Below $q^2 = 0.1\ \mathrm{GeV}^2/c^4$, $\mathcal{R}_{\mu/e}$ is significantly lower than 1 due to smaller phase space for $D^0 \to K^-\mu^+\nu_\mu$ with nonzero muon mass that cannot be neglected. Above $0.1\ \mathrm{GeV}^2/c^4$, $\mathcal{R}_{\mu/e}$ is close to 1. They are consistent with the SM prediction, and no deviation larger than 2σ is observed.

In summary, by analyzing 2.93 fb^{-1} of data collected at $\sqrt{s} = 3.773$ GeV with the BESIII detector, we present an improved measurement of the absolute BF of the SL decay $D^0 \to K^-\mu^+\nu_\mu$. Our result is consistent with the PDG value [26] and improves its precision by a factor of three. Combining the previous BESIII measurements of $D^0 \to K^-e^+\nu_e$, we calculate $\mathcal{R}_{\mu/e}$ ratios in the full q^2 range and various q^2 intervals. No significant evidence of LFU violation is found with current statistics and systematic uncertainties. By fitting the PDRs of this decay, we obtain $f^K_+(0)|V_{cs}| = 0.7133 \pm 0.0038_{\mathrm{stat}} \pm 0.0029_{\mathrm{syst}}$. Using $|V_{cs}|$ given by global fit in the SM [26] yields $f^K_+(0) = 0.7327 \pm 0.0039_{\mathrm{stat}} \pm 0.0030_{\mathrm{syst}}$, while using the $f^K_+(0)$ calculated in LQCD [27] results in $|V_{cs}| = 0.955 \pm 0.005_{\mathrm{stat}} \pm 0.004_{\mathrm{syst}} \pm 0.024_{\mathrm{LQCD}}$. These results are consistent with our measurements using $D^{0(+)} \to \bar{K}e^+\nu_e$ [24,43,44] and $D^+_s \to \mu^+\nu_\mu$ [45] within uncertainties and are important to test the LQCD calculation of $f^K_+(0)$ [17,27,46] and quark mixing matrix unitarity with better accuracy.

The BESIII collaboration thanks the staff of BEPCII and the IHEP computing center for their strong support. This work is supported in part by National Key Basic Research Program of China under Contract No. 2015CB856700; National Natural Science Foundation of China (NSFC) under Contracts No. 11305180, No. 11775230, No. 11235011, No. 11335008, No. 11425524, No. 11625523, and No. 11635010; the Chinese Academy of Sciences (CAS) Large-Scale Scientific Facility Program; the CAS Center for Excellence in Particle Physics (CCEPP); Joint Large-Scale Scientific Facility Funds of the NSFC and CAS under Contracts No. U1632109, No. U1332201, No. U1532257, and No. U1532258; CAS under Contracts No. KJCX2-YW-N29, No. KJCX2-YW-N45, and No. QYZDJ-SSW-SLH003; 100 Talents Program of CAS; National 1000 Talents Program of China; INPAC and Shanghai Key Laboratory for Particle Physics and Cosmology; German Research Foundation DFG under Contracts No. Collaborative Research Center CRC 1044, No. FOR 2359; Instituto Nazionale di Fisica Nucleare, Italy; Koninklijke Nederlandse Akademie van Wetenschappen (KNAW) under Contract No. 530-4CDP03; Ministry of Development of Turkey under Contract No. DPT2006K-120470; National Science and Technology fund; The Swedish Research Council; U.S. Department of Energy under Contracts No. DE-FG02-05ER41374, No. DE-SC-0010118, No. DE-SC-0010504, and No. DE-SC-0012069; University of Groningen (RuG) and the Helmholtzzentrum fuer Schwerionenforschung GmbH (GSI), Darmstadt; WCU Program of National Research Foundation of Korea under Contract No. R32-2008-000-10155-0.

[a]Also at Bogazici University, 34342 Istanbul, Turkey.
[b]Also at the Moscow Institute of Physics and Technology, Moscow 141700, Russia.
[c]Also at the Functional Electronics Laboratory, Tomsk State University, Tomsk 634050, Russia.
[d]Also at the Novosibirsk State University, Novosibirsk 630090, Russia.
[e]Also at the NRC "Kurchatov Institute," PNPI, Gatchina 188300, Russia.
[f]Also at Istanbul Arel University, 34295 Istanbul, Turkey.
[g]Also at Goethe University Frankfurt, 60323 Frankfurt am Main, Germany.
[h]Also at Key Laboratory for Particle Physics, Astrophysics and Cosmology, Ministry of Education; Shanghai Key Laboratory for Particle Physics and Cosmology; Institute of Nuclear and Particle Physics, Shanghai 200240, People's Republic of China.
[i]Government College Women University, Sialkot 51310, Punjab, Pakistan.
[j]Center for Underground Physics, Institute for Basic Science, Daejeon 34126, Korea.

[1] J. P. Lees *et al.* (*BABAR* Collaboration), Phys. Rev. Lett. **109**, 101802 (2012).

[2] J. P. Lees *et al.* (*BABAR* Collaboration), Phys. Rev. D **88**, 072012 (2013).
[3] R. Aaij *et al.* (LHCb Collaboration), Phys. Rev. Lett. **115**, 111803 (2015).
[4] M. Huschle *et al.* (Belle Collaboration), Phys. Rev. D **92**, 072014 (2015).
[5] Y. Sato *et al.* (Belle Collaboration), Phys. Rev. D **94**, 072007 (2016).
[6] R. Aaij *et al.* (LHCb Collaboration), Phys. Rev. Lett. **113**, 151601 (2014).
[7] R. Aaij *et al.* (LHCb Collaboration), J. High Energy Phys. 08 (2017) 055.
[8] Y. Amhis *et al.* (HFLAV Collaboration), Eur. Phys. J. C **77**, 895 (2017).
[9] S. Fajfer, J. F. Kamenik, and I. Nisandzic, Phys. Rev. D **85**, 094025 (2012).
[10] S. Fajfer, J. F. Kamenik, I. Nisandzic, and J. Zupan, Phys. Rev. Lett. **109**, 161801 (2012).
[11] A. Celis, M. Jung, X.-Q. Li, and A. Pich, J. High Energy Phys. 01 (2013) 054.
[12] A. Crivellin, G. D'Ambrosio, and J. Heeck, Phys. Rev. Lett. **114**, 151801 (2015).
[13] A. Crivellin, J. Heeck, and P. Stoffer, Phys. Rev. Lett. **116**, 081801 (2016).
[14] M. Bauer and M. Neubert, Phys. Rev. Lett. **116**, 141802 (2016).
[15] S. Fajfer, I. Nisandzic, and U. Rojec, Phys. Rev. D **91**, 094009 (2015).
[16] L. Riggio, G. Salerno, and S. Simula, Eur. Phys. J. C **78**, 501 (2018).
[17] V. Lubicz, L. Riggio, G. Salerno, S. Simula, and C. Tarantino (ETM Collaboration), Phys. Rev. D **96**, 054514 (2017).
[18] Throughout this Letter, the charge conjugate channels are implied unless otherwise stated.
[19] J. Zhang, C. X. Yue, and C. H. Li, Eur. Phys. J. C **78**, 695 (2018).
[20] Y. Fang, G. Rong, H. L. Ma, and J. Y. Zhao, Eur. Phys. J. C **75**, 10 (2015).
[21] L. Widhalm *et al.* (Belle Collaboration), Phys. Rev. Lett. **97**, 061804 (2006).
[22] D. Besson *et al.* (CLEO Collaboration), Phys. Rev. D **80**, 032005 (2009).
[23] B. Aubert *et al.* (*BABAR* Collaboration), Phys. Rev. D **76**, 052005 (2007).
[24] M. Ablikim *et al.* (BESIII Collaboration), Phys. Rev. D **92**, 072012 (2015).
[25] J. M. Link *et al.* (FOCUS Collaboration), Phys. Lett. B **607**, 233 (2005).
[26] M. Tanabashi *et al.* (Particle Data Group), Phys. Rev. D **98**, 030001 (2018).
[27] H. Na, C. T. H. Davies, E. Follana, G. P. Lepage, and J. Shigemitsu (HPQCD Collaboration), Phys. Rev. D **82**, 114506 (2010).
[28] M. Ablikim *et al.* (BESIII Collaboration), Nucl. Instrum. Methods Phys. Res., Sect. A **614**, 345 (2010).
[29] S. Agostinelli *et al.* (GEANT4 Collaboration), Nucl. Instrum. Methods Phys. Res., Sect. A **506**, 250 (2003).
[30] S. Jadach, B. F. L. Ward, and Z. Was, Comput. Phys. Commun. **130**, 260 (2000); Phys. Rev. D **63**, 113009 (2001).
[31] D. J. Lange, Nucl. Instrum. Methods Phys. Res., Sect. A **462**, 152 (2001); R. G. Ping, Chin. Phys. C **32**, 599 (2008).
[32] J. C. Chen, G. S. Huang, X. R. Qi, D. H. Zhang, and Y. S. Zhu, Phys. Rev. D **62**, 034003 (2000).
[33] D. Becirevic and A. B. Kaidalov, Phys. Lett. B **478**, 417 (2000).
[34] M. Ablikim *et al.* (BESIII Collaboration), Phys. Lett. B **734**, 227 (2014).
[35] H. Albrecht *et al.* (ARGUS Collaboration), Phys. Lett. B **241**, 278 (1990).
[36] See Supplemental Material at http://link.aps.org/supplemental/10.1103/PhysRevLett.122.011804 for the comparisons of some typical distributions between data and MC simulation, efficiency matrix, fits to $U_{\rm miss}$ distributions in 18 q^2 intervals, PDR and $\mathcal{R}_{\mu/e}$ in each q^2 interval, and statistical and systematic covariance matrices.
[37] T. Becher and R. J. Hill, Phys. Lett. B **633**, 61 (2006).
[38] J. P. Lees *et al.* (*BABAR* Collaboration), Phys. Rev. D **91**, 052022 (2015).
[39] C. G. Boyd, B. Grinstein, and R. F. Lebed, Nucl. Phys. **B461**, 493 (1996).
[40] J. M. Link *et al.* (FOCUS Collaboration), Phys. Lett. B **607**, 233 (2005).
[41] J. G. Korner and G. A. Schuler, Z. Phys. C **46**, 93 (1990).
[42] N. R. Soni and J. N. Pandya, Phys. Rev. D **96**, 016017 (2017).
[43] M. Ablikim *et al.* (BESIII Collaboration), Phys. Rev. D **96**, 012002 (2017).
[44] M. Ablikim *et al.* (BESIII Collaboration), Phys. Rev. D **92**, 112008 (2015).
[45] M. Ablikim *et al.* (BESIII Collaboration), arXiv:1811.10890.
[46] C. Aubin *et al.* (Fermilab Lattice and MILC and HPQCD Collaborations), Phys. Rev. Lett. **94**, 011601 (2005).

Determination of the Pseudoscalar Decay Constant $f_{D_s^+}$ via $D_s^+ \to \mu^+\nu_\mu$

M. Ablikim,[1] M. N. Achasov,[9,d] S. Ahmed,[14] M. Albrecht,[4] M. Alekseev,[56a,56c] A. Amoroso,[56a,56c] F. F. An,[1] Q. An,[53,43] Y. Bai,[42] O. Bakina,[26] R. Baldini Ferroli,[22a] Y. Ban,[34] K. Begzsuren,[24] D. W. Bennett,[21] J. V. Bennett,[5] N. Berger,[25] M. Bertani,[22a] D. Bettoni,[23a] F. Bianchi,[56a,56c] I. Boyko,[26] R. A. Briere,[5] H. Cai,[58] X. Cai,[1,43] O. Cakir,[46a] A. Calcaterra,[22a] G. F. Cao,[1,47] S. A. Cetin,[46b] J. Chai,[56c] J. F. Chang,[1,43] W. L. Chang,[1,47] G. Chelkov,[26,b,c] G. Chen,[1] H. S. Chen,[1,47] J. C. Chen,[1] M. L. Chen,[1,43] P. L. Chen,[54] S. J. Chen,[32] Y. B. Chen,[1,43] G. Cibinetto,[23a] F. Cossio,[56c] H. L. Dai,[1,43] J. P. Dai,[38,h] A. Dbeyssi,[14] D. Dedovich,[26] Z. Y. Deng,[1] A. Denig,[25] I. Denysenko,[26] M. Destefanis,[56a,56c] F. De Mori,[56a,56c] Y. Ding,[30] C. Dong,[33] J. Dong,[1,43] L. Y. Dong,[1,47] M. Y. Dong,[1,43,47] Z. L. Dou,[32] S. X. Du,[61] P. F. Duan,[1] J. Z. Fan,[45] J. Fang,[1,43] S. S. Fang,[1,47] Y. Fang,[1] R. Farinelli,[23a,23b] L. Fava,[56b,56c] S. Fegan,[25] F. Feldbauer,[4] G. Felici,[22a] C. Q. Feng,[53,43] M. Fritsch,[4] C. D. Fu,[1] Y. Fu,[1] Q. Gao,[1] X. L. Gao,[53,43] Y. Gao,[45] Y. G. Gao,[6] Z. Gao,[53,43] B. Garillon,[25] I. Garzia,[23a] A. Gilman,[50] K. Goetzen,[10] L. Gong,[33] W. X. Gong,[1,43] W. Gradl,[25] M. Greco,[56a,56c] L. M. Gu,[32] M. H. Gu,[1,43] Y. T. Gu,[12] A. Q. Guo,[1] L. B. Guo,[31] R. P. Guo,[36] Y. P. Guo,[25] A. Guskov,[26] Z. Haddadi,[28] S. Han,[58] X. Q. Hao,[15] F. A. Harris,[48] K. L. He,[1,47] F. H. Heinsius,[4] T. Held,[4] Y. K. Heng,[1,43,47] T. Holtmann,[4] Z. L. Hou,[1] H. M. Hu,[1,47] J. F. Hu,[38,h] T. Hu,[1,43,47] Y. Hu,[1] G. S. Huang,[53,43] J. S. Huang,[15] X. T. Huang,[37] X. Z. Huang,[32] Z. L. Huang,[30] T. Hussain,[55] W. Ikegami Andersson,[57] M. Irshad,[53,43] Q. Ji,[1] Q. P. Ji,[15] X. B. Ji,[1,47] X. L. Ji,[1,43] X. S. Jiang,[1,43,47] X. Y. Jiang,[33] J. B. Jiao,[37] Z. Jiao,[17] D. P. Jin,[1,43,47] S. Jin,[32] Y. Jin,[49] T. Johansson,[57] A. Julin,[50] N. Kalantar-Nayestanaki,[28] X. S. Kang,[33] M. Kavatsyuk,[28] B. C. Ke,[1] T. Khan,[53,43] A. Khoukaz,[51] P. Kiese,[25] R. Kliemt,[10] L. Koch,[27] O. B. Kolcu,[46b,f] B. Kopf,[4] M. Kornicer,[48] M. Kuemmel,[4] M. Kuessner,[4] A. Kupsc,[57] M. Kurth,[1] W. Kühn,[27] J. S. Lange,[27] M. Lara,[21] P. Larin,[14] L. Lavezzi,[56c] S. Leiber,[4] H. Leithoff,[25] C. Li,[57] Cheng Li,[53,43] D. M. Li,[61] F. Li,[1,43] F. Y. Li,[34] G. Li,[1] H. B. Li,[1,47] H. J. Li,[1,47] J. C. Li,[1] J. W. Li,[41] Ke Li,[1] Lei Li,[3] P. L. Li,[53,43] P. R. Li,[47,7] Q. Y. Li,[37] T. Li,[37] W. D. Li,[1,47] W. G. Li,[1] X. L. Li,[37] X. N. Li,[1,43] X. Q. Li,[33] Z. B. Li,[44] H. Liang,[53,43] Y. F. Liang,[40] Y. T. Liang,[27] G. R. Liao,[11] L. Z. Liao,[1,47] J. Libby,[20] C. X. Lin,[44] D. X. Lin,[14] B. Liu,[38,h] B. J. Liu,[1] C. X. Liu,[1] D. Liu,[53,43] D. Y. Liu,[38,h] F. H. Liu,[39] Fang Liu,[1] Feng Liu,[6] H. B. Liu,[12] H. L. Liu,[42] H. M. Liu,[1,47] Huanhuan Liu,[1] Huihui Liu,[16] J. B. Liu,[53,43] J. Y. Liu,[1,47] K. Liu,[45] K. Y. Liu,[30] Ke Liu,[6] Q. Liu,[47] S. B. Liu,[53,43] X. Liu,[29] Y. B. Liu,[33] Z. A. Liu,[1,43,47] Zhiqing Liu,[25] Y. F. Long,[34] X. C. Lou,[1,43,47] H. J. Lu,[17] J. D. Lu,[1,47] J. G. Lu,[1,43] Y. Lu,[1] Y. P. Lu,[1,43] C. L. Luo,[31] M. X. Luo,[60] X. L. Luo,[1,43] S. Lusso,[56c] X. R. Lyu,[47] F. C. Ma,[30] H. L. Ma,[1] L. L. Ma,[37] M. M. Ma,[1,47] Q. M. Ma,[1] X. N. Ma,[33] X. X. Ma,[1,47] X. Y. Ma,[1,43] Y. M. Ma,[37] F. E. Maas,[14] M. Maggiora,[56a,56c] Q. A. Malik,[55] A. Mangoni,[22b] Y. J. Mao,[34] Z. P. Mao,[1] S. Marcello,[56a,56c] Z. X. Meng,[49] J. G. Messchendorp,[28] G. Mezzadri,[23a] J. Min,[1,43] T. J. Min,[32] R. E. Mitchell,[21] X. H. Mo,[1,43,47] Y. J. Mo,[6] C. Morales Morales,[14] G. Morello,[22a] N. Yu. Muchnoi,[9,d] H. Muramatsu,[50] A. Mustafa,[4] S. Nakhoul,[10,g] Y. Nefedov,[26] F. Nerling,[10,g] I. B. Nikolaev,[9,d] Z. Ning,[1,43] S. Nisar,[8,k] S. L. Niu,[1,43] S. L. Olsen,[35,j] Q. Ouyang,[1,43,47] S. Pacetti,[22b] Y. Pan,[53,43] M. Papenbrock,[57] P. Patteri,[22a] M. Pelizaeus,[4] J. Pellegrino,[56a,56c] H. P. Peng,[53,43] K. Peters,[10,g] J. Pettersson,[57] J. L. Ping,[31] R. G. Ping,[1,47] A. Pitka,[4] R. Poling,[50] V. Prasad,[53,43] H. R. Qi,[2] M. Qi,[32] T. Y. Qi,[2] S. Qian,[1,43] C. F. Qiao,[47] N. Qin,[58] X. S. Qin,[4] Z. H. Qin,[1,43] J. F. Qiu,[1] K. H. Rashid,[55,i] C. F. Redmer,[25] M. Richter,[4] M. Ripka,[25] M. Rolo,[56c] G. Rong,[1,47] Ch. Rosner,[14] A. Sarantsev,[26,e] M. Savrié,[23b] C. Schnier,[4] K. Schoenning,[57] W. Shan,[18] X. Y. Shan,[53,43] M. Shao,[53,43] C. P. Shen,[2] P. X. Shen,[33] X. Y. Shen,[1,47] H. Y. Sheng,[1] X. Shi,[1,43] J. J. Song,[37] W. M. Song,[37] X. Y. Song,[1] S. Sosio,[56a,56c] C. Sowa,[4] S. Spataro,[56a,56c] G. X. Sun,[1] J. F. Sun,[15] L. Sun,[58] S. S. Sun,[1,47] X. H. Sun,[1] Y. J. Sun,[53,43] Y. K. Sun,[53,43] Y. Z. Sun,[1] Z. J. Sun,[1,43] Z. T. Sun,[21] Y. T. Tan,[53,43] C. J. Tang,[40] G. Y. Tang,[1] X. Tang,[1] I. Tapan,[46c] M. Tiemens,[28] B. Tsednee,[24] I. Uman,[46d] G. S. Varner,[48] B. Wang,[1] B. L. Wang,[47] C. W. Wang,[32] D. Y. Wang,[34] Dan Wang,[47] K. Wang,[1,43] L. L. Wang,[1] L. S. Wang,[1] M. Wang,[37] Meng Wang,[1,47] P. Wang,[1] P. L. Wang,[1] W. P. Wang,[53,43] X. F. Wang,[1] Y. Wang,[53,43] Y. F. Wang,[1,43,47] Y. Q. Wang,[25] Z. Wang,[1,43] Z. G. Wang,[1,43] Z. Y. Wang,[1] Zongyuan Wang,[1,47] T. Weber,[4] D. H. Wei,[11] P. Weidenkaff,[25] S. P. Wen,[1] U. Wiedner,[4] M. Wolke,[57] L. H. Wu,[1] L. J. Wu,[1,47] Z. Wu,[1,43] L. Xia,[53,43] X. Xia,[37] Y. Xia,[19] D. Xiao,[1] Y. J. Xiao,[1,47] Z. J. Xiao,[31] Y. G. Xie,[1,43] Y. H. Xie,[6] X. A. Xiong,[1,47] Q. L. Xiu,[1,43] G. F. Xu,[1] J. J. Xu,[1,47] L. Xu,[1] Q. J. Xu,[13] Q. N. Xu,[47] X. P. Xu,[41] F. Yan,[54] L. Yan,[56a,56c] W. B. Yan,[53,43] W. C. Yan,[2] Y. H. Yan,[19] H. J. Yang,[38,h] H. X. Yang,[1] L. Yang,[58] S. L. Yang,[1,47] Y. H. Yang,[32] Y. X. Yang,[11] Yifan Yang,[1,47] M. Ye,[1,43] M. H. Ye,[7] J. H. Yin,[1] Z. Y. You,[44] B. X. Yu,[1,43,47] C. X. Yu,[33] C. Z. Yuan,[1,47] Y. Yuan,[1] A. Yuncu,[46b,a] A. A. Zafar,[55] A. Zallo,[22a] Y. Zeng,[19] Z. Zeng,[53,43] B. X. Zhang,[1] B. Y. Zhang,[1,43] C. C. Zhang,[1] D. H. Zhang,[1] H. H. Zhang,[44] H. Y. Zhang,[1,43] J. Zhang,[1,47] J. L. Zhang,[59] J. Q. Zhang,[4] J. W. Zhang,[1,43,47] J. Y. Zhang,[1] J. Z. Zhang,[1,47] K. Zhang,[1,47] L. Zhang,[45] S. F. Zhang,[32] T. J. Zhang,[38,h] X. Y. Zhang,[37] Y. Zhang,[53,43] Y. H. Zhang,[1,43] Y. T. Zhang,[53,43] Yang Zhang,[1] Yao Zhang,[1] Yu Zhang,[47] Z. H. Zhang,[6] Z. P. Zhang,[53] Z. Y. Zhang,[58] G. Zhao,[1] J. W. Zhao,[1,43] J. Y. Zhao,[1,47] J. Z. Zhao,[1,43] Lei Zhao,[53,43] Ling Zhao,[1] M. G. Zhao,[33] Q. Zhao,[1] S. J. Zhao,[61] T. C. Zhao,[1] Y. B. Zhao,[1,43] Z. G. Zhao,[53,43] A. Zhemchugov,[26,b] B. Zheng,[54] J. P. Zheng,[1,43] W. J. Zheng,[37] Y. H. Zheng,[47] B. Zhong,[31] L. Zhou,[1,43] Q. Zhou,[1,47] X. Zhou,[58] X. K. Zhou,[53,43] X. R. Zhou,[53,43] X. Y. Zhou,[1] A. N. Zhu,[1,47] J. Zhu,[33] J. Zhu,[44] K. Zhu,[1] K. J. Zhu,[1,43,47] S. Zhu,[1] S. H. Zhu,[52] X. L. Zhu,[45] Y. C. Zhu,[53,43] Y. S. Zhu,[1,47] Z. A. Zhu,[1,47] J. Zhuang,[1,43] B. S. Zou,[1] and J. H. Zou[1]

(BESIII Collaboration)

[1]*Institute of High Energy Physics, Beijing 100049, People's Republic of China*
[2]*Beihang University, Beijing 100191, People's Republic of China*
[3]*Beijing Institute of Petrochemical Technology, Beijing 102617, People's Republic of China*
[4]*Bochum Ruhr-University, D-44780 Bochum, Germany*
[5]*Carnegie Mellon University, Pittsburgh, Pennsylvania 15213, USA*
[6]*Central China Normal University, Wuhan 430079, People's Republic of China*
[7]*China Center of Advanced Science and Technology, Beijing 100190, People's Republic of China*
[8]*COMSATS University Islamabad, Lahore Campus, Defence Road, Off Raiwind Road, 54000 Lahore, Pakistan*
[9]*G.I. Budker Institute of Nuclear Physics SB RAS (BINP), Novosibirsk 630090, Russia*
[10]*GSI Helmholtzcentre for Heavy Ion Research GmbH, D-64291 Darmstadt, Germany*
[11]*Guangxi Normal University, Guilin 541004, People's Republic of China*
[12]*Guangxi University, Nanning 530004, People's Republic of China*
[13]*Hangzhou Normal University, Hangzhou 310036, People's Republic of China*
[14]*Helmholtz Institute Mainz, Johann-Joachim-Becher-Weg 45, D-55099 Mainz, Germany*
[15]*Henan Normal University, Xinxiang 453007, People's Republic of China*
[16]*Henan University of Science and Technology, Luoyang 471003, People's Republic of China*
[17]*Huangshan College, Huangshan 245000, People's Republic of China*
[18]*Hunan Normal University, Changsha 410081, People's Republic of China*
[19]*Hunan University, Changsha 410082, People's Republic of China*
[20]*Indian Institute of Technology Madras, Chennai 600036, India*
[21]*Indiana University, Bloomington, Indiana 47405, USA*
[22a]*INFN Laboratori Nazionali di Frascati, I-00044, Frascati, Italy*
[22b]*INFN and University of Perugia, I-06100, Perugia, Italy*
[23a]*INFN Sezione di Ferrara, I-44122, Ferrara, Italy*
[23b]*University of Ferrara, I-44122, Ferrara, Italy*
[24]*Institute of Physics and Technology, Peace Ave. 54B, Ulaanbaatar 13330, Mongolia*
[25]*Johannes Gutenberg University of Mainz, Johann-Joachim-Becher-Weg 45, D-55099 Mainz, Germany*
[26]*Joint Institute for Nuclear Research, 141980 Dubna, Moscow region, Russia*
[27]*Justus-Liebig-Universitaet Giessen, II. Physikalisches Institut, Heinrich-Buff-Ring 16, D-35392 Giessen, Germany*
[28]*KVI-CART, University of Groningen, NL-9747 AA Groningen, Netherlands*
[29]*Lanzhou University, Lanzhou 730000, People's Republic of China*
[30]*Liaoning University, Shenyang 110036, People's Republic of China*
[31]*Nanjing Normal University, Nanjing 210023, People's Republic of China*
[32]*Nanjing University, Nanjing 210093, People's Republic of China*
[33]*Nankai University, Tianjin 300071, People's Republic of China*
[34]*Peking University, Beijing 100871, People's Republic of China*
[35]*Seoul National University, Seoul, 151-747 Korea*
[36]*Shandong Normal University, Jinan 250014, People's Republic of China*
[37]*Shandong University, Jinan 250100, People's Republic of China*
[38]*Shanghai Jiao Tong University, Shanghai 200240, People's Republic of China*
[39]*Shanxi University, Taiyuan 030006, People's Republic of China*
[40]*Sichuan University, Chengdu 610064, People's Republic of China*
[41]*Soochow University, Suzhou 215006, People's Republic of China*
[42]*Southeast University, Nanjing 211100, People's Republic of China*
[43]*State Key Laboratory of Particle Detection and Electronics, Beijing 100049, Hefei 230026, People's Republic of China*
[44]*Sun Yat-Sen University, Guangzhou 510275, People's Republic of China*
[45]*Tsinghua University, Beijing 100084, People's Republic of China*
[46a]*Ankara University, 06100 Tandogan, Ankara, Turkey*
[46b]*Istanbul Bilgi University, 34060 Eyup, Istanbul, Turkey*
[46c]*Uludag University, 16059 Bursa, Turkey*
[46d]*Near East University, Nicosia, North Cyprus, Mersin 10, Turkey*
[47]*University of Chinese Academy of Sciences, Beijing 100049, People's Republic of China*

[48]University of Hawaii, Honolulu, Hawaii 96822, USA
[49]University of Jinan, Jinan 250022, People's Republic of China
[50]University of Minnesota, Minneapolis, Minnesota 55455, USA
[51]University of Muenster, Wilhelm-Klemm-Str. 9, 48149 Muenster, Germany
[52]University of Science and Technology Liaoning, Anshan 114051, People's Republic of China
[53]University of Science and Technology of China, Hefei 230026, People's Republic of China
[54]University of South China, Hengyang 421001, People's Republic of China
[55]University of the Punjab, Lahore-54590, Pakistan
[56a]University of Turin, I-10125, Turin, Italy
[56b]University of Eastern Piedmont, I-15121, Alessandria, Italy
[56c]INFN, I-10125, Turin, Italy
[57]Uppsala University, Box 516, SE-75120 Uppsala, Sweden
[58]Wuhan University, Wuhan 430072, People's Republic of China
[59]Xinyang Normal University, Xinyang 464000, People's Republic of China
[60]Zhejiang University, Hangzhou 310027, People's Republic of China
[61]Zhengzhou University, Zhengzhou 450001, People's Republic of China

(Received 27 November 2018; revised manuscript received 18 January 2019; published 22 February 2019)

Using a 3.19 fb^{-1} data sample collected at an e^+e^- center-of-mass energy of $E_{\mathrm{cm}} = 4.178$ GeV with the BESIII detector, we measure the branching fraction of the leptonic decay $D_s^+ \to \mu^+\nu_\mu$ to be $\mathcal{B}_{D_s^+\to\mu^+\nu_\mu} = (5.49 \pm 0.16_{\mathrm{stat}} \pm 0.15_{\mathrm{syst}}) \times 10^{-3}$. Combining our branching fraction with the masses of the D_s^+ and μ^+ and the lifetime of the D_s^+, we determine $f_{D_s^+}|V_{cs}| = 246.2 \pm 3.6_{\mathrm{stat}} \pm 3.5_{\mathrm{syst}}$ MeV. Using the $c \to s$ quark mixing matrix element $|V_{cs}|$ determined from a global standard model fit, we evaluate the D_s^+ decay constant $f_{D_s^+} = 252.9 \pm 3.7_{\mathrm{stat}} \pm 3.6_{\mathrm{syst}}$ MeV. Alternatively, using the value of $f_{D_s^+}$ calculated by lattice quantum chromodynamics, we find $|V_{cs}| = 0.985 \pm 0.014_{\mathrm{stat}} \pm 0.014_{\mathrm{syst}}$. These values of $\mathcal{B}_{D_s^+\to\mu^+\nu_\mu}$, $f_{D_s^+}|V_{cs}|$, $f_{D_s^+}$ and $|V_{cs}|$ are each the most precise results to date.

DOI: 10.1103/PhysRevLett.122.071802

The leptonic decay $D_s^+ \to \ell^+\nu_\ell$ ($\ell = e$, μ, or τ) offers a unique window into both strong and weak effects in the charm quark sector. In the standard model (SM), the partial width of the decay $D_s^+ \to \ell^+\nu_\ell$ can be written as [1]

$$\Gamma_{D_s^+\to\ell^+\nu_\ell} = \frac{G_F^2}{8\pi}|V_{cs}|^2 f_{D_s^+}^2 m_\ell^2 m_{D_s^+}\left(1 - \frac{m_\ell^2}{m_{D_s^+}^2}\right)^2, \quad (1)$$

where $f_{D_s^+}$ is the D_s^+ decay constant, $|V_{cs}|$ is the $c \to s$ Cabibbo-Kobayashi-Maskawa (CKM) matrix element, G_F is the Fermi coupling constant, m_ℓ is the lepton mass, and $m_{D_s^+}$ is the D_s^+ mass. In recent years, much progress has been achieved in the measurements of $f_{D_s^+}$ and $|V_{cs}|$ with $D_s^+ \to \ell^+\nu_\ell$ decays at the CLEO [2–4], *BABAR* [5], Belle [6] and BESIII [7] experiments. However, compared to the precision of the most accurate lattice quantum chromodynamics (LQCD) calculation of $f_{D_s^+}$ [8], the accuracy of the measurements is still limited. Improved measurements of $f_{D_s^+}$ and $|V_{cs}|$ are critical to calibrate various theoretical calculations of $f_{D_s^+}$ [8–37], such as those from quenched and unquenched LQCD, QCD sum rules, etc., and to test the unitarity of the quark mixing matrix with better precision.

In the SM, the ratio of the branching fraction (BF) of $D_s^+ \to \tau^+\nu_\tau$ over that of $D_s^+ \to \mu^+\nu_\mu$ is predicted to be 9.74 with negligible uncertainty and the BFs of $D_s^+ \to \mu^+\nu_\mu$ and $D_s^- \to \mu^-\bar{\nu}_\mu$ decays are expected to be the same. However, hints of lepton flavor universality (LFU) violation in semileptonic B decays were recently reported at *BABAR*, LHCb, and Belle [38–42]. It has been argued that new physics mechanisms, such as a two-Higgs-doublet model with the mediation of charged Higgs bosons [43,44] or a seesaw mechanism due to lepton mixing with Majorana neutrinos [45], may cause LFU or CP violation. Tests of LFU and searches for CP violation in $D_s^+ \to \ell^+\nu_\ell$ decays are therefore important tests of the SM.

In this Letter, we present an experimental study of the leptonic decay $D_s^+ \to \mu^+\nu_\mu$ [46] by analyzing a 3.19 fb^{-1} data sample collected with the BESIII detector at an e^+e^- center-of-mass energy of $E_{\mathrm{cm}} = 4.178$ GeV. At this energy, D_s^+ mesons are produced mainly through the process $e^+e^- \to D_s^+D_s^{*-}$ + c.c. In an event where a D_s^- meson [called a single-tag (ST) D_s^- meson] is fully reconstructed, one can then search for a γ or π^0 and a D_s^+ meson in the recoiling system [called a double-tag (DT) event].

Details about the design and performance of the BESIII detector are given in Ref. [47]. The end cap time-of-flight (TOF) system was upgraded with multigap resistive plate chamber technology and now has a time resolution of 60 ps [48,49]. Monte Carlo (MC) events are generated with a GEANT4-based [50] detector simulation software package [51], which includes both the geometrical description of the detector and the detector's response. An inclusive MC sample is produced at $E_{\rm cm} = 4.178$ GeV, which includes all open charm processes, initial state radiation (ISR) production of the $\psi(3770)$, $\psi(3686)$, and J/ψ, and $q\bar{q}(q = u, d, s)$ continuum processes, along with Bhabha scattering, $\mu^+\mu^-$, $\tau^+\tau^-$, and $\gamma\gamma$ events. The open charm processes are generated using CONEXC [52]. The effects of ISR [53] and final state radiation (FSR) [54] are considered. The decay modes with known BF are generated using EVTGEN [55] and the other modes are generated using LUNDCHARM [56].

The ST D_s^- mesons are reconstructed from 14 hadronic decay modes, $D_s^- \to K^+K^-\pi^-$, $K^+K^-\pi^-\pi^0$, $K_S^0K^-$, $K_S^0K^-\pi^0$, $K_S^0K_S^0\pi^-$, $K_S^0K^+\pi^-\pi^-$, $K_S^0K^-\pi^+\pi^-$, $K^-\pi^+\pi^-$, $\pi^+\pi^-\pi^-$, $\eta_{\gamma\gamma}\pi^-$, $\eta_{\pi^0\pi^+\pi^-}\pi^-$, $\eta'_{\eta_{\gamma\gamma}\pi^+\pi^-}\pi^-$, $\eta'_{\gamma\rho^0}\pi^-$, and $\eta_{\gamma\gamma}\rho^-$, where the subscripts of $\eta^{(\prime)}$ represent the decay modes used to reconstruct $\eta^{(\prime)}$.

All charged tracks except for those from K_S^0 decays must originate from the interaction point (IP) with a distance of closest approach less than 1 cm in the transverse plane and less than 10 cm along the z axis. The polar angle θ of each track defined with respect to the positron beam must satisfy $|\cos\theta| < 0.93$. Measurements of the specific ionization energy loss (dE/dx) in the main drift chamber and the TOF are combined and used for particle identification (PID) by forming confidence levels for pion and kaon hypotheses (CL_π, CL_K). Kaon (pion) candidates are required to satisfy $CL_{K(\pi)} > CL_{\pi(K)}$.

To select K_S^0 candidates, pairs of oppositely charged tracks with distances of closest approach to the IP less than 20 cm along the z axis are assigned as $\pi^+\pi^-$ without PID requirements. These $\pi^+\pi^-$ combinations are required to have an invariant mass within ± 12 MeV of the nominal K_S^0 mass [57] and have a decay length of the reconstructed K_S^0 larger than 2σ of the vertex resolution away from the IP. The π^0 and η mesons are reconstructed via $\gamma\gamma$ decays. It is required that each electromagnetic shower starts within 700 ns of the event start time and its energy is greater than 25 (50) MeV in the barrel (end cap) region of the electromagnetic calorimeter (EMC) [47]. The opening angle between the shower and the nearest charged track has to be greater than 10°. The $\gamma\gamma$ combinations with an invariant mass $M_{\gamma\gamma} \in (0.115, 0.150)$ and $(0.50, 0.57)$ GeV$/c^2$ are regarded as π^0 and η mesons, respectively. A kinematic fit is performed to constrain $M_{\gamma\gamma}$ to the π^0 or η nominal mass [57]. The η candidates for the $\eta\pi^-$ ST channel are also reconstructed via $\pi^0\pi^+\pi^-$ candidates with an invariant mass within $(0.53, 0.57)$ GeV$/c^2$. The η' mesons are reconstructed via two decay modes, $\eta\pi^+\pi^-$ and $\gamma\rho^0$, whose invariant masses are required to be within (0.946,0.970) and $(0.940, 0.976)$ GeV$/c^2$, respectively. In addition, the minimum energy of the γ from $\eta' \to \gamma\rho^0$ decays must be greater than 0.1 GeV. The ρ^0 and ρ^+ mesons are reconstructed from $\pi^+\pi^-$ and $\pi^+\pi^0$ candidates, whose invariant masses are required to be larger than 0.5 GeV$/c^2$ and within $(0.67, 0.87)$ GeV$/c^2$, respectively.

The momentum of any pion not originating from a K_S^0, η, or η' decay is required to be greater than 0.1 GeV$/c$ to reject soft pions from D^* decays. For $\pi^+\pi^-\pi^-$ and $K^-\pi^+\pi^-$ combinations, the dominant peaking backgrounds from $K_S^0\pi^-$ and $K_S^0K^-$ events are rejected by requiring the invariant mass of any $\pi^+\pi^-$ combination be more than ± 0.03 GeV$/c^2$ away from the nominal K_S^0 mass [57].

To suppress non-$D_s^+D_s^{*-}$ events, the beam-constrained mass of the ST D_s^- candidate

$$M_{\rm BC} \equiv \sqrt{(E_{\rm cm}/2)^2 - |\vec{p}_{D_s^-}|^2} \tag{2}$$

is required to be within $(2.010, 2.073)$ GeV$/c^2$, where $\vec{p}_{D_s^-}$ is the momentum of the ST D_s^- candidate. This requirement retains D_s^- mesons directly from e^+e^- annihilation and indirectly from D_s^{*-} decay (See Fig. 1 in Ref. [58]). In each event, we only keep the candidate with the D_s^- recoil mass

$$M_{\rm rec} \equiv \sqrt{\left(E_{\rm cm} - \sqrt{|\vec{p}_{D_s^-}|^2 + m_{D_s^-}^2}\right)^2 - |\vec{p}_{D_s^-}|^2} \tag{3}$$

closest to the nominal D_s^{*+} mass [57] per tag mode per charge. Figure 1 shows the invariant mass ($M_{\rm tag}$) spectra of the accepted ST candidates. The ST yield for each tag mode is obtained by a fit to the corresponding $M_{\rm tag}$ spectrum. The signal is described by the MC-simulated shape convolved with a Gaussian function representing the resolution difference between data and MC simulation. For the tag mode $D_s^- \to K_S^0K^-$, the peaking background from $D^- \to K_S^0\pi^-$ is described by the MC-simulated shape and then smeared with the same Gaussian function used in the signal shape with its size as a free parameter. The nonpeaking background is modeled by a second- or third-order Chebychev polynomial function. Studies of the inclusive MC sample validate this parametrization of the background shape. The fit results on these invariant mass spectra are shown in Fig. 1. The events in the signal regions are kept for further analysis. The total ST yield in data is $N_{\rm ST}^{\rm tot} = 388660 \pm 2592$ (see tag-dependent ST yields and background yields in the signal regions in Table I of Ref. [58]).

At the recoil sides of the ST D_s^- mesons, the $D_s^+ \to \mu^+\nu_\mu$ candidates are selected with the surviving neutral and

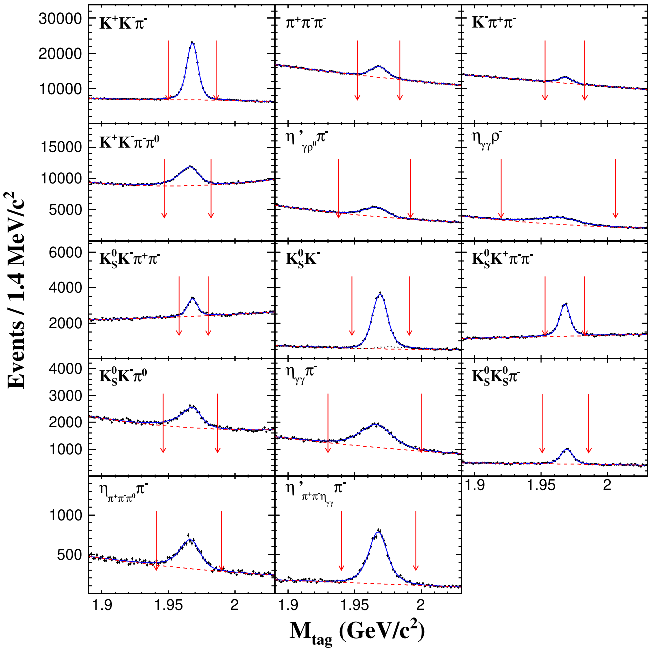

FIG. 1. Fits to the $M_{\rm tag}$ distributions of the accepted ST candidates. Dots with error bars are data. Blue solid curves are the fit results. Red dashed curves are the fitted backgrounds. The black dotted curve in the $K_S^0K^-$ mode is the $D^- \to K_S^0\pi^-$ component. The pairs of arrows denote the signal regions.

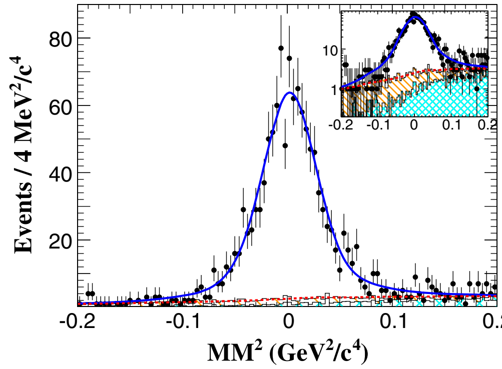

FIG. 2. Fit to the MM^2 distribution of the $D_s^+ \to \mu^+\nu_\mu$ candidates. Inset plot shows the same distribution in log scale. Dots with error bars are data. Blue solid curve is the fit result. Red dotted curve is the fitted background. Orange hatched and blue cross-hatched histograms are the BKGI component and the combined BKGII and BKGIII components, respectively (see text).

charged tracks. To select the soft $\gamma(\pi^0)$ from D_s^* and to separate signals from combinatorial backgrounds, we define two kinematic variables

$$\Delta E \equiv E_{\rm cm} - E_{\rm tag} - E_{\rm miss} - E_{\gamma(\pi^0)} \tag{4}$$

and

$$\mathrm{MM}^2 \equiv (E_{\rm cm} - E_{\rm tag} - E_{\gamma(\pi^0)} - E_\mu)^2 - |-\vec{p}_{\rm tag} - \vec{p}_{\gamma(\pi^0)} - \vec{p}_\mu|^2. \tag{5}$$

Here $E_{\rm miss} \equiv \sqrt{|\vec{p}_{\rm miss}|^2 + m^2_{D_s^+}}$ and $\vec{p}_{\rm miss} \equiv -\vec{p}_{\rm tag} - \vec{p}_{\gamma(\pi^0)}$ are the missing energy and momentum of the recoiling system of the soft $\gamma(\pi^0)$ and the ST D_s^-, where E_i and $\vec{p}_i$ [$i = \mu, \gamma(\pi^0)$ or tag] denote the energy and momentum of the muon, $\gamma(\pi^0)$ or ST D_s^-, respectively. MM^2 is the missing mass square of the undetectable neutrino. We loop over all remaining γ or π^0 candidates and choose the one giving a minimum $|\Delta E|$. The events with $\Delta E \in (-0.05, 0.10)$ GeV are accepted. The muon candidate is required to have an opposite charge to the ST D_s^- meson and a deposited energy in the EMC within (0.0,0.3) GeV. It must also satisfy a two dimensional (2D, e.g., $|\cos\theta_\mu|$ and momentum p_μ) requirement on the hit depth (d_μ) in the muon counter, as explained in Ref. [59]. To suppress the backgrounds with extra photon (s), the maximum energy of the unused showers in the DT selection ($E^{\rm max}_{{\rm extra}\gamma}$) is required to be less than 0.4 GeV and no additional charged track that satisfies the charged track selection criteria is allowed. To improve the MM^2 resolution, the candidate tracks, plus the missing neutrino, are subjected to a 4-constraint kinematic fit requiring energy and momentum conservation. In addition, the invariant masses of the two D_s mesons are constrained to the nominal D_s mass, the invariant mass of the $D_s^-\gamma(\pi^0)$ or $D_s^+\gamma(\pi^0)$ combination is constrained to the nominal D_s^* mass, and the combination with the smaller χ^2 is kept. Figure 2 shows the MM^2 distribution for the accepted DT candidate events.

To extract the DT yield, an unbinned constrained fit is performed to the MM^2 distribution. In the fit, the background events are classified into three categories: events with correctly reconstructed ST D_s^- and μ^+ but an unmatched $\gamma(\pi^0)$ from the D_s^{*-} (BKGI), events with a correctly reconstructed ST D_s^- but misidentified μ^+ (BKGII), and other events with a misreconstructed ST D_s^- (BKGIII). The signal and BKGI shapes are modeled with MC simulation. The signal shape is convolved with a Gaussian function with its mean and width as free parameters. The ratio of the signal yield over the BKGI yield is constrained to the value determined with the signal MC events. The size and shape of the BKGII and BKGIII components are fixed by analyzing the inclusive MC sample. From the fit to the MM^2 distribution, as shown in Fig. 2, we determine the number of $D_s^+ \to \mu^+\nu_\mu$ decays to be $N_{\rm DT} = 1135.9 \pm 33.1$.

The efficiencies for reconstructing the DT candidate events are determined with an exclusive MC sample of $e^+e^- \to D_s^+D_s^{*-}$, where the D_s^- decays to each tag mode and the D_s^+ decays to $\mu^+\nu_\mu$. Dividing them by the ST efficiencies determined with the inclusive MC sample yields the corresponding efficiencies of the $\gamma(\pi^0)\mu^+\nu_\mu$

reconstruction. The averaged efficiency of finding $\gamma(\pi^0)\mu^+\nu_\mu$ is $(52.67 \pm 0.19)\%$ as determined from

$$\varepsilon_{\gamma(\pi^0)\mu^+\nu_\mu} = f^{\rm cor}_{\mu\rm PID}\sum_i (N^i_{\rm ST}\varepsilon^i_{\rm DT})/(N^{\rm tot}_{\rm ST}\varepsilon^i_{\rm ST}), \qquad (6)$$

where $N^i_{\rm ST}$, $\varepsilon^i_{\rm ST}$, and $\varepsilon^i_{\rm DT}$ are the ST yield, ST efficiency, and DT efficiency in the ith ST mode, respectively. The factor $f^{\rm cor}_{\mu\rm PID} = 0.897$ accounts for the difference between the μ^+ PID efficiencies in data and MC simulation [$\varepsilon^{\rm data(MC)}_{\mu\rm PID}$]. These efficiencies are estimated using $e^+e^- \to \gamma\mu^+\mu^-$ samples but reweighted by the μ^+ 2D distribution of $D^+_s \to \mu^+\nu_\mu$. It is non-negligible mainly due to the imperfect simulation of d_μ and its applicability in different topology environments is verified via three aspects: (i) Studies with signal MC events show that $\varepsilon^{\rm MC}_{\mu\rm PID} = (74.79 \pm 0.03)\%$ for $D^+_s \to \mu^+\nu_\mu$ signals can be well reproduced by the 2D reweighted efficiency $\varepsilon^{\rm MC}_{\mu\rm PID} = (74.91 \pm 0.10)\%$ with $e^+e^- \to \gamma\mu^+\mu^-$ samples. (ii) Our nominal BF ($\mathcal{B}_{D^+_s\to\mu^+\nu_\mu}$) obtained later can be well reproduced by removing the d_μ requirement, with negligible difference but obviously lower precision due to much higher background [60]. (iii) The $\varepsilon^{\rm data(MC)}_{\mu\rm PID}$ for $e^+e^- \to \gamma_{\rm ISR}\psi(3686)$, $\psi(3686) \to \pi^+\pi^- J/\psi$, $J/\psi \to \mu^+\mu^-$ events can be well reproduced by the corresponding 2D reweighted efficiencies with $e^+e^- \to \gamma\mu^+\mu^-$ samples (see Table II of Ref. [58]). The BF of $D^+_s \to \mu^+\nu_\mu$ is then determined to be $(5.49 \pm 0.16_{\rm stat} \pm 0.15_{\rm syst}) \times 10^{-3}$ from

$$\mathcal{B}_{D^+_s\to\mu^+\nu_\mu} = f^{\rm rad}_{\rm cor}N_{\rm DT}/(N^{\rm tot}_{\rm ST}\varepsilon_{\gamma(\pi^0)\mu^+\nu_\mu}), \qquad (7)$$

where the radiative correction factor $f^{\rm rad}_{\rm cor} = 0.99$ is due to the contribution from $D^+_s \to \gamma\mathcal{D}^{*+}_s \to \gamma\mu^+\nu_\mu$ [61], with $\mathcal{D}^{*+}_s$ as a virtual vector or axial-vector meson. This contribution is almost identical with our signal process for low energy radiated photons. We further examine the BFs measured with individual tags which have very different background levels, and a good consistence is found (see Table I of Ref. [58] for tag-dependent DT yields, $\varepsilon_{\gamma(\pi^0)\mu^+\nu_\mu}$ and $\mathcal{B}_{D^+_s\to\mu^+\nu_\mu}$).

The systematic uncertainties in the BF measurement are estimated relative to the measured BF and are described below.

For uncertainties in the event selection criteria, the μ^+ tracking and PID efficiencies are studied with $e^+e^- \to \gamma\mu^+\mu^-$ events. After correcting the detection efficiency by $f^{\rm cor}_{\mu\rm PID}$, we assign 0.5% and 0.8% as the uncertainties in μ^+ tracking and PID efficiencies, respectively. The photon reconstruction efficiency has been previously studied with $J/\psi \to \pi^+\pi^-\pi^0$ decays [62]. The uncertainty of finding $\gamma(\pi^0)$ is weighted according to the BFs of $D^{*+}_s \to \gamma D^+_s$ and $D^{*+}_s \to \pi^0 D^+_s$ [57] and assigned to be 1.0%. The efficiencies for the requirements of $E^{\rm max}_{\rm extra\gamma}$ and no extra good charged track are studied with a DT hadronic sample. The systematic uncertainties are taken to be 0.3% and 0.9% considering the efficiency differences between data and MC simulation, respectively. The uncertainty of the ΔE requirement is estimated by varying the signal region by ± 0.01 GeV, and the maximum change of the BF, 0.5%, is taken as the systematic uncertainty.

To determine the uncertainty in the MM^2 fit, we change the fit range by ± 0.02 GeV$^2/c^4$, and the largest change of the BF is 0.6%. We change the signal shape by varying the $\gamma(\pi^0)$ match requirement and the maximum change is 0.2%. Two sources of uncertainty in the background estimation are considered. The effect of the background shape is obtained to be 0.2% by shifting the number of the main components of BKGII by $\pm 1\sigma$ of the uncertainties of the corresponding BFs [57], and varying the relative fraction of the main components of BKGII by 50%. The effect of the fixed number of the BKGII and BKGIII is estimated to be 0.5% by varying the nominal numbers by $\pm 1\sigma$ of their uncertainties. To evaluate the uncertainty in the fixed ratio of signal and BKGI, we perform an alternative fit to the MM^2 distribution of data without constraining the ratio of signal and BKGI. The change in the DT yield, 1.1%, is assigned as the relevant uncertainty.

The uncertainty in the number of ST D^-_s mesons is assigned to be 0.8% by examining the changes of the fit yields when varying the signal shape, background shape, bin size, and fit range and considering the background fluctuation in the fit. The uncertainty due to the limited MC size is 0.4%. The uncertainty in the imperfect simulation of the FSR effect is estimated as 0.4% by varying the amount of FSR photons in signal MC events [54]. The uncertainty due to the quoted BFs of D^{*-}_s subdecays from the Particle Data Group (PDG) [57] is examined by varying each subdecay BF by $\pm 1\sigma$. The efficiency change is found to be 0.4% and is taken as the associated uncertainty. The uncertainty in the radiative correction is assigned to be 1.0%, which is taken as 100% of its central value from theoretical calculation [61]. The ST efficiencies in the inclusive and signal MC samples are slightly different with each other due to different track multiplicities in these two environments. This may cause incomplete cancellation of the uncertainties of the ST efficiencies. The associated uncertainty is assigned as 0.6%, by taking into account the differences of the efficiencies of tracking/PID of $K^\pm$ and $\pi^\pm$, as well as the selections of neutral particles between data and MC simulation in different environments. The total systematic uncertainty is determined to be 2.7% by adding all the uncertainties in quadrature.

Combining our BF with the world average values of G_F, m_μ, $m_{D^+_s}$ and the lifetime of D^+_s [57] in Eq. (1) yields

$$f_{D^+_s}|V_{cs}| = 246.2 \pm 3.6_{\rm stat} \pm 3.5_{\rm syst}\ {\rm MeV}.$$

Here the systematic uncertainties arise mainly from the uncertainties in the measured BF (1.5%) and the lifetime of the D_s^+ (0.4%). Taking the CKM matrix element $|V_{cs}| = 0.97359^{+0.00010}_{-0.00011}$ from the global fit in the SM [57] or the averaged decay constant $f_{D_s^+} = 249.9 \pm 0.4$ MeV of recent LQCD calculations [8,10] as input, we determine

$$f_{D_s^+} = 252.9 \pm 3.7_{\rm stat} \pm 3.6_{\rm syst}\ {\rm MeV}$$

and

$$|V_{cs}| = 0.985 \pm 0.014_{\rm stat} \pm 0.014_{\rm syst}.$$

The additional systematic uncertainties according to the input parameters are negligible for $|V_{cs}|$ and 0.2% for $f_{D_s^+}$. The measured $|V_{cs}|$ is consistent with our measurements using $D \to \bar{K}\ell^+\nu_\ell$ [63–66] and $D_s^+ \to \eta^{(\prime)} e^+\nu_e$ [67], but with much better precision.

Combining the obtained $f_{D_s^+}|V_{cs}|$ and its counterpart $f_{D^+}|V_{cd}|$ measured in our previous work [68], along with $|V_{cd}/V_{cs}| = 0.23047 \pm 0.00045$ from the SM global fit [57], yields $f_{D_s^+}/f_{D^+} = 1.24 \pm 0.04_{\rm stat} \pm 0.02_{\rm syst}$. It is consistent with the CLEO measurement [2] within 1σ and the LQCD calculation within 2σ [8]. Alternatively, with the input of $f_{D_s^+}/f_{D^+} = 1.1749 \pm 0.0016$ calculated by LQCD [8], we obtain $|V_{cd}/V_{cs}|^2 = 0.048 \pm 0.003_{\rm stat} \pm 0.001_{\rm syst}$, which agrees with the one expected by $|V_{cs}|$ and $|V_{cd}|$ given by the CKMfitter within 2σ. Here, only the systematic uncertainty in the radiative correction is canceled since the two data samples were taken in different years.

Based on our result for $\mathcal{B}_{D_s^+\to\mu^+\nu_\mu}$ and those measured at the CLEO [2], *BABAR* [5], and Belle [6] experiments, along with a previous measurement at BESIII [7], the inverse-uncertainty weighted BF is determined to be $\bar{\mathcal{B}}_{D_s^+\to\mu^+\nu_\mu} = (5.49 \pm 0.17) \times 10^{-3}$ [69]. The ratio of $\bar{\mathcal{B}}_{D_s^+\to\mu^+\nu_\mu}$ over the PDG value of $\mathcal{B}_{D_s^+\to\tau^+\nu_\tau} = (5.48 \pm 0.23)\%$ [57] is determined to be $[(\mathcal{B}_{D_s^+\to\tau^+\nu_\tau})/(\bar{\mathcal{B}}_{D_s^+\to\mu^+\nu_\mu})] = 9.98 \pm 0.52$, which agrees with the SM predicted value of 9.74 within uncertainty.

The BFs of $D_s^+ \to \mu^+\nu_\mu$ and $D_s^- \to \mu^-\bar{\nu}_\mu$ decays are also measured separately. The results are $\mathcal{B}_{D_s^+\to\mu^+\nu_\mu} = (5.62 \pm 0.23_{\rm stat}) \times 10^{-3}$ and $\mathcal{B}_{D_s^-\to\mu^-\bar{\nu}_\mu} = (5.40 \pm 0.23_{\rm stat}) \times 10^{-3}$. The BF asymmetry is determined to be $A_{\rm CP} = [(\mathcal{B}_{D_s^+\to\mu^+\nu_\mu} - \mathcal{B}_{D_s^-\to\mu^-\bar{\nu}_\mu})/(\mathcal{B}_{D_s^+\to\mu^+\nu_\mu} + \mathcal{B}_{D_s^-\to\mu^-\bar{\nu}_\mu})] = (2.0 \pm 3.0_{\rm stat} \pm 1.2_{\rm syst})\%$, where the uncertainties in the tracking and PID efficiencies of the muon, the ST yields, the limited MC statistics, as well as the signal shape and fit range in MM^2 fits for D_s^+ and D_s^- have been studied separately and are not canceled.

In summary, by analyzing 3.19 fb^{-1} of e^+e^- collision data collected at $E_{\rm cm} = 4.178$ GeV with the BESIII detector, we have measured $\mathcal{B}(D_s^+ \to \mu^+\nu_\mu)$, the decay constant $f_{D_s^+}$, and the CKM matrix element $|V_{cs}|$. These are the most precise measurements to date, and are important to calibrate various theoretical calculations of $f_{D_s^+}$ and test the unitarity of the CKM matrix with better accuracy. We also search for LFU and CP violation in $D_s^+ \to \ell^+\nu_\ell$ decays, and no evidence is found.

The BESIII Collaboration thanks the staff of BEPCII and the IHEP computing center for their strong support. This work is supported in part by National Key Basic Research Program of China under Contract No. 2015CB856700; National Natural Science Foundation of China (NSFC) under Contracts No. 11235011, No. 11335008, No. 11425524, No. 11505034, No. 11575077, No. 11625523, No. 11635010, No. 11675200, and No. 11775230; the Chinese Academy of Sciences (CAS) Large-Scale Scientific Facility Program; the CAS Center for Excellence in Particle Physics (CCEPP); Joint Large-Scale Scientific Facility Funds of the NSFC and CAS under Contracts No. U1332201, No. U1532257, No. U1532258, and No. U1632109; CAS under Contracts No. KJCX2-YW-N29, No. KJCX2-YW-N45, No. QYZDJ-SSW-SLH003; 100 Talents Program of CAS; National 1000 Talents Program of China; INPAC and Shanghai Key Laboratory for Particle Physics and Cosmology; German Research Foundation DFG under Contracts No. Collaborative Research Center CRC 1044, FOR 2359; Istituto Nazionale di Fisica Nucleare, Italy; Koninklijke Nederlandse Akademie van Wetenschappen (KNAW) under Contract No. 530-4CDP03; Ministry of Development of Turkey under Contract No. DPT2006K-120470; National Science and Technology fund; The Swedish Research Council; U.S. Department of Energy under Contracts No. DE-FG02-05ER41374, No. DE-SC-0010118, No. DE-SC-0010504, and No. DE-SC-0012069; University of Groningen (RuG) and the Helmholtzzentrum fuer Schwerionenforschung GmbH (GSI), Darmstadt; WCU Program of National Research Foundation of Korea under Contract No. R32-2008-000-10155-0.

[a]Also at Bogazici University, 34342 Istanbul, Turkey
[b]Also at the Moscow Institute of Physics and Technology, Moscow 141700, Russia
[c]Also at the Functional Electronics Laboratory, Tomsk State University, Tomsk, 634050, Russia
[d]Also at the Novosibirsk State University, Novosibirsk, 630090, Russia
[e]Also at the NRC "Kurchatov Institute", PNPI, 188300, Gatchina, Russia
[f]Also at Istanbul Arel University, 34295 Istanbul, Turkey
[g]Also at Goethe University Frankfurt, 60323 Frankfurt am Main, Germany
[h]Also at Key Laboratory for Particle Physics, Astrophysics and Cosmology, Ministry of Education; Shanghai Key Laboratory for Particle Physics and Cosmology; Institute of Nuclear and Particle Physics, Shanghai 200240, People's Republic of China

[i]Also at Government College Women University, Sialkot - 51310. Punjab, Pakistan.
[j]Currently at: Center for Underground Physics, Institute for Basic Science, Daejeon 34126, Korea
[k]Also at Harvard University, Department of Physics, Cambridge, MA, 02138, USA

[1] D. Silverman and H. Yao, Phys. Rev. D **38**, 214 (1988).
[2] J. P. Alexander *et al.* (CLEO Collaboration), Phys. Rev. D **79**, 052001 (2009).
[3] P. Naik *et al.* (CLEO Collaboration), Phys. Rev. D **80**, 112004 (2009).
[4] P. U. E. Onyisi *et al.* (CLEO Collaboration), Phys. Rev. D **79**, 052002 (2009).
[5] P. del Amo Sanchez *et al.* (*BABAR* Collaboration), Phys. Rev. D **82**, 091103 (2010).
[6] A. Zupanc *et al.* (Belle Collaboration), J. High Energy Phys. 09 (2013) 139.
[7] M. Ablikim *et al.* (BESIII Collaboration), Phys. Rev. D **94**, 072004 (2016).
[8] A. Bazavov, C. Bernard, N. Brown, C. DeTar, A. X. El-Khadra, E. Gámiz, S. Gottlieb, U. M. Heller, J. Komijani, A. S. Kronfeld, J. Laiho, P. B. Mackenzie, E. T. Neil, J. N. Simone, R. L. Sugar, D. Toussaint, and R. S. Van de Water (Fermilab Lattice and MILC Collaborations), Phys. Rev. D **98**, 074512 (2018).
[9] A. Bazavov *et al.* (Fermilab Lattice and MILC Collaborations), Phys. Rev. D **90**, 074509 (2014).
[10] N. Carrasco, P. Dimopoulos, R. Frezzotti, P. Lami, V. Lubicz, F. Nazzaro, E. Picca, L. Riggio, G. C. Rossi, F. Sanfilippo, S. Simula, and C. Tarantino (ETM Collaboration), Phys. Rev. D **91**, 054507 (2015).
[11] P. A. Boyle, L. Del Debbio, A. Jüttner, A. Khamseh, F. Sanfilippo, and J. T. Tsang, J. High Energy Phys. 12 (2017) 008.
[12] Y. Yi-Bo *et al.*, Phys. Rev. D **92**, 034517 (2015).
[13] A. Bazavov *et al.* (Fermilab Lattice and MILC Collaborations), Phys. Rev. D **85**, 114506 (2012).
[14] C. T. H. Davies, C. McNeile, E. Follana, G. P. Lepage, H. Na, and J. Shigemitsu (HPQCD Collaboration), Phys. Rev. D **82**, 114504 (2010).
[15] H. Na, C. T. H. Davies, E. Follana, G. P. Lepage, and J. Shigemitsu (HPQCD Collaboration), Phys. Rev. D **86**, 054510 (2012).
[16] C. Aubin *et al.* (Fermilab Lattice and MILC Collaborations), Phys. Rev. Lett. **95**, 122002 (2005).
[17] E. Follana, C. T. H. Davies, G. P. Lepage, and J. Shigemitsu (HPQCD Collaboration), Phys. Rev. Lett. **100**, 062002 (2008).
[18] P. Dimopoulos *et al.* (ETM Collaboration), J. High Energy Phys. 01 (2012) 046.
[19] W. P. Chen, Y.-C. Chen, T.-W. Chiu, H.-Y. Chou, T.-S. Guu, and T.-H. Hsieh, Phys. Lett. B **736**, 231 (2014).
[20] Y. Namekawa, S. Aoki, K.-I. Ishikawa, N. Ishizuka, T. Izubuchi, K. Kanaya, Y. Kuramashi, M. Okawa, Y. Taniguchi, A. Ukawa, N. Ukita, and T. Yoshie (PACS-CS Collaboration), Phys. Rev. D **84**, 074505 (2011).
[21] A. Ali Khan, V. Braun, T. Burch, M. Göckeler, G. Lacagnina, A. Schäfer, and G. Schierholz (QCDSF Collaboration), Phys. Lett. B **652**, 150 (2007).
[22] T. W. Chiu, T.-H. Hsieh, J.-Y. Lee, P.-H. Liu, and H.-J. Chang, Phys. Lett. B **624**, 31 (2005).
[23] L. Lellouch and C.-J. David Lin (UKQCD Collaboration), Phys. Rev. D **64**, 094501 (2001).
[24] D. Becirevic, Ph. Boucaud, J. P. Leroy, V. Lubicz, G. Martinelli, F. Mescia, and F. Rapuano, Phys. Rev. D **60**, 074501 (1999).
[25] J. Bordes, J. Penarrocha, and K. Schilcher, J. High Energy Phys. 11 (2005) 014.
[26] S. Narison, arXiv:hep-ph/0202200.
[27] A. M. Badalian, B. L. B. Bakker, and Y. A. Simonov, Phys. Rev. D **75**, 116001 (2007).
[28] D. Ebert, R. N. Faustov, and V. O. Galkin, Phys. Lett. B **635**, 93 (2006).
[29] G. Cvetic, C. S. Kim, G.-L. Wang, and W. Namgung, Phys. Lett. B **596**, 84 (2004).
[30] H. M. Choi, Phys. Rev. D **75**, 073016 (2007).
[31] L. Salcedo, J. P. B. C. de Melo, D. Hadjmichef, and T. Frederico, Braz. J. Phys. **34**, 297 (2004).
[32] Z. G. Wang, W.-M. Yang, and S.-L. Wan, Nucl. Phys. **A744**, 156 (2004).
[33] J. F. Amundson, J. L. Rosner, M. A. Kelly, N. Horwitz, and S. L. Stone, Phys. Rev. D **47**, 3059 (1993).
[34] D. Becirevic, B. Blossier, A. Gérardin, A. Le Yaouanc, and F. Sanfilippo, Nucl. Phys. **B872**, 313 (2013).
[35] W. Lucha, D. Melikhov, and S. Simula, Phys. Lett. B **701**, 82 (2011).
[36] C. W. Hwang, Phys. Rev. D **81**, 054022 (2010).
[37] Z. G. Wang, Eur. Phys. J. C **75**, 427 (2015).
[38] J. P. Lees *et al.* (*BABAR* Collaboration), Phys. Rev. Lett. **109**, 101802 (2012).
[39] J. P. Lees *et al.* (*BABAR* Collaboration), Phys. Rev. D **88**, 072012 (2013).
[40] R. Aaij *et al.* (LHCb Collaboration), Phys. Rev. Lett. **115**, 111803 (2015).
[41] R. Aaij *et al.* (LHCb Collaboration), Phys. Rev. Lett. **113**, 151601 (2014).
[42] S. Wehle *et al.* (Belle Collaboration), Phys. Rev. Lett. **118**, 111801 (2017).
[43] S. Fajfer, I. Nisandzic, and U. Rojec, Phys. Rev. D **91**, 094009 (2015).
[44] G. C. Branco, P. M. Ferreira, L. Lavoura, M. N. Rebelo, M. Sher, and J. P. Silva, Phys. Rep. **516**, 1 (2012).
[45] G. C. Branco, R. G. Felipe, and F. R. Joaquim, Rev. Mod. Phys. **84**, 515 (2012).
[46] Charge-conjugate modes are always implied unless stated explicitly.
[47] M. Ablikim *et al.* (BESIII Collaboration), Nucl. Instrum. Methods Phys. Res., Sect. A **614**, 345 (2010).
[48] X. Li *et al.*, Radiat. Detect. Technol. Methods **1**, 13 (2017).
[49] Y. X. Guo *et al.*, Radiat. Detect. Technol. Methods **1**, 15 (2017).
[50] S. Agostinelli *et al.* (GEANT4 Collaboration), Nucl. Instrum. Methods Phys. Res., Sect. A **506**, 250 (2003).
[51] Z. Y. Deng *et al.*, Chin. Phys. C **30**, 371 (2006).
[52] R. G. Ping, Chin. Phys. C **38**, 083001 (2014).
[53] E. A. Kuraev and V. S. Fadin, Sov. J. Nucl. Phys. **41**, 466 (1985) Yad. Fiz. **41**, 733 (1985).

[54] E. Barberio and Z. Was, Comput. Phys. Commun. **79**, 291 (1994).

[55] D. J. Lange, Nucl. Instrum. Methods Phys. Res., Sect. A **462**, 152 (2001); R. G. Ping, Chin. Phys. C **32**, 599 (2008).

[56] J. C. Chen, G. S. Huang, X. R. Qi, D. H. Zhang, and Y. S. Zhu, Phys. Rev. D **62**, 034003 (2000).

[57] M. Tanabashi *et al.* (Particle Data Group), Phys. Rev. D **98**, 030001 (2018).

[58] See Supplemental Material at http://link.aps.org/supplemental/10.1103/PhysRevLett.122.071802 for the distributions of $M_{\rm BC}$, the ST yields and backgrounds in $M_{\rm tag}$ signal region, the DT yields, $\epsilon_{\gamma(\pi^0)\mu^+\nu_\mu}$ and $\mathcal{B}_{D_s^+\to\mu^+\nu_\mu}$ with different tags, and the validation of the correction of μ PID efficiency.

[59] The $|\cos\theta_{\mu,i}|$ is equally divided as $[0.2\times(i-1), 0.2\times i](i=1,2,3,4,$ or $5)$. In the first three $|\cos\theta_{\mu,i}|$ bins, we require d_μ greater than 17, $100\times p_\mu-(68+3\times i)$ and 33 cm for the muons with $p_\mu\le 0.85+0.03\times i$, $p_\mu\in(0.85+0.03\times i, 1.01+0.03\times i)$ and $p_\mu\ge 1.01+0.03\times i$, respectively. For other $|\cos\theta_{\mu,i}|$ bins, we require d_μ greater than 17 cm uniformly.

[60] Without the d_μ requirement, there will be higher background from $D_s^+\to\tau^+\nu_\tau, \tau^+\to\pi^+\bar{\nu}_\tau$.

[61] G. Burdman, T. Goldman, and D. Wyler, Phys. Rev. D **51**, 111 (1995).

[62] M. Ablikim *et al.* (BESIII Collaboration), Phys. Rev. D **83**, 112005 (2011).

[63] M. Ablikim *et al.* (BESIII Collaboration), Phys. Rev. D **92**, 072012 (2015).

[64] M. Ablikim *et al.* (BESIII Collaboration), Phys. Rev. D **96**, 012002 (2017).

[65] M. Ablikim *et al.* (BESIII Collaboration), Phys. Rev. D **92**, 112008 (2015).

[66] M. Ablikim *et al.* (BESIII Collaboration), Phys. Rev. Lett. **122**, 011804 (2019).

[67] M. Ablikim *et al.* (BESIII Collaboration), arXiv:1901.02133.

[68] M. Ablikim *et al.* (BESIII Collaboration), Phys. Rev. D **89**, 051104 (2014).

[69] To be consistent with results at CLEO and BESIII, the BFs measured by Belle and *BABAR* have been further corrected by $f^{\rm rad}_{\rm cor}$. The uncertainty in $f^{\rm rad}_{\rm cor}$ is common for individual measurements, but will be taken into account in the averaged BF. For the previous measurement in BESIII, we quote the BF without the LFU constraint.